THE IMPACT OF HIRANO BODIES ON ALZHEIMER'S DISEASE PROGRESSION

by

MATTHEW CHASE FURGERSON

(Under the Direction of Marcus Fechheimer and Ruth Furukawa)

ABSTRACT

Alzheimer's disease is a neurodegenerative condition characterized by three pathological hallmarks: amyloid beta plaques composed of amyloid beta (a fragment of the amyloid precursor protein), neurofibrillary tangles composed of tau, and Hirano bodies composed of filamentous actin (F-actin) and actin binding proteins (1). While both amyloid beta plaques and neurofibrillary tangles have been well studied, relatively little is known about Hirano bodies because of the absense of a model system. We have established cell culture models to study the role of Hirano bodies in amyloid precursor protein and tau-induced cell death. Exogenous expression of the amyloid precursor protein (APP) plus its c-terminal fragment C31, or expression of amyloid precursor protein intracellular domain (AICDc58, AICD) alone, initiates cell death. The addition of a hyperphosphorylated tau mimic 352PHPtau (2,3) or FTLD-tau mutants significantly increases cell death in the presence of both APP and C31 or AICDc58 alone. The mechanism of cell death induced by APP, its c-terminal fragments, and tau was investigated. Fe65, Tip60, p53, and caspases play a role in both tau-independent and tau-

dependent cell death. In addition, apoptosis was determined to contribute to cell death. The presence of model Hirano bodies protected against cell death initiated by some forms of tau and increased cell death initiated by others. Further investigation of the physiological role of Hirano bodies in a mouse model indicates that Hirano bodies initiate an inflammatory response in the brain as measured by reactive astrocytes. In addition, mice with Hirano bodies show a deficit in spatial working memory as measured using an 8-arm radial maze, while electrophysiological measurements of both short-term and long-term plasticity appear unaffected. These studies suggest that Hirano bodies can be either protective or detrimental and likely play a dynamic and complex role in neurodegeneration.

INDEX WORDS: Hirano body, APP, tau, NFT, amyloid, Alzheimer's disease, FTLD, transgenic mouse, electrophysiology, neurodegeneration.

THE IMPACT OF HIRANO BODIES ON ALZHEIMER'S DISEASE PROGRESSION

by

MATTHEW CHASE FURGERSON

B.S., Georgia College and State University, 2009

A Dissertation Submitted to the Graduate Faculty of The University of Georgia in Partial Fulfillment of the Requirements for the Degree

DOCTOR OF PHILOSOPHY

ATHENS, GEORGIA

2014

THE IMPACT OF HIRANO BODIES ON ALZHEIMER'S DISEASE PROGRESSION

by

MATTHEW C. FURGERSON

Major Professors:	Marcus Fechheimer and Ruth Furukawa
Committee:	James Lauderdale Richard Steet Claiborne Glover

Electronic Version Approved:

Julie Coffield
Dean of the Graduate School
The University of Georgia
July 2014

DEDICATION

This thesis is dedicated to my parents, Steve and Teresa Furgerson and my brother Joshua Furgerson. They have always provided a continual source of encouragement and love. Through their support, I have become the first member of my family to attempt or complete a graduate degree. Thank you for everything you have given me.

ACKNOWLEDGEMENTS

First, I would like to give thanks to my co-principle investigators, Drs. Marcus Fechheimer and Ruth Furukawa. They were both crucial to my success as a graduate student and development as a young scientist. Through their mentoring, they helped to foster creativity, independence, confidence, and patience. Dr. Fechheimer and Dr. Furukawa also offered advice and guidance during some of the most difficult personal circumstances in my life. I am grateful for that.

Second, I thank the members of both Dr. John Wagner's laboratory and Dr. Mike Tiemeyer's Laboratory. I would also like to thank members of my lab including William Spears, Yun Dong, Ali Bobo, Nelson May, Parker Evans, Connor Sweetnum, and Allison Wood. My time at UGA would not be the same without you all. I look forward to hearing of your successful endeavors.

Third, I would like to thank my committee members (Dr. Lauderdale, Dr. Glover, and Dr. Steet), collaborators (Dr. Wagner, Dr. Crystal, and Dr. Tiemeyer), and undergraduate advisor (Dr. Michael Gleason). You have all graciously set aside time to offer suggestions, perspective, and constructive critique during my graduate student career.

Finally, I would like to give thanks to my family, friends, and fiancé Katherine Firebaugh, with a special mention to my many brothers at Mt. Vernon Lodge No. 22 F&AM. I am blessed to have you all in my life.

TABLE OF CONTENTS

Page

LIST OF TABLES

Page

LIST OF FIGURES

Page

CHAPTER 1

INTRODUCTION AND LITERATURE REVIEW

ALZHEIMER'S DISEASE:

Neurodegenerative diseases are a class of diseases of the nervous system characterized by extensive neuron loss accompanied by cognitive and behavioral abnormalities. Alzheimer's disease is the most prevalent neurodegenerative disease worldwide and is the sixth leading cause of death in the United States. It is predicted that the number of patients with Alzheimer's disease will increase from 12.5 million to over 50 million by 2050 (Alz.org). Alzheimer's disease is diagnosed by the presence of pathological hallmarks, which include amyloid beta plaques and neurofibrillary tangles (NTFs). However, there are other common pathological hallmarks in Alzheimer's disease including Hirano bodies and granulovacuolar degeneration. Alzheimer's disease patients might also develop secondary pathologies, which are less frequently occurring and include Lewy bodies, Pick bodies, and TDP-43 aggregates (1). Alzheimer's disease can be divided into two types. The first is sporadic Alzheimer's disease, which is late onset and accounts for the vast majority of Alzheimer's disease cases (1,4,5). The second is familial Alzheimer's disease, which is both early onset and more aggressive and is linked to genetic mutations that impact the proteolytic processing of the amyloid precursor protein (APP) as discussed below (1,4,5). Neuron death occurs in the later stages of the disease; however, the memory loss associated with Alzheimer's disease precedes any detectable neuron loss (6). Furthermore, pathological hallmarks of the

disease can begin to deposit up to a decade before the onset of the disease (1). Therefore, understanding how these pathologies relate to disease progression is vital to development of therapeutics.

APP PROCESSING AND AMYLOID BETA PATHOLOGY:

APP, is a type I transmembrane protein whose encoding gene resides on human chromosome 21 (7). Of the three isoforms arising from alternative splicing (APP695, APP751, APP770), the 695 amino acid isoform is the most predominant species in the central nervous system (8,9). In addition to differences in isoforms, two mammalian orthologs of APP exist, APLP1 and APLP2 (10,11). While function of APP is still unknown, several putative roles have been suggested including modification of synaptic plasticity, cell adhesion, gene regulation, iron transport, calcium homeostasis, and axonal migration (12,13). The function of APP is further obscured by the fact that brain-specific APP knockout mice have little to no phenotype (14). Interestingly, APP and APLP2 double knockout mice show an early lethal phenotype not seen in APP or APLP2 single knockouts suggesting redundancy exists between APP and APLPs (14,15).

APP is subjected to a variety of cleavage events by various proteolytic enzymes including α-secretase, β-secretase, γ-secretase, and caspases (See Figure 1.1). Cleavage by both β and γ-secretases leads to the formation of amyloid beta (Aβ) molecules, which are released to the outside of the cell (1,16). These Aβ monomers aggregate to form insoluble structures called Aβ plaques as well as soluble and insoluble oligomeric aggregates (16-19). The γ-secretase enzyme has two adjacent cleavage sites within APP allowing two isoforms of Aβ, Aβ40 or Aβ42, to be generated (20,21). Aβ42 has a greater propensity to form aggregates because of its two additional hydrophobic residues, which were imbedded in the lipid bilayer (22-24). Familial

Alzheimer's disease mutations have been shown to alter Aβ synthesis. These mutations occur in either APP itself or the presenilin component of γ-secretase and result in one of two possible consequences. First, mutations can increase the production of total Aβ due to inducing an increase in APP/protease interaction or by increasing protease activity (25). Second, mutations may impact APP processing, resulting in γ-secretase cleavage events that preferentially produce the more pathogenic Aβ42 compared to Aβ40 (25). In addition to the amyloidogenic pathway just described, α-secretase can also cleave APP and impede the formation of Aβ by cleaving within the Aβ region of APP (See Figure 1.1) (20). The regulatory mechanism of APP cleavage by α-secretase versus β-secretase is unknown, but may be regulated via APP trafficking events (26,27).

Cleavage of APP by γ-secretase also releases an APP intracellular domain (AICD) that is 57 or 59 amino acids in length (28). This intracellular region of APP also contains a caspase cleavage site that produces a second molecule named C31 (See Figure 1.1) (29-31). Both AICD and C31 contain a YENPTY motif, which interacts with a variety of proteins (32), the best studied of which is the scaffolding protein Fe65 (33). AICD or C31/Fe65 complexes shuttle to the nucleus where they interact with the histone acetyltransferase tip60 to form a trimeric transcriptional complex in a signaling event similar to that of Notch (28,34-36). Multiple laboratories have measured the genes regulated by AICD, but the data sets are largely inconsistent (37-41). The few overlapping targets of these transcription assays include p53, glycogen synthase kinase 3 beta (GSK-3β), and regulators of cytoskeleton dynamics (42-44). In addition to a transcriptional role, intracellular fragments of APP have also been implicated in cell death (45-47). Interestingly, both AICD and C31 protein levels are significantly elevated in

brains of Alzheimer's disease patients compared to those of age-matched controls (45,48,49). However, the consequences of elevated protein levels is not understood.

TAU PATHOLOGY IN AD:

Neurofibrillary tangles (NFTs) are the second pathological hallmark of Alzheimer's disease patients and are composed of aggregations of tau (19). Tau is a microtubule-associated protein encoded by the MAPT gene (50). Under normal conditions tau is found as a monomer, but during Alzheimer's disease progression tau is dynamic and exists as soluble monomer, soluble oligomer, NFT, and other filamentous aggregation states (51-53). Interestingly, the levels of soluble tau monomers remain relatively equal between Alzheimer's disease and non-Alzheimer's disease patients while the total level of tau increases approximately 8-fold in Alzheimer's disease compared to non-Alzheimer's disease patients (54). Understanding tau aggregation states and normal function has been a major area of research and is essential to understanding why tau misbehaves during disease.

Little is known about tau secondary and tertiary structure because of its inherent flexibility (55,56). However, tau is known to contain three distinct domains: a microtubule-binding domain corresponding to amino acids 252-376 and two additional domains that flank this region (56-58). The first flanking domain is an N-terminal "projection domain," which extends away from microtubules and contains a proline-rich region upstream of the microtubule-binding domain (56-58). Finally, tau contains a short C-terminal tail flanking the downstream region of the microtubule binding region (57,58). Six isoforms of tau exist in the brain because of alternative splicing of exons 2, 3, and 10 of the 16 exons encoding the MAPT gene (See Figure 1.3). Tau isoforms can include exons 2 and 3, 2 only, or neither 2 nor 3. Since these

exons exist in the N-terminus (N), the combinations of exons 2 and 3 are referred to as 2N, 1N, or 0N depending on how tau is spliced (See Figure 1.3) (59-61). Exon 10 is one of 4 microtubule-binding repeats (R) that lie within the microtubule-binding domain of tau. Inclusion or exclusion of exon 10 results in either 4 repeats (4R) or 3 repeats (3R), respectively (59-61). Thus, the nomenclature 4R1N indicates a tau splice variant that contains exon 2 and exon 10, but not exon 3 (See Figure 3). Both 4R and 3R tau isoforms are spliced at approximately a 1:1 ratio and are found predominately in the central nervous system within axonal/somatic regions of neurons (59,62). The main function of tau was first described as a microtubule binding protein, which stabilizes microtubules, and it was later shown that 4R tau has a higher affinity for microtubules than 3R tau (50,63,64). This was the first result suggesting that there may be physiological and functional differences between isoforms. Since then, tau has been shown to have a diverse set of functions within neurons and glia (50,62,65-68).

There is a growing body of evidence supporting the interaction of tau with the actin cytoskeleton, which is mediated by the microtubule binding domain and proline-rich region of tau (See Table 1.1) (69-71). In addition to the interaction with cytoskeletal components, tau has been implicated in axonal transport, scaffolding, cell signaling, and apoptosis (50,62,65-68). Of these various functions, axonal transport and scaffolding have the most convincing evidence in support of their proposed function. There is an increasing gradient of tau bound to microtubules as the microtubules approach the axon terminal (66,67). Tau has been shown to regulate axonal transport by regulating the movement of kinesin along microtubules by causing kinesin to dissociate from microtubules when kinesin comes in contact with tau (66,67). The proline-rich region of tau has been shown to be a scaffold, which interacts with SH3-domain containing proteins such as the src kinase fyn (72-77). Tau-fyn complexes have been shown to travel to the

dendritic spines of neurons where the tau-fyn complex binds the scaffold protein PSD-95 (74,75). This trimeric complex then interacts with the NR2b subunit of NMDA receptors to initiate phosphorylation of the NMDA receptor resulting in an increase in receptor activity (62,78,79). These diverse roles of tau suggest its importance for neuronal survival. However, tau knockout mice are viable with no overt defects other than early delays in axonal development, which correct themselves with age (80,81). The absence of any obvious phenotype in tau knockout mice has been attributed to a putative redundancy between tau and other microtubule-associated proteins such as Map1A and Map2 (80,81). Consistent with this interpretation, MAP2 has been shown to associate with fyn (82). While it is undisputed that tau plays an important role in disease progression, the field is divided as to the cause. Some hypothesize that tau contributes to disease through loss of normal function while others support a gain of function of tau leading to promiscuous behavior (83).

In addition to its diverse range of functions within the cell, tau is subjected to extensive post-translational modification including acetylation, transglutamation, glycosylation, isomerization, nitration, sumoylation, phosphorylation, and ubiquitination (84-90). Of these modifications, phosphorylation has received the most attention. Tau contains ~30 serine and threonine residues that are subject to phosphorylation, which may regulate the many diverse functions of tau (42,91-93). In addition, there have been many kinases implicated in tau phosphorylation including PKA, GSK3β, Cdk5, SGK, Fyn, p70S6K, MARK, and SADK, but caution should be taken as some of these kinases have only been reported to modify tau *in vitro* using non-physiologically relevant concentrations of protein (42,91-93). Of these putative kinases, GSK-3β has the most compelling evidence as being a predominant tau kinase during disease progression (discussed in more depth below; See Links From APP to Tau) (42,91-95).

Under normal physiological conditions tau contains ~2 moles of phosphate per mole of tau; however, during Alzheimer's disease progression phosphate levels increase to ~8 moles per mole (51). This drastic increase in phosphate levels is referred to as hyperphosphorylation. The major consequence of hyperphosphorylation of tau is the induction of tau aggregation into NFTs. *In vitro* tau will not self-aggregate without the assistance of some inducing agent such as heparin (96-102). The flexible N-terminal and C-terminal domains normally prevent tau from aggregating to form NFTs. However, hyperphosphorylation of tau neutralizes this inhibition process (97,103,104).

In order for NFTs to form, the interaction between tau and microtubules must be abolished. Normally, the net positive charge of the microtubule-binding domain helps tau bind to negatively charged tubulin (105-107). Hyperphosphorylation of tau results in the neutralization of the microtubule-binding domain dissociating tau from microtubules (105-107). Indeed, multiple phospho-tau-specific antibodies have been shown to label NFTs, supporting this modification as a prerequisite in the pathway of NFT formation (103,104,108-113). After hyperphosphorylation, small aggregates of tau have been shown to sequester and misfold non-pathogenic tau as well as other MAPs such as MAP1 and MAP2 (111,113,114). Furthermore, removal of phosphates from purified NFTs *in vitro* by addition of phosphatase can drive disassembly of aggregated tau (115,116). Hyperphosphorylation was also found to protect tau from protease cleavage and degradation, which helps explain why total levels of tau are increased in Alzheimer's disease (116,117). Taken together, these and other results support the hypothesis that phosphorylation of tau drives tau aggregation.

FTLD-TAU:

Frontotemporal lobar degeneration (FTLD) is a term used to describe a heterogeneous group of non-Alzheimer's neurodegenerative conditions clinically characterized by motor dysfunction and distinct behavioral changes (118,119). FTLD can be further broken down into disease classes based on familial mutations in one of four genes including tau. FTLD-tau results in the formation of NFTs in the absence of overt amyloid pathology and is the second most prevalent cause of dementia after Alzheimer's disease (118-120). Diseases classified as FTLD-tau include familial supranuclear palsy, corticobasal degeneration, Picks disease, Argyrophilic grain disease, multi-system atrophy with globular inclusions, and frontotemporal dementia with Parkinsonism linked to chromosome 17 (FTDP-17) (121). These different diseases are differentiated from one another by the types of behavioral changes that patients develop as well as the characterization of the NFT pathology and any secondary pathology (122). The majority of these behavioral changes fall into either semantic dementia (SD) or progressive non-fluent aphasia (PNFA). SD is characterized by fluent speech and correct syntax, but difficulty with word comprehension, whereas patients with PNFA maintain a greater word comprehension ability, but experience difficulty speaking fluently, use short sentences, and frequently stutter (123-127).

At least 45 mutations in tau have been identified, 39 of which are coding mutations further split into deletions or non-synonymous mutations mainly occurring in exons within the microtubule binding domain (128-130). The remaining 7 mutations occur within or adjacent to introns flanking exon 10 (within the tau microtubule binding domain) thereby impacting tau splicing (128). Interestingly, the same mutation in tau can lead to different FTLD-tau diseases even within the same family, though it is unclear how this occurs (131). Mutations in tau that

impact splicing shift the ratio of 3R to 4R tau in either direction (See Table 1.2) and result in NFTs containing only 3R or 4R isoforms (121).

Several tau mutants have been studied in great detail *in vitro* and *in vivo*. These mutations have been found to influence tau posttranslational modification, function, and pathology (See Table 1.2). FTLD-tau mutations do not appear to significantly alter the flexible secondary structure of tau (98,132,133). While wild-type tau requires an inducer for *in vitro* aggregation, tau mutants show a greater propensity to self-aggregate (96-102). Tau mutations also increase hyperphosphorylation of tau, which detaches tau from microtubules and increases susceptibility to aggregation *in vivo* (111,134,135). Mutations in the tau microtubule binding domain, but not other regions of tau, have also been shown to cause deficits in microtubule stability and axonal transport (66,67,98,136-140). Furthermore, these mutations can reduce the ability of tau to interact with binding partners such as fyn and JIP1 and shift the distribution of tau from axonal/somatic to dendritic compartments (62,74-76,135).

There have been several mutant tau mouse models of FTLD. Reactive astrocytes and microglia appear to be an early phenotype of many of these models and all develop some variety of memory impairment and/or motor dysfunction (141-148). One such mutant mouse (P301L tau) has been extensively studied (110,149-154). Comparisons of mice expressing human 4R wild type or P301L tau driven by CamKIIa or Thy1 promoters revealed interesting results. Wild -type tau-expressing mice had no NFTs and showed cognitive decline earlier than P301L mice. This earlier cognitive decline quickly plateaus. However, P301L mice take longer to show deficits, but ultimately have much more severe memory impairments following hyperphosphorylation of tau and NFT formation (155-160). Another group showed that cognitive decline in an inducible expression P301L mouse correlates with soluble tau better than

with NFTs. Furthermore, this study showed that turning off tau expression reversed cognitive decline and reduced levels of soluble tau, but had no impact on NFT burden (161). This led to the first hypothesis that hyperphosphorylated oligomeric aggregates of tau and not NFTs may underlie the neurodegenerative properties of tau. Later, another group performed *in vivo* microscopy on live P301L tau transgenic mice. Using the vasculature of the brain, they created road maps in order to study the same neurons over an extended time course lasting weeks. They found that at any given time, a small fraction of neurons developed NFTs. However, these tangle-bearing neurons never succumbed to cell death, while those that did not form tangles died (108). This study both supports the hypothesis that oligomeric aggregates are toxic but also suggests that NFT formation might be protective.

LINKS FROM APP TO TAU:

There are two putative links between APP and tau involved during disease progression, involving either Aβ or AICD/C31. Many studies have focused on Aβ to tau signaling because of the involvement of Aβ in the development of Alzheimer's disease pathology. Initial studies showed that adding amyloid beta to cells in culture increases levels of GSK3β (162-165). Since GSK3β is one of the predominant tau kinases, it led researchers to hypothesize that Aβ may promote an increase in tau phosphorylation. Indeed, addition of Aβ to neuronal cultures resulted in increases in site-specific phosphorylation of tau (166). Furthermore, injecting Aβ into the brain of a P301L tau mutant mouse exacerbated tau hyperphosphorylation and NFT formation as much as 5-fold (150). Researchers also began to investigate whether tau was required for Aβ-induced cell death. One group independently incubated Aβ with primary neurons isolated from control and tau knockout mice. They found that only neurons with endogenous tau were

susceptible to Aβ-induced neuron loss while those from tau knockouts remained largely unharmed (167). These results prompted studies using *in vivo* models. Alzheimer's disease model mice expressing mutant APP transgenes are susceptible to excitotoxic seizures, but the same transgene in a tau knockout background reduces seizure severity and frequency (62,168). Despite the attempts to tease out the signaling events between Aβ and tau, it is unclear what pathways are involved.

More recently, some researchers have shifted their attention from Aβ to AICD as a potential link of APP to tau. Aβ addition to APP knockout cells failed to induce cell death (169). Later studies proposed that APP can dimerize with Aβ and that this event is important for Aβ-induced cell death (170,171). Furthermore, it was later shown that APP dimerization promotes production of c-terminal fragments of APP (45,172). These studies may indicate that Aβ signals to tau through production of AICD/C31. AICD/C31 has been shown to upregulate the activity of GSK3β as well as increase GSK3β protein levels (42,173). One major limitation of Alzheimer's disease model mice is the inability of mutant APP or PSEN transgene expression to induce tau pathology without the co-expression of a mutant tau transgene (174-179). A model mouse expressing an AICD transgene resulted in both cognitive decline and neuron loss despite the absence of Aβ (48,173,180). Unlike any other Alzheimer's disease model mice, this AICD transgenic model induced hyperphosphorylation of endogenous tau as well as production of insoluble tau species without the expression of a mutant tau transgene (48,173,180). Administration of a GSK3β inhibitor reversed many of these symptoms (48). In the future it would be interesting to investigate the relationship between AICD and tau in disease progression.

HIRANO BODIES AND MODEL SYSTEMS OF HIRANO BODIES:

Hirano bodies were first discovered as refractive rod-shaped pathological inclusions found in brains from human patients with amyotrophic lateral sclerosis and Parkinsonism-type dementia (181). Hirano bodies were later reported in patients with Alzheimer's disease or Pick's disease and have since been found associated with an even wider array of conditions and tissues (See Table 1.3) (181-186). These inclusions are rarely seen in neural axons and appear more frequently in brains containing more NFTs (182,187,188). Ultrastructural analysis of these inclusions revealed regularly spaced fibrils that are 6-10 nm in diameter with differential appearance of filament positioning depending on the plane of section (187,189,190). These structures are comprised of bundles of filamentous actin (F-actin) and actin-interacting proteins (See Table 1.4) (191,192). Since their discovery, much of what is known about Hirano bodies has involved investigation of their structure, components (See Table 1.4), tissue and cell location (See Table 1.3), and conditions in which they are associated (Table 1.3). Because of a lack of a model system, early studies were limited to post-mortem tissue from autopsy and necropsy. Despite decades of work, it is still unclear what the physiological roles of Hirano bodies are or how Hirano bodies impact disease progression. More recently, studies investigating properties of the 34 kDa actin binding protein have led to the creation of a model system to study Hirano bodies (193-195).

The 34 kDa actin-binding protein is a calcium-sensitive actin-bundling protein first discovered in *Dictyostelium* (196-200). After its initial discovery, truncation mutants of 34 kDa protein were generated to determine which regions of the protein were important for actin binding (193). One such c-terminal truncation named CT (containing amino acids 124-295) showed a gain of function in F-actin binding compared to the full-length wild-type protein (193).

Unlike wild-type 34 kDa actin-bundling protein, CT is calcium-insensitive, and its activated binding is believed to arise from the removal of an inhibitory domain in the N-terminus of the protein (193,194). When CT was expressed in *Dictyostelium,* it resulted in the formation of large intracellular actin-rich aggregates. Furthermore, it was shown that CT expression did not affect total actin levels and instead induced a redistribution in the ratio of globular actin to F-actin (195). These actin aggregates only moderately slow *Dictyostelium* growth and development and were not detrimental to cell survival (195). Ultrastructural analysis of CT-induced actin-rich deposits revealed highly ordered F-actin filaments identical to those in Hirano bodies found in human tissue (195). CT expression in mammalian cell lines as well as primary neurons also result in formation of model Hirano bodies. These cells experience no growth or migration phenotypes (201). Model Hirano bodies formed in these cells contain many of the same protein components as Hirano bodies formed in humans (See Table 1.5) as well as the same ultrastructure and filament spacing (195,201,202). Since model Hirano bodies were sometimes seen within membrane bound compartments and model Hirano body size is limited, it was hypothesized that they may be turned-over through autophagy (188). Later, autophagy mutant strains of *Dictyostelium* and proteasome inhibitors were used to show that model Hirano bodies are degraded through both autophagy and proteasome pathways (203). Since AICD was reported to colocalize with Hirano bodies in human Alzheimer's disease patients, the impact of model Hirano bodies on AICD was investigated in cell culture (204). Both AICD and Fe65 were found to colocalize with model Hirano bodies. Normally AICD is found largely colocalized to the nucleus, where it plays a role in transcription (35). Interestingly, model Hirano bodies drastically reduce AICD nuclear localization. In addition, model Hirano bodies were found to

mitigate AICD-induced cell death and AICD-induced transcription (202). These results implicate a potential protective role of Hirano bodies.

In order to investigate the physiological role of Hirano bodies, a mouse with brain-specific expression of CT-GFP was generated. Mice develop rod-shaped eosinophilic inclusions in the CA3 region of the hippocampus at 6 months of age. Furthermore, these inclusions contain an identical ultrastructure to authentic Hirano bodies (205,206). These inclusions do not damage neurons or impact long-term plasticity. However, expression of CT-GFP and formation of model Hirano bodies were found to induce deficits in short-term plasticity as measured by a paired-pulse stimulus protocol (206). While control mice showed a strong paired-pulse facilitation, CT-GFP expressing mice showed paired-pulse depression (206). These results suggest that CT-GFP expression and model Hirano body formation may be detrimental. While this model mouse gives important insight, model Hirano bodies did not form in the CA1 region of the hippocampus where Hirano bodies are normally found in human patients (187,188). It will be important to generate a more physiologically relevant mouse model to study the function of Hirano bodies.

REFERENCES:

1. Hardy, J. (2006) A hundred years of Alzheimer's disease research. *Neuron* **52**, 3-13
2. Eidenmüller, J., Fath, T., Maas, T., Pool, M., Sontag, E., and Brandt, R. (2001) Phosphorylation-mimicking glutamate clusters in the proline-rich region are sufficient to simulate the functional deficiencies of hyperphosphorylated tau protein. *Biochem. J.* **357**, 759-767
3. Fath, T., Eldenmüller, J., and Brandt, R. (2002) Tau-mediated cytotoxicity in a pseudohyperphosphorylation model of Alzheimer's disease. *J. Neurosci* **22**, 9733-9741
4. Maulik, M., Westaway, D., Jhamandas, J. H., and Kar, S. (2013) Role of cholesterol in APP metabolism and its significance in Alzheimer's disease pathogenesis. *Molecular neurobiology* **47**, 37-63
5. Haass, C., Kaether, C., Thinakaran, G., and Sisodia, S. (2012) Trafficking and proteolytic processing of APP. *Cold Spring Harbor perspectives in medicine* **2**, a006270
6. Ball, M. J. (1977) Neuronal loss, neurofibrillary tangles and granulovacuolar degeneration in the hippocampus with ageing and dementia. A quantitative study. *Acta Neuropathol* **37**, 111-118
7. Kang, J., Lemaire, H. G., Unterbeck, A., Salbaum, J. M., Masters, C. L., Grzeschik, K. H., Multhaup, G., Beyreuther, K., and Muller-Hill, B. (1987) The precursor of Alzheimer's disease amyloid A4 protein resembles a cell-surface receptor. *Nature* **325**, 733-736
8. Tanaka, S., Shiojiri, S., Takahashi, Y., Kitaguchi, N., Ito, H., Kameyama, M., Kimura, J., Nakamura, S., and Ueda, K. (1989) Tissue-specific expression of three types of beta-protein precursor mRNA: enhancement of protease inhibitor-harboring types in

Alzheimer's disease brain. *Biochemical and biophysical research communications* **165**, 1406-1414

9. Moir, R. D., Lynch, T., Bush, A. I., Whyte, S., Henry, A., Portbury, S., Multhaup, G., Small, D. H., Tanzi, R. E., Beyreuther, K., and Masters, C. L. (1998) Relative increase in Alzheimer's disease of soluble forms of cerebral Abeta amyloid protein precursor containing the Kunitz protease inhibitory domain. *J Biol Chem* **273**, 5013-5019
10. Jacobsen, K. T., and Iverfeldt, K. (2009) Amyloid precursor protein and its homologues: a family of proteolysis-dependent receptors. *Cellular and molecular life sciences : CMLS* **66**, 2299-2318
11. Niederwolfsgruber, E., Schmitt, T. L., Blasko, I., Trieb, K., Steger, M. M., Maczek, C., Hager, J., Bobak, K., Steiner, E., and Grubeck-Loebenstein, B. (1998) The production of the Alzheimer amyloid precursor protein (APP) in extraneuronal tissue does not increase in old age. *The journals of gerontology. Series A, Biological sciences and medical sciences* **53**, B186-190
12. Nalivaeva, N. N., and Turner, A. J. (2013) The amyloid precursor protein: a biochemical enigma in brain development, function and disease. *FEBS letters* **587**, 2046-2054
13. Hoe, H. S., Lee, H. K., and Pak, D. T. (2012) The upside of APP at synapses. *CNS neuroscience & therapeutics* **18**, 47-56
14. Zheng, H., Jiang, M., Trumbauer, M. E., Hopkins, R., Sirinathsinghji, D. J., Stevens, K. A., Conner, M. W., Slunt, H. H., Sisodia, S. S., Chen, H. Y., and Van der Ploeg, L. H. (1996) Mice deficient for the amyloid precursor protein gene. *Annals of the New York Academy of Sciences* **777**, 421-426

15. von Koch, C. S., Zheng, H., Chen, H., Trumbauer, M., Thinakaran, G., van der Ploeg, L. H., Price, D. L., and Sisodia, S. S. (1997) Generation of APLP2 KO mice and early postnatal lethality in APLP2/APP double KO mice. *Neurobiol Aging* **18**, 661-669

16. Nikaido, T., Austin, J., Trueb, L., Hutchison, J., Rinehart, R., Stuckenbrok, H., and Miles, B. (1970) Isolation and preliminary characterization of Alzheimer plaques from presenile and senile dementia. *Trans Am Neurol Assoc* **95**, 47-50

17. Evin, G., and Weidemann, A. (2002) Biogenesis and metabolism of Alzheimer's disease Abeta amyloid peptides. *Peptides* **23**, 1285-1297

18. Mucke, L., Masliah, E., Yu, G.-Q., Mallory, M., Rockenstein, E. M., Tatsuno, G., Hu, K., Kholodenko, D., Johnson-Wood, K., and McConlogue, L. (2000) High-level neuronal expression of Abeta $_{1-42}$ in wild type human amyloid protein precursor transgenic mice: synaptotoxicity without plaque formation. *J. Neurosci* **20**, 4050-4058

19. Oddo, S., and LaFerla, F. M. (2006) The role of nicotinic acetylcholine receptors in Alzheimer's disease. *Journal of physiology, Paris* **99**, 172-179

20. Thinakaran, G., and Koo, E. H. (2008) APP Trafficking, Processing, and Function. *J. Biol. Chem.* **epub,** http://www.jbc.org/cgi/doi/10.1074/jbc.R800019200

21. Johnson-Wood, K., Lee, M., Motter, R., Gordon, G., Barbour, R., Khan, K., Gordon, M., Tan, H., Games, D., Lieberburg, I., Schenk, D., Seubert, P., and McConlogue, L. (1997) Amyloid precursor protein processing and Aβ42 deposition in a transgenic mouse model of Alzheimer disease. *Proc. Natl. Acad. Sci. USA* **94**, 1550-1555

22. Hilbich, C., Kisters-Woike, B., Reed, J., Masters, C. L., and Beyreuther, K. (1991) Aggregation and secondary structure of synthetic amyloid beta A4 peptides of Alzheimer's disease. *Journal of molecular biology* **218**, 149-163

23. Soreghan, B., Kosmoski, J., and Glabe, C. (1994) Surfactant properties of Alzheimer's A beta peptides and the mechanism of amyloid aggregation. *J Biol Chem* **269**, 28551-28554

24. Morelli, L., Prat, M. I., and Castano, E. M. (1999) Differential accumulation of soluble amyloid beta peptides 1-40 and 1-42 in human monocytic and neuroblastoma cell lines. Implications for cerebral amyloidogenesis. *Cell and tissue research* **298**, 225-232

25. Piaceri, I., Nacmias, B., and Sorbi, S. (2013) Genetics of familial and sporadic Alzheimer's disease. *Frontiers in bioscience* **5**, 167-177

26. Park, H. J., Shabashvili, D., Nekorchuk, M. D., Shyqyriu, E., Jung, J. I., Ladd, T. B., Moore, B. D., Felsenstein, K. M., Golde, T. E., and Kim, S. H. (2012) Retention in endoplasmic reticulum 1 (RER1) modulates amyloid-beta (Abeta) production by altering trafficking of gamma-secretase and amyloid precursor protein (APP). *J Biol Chem* **287**, 40629-40640

27. Prabhu, Y., Burgos, P. V., Schindler, C., Farias, G. G., Magadan, J. G., and Bonifacino, J. S. (2012) Adaptor protein 2-mediated endocytosis of the beta-secretase BACE1 is dispensable for amyloid precursor protein processing. *Molecular biology of the cell* **23**, 2339-2351

28. Kimberly, W. T., Zheng, J. B., Guenette, S. Y., and Selkoe, D. J. (2001) The intracellular domain of the beta-amyloid precursor protein is stabilized by Fe65 and translocates to the nucleus in a notch-like manner. *J. Biol. Chem.* **276**, 40288-40292

29. Weidemann, A., Paliga, K., Durrwang, U., Reinhard, F. B., Schuckert, O., Evin, G., and Masters, C. L. (1999) Proteolytic processing of the Alzheimer's disease amyloid precursor protein within its cytoplasmic domain by caspase-like proteases. *J Biol Chem* **274**, 5823-5829

30. Gervais, F. G., Xu, D., Robertson, G. S., Vaillancourt, J. P., Zhu, Y., Huang, J., LeBlanc, A., Smith, D., Rigby, M., Shearman, M. S., Clarke, E. E., Zheng, H., Van Der Ploeg, L., Ruffolo, S. C., Thornberry, N. A., Xanthoudakis, S., Zamboni, R. J., Roy, S., and Nicholson, D. W. (1999) Involvement of Caspases in Proteolytic Cleavage of Alzheimer's Amyloid-β Precursor Protein and Amyloidogenic Aβ peptide Foramtion. *Cell* **97**, 395-406

31. Barnes, N. Y., Li, L., Yoshikawa, K., Schwartz, L. M., Oppenheim, R. W., and Milligan, C. E. (1998) Increased production of amyloid precursor protein provides a substrate for caspase-3 in dying motoneurons. *J Neurosci* **18**, 5869-5880

32. Pardossi-Piquard, R., and Checler, F. (2012) The physiology of the b-amyloid precursor protein intracellular domain AICD. *J. Neurochem.* **120 (Suppl. 1)**, 109-124

33. Minopoli, G., Gargiulo, A., Parisi, S., and Russo, T. (2012) Fe65 matters: new light on an old molecule. *IUBMB life* **64**, 936-942

34. Borg, J. P., Ooi, J., Levy, E., and Margolis, B. (1996) The phosphotyrosine interaction domains of X11 and FE65 bind to distinct sites on the YENPTY motif of amyloid precursor protein. *Molecular and cellular biology* **16**, 6229-6241

35. Cao, X., and Südhof, T. C. (2004) Dissection of amyloid-beta precursor protein-dependent transcriptional transactivation. *J. Biol. Chem.* **279**, 24601-14611

36. Cao, X., and Südhof, T. C. (2001) A transcriptionally active complex of APP with Fe65 and histone acetyltransferase Tip60. *Science* **293**, 115-120

37. Li, H., Wang, B., Wang, Z., Guo, Q., Tabuchi, K., Hammer, R. E., Sudhof, T. C., and Zheng, H. (2010) Soluble amyloid precursor protein (APP) regulates transthyretin and

Klotho gene expression without rescuing the essential function of APP. *Proc Natl Acad Sci U S A* **107**, 17362-17367

38. Ohkawara, T., Nagase, H., Koh, C. S., and Nakayama, K. (2011) The amyloid precursor protein intracellular domain alters gene expression and induces neuron-specific apoptosis. *Gene* **475**, 1-9

39. Aydin, D., Filippov, M. A., Tschape, J. A., Gretz, N., Prinz, M., Eils, R., Brors, B., and Muller, U. C. (2011) Comparative transcriptome profiling of amyloid precursor protein family members in the adult cortex. *BMC genomics* **12**, 160

40. von Rotz, R. C., Kohli, B. M., Bosset, J., Meier, M., Suzuki, T., Nitsch, R. M., and Konietzko, U. (2004) The APP intracellular domain forms nuclear multiprotein complexes and regulates the transcription of its own precursor. *Journal of cell science* **117**, 4435-4448

41. Muller, T., Concannon, C. G., Ward, M. W., Walsh, C. M., Tirniceriu, A. L., Tribl, F., Kogel, D., Prehn, J. H., and Egensperger, R. (2007) Modulation of gene expression and cytoskeletal dynamics by the amyloid precursor protein intracellular domain (AICD). *Molecular biology of the cell* **18**, 201-210

42. Kim, H.-S., Kim, E.-M., Lee, J.-P., Park, C. H., Kim, S., Seo, J.-H., Chang, K.-A., Yu, E., Jeong, S.-J., Chong, Y. H., and Suh, A. Y.-H. (2003) C-terminal fragments of amyloid precursor protein exert neurotoxicity by inducing glycogen synthase kinase-3b expression. *FASEB J.* **17**, 1951-1954

43. Alves da Costa, C., Sunyach, C., Pardossi-Piquard, R., Sevalle, J., Vincent, B., Boyer, N., Kawarai, T., Girardot, N., St George-Hyslop, P., and Checler, F. (2006) Presenilin-

dependent gamma-secretase-mediated control of p53-associated cell death in Alzheimer's disease. *J. Neurosci* **26**, 6377-6385

44. Ozaki, T., Li, Y., Kikuchi, H., Tomita, T., Iwatsubo, T., and Nakagawara, A. (2006) The intracellular domain of the amyloid precursor protein (AICD) enhances the p53-mediated apoptosis. *Biochemical and biophysical research communications* **351**, 57-63

45. Lu, D. C., Rabizadeh, S., Chandra, S., Shayya, R. F., Ellerby, L. M., Ye, X., Salvesen, G. S., Koo, E. H., and Bredesen, D. E. (2000) A second cytotoxic proteolytic peptide derived from amyloid B-protein precursor. *Nat Med* **6**, 397-404

46. Lu, D. C., Soriano, S., Bredesen, D. E., and Koo, E. H. (2003) Caspase cleavage of the amyloid precursor protein modulates amyloid beta-protein toxicity. *J. Neurochem.* **87**, 733-741

47. Kinoshita, A., Whelan, C. M., Berezovska, O., and Hyman, B. T. (2002) The gamma secretase-generated carboxyl-terminal domain of the amyloid precursor protein induces apoptosis via Tip60 in H4 cells. *J. Biol. Chem.* **277**, 28530-28536

48. Ghosal, K., Vogt, D. L., Liang, M., Shen, Y., Lamb, B. T., and Pimplikar, S. W. (2009) Alzheimer's disease-like pathological features in transgenic mice expressing the APP intracellular domain. *Proc Natl Acad Sci U S A* **106**, 18367-18372

49. Nakayama, K., Ohkawara, T., Hiratochi, M., Koh, C. S., and Nagase, H. (2008) The intracellular domain of amyloid precursor protein induces neuron-specific apoptosis. *Neurosci Lett* **444**, 127-131

50. Weingarten, M. D., Lockwood, A. H., Hwo, S. Y., and Kirschner, M. W. (1975) A protein factor essential for microtubule assembly. *Proc Natl Acad Sci U S A* **72**, 1858-1862

51. Kopke, E., Tung, Y. C., Shaikh, S., Alonso, A. C., Iqbal, K., and Grundke-Iqbal, I. (1993) Microtubule-associated protein tau. Abnormal phosphorylation of a non-paired helical filament pool in Alzheimer disease. *J Biol Chem* **268**, 24374-24384

52. Grundke-Iqbal, I., Iqbal, K., Quinlan, M., Tung, Y. C., Zaidi, M. S., and Wisniewski, H. M. (1986) Microtubule-associated protein tau. A component of Alzheimer paired helical filaments. *J Biol Chem* **261**, 6084-6089

53. Bancher, C., Brunner, C., Lassmann, H., Budka, H., Jellinger, K., Seitelberger, F., Grundke-Iqbal, I., Iqbal, K., and Wisniewski, H. M. (1989) Tau and ubiquitin immunoreactivity at different stages of formation of Alzheimer neurofibrillary tangles. *Prog Clin Biol Res* **317**, 837-848

54. Khatoon, S., Grundke-Iqbal, I., and Iqbal, K. (1992) Brain levels of microtubule-associated protein tau are elevated in Alzheimer's disease: a radioimmuno-slot-blot assay for nanograms of the protein. *J Neurochem* **59**, 750-753

55. Wille, H., Drewes, G., Biernat, J., Mandelkow, E. M., and Mandelkow, E. (1992) Alzheimer-like paired helical filaments and antiparallel dimers formed from microtubule-associated protein tau in vitro. *The Journal of cell biology* **118**, 573-584

56. Schweers, O., Schonbrunn-Hanebeck, E., Marx, A., and Mandelkow, E. (1994) Structural studies of tau protein and Alzheimer paired helical filaments show no evidence for beta-structure. *J Biol Chem* **269**, 24290-24297

57. Hirokawa, N., Shiomura, Y., and Okabe, S. (1988) Tau proteins: the molecular structure and mode of binding on microtubules. *The Journal of cell biology* **107**, 1449-1459

58. Steiner, B., Mandelkow, E. M., Biernat, J., Gustke, N., Meyer, H. E., Schmidt, B., Mieskes, G., Soling, H. D., Drechsel, D., Kirschner, M. W., and et al. (1990)

Phosphorylation of microtubule-associated protein tau: identification of the site for Ca2(+)-calmodulin dependent kinase and relationship with tau phosphorylation in Alzheimer tangles. *The EMBO journal* **9**, 3539-3544

59. Lee, G., Cowan, N., and Kirschner, M. (1988) The primary structure and heterogeneity of tau protein from mouse brain. *Science* **239**, 285-288

60. Goedert, M., Wischik, C. M., Crowther, R. A., Walker, J. E., and Klug, A. (1988) Cloning and sequencing of the cDNA encoding a core protein of the paired helical filament of Alzheimer disease: identification as the microtubule-associated protein tau. *Proc Natl Acad Sci U S A* **85**, 4051-4055

61. Himmler, A., Drechsel, D., Kirschner, M. W., and Martin, D. W., Jr. (1989) Tau consists of a set of proteins with repeated C-terminal microtubule-binding domains and variable N-terminal domains. *Molecular and cellular biology* **9**, 1381-1388

62. Ittner, L. M., Ke, Y. D., Delerue, F., Bi, M., Gladbach, A., van Eersel, J., Wolfing, H., Chieng, B. C., Christie, M. J., Napier, I. A., Eckert, A., Staufenbiel, M., Hardeman, E., and Gotz, J. (2010) Dendritic function of tau mediates amyloid-beta toxicity in Alzheimer's disease mouse models. *Cell* **142**, 387-397

63. Goode, B. L., Chau, M., Denis, P. E., and Feinstein, S. C. (2000) Structural and functional differences between 3-repeat and 4-repeat tau isoforms. Implications for normal tau function and the onset of neurodegenetative disease. *J Biol Chem* **275**, 38182-38189

64. Lu, M., and Kosik, K. S. (2001) Competition for microtubule-binding with dual expression of tau missense and splice isoforms. *Molecular biology of the cell* **12**, 171-184

65. Wang, J. Z., and Liu, F. (2008) Microtubule-associated protein tau in development, degeneration and protection of neurons. *Progress in neurobiology* **85**, 148-175

66. Dixit, R., Ross, J. L., Goldman, Y. E., and Holzbaur, E. L. (2008) Differential regulation of dynein and kinesin motor proteins by tau. *Science* **319**, 1086-1089

67. Trinczek, B., Ebneth, A., Mandelkow, E. M., and Mandelkow, E. (1999) Tau regulates the attachment/detachment but not the speed of motors in microtubule-dependent transport of single vesicles and organelles. *Journal of cell science* **112 (Pt 14)**, 2355-2367

68. Brandt, R., Leger, J., and Lee, G. (1995) Interaction of tau with the neural plasma membrane mediated by tau's amino-terminal projection domain. *The Journal of cell biology* **131**, 1327-1340

69. Farias, G. A., Munoz, J. P., Garrido, J., and Maccioni, R. B. (2002) Tubulin, actin, and tau protein interactions and the study of their macromolecular assemblies. *Journal of cellular biochemistry* **85**, 315-324

70. Yu, J. Z., and Rasenick, M. M. (2006) Tau associates with actin in differentiating PC12 cells. *FASEB J* **20**, 1452-1461

71. He, H. J., Wang, X. S., Pan, R., Wang, D. L., Liu, M. N., and He, R. Q. (2009) The proline-rich domain of tau plays a role in interactions with actin. *BMC cell biology* **10**, 81

72. Reynolds, C. H., Garwood, C. J., Wray, S., Price, C., Kellie, S., Perera, T., Zvelebil, M., Yang, A., Sheppard, P. W., Varndell, I. M., Hanger, D. P., and Anderton, B. H. (2008) Phosphorylation regulates tau interactions with Src homology 3 domains of phosphatidylinositol 3-kinase, phospholipase Cgamma1, Grb2, and Src family kinases. *J Biol Chem* **283**, 18177-18186

73. Liu, Y., Lv, K., Li, Z., Yu, A. C., Chen, J., and Teng, J. (2012) PACSIN1, a Tau-interacting protein, regulates axonal elongation and branching by facilitating microtubule instability. *J Biol Chem* **287**, 39911-39924

74. Lee, G., Newman, S. T., Gard, D. L., Band, H., and Panchamoorthy, G. (1998) Tau interacts with src-family non-receptor tyrosine kinases. *Journal of cell science* **111 (Pt 21)**, 3167-3177

75. Bhaskar, K., Yen, S. H., and Lee, G. (2005) Disease-related modifications in tau affect the interaction between Fyn and Tau. *J Biol Chem* **280**, 35119-35125

76. Ittner, L. M., Ke, Y. D., and Gotz, J. (2009) Phosphorylated Tau interacts with c-Jun N-terminal kinase-interacting protein 1 (JIP1) in Alzheimer disease. *J Biol Chem* **284**, 20909-20916

77. Barbato, C., Canu, N., Zambrano, N., Serafino, A., Minopoli, G., Ciotti, M. T., Amadoro, G., Russo, T., and Calissano, P. (2005) Interaction of Tau with Fe65 links tau to APP. *Neurobiology of disease* **18**, 399-408

78. Mondragon-Rodriguez, S., Trillaud-Doppia, E., Dudilot, A., Bourgeois, C., Lauzon, M., Leclerc, N., and Boehm, J. (2012) Interaction of endogenous tau protein with synaptic proteins is regulated by N-methyl-D-aspartate receptor-dependent tau phosphorylation. *J Biol Chem* **287**, 32040-32053

79. Belkadi, A., and LoPresti, P. (2008) Truncated Tau with the Fyn-binding domain and without the microtubule-binding domain hinders the myelinating capacity of an oligodendrocyte cell line. *J Neurochem* **107**, 351-360

80. Harada, A., Oguchi, K., Okabe, S., Kuno, J., Terada, S., Ohshima, T., Sato-Yoshitake, R., Takei, Y., Noda, T., and Hirokawa, N. (1994) Altered microtubule organization in small-calibre axons of mice lacking tau protein. *Nature* **369**, 488-491

81. Dawson, H. N., Ferreira, A., Eyster, M. V., Ghoshal, N., Binder, L. I., and Vitek, M. P. (2001) Inhibition of neuronal maturation in primary hippocampal neurons from tau deficient mice. *Journal of cell science* **114**, 1179-1187

82. Lim, R. W., and Halpain, S. (2000) Regulated association of microtubule-associated protein 2 (MAP2) with Src and Grb2: evidence for MAP2 as a scaffolding protein. *J Biol Chem* **275**, 20578-20587

83. Trojanowski, J. Q., and Lee, V. M. (2005) Pathological tau: a loss of normal function or a gain in toxicity? *Nature neuroscience* **8**, 1136-1137

84. Arnold, C. S., Johnson, G. V., Cole, R. N., Dong, D. L., Lee, M., and Hart, G. W. (1996) The microtubule-associated protein tau is extensively modified with O-linked N-acetylglucosamine. *J Biol Chem* **271**, 28741-28744

85. Cripps, D., Thomas, S. N., Jeng, Y., Yang, F., Davies, P., and Yang, A. J. (2006) Alzheimer disease-specific conformation of hyperphosphorylated paired helical filament-Tau is polyubiquitinated through Lys-48, Lys-11, and Lys-6 ubiquitin conjugation. *J Biol Chem* **281**, 10825-10838

86. Dorval, V., and Fraser, P. E. (2006) Small ubiquitin-like modifier (SUMO) modification of natively unfolded proteins tau and alpha-synuclein. *J Biol Chem* **281**, 9919-9924

87. Reyes, J. F., Reynolds, M. R., Horowitz, P. M., Fu, Y., Guillozet-Bongaarts, A. L., Berry, R., and Binder, L. I. (2008) A possible link between astrocyte activation and tau nitration in Alzheimer's disease. *Neurobiology of disease* **31**, 198-208

88. Miyasaka, T., Watanabe, A., Saito, Y., Murayama, S., Mann, D. M., Yamazaki, M., Ravid, R., Morishima-Kawashima, M., Nagashima, K., and Ihara, Y. (2005) Visualization of newly deposited tau in neurofibrillary tangles and neuropil threads. *J Neuropathol Exp Neurol* **64**, 665-674

89. Cohen, T. J., Guo, J. L., Hurtado, D. E., Kwong, L. K., Mills, I. P., Trojanowski, J. Q., and Lee, V. M. (2011) The acetylation of tau inhibits its function and promotes pathological tau aggregation. *Nat Commun* **2**, 252

90. Min, S. W., Cho, S. H., Zhou, Y., Schroeder, S., Haroutunian, V., Seeley, W. W., Huang, E. J., Shen, Y., Masliah, E., Mukherjee, C., Meyers, D., Cole, P. A., Ott, M., and Gan, L. (2010) Acetylation of tau inhibits its degradation and contributes to tauopathy. *Neuron* **67**, 953-966

91. Baumann, K., Mandelkow, E. M., Biernat, J., Piwnica-Worms, H., and Mandelkow, E. (1993) Abnormal Alzheimer-like phosphorylation of tau-protein by cyclin-dependent kinases cdk2 and cdk5. *FEBS letters* **336**, 417-424

92. Ishiguro, K., Shiratsuchi, A., Sato, S., Omori, A., Arioka, M., Kobayashi, S., Uchida, T., and Imahori, K. (1993) Glycogen synthase kinase 3 beta is identical to tau protein kinase I generating several epitopes of paired helical filaments. *FEBS letters* **325**, 167-172

93. Hosoi, T., Uchiyama, M., Okumura, E., Saito, T., Ishiguro, K., Uchida, T., Okuyama, A., Kishimoto, T., and Hisanaga, S. (1995) Evidence for cdk5 as a major activity phosphorylating tau protein in porcine brain extract. *Journal of biochemistry* **117**, 741-749

94. Hong, M., Chen, D. C., Klein, P. S., and Lee, V. M. (1997) Lithium reduces tau phosphorylation by inhibition of glycogen synthase kinase-3. *J Biol Chem* **272**, 25326-25332

95. Munoz-Montano, J. R., Moreno, F. J., Avila, J., and Diaz-Nido, J. (1997) Lithium inhibits Alzheimer's disease-like tau protein phosphorylation in neurons. *FEBS letters* **411**, 183-188

96. von Bergen, M., Barghorn, S., Muller, S. A., Pickhardt, M., Biernat, J., Mandelkow, E. M., Davies, P., Aebi, U., and Mandelkow, E. (2006) The core of tau-paired helical filaments studied by scanning transmission electron microscopy and limited proteolysis. *Biochemistry* **45**, 6446-6457

97. von Bergen, M., Barghorn, S., Jeganathan, S., Mandelkow, E. M., and Mandelkow, E. (2006) Spectroscopic approaches to the conformation of tau protein in solution and in paired helical filaments. *Neuro-degenerative diseases* **3**, 197-206

98. Barghorn, S., Zheng-Fischhofer, Q., Ackmann, M., Biernat, J., von Bergen, M., Mandelkow, E. M., and Mandelkow, E. (2000) Structure, microtubule interactions, and paired helical filament aggregation by tau mutants of frontotemporal dementias. *Biochemistry* **39**, 11714-11721

99. Wilson, D. M., and Binder, L. I. (1997) Free fatty acids stimulate the polymerization of tau and amyloid beta peptides. In vitro evidence for a common effector of pathogenesis in Alzheimer's disease. *The American journal of pathology* **150**, 2181-2195

100. Goedert, M., Jakes, R., Spillantini, M. G., Hasegawa, M., Smith, M. J., and Crowther, R. A. (1996) Assembly of microtubule-associated protein tau into Alzheimer-like filaments induced by sulphated glycosaminoglycans. *Nature* **383**, 550-553

101. Goedert, M. (1999) Filamentous nerve cell inclusions in neurodegenerative diseases: tauopathies and alpha-synucleinopathies. *Phil. Trans. Roy. Soc. Lond. B-Biol. Sci.* **354**, 1101-1118

102. Chang, E., and Kuret, J. (2008) Detection and quantification of tau aggregation using a membrane filter assay. *Analytical biochemistry* **373**, 330-336

103. Alonso, A., Zaidi, T., Novak, M., Grundke-Iqbal, I., and Iqbal, K. (2001) Hyperphosphorylation induces self-assembly of tau into tangles of paired helical filaments/straight filaments. *Proc Natl Acad Sci U S A* **98**, 6923-6928

104. Alonso, A. D., Zaidi, T., Novak, M., Barra, H. S., Grundke-Iqbal, I., and Iqbal, K. (2001) Interaction of tau isoforms with Alzheimer's disease abnormally hyperphosphorylated tau and in vitro phosphorylation into the disease-like protein. *J Biol Chem* **276**, 37967-37973

105. Jho, Y. S., Zhulina, E. B., Kim, M. W., and Pincus, P. A. (2010) Monte carlo simulations of tau proteins: effect of phosphorylation. *Biophysical journal* **99**, 2387-2397

106. Kar, S., Fan, J., Smith, M. J., Goedert, M., and Amos, L. A. (2003) Repeat motifs of tau bind to the insides of microtubules in the absence of taxol. *The EMBO journal* **22**, 70-77

107. Kar, S., Florence, G. J., Paterson, I., and Amos, L. A. (2003) Discodermolide interferes with the binding of tau protein to microtubules. *FEBS letters* **539**, 34-36

108. de Calignon, A., Fox, L. M., Pitstick, R., Carlson, G. A., Bacskai, B. J., Spires-Jones, T. L., and Hyman, B. T. (2010) Caspase activation precedes and leads to tangles. *Nature* **464**, 1201-1204

109. Augustinack, J. C., Schneider, A., Mandelkow, E. M., and Hyman, B. T. (2002) Specific tau phosphorylation sites correlate with severity of neuronal cytopathology in Alzheimer's disease. *Acta Neuropathol* **103**, 26-35

110. Noble, W., Olm, V., Takata, K., Casey, E., Mary, O., Meyerson, J., Gaynor, K., LaFrancois, J., Wang, L., Kondo, T., Davies, P., Burns, M., Veeranna, Nixon, R., Dickson, D., Matsuoka, Y., Ahlijanian, M., Lau, L. F., and Duff, K. (2003) Cdk5 is a key factor in tau aggregation and tangle formation in vivo. *Neuron* **38**, 555-565

111. Alonso, A. C., Grundke-Iqbal, I., and Iqbal, K. (1996) Alzheimer's disease hyperphosphorylated tau sequesters normal tau into tangles of filaments and disassembles microtubules. *Nat Med* **2**, 783-787

112. Alonso, A. D., Di Clerico, J., Li, B., Corbo, C. P., Alaniz, M. E., Grundke-Iqbal, I., and Iqbal, K. (2010) Phosphorylation of tau at Thr212, Thr231, and Ser262 combined causes neurodegeneration. *J Biol Chem* **285**, 30851-30860

113. Alonso, A. D., Grundke-Iqbal, I., Barra, H. S., and Iqbal, K. (1997) Abnormal phosphorylation of tau and the mechanism of Alzheimer neurofibrillary degeneration: sequestration of microtubule-associated proteins 1 and 2 and the disassembly of microtubules by the abnormal tau. *Proc Natl Acad Sci U S A* **94**, 298-303

114. Alonso, A. C., Li, B., Grundke-Iqbal, I., and Iqbal, K. (2008) Mechanism of tau-induced neurodegeneration in Alzheimer disease and related tauopathies. *Current Alzheimer research* **5**, 375-384

115. Gong, C. X., Shaikh, S., Wang, J. Z., Zaidi, T., Grundke-Iqbal, I., and Iqbal, K. (1995) Phosphatase activity toward abnormally phosphorylated tau: decrease in Alzheimer disease brain. *J Neurochem* **65**, 732-738

116. Wang, J. Z., Gong, C. X., Zaidi, T., Grundke-Iqbal, I., and Iqbal, K. (1995) Dephosphorylation of Alzheimer paired helical filaments by protein phosphatase-2A and -2B. *J Biol Chem* **270**, 4854-4860

117. Poppek, D., Keck, S., Ermak, G., Jung, T., Stolzing, A., Ullrich, O., Davies, K. J., and Grune, T. (2006) Phosphorylation inhibits turnover of the tau protein by the proteasome: influence of RCAN1 and oxidative stress. *The Biochemical journal* **400**, 511-520

118. Cairns, N. J., Bigio, E. H., Mackenzie, I. R., Neumann, M., Lee, V. M., Hatanpaa, K. J., White, C. L., 3rd, Schneider, J. A., Grinberg, L. T., Halliday, G., Duyckaerts, C., Lowe, J. S., Holm, I. E., Tolnay, M., Okamoto, K., Yokoo, H., Murayama, S., Woulfe, J., Munoz, D. G., Dickson, D. W., Ince, P. G., Trojanowski, J. Q., Mann, D. M., and Consortium for Frontotemporal Lobar, D. (2007) Neuropathologic diagnostic and nosologic criteria for frontotemporal lobar degeneration: consensus of the Consortium for Frontotemporal Lobar Degeneration. *Acta Neuropathol* **114**, 5-22

119. Mackenzie, I. R., Neumann, M., Bigio, E. H., Cairns, N. J., Alafuzoff, I., Kril, J., Kovacs, G. G., Ghetti, B., Halliday, G., Holm, I. E., Ince, P. G., Kamphorst, W., Revesz, T., Rozemuller, A. J., Kumar-Singh, S., Akiyama, H., Baborie, A., Spina, S., Dickson, D. W., Trojanowski, J. Q., and Mann, D. M. (2010) Nomenclature and nosology for neuropathologic subtypes of frontotemporal lobar degeneration: an update. *Acta Neuropathol* **119**, 1-4

120. Liscic, R. M., Grinberg, L. T., Zidar, J., Gitcho, M. A., and Cairns, N. J. (2008) ALS and FTLD: two faces of TDP-43 proteinopathy. *European journal of neurology : the official journal of the European Federation of Neurological Societies* **15**, 772-780

121. Rohan, Z., and Matej, R. (2014) Current concepts in the classification and diagnosis of frontotemporal lobar degenerations: a practical approach. *Archives of pathology & laboratory medicine* **138**, 132-138

122. McKhann, G. M., Albert, M. S., Grossman, M., Miller, B., Dickson, D., Trojanowski, J. Q., Work Group on Frontotemporal, D., and Pick's, D. (2001) Clinical and pathological diagnosis of frontotemporal dementia: report of the Work Group on Frontotemporal Dementia and Pick's Disease. *Archives of neurology* **58**, 1803-1809

123. Hodges, J. R., Martinos, M., Woollams, A. M., Patterson, K., and Adlam, A. L. (2008) Repeat and Point: differentiating semantic dementia from progressive non-fluent aphasia. *Cortex; a journal devoted to the study of the nervous system and behavior* **44**, 1265-1270

124. Hodges, J. R., and Patterson, K. (2007) Semantic dementia: a unique clinicopathological syndrome. *Lancet neurology* **6**, 1004-1014

125. Hodges, J. R., Patterson, K., Oxbury, S., and Funnell, E. (1992) Semantic dementia. Progressive fluent aphasia with temporal lobe atrophy. *Brain : a journal of neurology* **115 (Pt 6)**, 1783-1806

126. Turner, R. S., Kenyon, L. C., Trojanowski, J. Q., Gonatas, N., and Grossman, M. (1996) Clinical, neuroimaging, and pathologic features of progressive nonfluent aphasia. *Ann Neurol* **39**, 166-173

127. Grossman, M., Mickanin, J., Onishi, K., Hughes, E., D'Esposito, M., Ding, X. S., Alavi, A., and Reivich, M. (1996) Progressive Nonfluent Aphasia: Language, Cognitive, and PET Measures Contrasted with Probable Alzheimer's Disease. *Journal of cognitive neuroscience* **8**, 135-154

128. Goedert, M., Ghetti, B., and Spillantini, M. G. (2012) Frontotemporal dementia: implications for understanding Alzheimer disease. *Cold Spring Harbor perspectives in medicine* **2**, a006254

129. Rademakers, R., Cruts, M., and van Broeckhoven, C. (2004) The role of tau (MAPT) in frontotemporal dementia and related tauopathies. *Human mutation* **24**, 277-295

130. Ingram, E. M., and Spillantini, M. G. (2002) Tau gene mutations: dissecting the pathogenesis of FTDP-17. *Trends in molecular medicine* **8**, 555-562

131. Bugiani, O., Murrell, J. R., Giaccone, G., Hasegawa, M., Ghigo, G., Tabaton, M., Morbin, M., Primavera, A., Carella, F., Solaro, C., Grisoli, M., Savoiardo, M., Spillantini, M. G., Tagliavini, F., Goedert, M., and Ghetti, B. (1999) Frontotemporal dementia and corticobasal degeneration in a family with a P301S mutation in tau. *J Neuropathol Exp Neurol* **58**, 667-677

132. Gamblin, T. C., King, M. E., Dawson, H., Vitek, M. P., Kuret, J., Berry, R. W., and Binder, L. I. (2000) In vitro polymerization of tau protein monitored by laser light scattering: method and application to the study of FTDP-17 mutants. *Biochemistry* **39**, 6136-6144

133. von Bergen, M., Barghorn, S., Li, L., Marx, A., Biernat, J., Mandelkow, E. M., and Mandelkow, E. (2001) Mutations of tau protein in frontotemporal dementia promote aggregation of paired helical filaments by enhancing local beta-structure. *J Biol Chem* **276**, 48165-48174

134. Goedert, M., Spillantini, M. G., Cairns, N. J., and Crowther, R. A. (1992) Tau proteins of Alzheimer paired helical filaments: abnormal phosphorylation of all six brain isoforms. *Neuron* **8**, 159-168

135. Gotz, J., Probst, A., Spillantini, M. G., Schafer, T., Jakes, R., Burki, K., and Goedert, M. (1995) Somatodendritic localization and hyperphosphorylation of tau protein in

transgenic mice expressing the longest human brain tau isoform. *The EMBO journal* **14**, 1304-1313

136. Ittner, L. M., Fath, T., Ke, Y. D., Bi, M., van Eersel, J., Li, K. M., Gunning, P., and Gotz, J. (2008) Parkinsonism and impaired axonal transport in a mouse model of frontotemporal dementia. *Proc Natl Acad Sci U S A* **105**, 15997-16002

137. Stamer, K., Vogel, R., Thies, E., Mandelkow, E., and Mandelkow, E. M. (2002) Tau blocks traffic of organelles, neurofilaments, and APP vesicles in neurons and enhances oxidative stress. *The Journal of cell biology* **156**, 1051-1063

138. Ishihara, T., Hong, M., Zhang, B., Nakagawa, Y., Lee, M. K., Trojanowski, J. Q., and Lee, V. M. (1999) Age-dependent emergence and progression of a tauopathy in transgenic mice overexpressing the shortest human tau isoform. *Neuron* **24**, 751-762

139. Dayanandan, R., Van Slegtenhorst, M., Mack, T. G., Ko, L., Yen, S. H., Leroy, K., Brion, J. P., Anderton, B. H., Hutton, M., and Lovestone, S. (1999) Mutations in tau reduce its microtubule binding properties in intact cells and affect its phosphorylation. *FEBS letters* **446**, 228-232

140. Hasegawa, M., Smith, M. J., and Goedert, M. (1998) Tau proteins with FTDP-17 mutations have a reduced ability to promote microtubule assembly. *FEBS letters* **437**, 207-210

141. Leroy, K., Bretteville, A., Schindowski, K., Gilissen, E., Authelet, M., De Decker, R., Yilmaz, Z., Buee, L., and Brion, J. P. (2007) Early axonopathy preceding neurofibrillary tangles in mutant tau transgenic mice. *The American journal of pathology* **171**, 976-992

142. Garcia-Cabrero, A. M., Guerrero-Lopez, R., Giraldez, B. G., Llorens-Martin, M., Avila, J., Serratosa, J. M., and Sanchez, M. P. (2013) Hyperexcitability and epileptic seizures in a model of frontotemporal dementia. *Neurobiology of disease* **58**, 200-208

143. Flunkert, S., Hierzer, M., Loffler, T., Rabl, R., Neddens, J., Duller, S., Schofield, E. L., Ward, M. A., Posch, M., Jungwirth, H., Windisch, M., and Hutter-Paier, B. (2013) Elevated levels of soluble total and hyperphosphorylated tau result in early behavioral deficits and distinct changes in brain pathology in a new tau transgenic mouse model. *Neuro-degenerative diseases* **11**, 194-205

144. Tatebayashi, Y., Miyasaka, T., Chui, D. H., Akagi, T., Mishima, K., Iwasaki, K., Fujiwara, M., Tanemura, K., Murayama, M., Ishiguro, K., Planel, E., Sato, S., Hashikawa, T., and Takashima, A. (2002) Tau filament formation and associative memory deficit in aged mice expressing mutant (R406W) human tau. *Proc Natl Acad Sci U S A* **99**, 13896-13901

145. Gotz, J., Chen, F., Barmettler, R., and Nitsch, R. M. (2001) Tau filament formation in transgenic mice expressing P301L tau. *J Biol Chem* **276**, 529-534

146. Yoshiyama, Y., Higuchi, M., Zhang, B., Huang, S.-M., Iwata, N., Saido, T. C., Maeda, J., Suhara, t., Trojanowski, J. Q., and Lee, V. M. (2007) Synapse loss and microglial activation precede tangles in a P301S tauopathy mouse model. *Neuron* **53**, 337-351

147. Schindowski, K., Bretteville, A., Leroy, K., Begard, S., Brion, J. P., Hamdane, M., and Buee, L. (2006) Alzheimer's disease-like tau neuropathology leads to memory deficits and loss of functional synapses in a novel mutated tau transgenic mouse without any motor deficits. *The American journal of pathology* **169**, 599-616

148. Barten, D. M., Fanara, P., Andorfer, C., Hoque, N., Wong, P. Y., Husted, K. H., Cadelina, G. W., Decarr, L. B., Yang, L., Liu, V., Fessler, C., Protassio, J., Riff, T., Turner, H., Janus, C. G., Sankaranarayanan, S., Polson, C., Meredith, J. E., Gray, G., Hanna, A., Olson, R. E., Kim, S. H., Vite, G. D., Lee, F. Y., and Albright, C. F. (2012) Hyperdynamic microtubules, cognitive deficits, and pathology are improved in tau transgenic mice with low doses of the microtubule-stabilizing agent BMS-241027. *J Neurosci* **32**, 7137-7145

149. Lewis, J., McGowan, E., Rockwood, J., Melrose, H., Nacharaju, P., Van Slegtenhorst, M., Gwinn-Hardy, K., Paul Murphy, M., Baker, M., Yu, X., Duff, K., Hardy, J., Corral, A., Lin, W. L., Yen, S. H., Dickson, D. W., Davies, P., and Hutton, M. (2000) Neurofibrillary tangles, amyotrophy and progressive motor disturbance in mice expressing mutant (P301L) tau protein. *Nature genetics* **25**, 402-405

150. Gotz, J., Chen, F., Barmettler, R., and Nitsch, R. M. (2001a) Formation of neurofibrillary tangles in P301L tau transgenic mice induced by Abeta 42 fibrils. *Science* **293**, 1491-1495

151. Götz, J., Chen, F., Barmettler, R., and Nitsch, R. M. (2001) Tau filament formation in transgenic mice expressing P301L tau. *J. Biol. Chem.* **276**, 529-534

152. Gotz, J., Tolnay, M., Barmettler, R., Chen, F., Probst, A., and Nitsch, R. M. (2001) Oligodendroglial tau filament formation in transgenic mice expressing G272V tau. *The European journal of neuroscience* **13**, 2131-2140

153. Ho, L., Xiang, Z., Mukherjee, P., Zhang, W., De Jesus, N., Mirjany, M., Yemul, S., and Pasinetti, G. M. (2001) Gene expression profiling of the tau mutant (P301L) transgenic mouse brain. *Neurosci Lett* **310**, 1-4

154. Giasson, B. I., Forman, M. S., Higuchi, M., Golbe, L. I., Graves, C. L., Kotzbauer, P. T., Trojanowski, J. Q., and Lee, V. M. (2003) Initiation and synergistic fibrillization of tau and alpha-synuclein. *Science* **300**, 636-640

155. Hoover, B. R., Reed, M. N., Su, J., Penrod, R. D., Kotilinek, L. A., Grant, M. K., Pitstick, R., Carlson, G. A., Lanier, L. M., Yuan, L. L., Ashe, K. H., and Liao, D. (2010) Tau mislocalization to dendritic spines mediates synaptic dysfunction independently of neurodegeneration. *Neuron* **68**, 1067-1081

156. Terwel, D., Lasrado, R., Snauwaert, J., Vandeweert, E., Van Haesendonck, C., Borghgraef, P., and Van Leuven, F. (2005) Changed conformation of mutant Tau-P301L underlies the moribund tauopathy, absent in progressive, nonlethal axonopathy of Tau-4R/2N transgenic mice. *J Biol Chem* **280**, 3963-3973

157. Kimura, T., Fukuda, T., Sahara, N., Yamashita, S., Murayama, M., Mizoroki, T., Yoshiike, Y., Lee, B., Sotiropoulos, I., Maeda, S., and Takashima, A. (2010) Aggregation of detergent-insoluble tau is involved in neuronal loss but not in synaptic loss. *J Biol Chem* **285**, 38692-38699

158. SantaCruz, K., Lewis, J., Spires, T., Paulson, J., Kotilinek, L., Ingellsson, M., Guimaraes, A., DeTure, M., Ramsden, M., McGowan, E., Forster, C., Yue, M., Orne, J., Janus, C., Mariash, A., Kiskowski, M., Hyman, B., Hutton, M., and Ashe, K. H. (2005) Tau Suppression in a Neurodegenerative Mouse Model Improves Memory Function. *Science* **309**, 476-481

159. Sydow, A., Van der Jeugd, A., Zheng, F., Ahmed, T., Balschun, D., Petrova, O., Drexler, D., Zhou, L., Rune, G., Mandelkow, E., D'Hooge, R., Alzheimer, C., and Mandelkow, E.

M. (2011) Tau-induced defects in synaptic plasticity, learning, and memory are reversible in transgenic mice after switching off the toxic tau mutant. *J Neurosci* **31**, 2511-2525

160. Sydow, A., Van der Jeugd, A., Zheng, F., Ahmed, T., Balschun, D., Petrova, O., Drexler, D., Zhou, L., Rune, G., Mandelkow, E., D'Hooge, R., Alzheimer, C., and Mandelkow, E. M. (2011) Reversibility of Tau-related cognitive defects in a regulatable FTD mouse model. *Journal of molecular neuroscience : MN* **45**, 432-437

161. Andorfer, C., Acker, C. M., Kress, Y., Hof, P. R., Duff, K., and Davies, P. (2005) Cell-cycle reentry and cell death in transgenic mice expressing nonmutant human tau isoforms. *J Neurosci* **25**, 5446-5454

162. Takashima, A., Noguchi, K., Michel, G., Mercken, M., Hoshi, M., Ishiguro, K., and Imahori, K. (1996) Exposure of rat hippocampal neurons to amyloid beta peptide (25-35) induces the inactivation of phosphatidyl inositol-3 kinase and the activation of tau protein kinase I/glycogen synthase kinase-3 beta. *Neurosci Lett* **203**, 33-36

163. Takashima, A., Noguchi, K., Sato, K., Hoshino, T., and Imahori, K. (1993) Tau protein kinase I is essential for amyloid beta-protein-induced neurotoxicity. *Proc Natl Acad Sci U S A* **90**, 7789-7793

164. Busciglio, J., Lorenzo, A., Yeh, J., and Yankner, B. A. (1995) beta-amyloid fibrils induce tau phosphorylation and loss of microtubule binding. *Neuron* **14**, 879-888

165. Ferreira, A., Lu, Q., Orecchio, L., and Kosik, K. S. (1997) Selective phosphorylation of adult tau isoforms in mature hippocampal neurons exposed to fibrillar A beta. *Molecular and cellular neurosciences* **9**, 220-234

166. Johansson, S., Jamsa, A., Vasange, M., Winblad, B., Luthman, J., and Cowburn, R. F. (2006) Increased tau phosphorylation at the Ser396 epitope after amyloid beta-exposure in organotypic cultures. *Neuroreport* **17**, 907-911

167. Rapoport, M., Dawson, H. N., Binder, L. I., Vitek, M. P., and Ferreira, A. (2002) Tau is essential to beta -amyloid-induced neurotoxicity. *Proc Natl Acad Sci U S A* **99**, 6364-6369

168. Roberson, E. D., Scearce-Levie, K., Palop, J. J., Yan, F., Cheng, I. H., Wu, T., Gerstein, H., Yu, G.-Q., and Mucke, L. (2007) Reducing endogenous tau ameliorates amyloid beta-induced deficits in an Alzheimer's disease mouse model. *Science* **316**, 750-754

169. White, A. R., Zheng, H., Galatis, D., Maher, F., Hesse, L., Multhaup, G., Beyreuther, K., Masters, C. L., and Cappai, R. (1998) Survival of cultured neurons from amyloid precursor protein knock-out mice against Alzheimer's amyloid-beta toxicity and oxidative stress. *J Neurosci* **18**, 6207-6217

170. Lu, D. C., Shaked, G. M., Masliah, E., Bredesen, D. E., and Koo, E. H. (2003) Amyloid beta protein toxicity mediated by the formation of amyloid-beta protein precursor complexes. *Ann. Neurol.* **54**, 781-789

171. Shaked, G. M., Kummer, M. P., Lu, D. C., Galvan, V., Bredesen, D. E., and Koo, E. H. (2006) Abeta induces cell death by direct interaction wiwth its cognate extracellular domain on app (app597-624). *FASEB J.* **20**, 1254-1256

172. Park, S. A., Shaked, G. M., Bredesen, D. E., and Koo, E. H. (2009) Mechanism of cytotoxicity mediated by the C31 fragment of the amyloid precursor protein. *Biochemical and biophysical research communications* **388**, 450-455

173. Ghosal, K., Stathopoulos, A., and Pimplikar, S. W. (2010) APP intracellular domain impairs adult neurogenesis in transgenic mice by inducing neuroinflammation. *PLOS ONE* **5**, e11866

174. Mucke, L., Masliah, E., Yu, G. Q., Mallory, M., Rockenstein, E. M., Tatsuno, G., Hu, K., Kholodenko, D., Johnson-Wood, K., and McConlogue, L. (2000) High-level neuronal expression of abeta 1-42 in wild-type human amyloid protein precursor transgenic mice: synaptotoxicity without plaque formation. *J Neurosci* **20**, 4050-4058

175. Palop, J. J., Chin, J., Roberson, E. D., Wang, J., Thwin, M. T., Bien-Ly, N., Yoo, J., Ho, K. O., Yu, G. Q., Kreitzer, A., Finkbeiner, S., Noebels, J. L., and Mucke, L. (2007) Aberrant excitatory neuronal activity and compensatory remodeling of inhibitory hippocampal circuits in mouse models of Alzheimer's disease. *Neuron* **55**, 697-711

176. Moechars, D., Lorent, K., De Strooper, B., Dewachter, I., and Van Leuven, F. (1996) Expression in brain of amyloid precursor protein mutated in the alpha-secretase site causes disturbed behavior, neuronal degeneration and premature death in transgenic mice. *The EMBO journal* **15**, 1265-1274

177. Borchelt, D. R., Thinakaran, G., Eckman, C. B., Lee, M. K., Davenport, F., Ratovitsky, T., Prada, C. M., Kim, G., Seekins, S., Yager, D., Slunt, H. H., Wang, R., Seeger, M., Levey, A. I., Gandy, S. E., Copeland, N. G., Jenkins, N. A., Price, D. L., Younkin, S. G., and Sisodia, S. S. (1996) Familial Alzheimer's disease-linked presenilin 1 variants elevate Abeta1-42/1-40 ratio in vitro and in vivo. *Neuron* **17**, 1005-1013

178. Jankowsky, J. L., Fadale, D. J., Anderson, J., Xu, G. M., Gonzales, V., Jenkins, N. A., Copeland, N. G., Lee, M. K., Younkin, L. H., Wagner, S. L., Younkin, S. G., and Borchelt, D. R. (2004) Mutant presenilins specifically elevate the levels of the 42 residue

beta-amyloid peptide in vivo: evidence for augmentation of a 42-specific gamma secretase. *Human molecular genetics* **13**, 159-170

179. Oddo, S., Caccamo, A., Kitazawa, M., Tseng, B. P., and LaFerla, F. M. (2003) Amyloid deposition precedes tangle formation in a triple transgenic model of Alzheimer's disease. *Neurobiol Aging* **24**, 1063-1070

180. Ghosal, K., and Pimplikar, S. W. (2011) Aging and excitotoxic stress exacerbate neural circuit reorganization in amyloid precursor protein intracellular domain transgenic mice. *Neurobiol Aging* **32**, 2320 2321-2329

181. Hirano, A., Dembitzer, H. M., Kurland, L. T., and Zimmerman, H. M. (1968) The fine structure of some intraganglionic alterations. Neurofibrillary tangles, granulovacuolar bodies and "rod-like" structures as seen in Guam amyotrophic lateral sclerosis and parkinsonism-dementia complex. *J Neuropathol Exp Neurol* **27**, 167-182

182. Schochet, S. S., Jr., Lampert, P. W., and Lindenberg, R. (1968) Fine structure of the Pick and Hirano bodies in a case of Pick's disease. *Acta Neuropathol (Berl)* **11**, 330-337

183. Cartier, L., Galvez, S., and Gajdusek, D. C. (1985) Familial clustering of the ataxic form of Creutzfeldt-Jakob disease with Hirano bodies. *J Neurol Neurosurg Psychiatry* **48**, 234-238

184. Gibson, P. H., and Tomlinson, B. E. (1977) Numbers of Hirano bodies in the hippocampus of normal and demented people with Alzheimer's disease. *J Neurol Sci* **33**, 199-206

185. Martinez-Saez, E., Gelpi, E., Rey, M. J., Ferrer, I., Ribalta, T., Botta-Orfila, T., Nos, C., Yague, J., and Sanchez-Valle, R. (2012) Hirano body-rich subtypes of Creutzfeldt-Jakob disease. *Neuropathol Appl Neurobiol* **38**, 153-161

186. Mitake, S., Ojika, K., and Hirano, A. (1997) Hirano bodies and Alzheimer's disease. *Kao Hsiung I Hsueh Ko Hsueh Tsa Chih* **13**, 10-18

187. Schochet, S. S., Jr., and McCormick, W. F. (1972) Ultrastructure of Hirano bodies. *Acta Neuropathol* **21**, 50-60

188. Gibson, P. H. (1978) Light and electron microscopic observations on the relationship between Hirano bodies, neuron and glial perikarya in the human hippocampus. *Acta Neuropathol (Berl)* **42**, 165-171

189. Ogata, J., Budzilovich, G. N., and Cravioto, H. (1972) A study of rod-like structures (Hirano bodies) in 240 normal and pathological brains. *Acta Neuropathol* **21**, 61-67

190. Mori, H., Tomonaga, M., Baba, N., and Kanaya, K. (1986) The structure analysis of Hirano bodies by digital processing on electron micrographs. *Acta Neuropathol* **71**, 32-37

191. Galloway, P. G., Perry, G., and Gambetti, P. (1987) Hirano body filaments contain actin and actin-associated proteins. *J Neuropathol Exp Neurol* **46**, 185-199

192. Goldman, J. E. (1983) The association of actin with Hirano bodies. *J Neuropathol Exp Neurol* **42**, 146-152

193. Lim, R. W. L., Furukawa, R., Eagle, S., Cartwright, R. C., and Fechheimer, M. (1999a) Three distinct F-actin binding sites in the Dictyostelium discoideum 34,000 dalton actin bundling protein. *Biochemistry* **38**, 800-812

194. Lim, R. W. L., Furukawa, R., and Fechheimer, M. (1999b) Evidence of intramolecular regulation of the Dictyostelium discoideum 34,000 dalton F-actin bundling protein. *Biochemistry* **38**, 16323-16332

195. Maselli, A. G., Davis, R., Furukawa, R., and Fechheimer, M. (2002) Formation of Hirano bodies in Dictyostelium and mammalian cells induced by expression of a modified form of an actin cross-linking protein. *J. Cell Sci.* **115**, 1939-1952

196. Fechheimer, M., and Taylor, D. L. (1984) Isolation and characterization of a 30,000-dalton calcium-sensitive actin cross-linking protein from Dictyostelium discoideum. *J. Biol. Chem.* **259**, 4514-4520

197. Furukawa, R., and Fechheimer, M. (1987) An Actin Monomer Binding Protein from Dictyostelium discoideum. *J. Cell Biol.* **105**, 195a

198. Fechheimer, M., and Furukawa, R. (1993) A 27,000 dalton core of the Dictyostelium 34,000 dalton protein retains Ca+2-regulated actin cross-linking but lacks bundling activity. *J. Cell Biol.* **120**, 1169-1176

199. Lim, R. W. L., and Fechheimer, M. (1997) Overexpression, Purification, and Characterization of Recombinant Dictyostelium discoideum calcium regulated 34,000 dalton F-actin bundling protein from Escherichia coli. *Prot. Expr. Purif.* **9**, 182-190

200. Furukawa, R., and Fechheimer, M. (1997) The Structure, Function, and Assembly of Actin Filament Bundles. *Int. Rev. Cytol.* **175**, 29-90

201. Davis, R. C., Furukawa, R., and Fechheimer, M. (2008) A cell culture model for investigation of Hirano bodies. *Acta Neuropathol* **115**, 205-217

202. Ha, S., Furukawa, R., and Fechheimer, M. (2011) Association of AICD and Fe65 with Hirano bodies reduces transcriptional activation and initiation of apoptosis. *Neurobiol Aging* **32**, 2287-2298

203. Kim, D. H., Davis, R. C., Furukawa, R., and Fechheimer, M. (2009) Autophagy contributes to degradation of Hirano bodies. *Autophagy* **5**, 44-51

204. Munoz, D. G., Wang, D., and Greenberg, B. D. (1993) Hirano bodies accumulate C-terminal sequences of beta-amyloid precursor protein (beta-APP) epitopes. *J Neuropathol Exp Neurol* **52**, 14-21

205. Hirano, A., Dembitzer, H. M., Kurland, L. T., and Zimmerman, H. M. (1968) The fine structure of some intraganlionic alterations. *J. Neuropathol. Expt. Neurol.* **27**, 167-182

206. Ha, S., Furukawa, R., Stramiello, M., Wagner, J. J., and Fechheimer, M. (2011) Transgenic mouse model for the formation of Hirano bodies. *BMC neurosci* **12**, 97

207. Banwait, S., Galvan, V., Zhang, J., Gorostiza, O. F., Ataie, M., Huang, W., Crippen, D., Koo, E. H., and Bredesen, D. E. (2008) C-terminal cleavage of the amyloid-beta protein precursor at Asp664: a switch associated with Alzheimer's disease. *J. Alzheimer's Disease* **13**, 1-16

208. Eggert, S., Midthune, B., Cottrell, B., and Koo, E. H. (2009) Induced dimerization of the amyloid precursor protein leads to decreased amyloid-beta protein production. *J Biol Chem* **284**, 28943-28952

209. Kinoshita, A., Whelan, C. M., Smith, C. J., Berezovska, O., and Hyman, B. T. (2002) Direct visualization of the gamma secretase-generated carboxyl-terminal domain of the amyloid precursor protein: association with Fe65 and translocation to the nucleus. *J. Neurochem.* **82**, 839-847

210. Griffith, L. M., and Pollard, T. D. (1978) Evidence for actin filament-microtubule interaction mediated by microtubule-associated proteins. *The Journal of Cell Biology* **78**, 958-965

211. Selden, S. C., and Pollard, T. D. (1983) Phosphorylation of microtubule-associated proteins regulates their interaction with actin filaments. *J Biol Chem* **258**, 7064-7071

212. Kotani, S., Nishida, E., Kumagai, H., and Sakai, H. (1985) Calmodulin inhibits interaction of actin with MAP2 and Tau, two major microtubule-associated proteins. *The Journal of Biological Chemistry* **260**, 10779-10783

213. Yamauchi, P. S., and Purich, D. L. (1993) Microtubule-associated protein interactions with actin filaments: evidence for differential behavior of neuronal MAP-2 and tau in the presence of phosphatidyl-inositol. *Biochemical and Biophysical Research Communications* **190**, 710-715

214. Farias, G. A., Munoz, J. P., Garrido, J., and Maccioni, R. B. (2002) Tubulin, actin, and tau protein interactions and the study of their macromolecular assemblies. *Journal of Cellular Biochemistry* **85**, 315-324

215. Correas, I., Padilla, R., and Avila, J. (1990) The tubulin-binding sequence of brain microtubule-associated proteins, tau and MAP-2, is also involved in actin binding. *Biochem J* **269**, 61-64

216. He, H. J., Wang, X. S., Pan, R., Wang, D. L., Liu, M. N., and He, R. Q. (2009) The proline-rich domain of tau plays a role in interactions with actin. *BMC Cell Biol* **10**, 81

217. Fulga, T. A., Elson-Schwab, I., Khurana, V., Steinhib, M. L., Spires, T. L., T., H. B., and Feany, M. B. (2007) Abnormal bundling and accumulation of F-actin mediates tau-induced neuronal degeneration in vivo. *Nat. Cell Biol.* **9**, 139-148

218. Whiteman, I. T., Minamide, L. S., Goh de, L., Bamburg, J. R., and Goldsbury, C. (2011) Rapid changes in phospho-MAP/tau epitopes during neuronal stress: cofilin-actin rods primarily recruit microtubule binding domain epitopes. *PLoS ONE* **6**, e20878

219. Galloway, P. G., Perry, G., Kosik, K. S., and Gambetti, P. (1987) Hirano bodies contain tau protein. *Brain Res* **403**, 337-340

220. Peterson, C., Kress, Y., Vallee, R., and Goldman, J. E. (1988) High molecular weight microtubule-associated proteins bind to actin lattices (Hirano bodies). *Acta Neuropathol* **77**, 168-174

221. Yu, J. Z., and Rasenick, M. M. (2006) Tau associates with actin in differentiating PC12 cells. *FASEB journal : official publication of the Federation of American Societies for Experimental Biology* **20**, 1452-1461

222. Hayashi, S., Toyoshima, Y., Hasegawa, M., Umeda, Y., Wakabayashi, K., Tokiguchi, S., Iwatsubo, T., and Takahashi, H. (2002) Late-onset frontotemporal dementia with a novel exon 1 (Arg5His) tau gene mutation. *Ann Neurol* **51**, 525-530

223. Gotz, J., Tolnay, M., Barmettler, R., Chen, F., Probst, A., and Nitsch, R. M. (2001) Oligodendroglial tau filament formation in transgenic mice expressing G272V tau. *Eur J Neurosci* **13**, 2131-2140

224. Wszolek, Z. K., Tsuboi, Y., Ghetti, B., Pickering-Brown, S., Baba, Y., and Cheshire, W. P. (2006) Frontotemporal dementia and parkinsonism linked to chromosome 17 (FTDP-17). *Orphanet J Rare Dis* **1**, 30

225. Bunker, J. M., Kamath, K., Wilson, L., Jordan, M. A., and Feinstein, S. C. (2006) FTDP-17 mutations compromise the ability of tau to regulate microtubule dynamics in cells. *The Journal of Biological Chemistry* **281**, 11856-11863

226. Hong, M., Zhukareva, V., Vogelsberg-Ragaglia, V., Wszolek, Z., Reed, L., Miller, B. I., Geschwind, D. H., Bird, T. D., McKeel, D., Goate, A., Morris, J. C., Wilhelmsen, K. C., Schellenberg, G. D., Trojanowski, J. Q., and Lee, V. M. (1998) Mutation-specific functional impairments in distinct tau isoforms of hereditary FTDP-17. *Science* **282**, 1914-1917

227. Lewis, J., McGowan, E., Rockwood, J., Melrose, H., Nacharaju, P., Van Slegtenhorst, M., Gwinn-Hardy, K., Paul Murphy, M., Baker, M., Yu, X., Duff, K., Hardy, J., Corral, A., Lin, W. L., Yen, S. H., Dickson, D. W., Davies, P., and Hutton, M. (2000) Neurofibrillary tangles, amyotrophy and progressive motor disturbance in mice expressing mutant (P301L) tau protein. *Nature Genetics* **25**, 402-405

228. Gotz, J., Chen, F., Barmettler, R., and Nitsch, R. M. (2001) Tau filament formation in transgenic mice expressing P301L tau. *The Journal of Biological Chemistry* **276**, 529-534

229. Tatebayashi, Y., Miyasaka, T., Chui, D. H., Akagi, T., Mishima, K., Iwasaki, K., Fujiwara, M., Tanemura, K., Murayama, M., Ishiguro, K., Planel, E., Sato, S., Hashikawa, T., and Takashima, A. (2002) Tau filament formation and associative memory deficit in aged mice expressing mutant (R406W) human tau. *Proceedings of the National Academy of Sciences of the United States of America* **99**, 13896-13901

230. Tackenberg, C., and Brandt, R. (2009) Divergent pathways mediate spine alterations and cell death induced by amyloid-beta, wild-type tau, and R406W tau. *The Journal of neuroscience : the official journal of the Society for Neuroscience* **29**, 14439-14450

231. Gauthier-Kemper, A., Weissmann, C., Golovyashkina, N., Sebo-Lemke, Z., Drewes, G., Gerke, V., Heinisch, J. J., and Brandt, R. (2011) The frontotemporal dementia mutation R406W blocks tau's interaction with the membrane in an annexin A2-dependent manner. *The Journal of Cell Biology* **192**, 647-661

232. Momeni, P., Pittman, A., Lashley, T., Vandrovcova, J., Malzer, E., Luk, C., Hulette, C., Lees, A., Revesz, T., Hardy, J., and de Silva, R. (2009) Clinical and pathological features of an Alzheimer's disease patient with the MAPT Delta K280 mutation. *Neurobiology of aging* **30**, 388-393

233. Khlistunova, I., Biernat, J., Wang, Y., Pickhardt, M., von Bergen, M., Gazova, Z., Mandelkow, E., and Mandelkow, E. M. (2006) Inducible expression of Tau repeat domain in cell models of tauopathy: aggregation is toxic to cells but can be reversed by inhibitor drugs. *The Journal of Biological Chemistry* **281**, 1205-1214

234. Wang, Y. P., Biernat, J., Pickhardt, M., Mandelkow, E., and Mandelkow, E. M. (2007) Stepwise proteolysis liberates tau fragments that nucleate the Alzheimer-like aggregation of full-length tau in a neuronal cell model. *Proceedings of the National Academy of Sciences of the United States of America* **104**, 10252-10257

235. Yamamoto, T., and Hirano, A. (1985) Hirano bodies in the perikaryon of the Purkinje cell in a case of Alzheimer's disease. *Acta Neuropathol* **67**, 167-169

236. Schmidt, M. L., Lee, V. M., and Trojanowski, J. Q. (1989) Analysis of epitopes shared by Hirano bodies and neurofilament proteins in normal and Alzheimer's disease hippocampus. *Lab Invest* **60**, 513-522

237. David-Ferreira, J. F., David-Ferreira, K. L., Gibbs, C. J., Jr., and Morris, J. A. (1968) Scrapie in mice: ultrastructural observations in the cerebral cortex. *Proceedings of the Society for Experimental Biology and Medicine. Society for Experimental Biology and Medicine* **127**, 313-320

238. Okamoto, K., Hirai, S., and Hirano, A. (1982) Hirano bodies in myelinated fibers of hepatic encephalopathy. *Acta Neuropathol* **58**, 307-310

239. Lass, R., and Hagel, C. (1994) Hirano bodies and chronic alcoholism. *Neuropath. Appl. Neurobiol.* **20**, 12-21

240. Fu, Y., Ward, J., and Young, H. F. (1975) Unusual, rod-shaped cytoplasmic inclusions (Hirano bodies) in a cerebellar hemangioblastoma. *Acta Neuropathol* **31**, 129-135

241. Gessaga, E. C., and Anzil, A. P. (1975) Rod-Shaped Filamentous Inclusions and Other Ultrastructural Features in a Cerebellar Astrocytoma. *Acta Neuropath.* **33**, 119-127

242. Sima, A. A., and Hinton, D. (1983) Hirano-bodies in the distal symmetric polyneuropathy of the spontaneously diabetic BB-Wistar rat. *Acta Neurol Scand* **68**, 107-112

243. Fisher, E. R., Gonzalez, A. R., Khurana, R. C., and Danowski, T. S. (1972) Unique, Concentrically Laminated, Membranous Inclusions in Myofibers. *Am. J. Clin. Pathol.* **58**, 239-244

244. Tomonaga, M. (1983) Hirano body in extraocular muscle. *Acta Neuropathol* **60**, 309-313

245. Fernandez, R., Fernandez, J. M., Cervera, C., Teijeira, S., Teijeiro, A., Dominguez, C., and Navarro, C. (1999) Adult glycogenosis II with paracrystalline mitochondrial inclusions and Hirano bodies in skeletal muscle. *Neuromuscul Disord* **9**, 136-143

246. Anzil, A., Herrlinger, H., Blinzinger, K., and Heldrich, A. (1974) Ultrastructure of Brain and Nerve Biopsy tissue in Wilson Disease. *Arch Neurol.* **31**, 94-100

247. Nagara, H., Yajima, K., and Suzuki, K. (1980) An Ultrastructural Study on the Cerebellum of the brindled mouse. *Acta Neuropathol* **52**, 41-50

248. Peterson, C., Suzuki, K., Kress, Y., and Goldman, J. E. (1986) Abnormalities of dendritic actin organization in the brindled mouse. *Brain Res* **382**, 205-212

249. Schmidt, C. F., Bärmann, M., Isenberg, G., and Sackmann, E. (1989) Chain dynamics, mesh size, and diffusive transport in networks of polymerized actin. A quasielastic light scattering and microfluorescence study. *Macromolecules* **22**, 3638-3649

250. Melidone, R., Keating, J. H., Pfannl, R., and Alroy, J. (2012) Cerebral Hirano-like bodies in an alpaca (Vicugna pacos): histologic and ultrastructural characterization. *Veterinary pathology* **49**, 723-726

251. Field, E. J., Mathews, J. D., and Raine, C. S. (1969) Electron Microscopic Observations on the Cerebellar Cortex in Kuru. *J. Neurol. Sci.* **8**, 209-224

252. Field, E. J., and Narang, H. K. (1972) An Electron-microscopic study of Scrapie in the Rat: Further Observations on "Inclusion bodies" and Virus-like particles. *J. Neurol. Sci.* **17**, 347-364

253. Beal, J. A. (1978) Morphogenesis of the Hirano body in neurons of the squirrel monkey dorsal horn. *J Neurocytol* **7**, 395-403

254. Wisniewski, H. M., and Terry, R. D. (1973) Morphology of the aging brain, human and animal. *Progress in brain research* **40**, 167-186

255. Yagishita, S., Itoh, Y., Nakano, T., Ono, Y., and Amano, N. (1979) Crystalloid inclusions reminiscent of Hirano bodies in autolyzed peripheral nerve of normal wistar rats. *Acta Neuropathol (Berl)* **47**, 231-236

256. Hirano, A., and Dembitzer, H. M. (1976) The fine structure of astrocytes in the adult staggerer. *J Neuropathol Exp Neurol* **35**, 63-74

257. Minagawa, M., Maeshiro, H., Shioda, K., and Hirano, A. (1985) Membranous lipodystrophy (Nasu disease): clinical and neuropathological study of a case. *Clinical neuropathology* **4**, 38-45

258. Nagara, H., Doi, H., Iwaki, T., Kuramitsu, M., and Tateishi, J. (1986) Intracytoplasmic inclusion of Hirano type in Purkinje cells. *Clinical neuropathology* **5**, 131-133

259. Peress, N. S., and Perillo, E. (1995) Differential expression of TFG Beta 1, 2, and 3 isotypes in Alzheimer's disease: a comparative immunohistochemical study with cerebral infarction, aged human and mouse control brainsq. *J. Neuropathol. Exp. Neurol.* **54**, 802-811

260. Singhrao, S. K. (2013) C1q, the classical complement pathway protein binds Hirano bodies in Pick's disease. *Microscopy research and technique* **76**, 606-611

261. Satoh, J., Tabunoki, H., Ishida, T., Saito, Y., and Arima, K. (2013) Ubiquilin-1 immunoreactivity is concentrated on Hirano bodies and dystrophic neurites in Alzheimer's disease brains. *Neuropathol Appl Neurobiol*

262. Rossiter, J. P., Anderson, L. L., Yang, F., and Cole, G. M. (2000) Caspase-cleaved actin (fractin) immunolabelling of Hirano bodies. *Neuropathol. Appl. Neurobiol.* **26**, 342-346

263. Kokoulina, P., and Rohn, T. T. (2010) Caspase-cleaved transactivation response DNA-binding protein 43 in Parkinson's disease and dementia with Lewy bodies. *Neuro-degenerative diseases* **7**, 243-250

264. Zhu, X., Raina, A. K., Rottkamp, C. A., Aliev, G., Perry, G., Boux, H., and Smith, M. A. (2001) Activation and redistribution of c-jun N-terminal kinase/stress activated protein kinase in degenerating neurons in Alzheimer's disease. *J Neurochem* **76**, 435-441

265. Santa-Maria, I., Santpere, G., MacDonald, M. J., de Barreda, E. G., Hernandez, F., Moreno, F. J., Ferrer, I., and Avila, J. (2008) Coenzyme Q induces tau aggregation, tau filaments, and Hirano bodies. *J. Neuropathol. Exp. Neurol.* **67**, 428-434

266. Maciver, S. K., and Harrington, C. R. (1995) Two actin binding proteins, actin depolymerizing factor and cofilin, are associated with Hirano bodies. *Neuroreport* **6**, 1985-1988

267. Jordan-Sciutto, K., Dragich, J., Walcott, D., and Bowser, R. (1998) The presence of FAC1 protein in Hirano bodies. *Neuropathol Appl Neurobiol* **24**, 359-366

268. Renkawek, K., Bosman, G. J., and de Jong, W. W. (1994) Expression of small heat-shock protein hsp 27 in reactive gliosis in Alzheimer disease and other types of dementia. *Acta Neuropathol* **87**, 511-519

269. Lee, H.-g., Ueda, M., Miyamoto, Y., Yoneda, Y., Perry, G., Smith, M. A., and Zhu, X. (2006) Aberrant localization of importin a1 in hippocampal neurons in Alzheimer disease. *Brain Res.* **1124**, 1-4

270. Lee, S. C., Zhao, M. L., Hirano, A., and Dickson, D. W. (1999) Inducible nitric oxide synthase immunoreactivity in the Alzheimer disease hippocampus: association with Hirano bodies, neurofibrillary tangles, and senile plaques. *J Neuropathol Exp Neurol* **58**, 1163-1169

271. Perry, G., Zhu, X., Babar, A. K., Siedlak, S. L., Yang, Q., Ito, G., Iwatsubo, T., Smith, M. A., and Chen, S. G. (2008) Leucine-rich repeat kinase 2 colocalizes with alpha-synuclein in Parkinson's disease, but not tau-containing deposits in tauopathies. *Neuro-degenerative diseases* **5**, 222-224

272. Previll, L. A., Crosby, M. E., Castellani, R. J., Bowser, R., Perry, G., Smith, M. A., and Zhu, X. (2007) Increased expression of p130 in Alzheimer's disease. *Neurochem. Res.* **32**, 639-644

273. Shao, C. Y., Mirra, S. S., Sait, H. B., Sacktor, T. C., and Sigurdsson, E. M. (2011) Postsynaptic degeneration as revealed by PSD-95 reduction occurs after advanced Abeta and tau pathology in transgenic mouse models of Alzheimer's disease. *Acta Neuropathol* **122**, 285-292

274. Renkawek, K., Bosman, G. J., and de Jong, W. W. (1994) Expression of small heat shock protein hsp 27 in reactive gliosis in Alzheimer disease and other types of dementia. *Acta Neuropathol. (Berl)* **87**, 511-519

275. Hong, Y., Chan, C. B., Kwon, I. S., Li, X., Song, M., Lee, H. P., Liu, X., Sompol, P., Jin, P., Lee, H. G., Yu, S. P., and Ye, K. (2012) SRPK2 phosphorylates tau and mediates the cognitive defects in Alzheimer's disease. *J Neurosci* **32**, 17262-17272

276. Rohn, T. T. (2008) Caspase-cleaved TAR DNA-binding protein-43 is a major pathological finding in Alzheimer's disease. *Brain Res* **1228**, 189-198

277. Rohn, T. T., and Kokoulina, P. (2009) Caspase-cleaved TAR DNA-binding protein-43 in Pick's disease. *International journal of physiology, pathophysiology and pharmacology* **1**, 25-32

278. Maselli, A. G., Furukawa, R., Thomson, S. A. M., Davis, R. C., and Fechheimer, M. (2003) Formation of Hirano bodies induced by expression of an actin cross-linking protein with a gain of function mutation. *Eucaryot. Cell* **2**, 778-787

279. Furukawa, R., Maselli, A. G., Thomson, S. A. M., Lim, R. W.-L., Stokes, J. V., and Fechheimer, M. (2003) Calcium Regulation of Actin Cross-linking Is Important For Function of the Actin Cytoskeleton in Dictyostelium. *J. Cell Science* **116**, 187-196

280. Furgerson, M., Fechheimer, M., and Furukawa, R. (2012) Model Hirano bodies protect against tau-independent and tau-dependent cell death initiated by the amyloid precursor protein intracellular domain. *PLOS ONE* **7**, e44996

Figure 1.1. Proteolytic processing of the amyloid precursor protein. Cleavage of the amyloid precursor protein by β-secretase produces the C99 molecule upon release of the soluble APP extracellular domain. Cleavage of APP by both beta secretase and gamma secretase results in the extracellular production of amyloid beta, which can either be cleared from the brain or aggregate to form plaque. Cleavage of APP by α-secretase occurs within the amyloid beta region of APP thereby impeding the formation of amyloid beta and producing the C83 molecule. γ-secretase cleavage produces an intracellular peptide, AICD. Further cleavage of the AICD molecule by caspase produces a smaller c-terminal fragment of APP, C31. AICD and C31 are believed to regulate transcription, which is in part regulated by the interaction of scaffolding proteins with the ACID or C31 YENPTY motif.

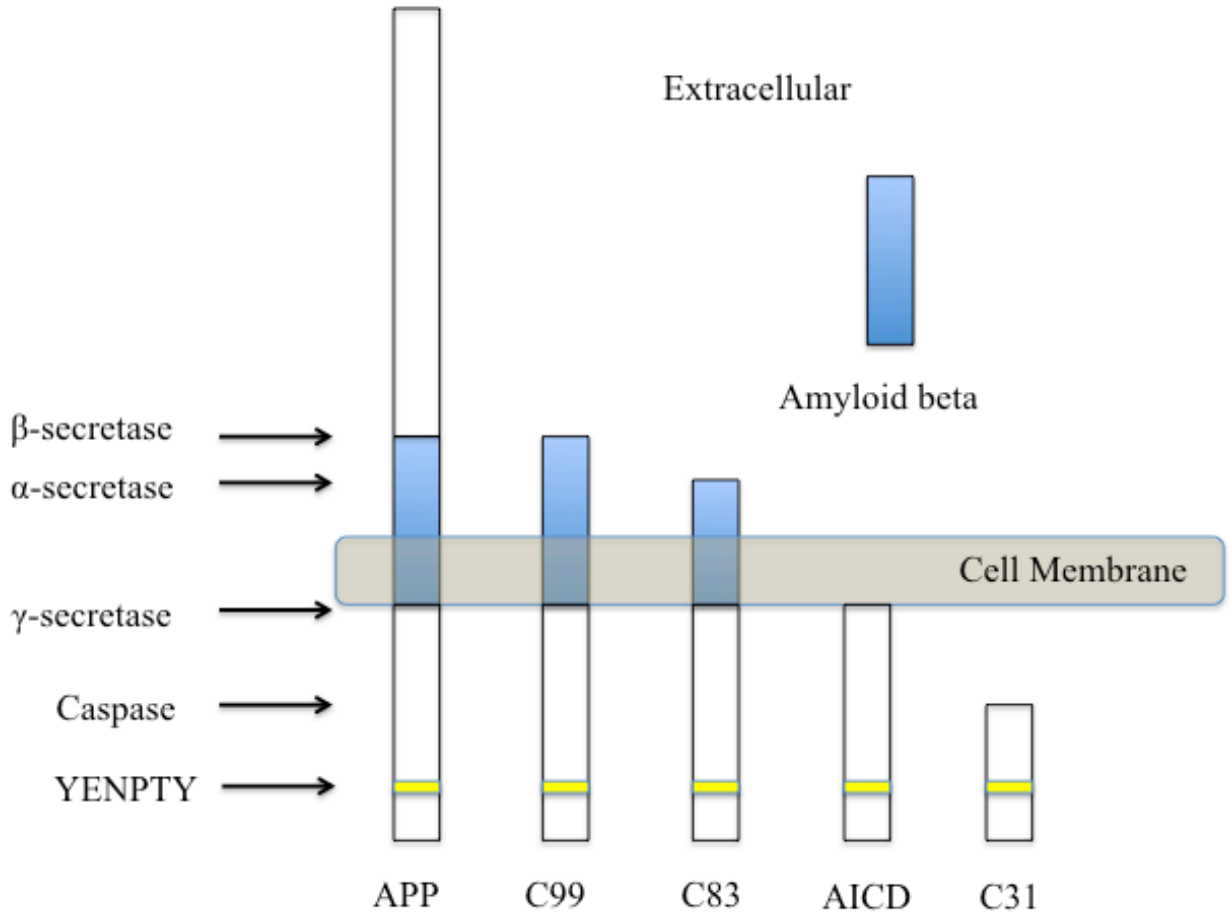
Extracellular
Amyloid beta
β-secretase
α-secretase
γ-secretase
Caspase
YENPTY
Cell Membrane
APP
C99
C83
AICD
C31

Figure 1.2. AICD/C31 signaling and induction of cell death. **A**. APP has been shown to dimerize with either APP or AICD/C31 leading to increased production of APP c-terminal fragments (AICD and C31) (45,170,172,207,208). Fe65 may mediate this dimerization event. Although the exact organization of these APP complexes is unknown, several possibilities exist. 1) APP and Fe65 associate and cleavage of the cytoplasmic tail releases the AICD/C31-Fe65 complex. 2) An APP-APP dimerization event increases cleavage of the intracellular domain of APP, releasing one or two AICD/C31-Fe65 complexes. 3) An APP-AICD/C31 dimerization event increases cleavage of the intracellular domain of APP, releasing one or two AICD/C31-Fe65 complexes. **B**. AICD or C31 associate with the Fe65 scaffolding protein, possibly by dimerizing with APP (45,46,170). Fe65 enters the nucleus with or without AICD or C31 to activate the histone acetyl transferase Tip60 and initiate transcription (35,36,209). Expression of AICD or C31 has been shown to initiate cell death pathways, which are dependent on Tip60, Fe65, and caspase (42,45-47,172).

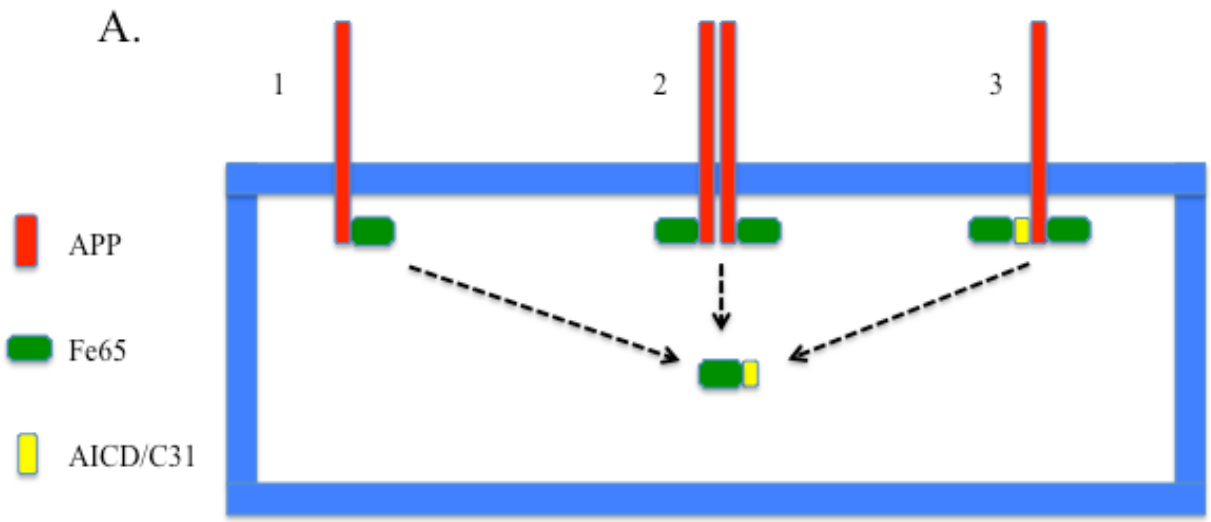
A.
1
2
3
APP
Fe65
AICD/C31

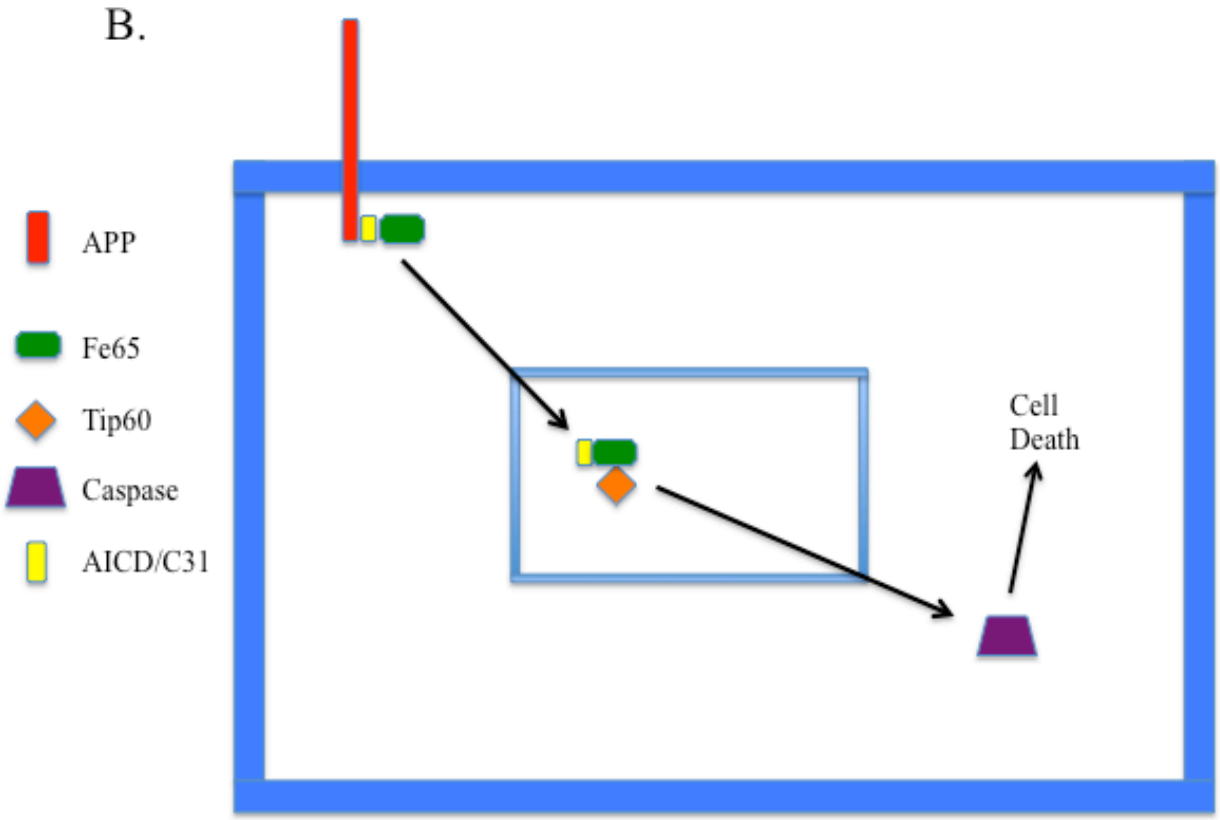
B.
APP
Fe65
Tip60
Caspase
AICD/C31
Cell
Death

Figure 1.3. Tau splicing isoforms. The MAPT gene encodes the tau protein. Tau can be alternatively sliced to generate six isoforms ranging from 441 amino acids to 352 amino acids. Tau isoforms can contain exons (E) 2-3, 2 only, or neither 2 nor 3. In addition, tau isoforms are categorized by the number of microtubule-binding repeat domains they contain. Tau isoforms contain either 3 or 4 microtubule-binding domains. The second microtubule-binding domain designated R2 is encoded by exon 10 and is alternatively spliced.

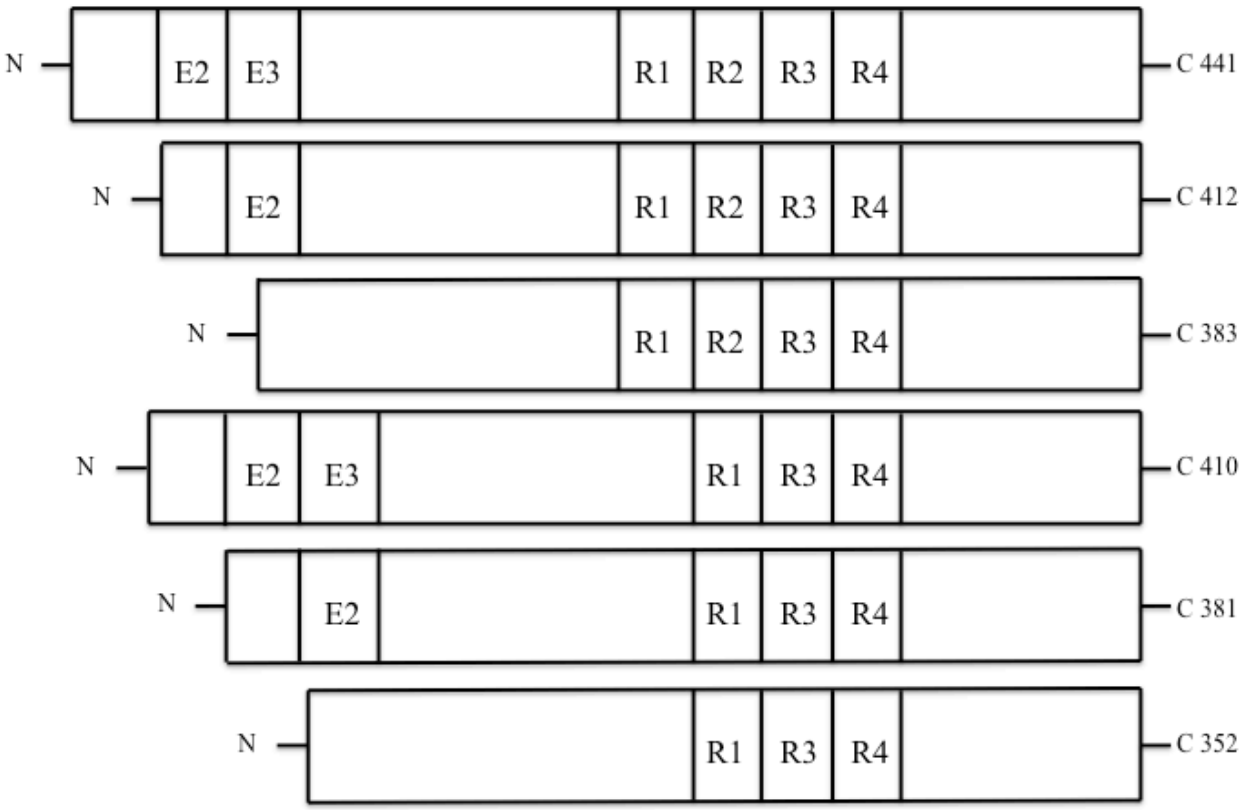
N
E2
E3
R1
R2
R3
R4
C 441
N
E2
R1
R2
R3
R4
C 412
N
R1
R2
R3
R4
C 383
N
E2
E3
R1
R3
R4
C 410
N
E2
R1
R3
R4
C 381
N
R1
R3
R4
C 352

Table 1.1 Evidence of tau-actin interactions

Assay	*Result*	*Reference*
Viscosity	MAPs increase viscosity of actin, actin+tubulin mixtures	(210)
Viscosity	Critical gelation concentration of mixtures of actin and MAPs increased with increased phosphorylation	(211)
Viscosity, turbidity, TEM	Tau assembles F-actin, increases turbidity, bundles actin	(212)
Viscosity	Phospholipids have no effect on viscosity of tau-actin mixtures	(213)
ELISA, TEM	Actin inhibits tau-tubulin interactions. Tau promotes actin bundling and is observed at cross-links	(214)
TEM, cosedimentation, affinity chromatography	MT binding domain tau peptide and full length tau bind actin, but only full length tau bundles actin	(215)
Cosedimentation, TEM, AFM	Tau MT binding domain or proline-rich region sufficient for actin binding	(216)
Overexpression of FTDP-17 tau in Drosophila	FTDP-17 tau expression causes phospho-tau reactive actin inclusions	(217)
Primary chick neuron culture, colocalization	Cell stress induces phospho-tau accumulation in actin-cofilin rods	(218)
N2A cell culture; human brain immunohistochemistry	Endogenous tau colocalizes with HBs in culture and in AD	(201, 219, 220)
NGF treated PC12 cells, colocalization	Tau colocalizes with actin in lammellipodia	(221)

Table modified from W. Spears M.S. dissertation UGA 2012

Table 1.2. Tau mutations produce different phenotypes

Tau mutant	*Method*	*Result*	*Reference*
R5H	Genomic DNA sequencing, MT assembly assay	Patient with tau R5H allele shows NFTs, plaques. Recombinant R5H shows reduced ability to promote MT Assembly	(222)
G272V	Overexpression of 441 G272V human tau driven by prion protein promoter	Oligodendroglial hyperphosphorylated tau filaments, reduced tau solubility	(223)
G272V	Clinical symptoms	Onset 41-50 yrs, duration 6-10 yrs, late dementia, parkinsonism rare, early personality change, language difficulties	(224)
G272V, P301L, ΔK280	Live cell tracking of GFP-tubulin+Tau transfected MCF7 cells	G272V tau reduced ability to regulate MT dynamics	(225)
P301L, R406W	Light scattering, cosedimentation, frontal gray matter tau extraction	Reduced ability to bind and promote MT assembly. R406W had lowest MT binding capacity. Human P301L insoluble tau composed of 4R. R406W composed of all 6 isoforms	(226)
P301L	Clinical symptoms	Onset 41-50, duration 6-10 yrs, rare parkinsonism, late dementia, early personality change, language difficulties, amyotrophy	(224)
P301L	4R0N or 4R2N P301L expression in mice	NFT formation, neuron loss, age-dependent increase in insoluble tau, tau filament formation, astrocyte activation	(227, 228)
P301L	CamKII driven 4R0N mouse tau expression, primary neuron culture	Mice show memory and synaptic plasticity deficits, tau accumulation in dendritic spines, decreased synaptic expression of AMPA and NMDA subunits	(155)
R406W	CamKII driven forebrain expression of 4R2N	Tau inclusions, filament formation, memory deficits. All tau isoforms expressed were incorporated in tangles	(229)
R406W, P301L	Primary neuron culture	Wt and R406W tau expression potentiated cell death in the presence of APP, not P301L	(230)
R406W	Clinical symptons	Onset >50 yrs, duration >15 yrs, early dementia, personality change, mutism	(224)
R406W	Primary neuron culture	R406W decreases phosphorylation, abolishes tau interaction with the plasma membrane mediated by Annexin A2	(231)
ΔK280	Genomic DNA sequencing, IHC	NFTs, preferential 3R tau deposits, may increase splicing of 3R tau	(232)
K18ΔK280	CaMKII driven expression	Mice show hyperphosphorylation of endogenous mouse tau, neuron loss, NFTs, tau mislocalization	(159)
K18ΔK280	N2a cell culture	Binds weakly to MTs, high propensity for aggregation which is correlated with further proteolysis and cell death	(98, 233, 234)

Table modified from W. Spears M.S. dissertation UGA 2012

Figure 1.4 Illustration of Tau mutations and sites of phosphorylation. There have been multiple FTLD-tau mutations characterized, and some of the most studied are highlighted (red). Most of these mutations occur within the microtubule binding repeats, but others occur in the N- and C- terminal domains. In addition, there have been many sites on tau that are substrates for phosphorylation. The serine, threonine, and tyrosine sites most closely linked to Alzheimer's disease are labeled yellow. The Paired helical filament forming region of tau is labeled (PHF). This region is the primary component of NFTs.

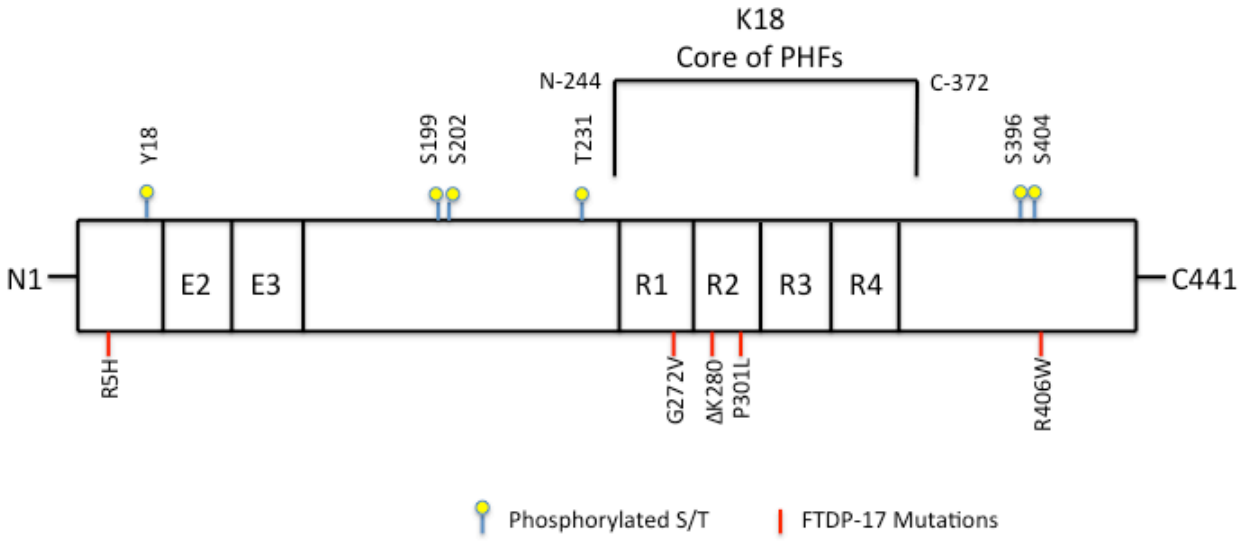
K18
Core of PHFs
N-244
C-372
Y18
S199
S202
T231
S396
S404
N1
E2
E3
R1
R2
R3
R4
C441
R5H
G272V
ΔK280
P301L
R406W
Phosphorylated S/T
FTDP-17 Mutations

Table 1.3. Diseases associated with Hirano bodies

Source	*Cell type/Tissue*	*References*
Alzheimer's disease	Hippocampus CA1, Purkinje cells, Oligodendrocytes	(184,186,190,235,236)
Parkinson's disease	Hippocampus CA1	(205)
Pick's disease	Hippocampus CA1	(182)
Amyotrophic lateral sclerosis (ALS)	Hippocampus CA1	(205)
Creutzfeldt-Jakob disease	Hippocampus CA1	(183,185)
Mice with scrapie	Cerebellar cortex	(237)
Chronic alcoholism	Hippocampus CA1; Substantia nigra	(238)
Hepatic encephalopathy	Substantia nigra, Denate nucleus	(239)
Neuroblastoma; Astrocytoma	Stromal cells, Glial cells	(240,241)
Diabetes (rat model)	Peripheral nerves, Oligodendrocytes	(242)
Muscle degeneration	Myofibers	(243-245)
Brindled mice (Menke's); Wilson's Disease	Cerebellum, neocortex, cerebral cortex	(246-248)
General aging	Hippocampus CA1	(189,249)
Aged Alpaca	Cerebral cortex	(250)
Humans and chimpanzees with Kuru	Cortex and Cerebellum	(251,252)
Normal aged chimpanzees and monkeys	Cortex	(251,253,254)
Wistar Rats	Cortex	(255)
Hamster model of demyelinated hind-leg paralysis	Cerebellum	(256)
Nasu-Hakola's disease	Cerebral Cortex	(257)
Infantile neuroaxonal dystrophy	NA	(255)

Crow-Fukase syndrome	Purkinje Cells	(258)

Table was adapted from (201)

Table 1.4. Components of Hirano bodies

Protein	***Function***	***References***
Actin (F-actin)	Cytoskeleton	(191,192)
a-actinin	F-actin cross-linking protein	(191)
a-1-antichymotrypsin	Protease Inhibitor	(259)
C1q Complement Protein	Immune Response	(260)
C9orf72	Unknown Function	(261)
Caspase cleaved actin (Fractin)	Unknown function	(262)
Caspase cleaved Transactivation Response DNA-binding Protein 43 (TDP-43)	Unknown Function	(263)
Jun N-terminal Kinase/Stress Activated Protein Kinase (JNK/SAPKγ)	Cell Signaling	(264)
Coenzyme Q_{10} (Ubiquinone)	Electron transport chain	(265)
Cofilin	Actin binding protein	(266)
C-terminal fragment of b-APP (AICD)	Transcription regulator	(204)
FAC1	*Transcription repressor*	(267)
Heat-shock protein 27 (Hsp27)	*Thermo-tolerance*	(268)
Hippocampus acetylcholine neurostimulating peptide (HCNP)	Hormone	(262)
Importin a	Cytoplasmic-nuclear transport	(269)
Inducible nitric oxide synthase (iNOS)	Stress response	**(270)**
Leucine-rich Repeat Kinase 2 (LRRK2)	Cell Signaling	(271)
MAP1 and MAP2	Microtubule binding protein	(220)
Neurofilament subunits L and M	Cytoskeleton	(236)
P130 (retinoblastoma related protein)	Transcription regulator	(272)

Phosphorylated Tau (pTau-199/202)	Microtubule binding protein	Unpublished
PSD-95	Synaptic scaffold protein	(273)
Small heat shock protein 27 (HSP 27)	Stress response	(274)
Serine-arginine protein kinase 2 (SRPK2)	Cell Signaling	(275)
Tau protein	Microtubule binding protein	(204)
Transactivation Response DNA-binding Protein 43 (TDP-43)	Transcriptional repressor/Splicing	(276,277)
Transforming growth factor b3	Hormone	(259)
Tropomyosin	Actin binding protein	(219)
Ubiquillin-1	Cytoskeleton scaffold	(261)
Vinculin	Actin binding protein	(191)

Table was adapted from (201)

Table 1.5. Components of Model Hirano bodies

Protein	*Function*	*References*
Actin	Cytoskeleton	(195,278,279)
COOH fragments of APP (AICD)	Transcription Regulator	(202,280)
α-actinin	F-actin cross-linking protein	(201,279)
Cofilin	Actin binding protein	(195,201)
Elongation Factor 1α (eEF-1α)	Translation	(195)
Importin α	Cytoplasmic-nuclear transport	(201)
Myosin II	Motor protein	(195,201)
Talin	F-actin cross-linking protein	(201)
Tau	Microtubule binding protein	(201,280)
Tropomyosin	Actin binding protein	(201)
Ubiquitin	Protein degradation	(201)
Vinculin	Actin binding protein	(201)
Zyxin	Focal adhesions	(201)
Fe65	Scaffolding Protein	(202)
Mena	Actin Associated Protein	Unpublished
Heat-shock protein 27 (Hsp27)	Thermo-tolerance	Unpublished

Table adapted from (201)

CHAPTER 2

MODEL HIRANO BODIES PROTECT AGAINST TAU-INDEPENDENT AND TAU-DEPENDENT CELL DEATH INITIATED BY THE AMYLOID PRECURSOR PROTEIN INTRACELLULAR DOMAIN[1]

---

[1] Furgerson, M. Fechheimer, M. and R. Furukawa. 2012. *PLoS ONE.* 7:9-19 Reprinted here with permission of publisher.

ABSTRACT:

The main pathological hallmarks of Alzheimer's disease are amyloid-beta plaques and neurofibrillary tangles, which are primarily composed of amyloid precursor protein (APP) and tau, respectively. These proteins and their role in the mechanism of neurodegeneration have been extensively studied. Hirano bodies are a frequently occurring pathology in Alzheimer's disease as well as other neurodegenerative diseases. However, the physiological role of Hirano bodies in neurodegenerative diseases has yet to be determined. We have established cell culture models to study the role of Hirano bodies in amyloid precursor protein and tau-induced cell death mechanisms. Exogenous expression of APP and either of its c-terminal fragments C31 or AICDc58 enhance cell death. The presence of tau is not required for this enhanced cell death. However, the addition of a hyperphosphorylated tau mimic 352PHPtau (1,2) significantly increases cell death in the presence of both APP and C31 or AICDc58 alone. The mechanism of cell death induced by APP and its c-terminal fragments and tau was investigated. Fe65, Tip60, p53, and caspases play a role in tau-independent and tau-dependent cell death. In addition, apoptosis was determined to contribute to cell death. The presence of model Hirano bodies protected against cell death, indicating Hirano bodies may play a protective role in neurodegeneration.

INTRODUCTION:

Alzheimer's disease is a growing, worldwide neurodegenerative disease affecting millions of elderly. Alzheimer's disease (AD) patients experience progressive dementia as a result of severe neurodegeneration. The autopsied brains of AD patients reveal two hallmark neuropathological protein aggregates, amyloid-beta plaques and neurofibrillary tangles

(reviewed in (3,4)) and also have a higher frequency of intracellular F-actin-rich Hirano bodies than age matched normal subjects (4-8). Investigating how these pathologies relate to molecular events leading to neurodegeneration is an extensive and often controversial area of research.

The amyloid cascade hypothesis of Alzheimer's disease (9-14) and subsequent refinements positing that oligomeric amyloid-beta species are neurotoxic (15) (reviews (16-18)) have explained a vast amount of the data and pathology in both humans and model systems. Proteolytic processing of the type 1 transmembrane protein amyloid precursor protein (APP) (19-21) and sequential cleavage of APP by beta- and gamma-secretase releases an extracellular peptide, amyloid-beta, which aggregates to form plaques (reviewed in (22)). Gamma-secretase cleavage of APP also results in the release of a c-terminal intracellular domain, AICD. Additional caspase cleavage results in another smaller c-terminal intracellular peptide, C31 (reviewed in (22)). Although controversial, it is thought that AICD can participate in signaling pathways (reviewed in (23-25)).

The second pathological hallmark, neurofibrillary tangles, is derived from the aggregation of the microtubule binding protein tau (26,27). Tauopathies such as Frontal Temporal Dementias with Parkinsonism (FTDP) are diseases linked to mutations in tau (reviewed in (28,29)). These diseases exhibit tau pathology, but unlike AD, no amyloid-beta pathology exists. Thus, mutant tau contributes to neurodegeneration without amyloid-beta. Numerous observations suggest a link between the cleavage products of APP and tau in neurodegeneration. Amyloid-beta plaques appear before neurofibrillary tangles in brains during neurodegeneration. Furthermore, reduction of tau levels in a mouse model of Alzheimer's disease prevented amyloid-beta induced defects (30,31). Turning off tau expression in a mouse model of tauopathy rescued memory defects even though cells still contain neurofibrillary

tangles (32). These observations suggests that tau pathology arises downstream of amyloid-beta pathology. However, the exact mechanism, interaction, and timing of these two pathologies remain to be elucidated.

In contrast to the extensive research on APP and tau, very little attention has been given to Hirano bodies, intracellular protein inclusions. They develop in the brain during normal aging, but are highly prevalent in neurodegenerative diseases such as AD, amyotrophic lateral sclerosis, Creutzfeldt-Jakob disease, and some tauopathies (4,8,33-39). Hirano bodies are highly ordered filamentous actin (F-actin) arranged in a paracrystalline structure (40,41). Electron microscopy has shown that the F-actin appears arranged as either a herringbone or crosshatch pattern depending on the plane of section. Due to the lack of a model system, previous research has focused on studying their ultrastructure and identifying their components (5,35,42,43).

Recently, the creation of model Hirano bodies was discovered through the expression of a truncated version of the 34 kDa actin bundling protein. This truncation consists of the carboxyl-terminal region of 34 kDa protein (CT) (44). Model Hirano bodies induced by CT expression have been successfully created in Dictyostelium, a variety of mammalian cell lines, and in transgenic mice (44-46). Model Hirano bodies are indistinguishable from authentic Hirano bodies on an ultrastructural level and contain some of the same protein components including tau and c-terminal fragments of APP (8,37,45,47,48).

Previous work from our laboratory has shown that model Hirano bodies protect against AICDc58-dependent cell death in H4 cells (49). This work also showed that model Hirano bodies lowered the transcriptional activation from exogenous AICDc58 (49). We have extended these studies by investigating the effect of model Hirano bodies on the presence of exogenous

APP, AICDc58, and C31. Since tau co-localized with Hirano bodies and tau exhibits pathology in neurodegenerative diseases, we have studied the effect of tau in the presence of APP, AICDc58, and C31 and model Hirano bodies. We provide direct evidence for enhanced cell death between APP/AICDc58, APP/C31 and 352PHPtau, and AICDc58/352PHPtau. We show that these enhanced cell death conditions are partially attributed to activation of apoptotic pathways. Furthermore, we show that model Hirano bodies protect against APP/AICDc58, AICDc58/352PHPtau, APP/C31, and APP/C31/352PHPtau-induced cell death. Understanding the physiological role of Hirano bodies and their interactions with tau and fragments of APP may provide fundamental new insights to understanding Alzheimer's disease and the presence of Hirano bodies in other neurodegenerative diseases.

RESULTS:

Model Hirano bodies protect against APP and C31-induced cell death

It was shown previously that APP enhances the level of cell death induced by C31 (50). We investigated the effect of Hirano bodies on C31-induced cell death. We transiently expressed APP-C31-myc and/or APP to induce cell death in N2A cells as described previously (50), and measured cell death in the presence or absence of model Hirano bodies as shown in Figure 2.1. Expression of either APP or APP-C31-myc alone induced low levels of cell death in the presence or absence of model Hirano bodies. Cells lacking model Hirano bodies and expressing APP/C31 showed a significant increase in cell death as previously reported (50). In contrast, cells expressing model Hirano bodies and both APP/C31 showed a significant reduction in cell death levels (**$p < 0.01$ compared to cells without model Hirano bodies).

Since N2A cells contain moderate levels of endogenous tau (51), we investigated whether APP/C31-induced cell death requires the presence of tau. To address this question, we utilized astroglioma derived H4 cells that have very low levels of endogenous tau (51,52). Hirano bodies have been proposed to have a glial origin (53) and astrocytes have been shown to be important mediators of cell death induced by beta amyloid and tau (54). APP and/or C31 were transiently expressed in H4 cells and cell death was measured as shown in Figure 2.2. Low levels of cell death were observed in the presence of exogenously expressed APP-C31-myc as previously observed in N2A cells. Expression of exogenous APP increased the level of cell death in H4 cells similar to the results obtained in N2A cells. In the presence of very low amounts of endogenous tau, model Hirano bodies still protected H4 cells against APP-induced cell death (*$p < 0.05$). In the presence of both exogenous APP and APP-C31-myc, enhanced cell death occurred in H4 cells in the presence or absence of model Hirano bodies. The presence of model Hirano bodies significantly lowered the amount of cell death induced by APP/C31 expression (**$p < 0.01$). Cell death pathways of APP and C31 can operate independently of tau. In addition, the presence of model Hirano bodies protect cells from APP/C31-induced cell death.

Previously, we observed AICDc58-dependent cell death in H4 cells without expression of either exogenous APP or tau (49,55) and that model Hirano bodies protect against cell death. We investigated whether model Hirano bodies would protect against the enhanced cell death induced by APP/AICDc58 by cotransfection of APPc58-myc plasmid and APP. Expression of either exogenous APPc58-myc alone or APP/AICDc58 caused a significant amount of cell death as shown in Figure 2.3. The presence of model Hirano bodies decreased the amount of cell death by approximately 50% (*$p < 0.05$). This level of protection is in agreement with previous data (49). AICDc58-induced cell death was increased approximately 60% in the presence of

exogenous APP. The presence of model Hirano bodies significantly reduced APP/AICDc58 cell death (**$p < 0.01$).

Model Hirano bodies protect against tau-dependent cell death

The effect of tau on AICDc58-induced cell death was investigated. Wild type fetal human tau (352 residues, 3R0N) tau (352WTtau) or 352tau fetal human tau (352PHPtau) with S198, S199, S202, T231, S235, S396, S404, S409, S413, and S422 mutated to glutamate to mimic phosphorylated residues (2) was utilized. Tau phosphorylation has been implicated in neurodegeneration and expression of 352PHPtau has been shown to induce death in a cell culture system at an earlier time point than wild type tau (1,2). Exogenous APPc58-myc was transfected alone and with either 352WTtau or 352PHPtau in the presence or absence of Hirano bodies. 352WTtau, like 352PHPtau, causes low levels of cell death when co-expresssed with GFP shown in Figure 2.4. Expression of exogenous AICDc58 alone causes a significant amount of cell death. AICDc58/352WTtau slightly increases cell death compared to AICDc58 alone. In contrast, 352PHPtau/AICDc58 enhanced increases cell death and is significantly higher than both AICDc58-induced cell death (***$p < 0.005$) and AICDc58/352WTtau (**$p < 0.01$). The presence of model Hirano bodies significantly reduced AICDc58, AICDc58/352WTtau, and AICDc58/352PHP-induced cell death (**$p < 0.01$).

The effect of tau on APP/C31-induced cell death was investigated. H4 cells were transfected with APP or APP/C31 and 352WTtau or 352PHPtau in the presence or absence of model Hirano bodies. Surprisingly, the 3.0 μg of APP plasmid used to initiate APP and APP-C31-myc-induced cell death in H4 cells killed virtually every cell in the presence of APP, 352PHPtau and APP-C31-myc (data not shown). Therefore, the amount of APP plasmid was

reduced to 1.5 μg in order to achieve a maximum of approximately 50% cell death in the presence of exogenous APP-C31-myc and 352PHPtau as shown in Figure 2.5. A small amount of cell death occurred with expression of 352PHPtau or C31/352PHPtau. At this new concentration of APP plasmid, APP/C31 had significantly lower cell death than with APP/C31/352PHPtau, indicating that the addition of 352PHPtau is responsible for most of the death (**$p < 0.01$ compared to APP/c31). When model Hirano bodies were present, the amount of APP/c31/352PHPtau-induced cell death was significantly reduced (**$p < 0.01$ compared to cells without model Hirano bodies).

Both tau-independent and -dependent cell death involve apoptosis

To discover how model Hirano bodies protect against tau-independent and tau-dependent cell death, we investigated possible mechanisms of cell death. We previously showed that AICDc58 and Fe65 co-localize with model Hirano bodies and that model Hirano bodies significantly reduced AICDc58-induced cell death and the transcriptional activity mediated by AICDc58, Fe65, and Tip60 (49). In addition, it has been previously shown that AICDc58-induced cell death involves Tip60 (55). The contribution of Fe65 and Tip60 in cell death was investigated by utilizing mutations in these proteins. We utilized a previously characterized dominant negative mutation in Fe65, C655F, which abolished its ability to interact with the YENPTY domain of APP or its c-terminal fragments (56). Exogenous expression of C655F Fe65 significantly reduced both tau-independent (APP/c31) (***$p < 0.005$) and tau–dependent (APP/C31/352PHPtau) cell death (***$p < 0.005$) as shown in Figure 2.6, implicating Fe65 in both cell death pathways. We utilized a previously characterized dominant negative mutant form of Tip60, Q377E G380E, which abolished the catalytic activity of Tip60 (55). Expression of Q377E G380E Tip60 (mTip60) significantly reduced both tau-independent (APP/C31) and tau–

dependent (APP/C31/352PHPtau) cell death by at least 50% as shown in Figure 2.7 (***$p < 0.005$). This result indicates a role of Tip60 in both cell death pathways.

It has been reported that AICD and presenilin mediate the upregulation of p53 in cells (57). Furthermore, Tip60 has been shown to acetylate p53 directly, causing it to initiate transcription of apoptotic genes (58-60). We tested the role of p53 in APP/c31-induced cell death in the presence or absence of 352PHPtau using a cell permeable inhibitor of p53, α-pifithrin (61). Cell death in H4 cells was induced by exogenous expression of APP/C31 or APP/C31/352PHPtau. Cell viability was measured in the presence or absence of α-pifithrin as shown in Figure 2.8. α-pifithrin significantly reduced both tau-independent (APP/C31) (***$p < 0.005$) and tau-dependent (APP/c31/352PHPtau) cell death (**$p < 0.01$).

APP and C31-induced cell death in N2A cells and AICD-induced cell death in H4 cells have been shown to involve caspases (50,55). Caspase inhibitors were utilized to investigate whether caspases are involved in APP/C31 and APP/C31/352PHPtau death pathways. Broad-spectrum caspase inhibitor (Ac-VAD-CHO) as well as inhibitors of caspase 8 (Z-IGTD-FMK) and caspase 3 (Z-DEVD-FMK) was utilized in cell death assays in H4 cells as shown in Figure 2.9. Both the broad and the caspase 8 inhibitors, but not caspase 3 inhibitor, significantly reduced both tau-independent (APP/C31) (**$p < 0.01$) and tau-dependent (APP/C31/352PHPtau) cell death (*$p < 0.05$). Since both p53 and caspases were involved, we hypothesized that apoptosis is likely the mechanism of cell death. To verify that p53 and caspase activation is leading to apoptosis, H4 cells undergoing both tau-independent (APP/C31) and tau-dependent (APP/C31/352PHPtau) cell death were stained with Annexin V. A large population of H4 cells undergoing both tau-independent and tau-dependent cell death were stained by Annexin V, indicating apoptosis is initiated in cell death as shown in Figure 2.10. H4 cells with model

Hirano bodies showed a significant reduction in the amount of Annexin V positive cells compared to H4 cells without model Hirano bodies (*$p < 0.05$) as shown in Figure 2.10. This observation is consistent with the results above that Fe65, Tip60, caspases, and p53 are involved in both tau-independent and tau-dependent cell death and that model Hirano bodies protect against cell death.

Our results show that Hirano bodies protect against cell death induced by APP/C31 and AICDc58 in the presence or absence of 352PHPtau. Both tau and the c-terminal region of APP have been shown to co-localize with Hirano bodies in post mortem samples as well as in model Hirano bodies in cell culture (8,37,45,49). This suggests that the protective role of Hirano bodies may be due to sequestering these proteins. To determine if C31 and 352PHPtau co-localize with model Hirano bodies, H4 cells were transfected with C31/352PHPtau and either CT-GFP to induce model Hirano bodies or pEGFPN-1 as a control. In GFP control cells, 352PHPtau is predominantly found in the cytoplasm while APP-C31-myc is uniformly distributed throughout the cell as shown in Figure 2.11. Surprisingly, in the presence of model Hirano bodies, APP-C31-myc and 352PHPtau are predominantly co-localized with model Hirano bodies. Although APP-C31-myc and 352PHPtau co-localize with model Hirano bodies (Figure 2.7) and cell death induced by these proteins is reduced in the presence of model Hirano bodies, it does not prove that model Hirano bodies reduce cell death by sequestration of these proteins. To address whether the presence of model Hirano bodies protect cells from death specifically, H4 cells expressing GFP or CT-GFP were incubated with and without 100 μM etoposide, a well characterized inducer of apoptosis. Expression of either GFP or CT-GFP in the absence of etoposide results in very low levels of cell death as shown in Figure 2.12. Cells expressing both GFP and CT-GFP incubated with etoposide had a significant increase in cell death (***$p <$

0.005). The presence of model Hirano bodies had no impact on cell death induced by etoposide. Thus, model Hirano bodies have some specificity protecting against cell death.

DISCUSSION:

The cause of Alzheimer's disease is unknown (13). The amyloid cascade hypothesis and subsequent refinement that oligomeric species of abeta contribute to neuronal cell death provide a framework for investigation and explains a wide range of data (16,18,62,63). AICD is an intracellular product of the processing of APP that produces amyloid-beta. The role of AICD in neurodegeneration is controversial. The lifetime of AICD is short (64,65) (but tagged versions have a longer lifetime (66-68)) impeding efforts to identify which cellular pathways it participates in. In spite of this, it has been shown that AICD does activate gene transcription but there are many targets that vary depending on the cell line and strategy used in the investigation (reviewed in (14,24,69)). All of these factors lead to controversy and caution in ascribing signaling activity to AICD.

In this study, we have investigated the role of Hirano bodies, intracellular F-actin-rich inclusions, found in a variety of post-mortem neurodegenerative diseases including Alzheimer's disease (6,39,70,71) and cell death induced by APP, AICDc58 and C31 and tau. Previously, we had shown that the presence of model Hirano bodies reduced transcription of AICDc58 and Fe65 and reduced AICDc58-induced cell death (49). We have shown that the intracellular c-terminal fragments of APP, AICDc58 and C31 both induce cell death but that C31 requires the presence of APP to achieve significant levels of cell death. In addition, AICDc58-induced death increases in the presence of APP. These results are in agreement with previous results (49,50,55,72 2287,73,74). The presence of model Hirano bodies significantly reduce the level of cell death.

Transcription and Cell Death

Since the transactivating activity of the APP/Fe65/Tip60 complex has been consistently observed (reviewed in (24,25,74,75)), we utilized mutants in either Fe65 or Tip60 to elucidate whether they play a role in cell death induced by exogenous AICDc58 or APP/C31. Mutations within the active site of Tip60 reduce AICD transcriptional activity and prevent AICD-induced cell death (55,56,76). Our data is consistent with the gene activation activity of this complex since expression of dominant negative mutant Fe65 and Tip60 significantly reduce both APP/c31 and APP/C31/352PHPtau-induced cell death.

Our results disagree with a prior study which showed a mutant form of AICD (Y682A/Y687A) that was suggested not to bind Fe65, was still active in promoting cell death (55). A possible explanation for this discrepancy is that the AICD mutation (Y682A/Y687A) was not proven to prevent interaction with Fe65 (55). Furthermore, AICD mutants with either Y682A or Y687A reduce, but do not abolish the interaction of AICD with Fe65. In contrast, the C655F Fe65 mutant used in our study has been shown to prevent this interaction (56). Thus, all work is consistent with the finding that Fe65 and Tip60 contribute to AICD-induced cell death.

While the mechanism of AICD and tau-dependent cell death is unknown, AICD-induced cell death in the absence of tau involves induction of apoptosis (55). We have shown that APP/C31 also induces apoptosis. Tip60 has been shown to regulate the specificity of p53, activating transcriptional preference for pro-apoptotic genes (58-60). Furthermore, presenilin-dependent release of AICD is reported to enhance activity and expression of p53 to promote neurodegeneration (57). An additional report shows that Fe65 can either activate or repress target genes, and promote cell death by controlling expression of caspase 4 (77). Our data is

consistent with these findings since our results show that cell death requires both p53 and caspase activation and cells were stained with Annexin V.

While the cause of neurodegenerative diseases is unknown, there are data that suggests that AICD and/or C31 may play a role. AICD levels have been shown to be significantly higher in AD patient brains compared to age matched controls and correlates to levels of phosphorylated tau in these brains (78,79). Caspase cleaved APP is also higher in AD brains suggesting that C31 is produced at a much higher rate in AD patients (80). Additionally, there is evidence that c-terminal fragments of APP could associate with amyloid beta-induced cell death by a mechanism involving amyloid beta binding directly to APP, inducing its cleavage (50,81). In addition, AICD expression in mice has been shown to increase levels of insoluble tau and phosphorylated tau, impaired neurogenesis, and promoted neurodegeneration compared to wild type mice (78,82). These transgenic mice also show susceptibility to excitotoxicity stressors, which do not affect wild type mice (83,84). In contrast, a small subset of the familial mutations found in presenilin 1 have been shown to decrease AICD production, suggesting that AICD might not play a role in Alzheimer's disease (85). The mutant presenilins also lower notch intracellular domain levels (85). However, the gamma secretase complex has over 50 substrates in cells and other signaling pathways may also be affected by these presenilin mutations (86).

In addition, the role of AICD and Fe65 has been investigated in model mice overexpressing these proteins. Transgenic mice have elevated levels of active GSK-3β, which is also observed with AD patients (87). These mice also exhibit hyperphosphorylated tau, increased levels of insoluble tau, and neurodegeneration also found in Alzheimer's patients (78). Finally, APP (D664A) mutant mice which cannot be cleaved by caspases have reduced levels of seizures

compared to APP transgenic mice (84), suggesting a role for further proteolytic processing of AICD to C31 in neurodegeneration.

Interaction of Tau and c-terminal Fragments of APP

The interaction of tau with APP and its proteolytic fragments in the progression of Alzheimer's disease has been shown in numerous studies (reviewed (16,62)). However, a direct link between tau and AICD in cell death has not been documented. We have shown for the first time that both AICDc58 as well as APP/C31-induced cell death significantly increases in the presence of 352PHPtau, a mutant form of tau that mimics hyperphosphorylation (1,2). The amount of exogenous APP required to induce cell death in the presence of both C31 and 352PHPtau is lower than for APP/C31 alone. Furthermore, the amount of cell death induced by exogenous APP/C31/352PHPtau is greater than that induced by either APP/C31 or 352PHPtau alone, indicating a relationship between APP, C31, and tau in causing cell death. The presence of model Hirano bodies significantly decreased the level of cell death. In contrast, 352WTtau, unlike 352PHPtau did not significantly increase AICDc58-induced cell death. The mechanism underlying the ability of 352PHPtau to significantly increase AICDc58-induced cell death compared to 352WTtau is not clear. It has been shown that phosphorylation of specific residues on tau is required to prime tau for additional phosphorylation (88-91). It has also been shown that 352PHPtau becomes phosphorylated in cell cultures (92). It is possible that the additional phosphorylation of 352PHPtau contributes to the enhanced cell death observed in the presence of either AICDc58 or C31 but the exact mechanism is unknown.

Numerous prior studies support the interaction of APP and tau in progression of Alzheimer's disease. A link between APP and tau has been supported in whole animal models

(30,31,93). Others have shown that cognitive decline in transgenic mice, due to expression of familial disease mutant forms of APP, are ameliorated by deletion of tau (30,31,94). It has recently been shown that amyloid-beta can cause tau hyperacetylation in primary neurons through an unknown mechanism (93,95). Acetylation of tau prevents its degradation by competing with ubiquitination, which targets tau to the proteasome. Phosphorylated forms of tau begin to accumulate leading to hyperphosphorylated states (93). We suggest tau enhances the level of APP/AICDc58 and APP/C31-induced cell death could contribute to progression of Alzheimer's disease.

Model Hirano bodies protect against cell death

Hirano bodies are found in increased frequency in autopsied brains with neurodegenerative diseases compared to control brains (6,39,70,71). The physiological role of Hirano bodies is unknown. Development of cell culture and transgenic mouse models of Hirano bodies provide avenues of study that are not available using autopsy and necropsy samples (45,46) to determine the physiological role of Hirano bodies. Our results obtained using the cell culture model system show that cell death induced by either APP/C31 in the presence or absence of 352PHPtau or APP/AICDc58 is significantly reduced in the presence of model Hirano bodies. Both tau and the c-terminal region of APP have been shown to co-localize with Hirano bodies in post-mortem samples as well as in model Hirano bodies in cell culture (8,37,45,49). In addition, the APP binding adaptor protein Fe65 has also been shown to co-localize with Hirano bodies in brain and cell cultures (8,49). Both C31 and 352PHPtau co-localize with model Hirano bodies, but unlike 352PHPtau, the distribution of C31 changes from diffuse in control samples to concentrated and co-localized with Hirano bodies. The interaction of tau with Hirano bodies could occur through tau and its phosphorylated forms binding directly to F-actin (96). Other

findings in different experimental models suggest that tau promotes the formation of Hirano bodies and that actin promotes tau-dependent toxicity (96,97). It is not known if specific isoforms of tau or whether phosphorylation of tau is required for interaction with model Hirano bodies.

We suggest that model Hirano bodies could confer protection against cell death by sequestering c-terminal fragments of APP and possibly tau, preventing them from either participating in signaling pathways which contribute to cell death or gene transcription. Model Hirano bodies can be degraded by either autophagy or through the proteasome pathway (98). Via these pathways, deleterious proteins bound to the model Hirano bodies are cleared from the cell, possibly conferring protection from cell death. We showed that model Hirano bodies are unable to protect cells against etoposide-induced apoptosis. This lack of protection suggests that Hirano bodies may have a specific role in protection against cell death.

It will be important in the future to determine the effects of model Hirano bodies on the progression of neurodegeneration in animal model systems to determine whether they represent a neuroprotective mechanism.

MATERIALS AND METHODS:

Plasmids: pEGFPN-1 was obtained from Clontech. CT-EGFP was previously described (45). APPc58-myc was generously provided by Dr. Bradley T. Hyman, Harvard Medical School (55). APP was generously provided by Dr. Thomas C. Sudhof, Stanford University School of Medicine (56,76). 352tau is fetal human tau (352 residues) and 352PHP-tau is fetal human tau (352 residues) with S198, S199, S202, T231, S235, S396, S404, S409, S413, and S422 mutated to glutamate to mimic phosphorylated residues was generously provided by Dr. Roland Brandt,

University of Heidelberg (2). APP-C31-myc was constructed by deleting the coding region of c58-myc from APPc58-myc, inserting the coding sequence of C31 (664-695 of APP) made by PCR amplification using APPc58-myc as a template, and ligating into plasmid that remained from APPc58-myc after deletion of the APPc58-myc coding sequence. Mutagenesis of Tip60 and Fe65 (56,76) (generously provided by Dr. Thomas C. Sudhof, Stanford University School of Medicine) were performed using Stratagene Quickchange mutagenesis kit. DNA sequencing (Genewiz) was performed to confirm sequence fidelity of the Q377E G380E Tip60 and C655F Fe65 mutations and APPc31-myc.

Cell Culture and Transfection: All cell lines were grown in DMEM supplemented with 10% fetal bovine serum (FBS) at 37°C and 5% CO_2. Cells were plated in a 96-well plate (Nunc) or 35 mm dishes approximately 24 hours prior to transfection. Transient transfections were performed using Fugene 6 (Roche Diagnostics) or Lipofectamine LTX with Plus reagent (Invitrogen) according to the manufacturer's recommendations. Approximately 4 hours after transfection, cells were washed with PBS, resuspended in DMEM plus 10% FBS and grown for approximately 48 hours before cell death assays were performed. N2A mouse neuroblastoma cells (ATCC) were transfected using Fugene 6 with 2.5 μg APPc58-myc, 1 μg APP-C31-myc, and 2 μg pEGFPN-1 or CT-EGFP. H4 human astroglioma cells (ATCC) were transfected with Fugene 6 with 3 μg or 1.5 μg APP (tau-dependent and tau-independent conditions, respectively), 1 μg APP-C31-myc and either 2 μg pEGFPN-1 or CT-EGFP for the tau-independent assays. For tau-dependent assays, 1 μg 352PHP-tau or 352WTtau was used. For AICDc58 experiments, 1 μg APPc58-myc, 1.5 μg APP, and 1 μg 352PHPtau or 352WTtau were used. Other experiments used 3 μg APP, 3.5 μg APPc58-myc, and 1 μg APP-C31myc with either 2 μg of pEGFPN-1 or

CT-EGFP. For experiments with Fe65 and Tip60, 1 μg Q377E G380E Tip60 or C655F Fe65 was used. Lipofectamine LTX transfection was used in Figures 2.4 and 2.11 with 250 ng of APP, APPc58-myc, 352PHPtau, 352WT tau, pEGFPN-1 or CT-EGFP.

Flow cytometry was used to verify that the presence of multiple plasmids did not affect the level of protein expression (Figure 2.13).

Inhibitors used during the cell death assays were added immediately after removal of the Fugene 6 transfection reagent. A final concentration of 20 μM α-pifithrin (Sigma) and 100 μM caspase inhibitors Z-IGTD-FMK (caspase 8), Z-DEVD-FMK (caspase3), and Ac-VAD-CHO (broad caspases) (MP Biomedicals) were used and incubated for 48 hours before cell death assays were performed. A final concentration of 100 μM etoposide (Sigma-Aldrich) was added approximately 24 hours after the transfection reagent was removed. After two hours, cells were washed with PBS and resuspended in DMEM plus 10% FBS and incubated at 37°C with 5% CO_2 for 16 hours prior to cell death assays.

Cell Death Assays: Cells were incubated with 9 nM Sytox Orange nucleic acid dye (Invitrogen) and 264 μM Hoechst 33258 at 37°C and 5% CO_2 for 10 minutes prior to microscopy. Fluorescence and visible cell images were obtained using a Zeiss IM-35 epi-fluorescence microscope equipped with a CCD 300-T-RC camera (Dage MTI) controlled by Scion Image software. GFP and Sytox Orange fluorescence and phase images were superimposed in Photoshop and live and dead cells were counted (see supplemental material for representative images S2). Since N2A and H4 cell lines have low transfection efficiencies (~15%), the

presence of EGFP or CT-EGFP was used to indicate transfected cells. A minimum of 50 cells was counted per sample and each condition was sampled at least three independent times. The mean value is plotted in the histograms with error bars representing the standard deviation. Statistics were performed using the Student's T-test.

Annexin V Staining: Approximately 24 hours after transfection, cells were washed with annexin binding buffer (10 mM HEPES, 140 mM NaCl, 2.5 mM $CaCl_2$, pH 7.4) and stained with 5 μL Pacific blue-conjugated annexin V (Invitrogen) for 30 minutes at 37°C and 5% CO_2. Cells were washed once with annexin V binding buffer, re-suspended in annexin V binding buffer with 9 nM Sytox orange, and incubated at 37°C and 5% CO_2 for 15 minutes prior to assessment by fluorescence microscopy (see Figure 2.14 for representative images). The fraction of apoptotic cells were scored as GFP positive cells that were also Annexin V positive divided by the total number of GFP positive cells. Sytox orange was utilized to eliminate Annexin V positive cells that had a compromised membrane. A minimum of 50 cells was counted per sample and each condition was sampled at least three independent times. The mean value is plotted in the histograms with error bars representing the standard deviation. Statistics were performed using the Student's T-test.

Immunofluorescence: Approximately 24 hours prior to transfection, cells were plated onto glass coverslips. Cells were cotransfected with 1.5 μg each of pEGFPN-1 or CT-GFP and 352PHPtau/APP-C31-myc using 3.5 μL Lipofectamine LTX and 1.0 μL Plus reagent according to the manufacturer's instructions (Invitrogen). Approximately 4 hours after transfection, cells were washed with PBS, resuspended in DMEM with 10% FBS. Approximately 24 hours after transfection, the cells were washed in PBS and fixed for 10 minutes in 3.7% formaldehyde in PBS and 1.0 mM EGTA (pH 7.0). Cells were permeablized for 5 minutes in 0.1% Triton X-100

in PBS and 1 mM EGTA (pH 7.0). Cells were washed three times in PBS and blocked for 1 hour with 10.0% BSA in PBS. Cells were washed three times in PBS and incubated with mouse anti-myc 1:1000 (Cell Signaling) and rabbit anti-FLAG 1:100 (Sigma) primary antibodies for 1 hour. After three washes in PBS, cells were incubated with Alexa 350-labeled goat anti-rabbit 1:200 (Invitrogen) and TRITC-labeled goat anti-mouse 1:700 (Sigma) secondary antibodies for 1 hour. Cells were washed three times in PBS and mounted with Crystal Mount (Biomeda). Images were obtained using a Deltavision microscope and subjected to deconvolution using Applied Precision software.

ACKNOWLEDGEMENTS:

The authors thank Drs. T. Sudhof (Stanford) and B. Hyman (Harvard) for generously providing the APP, APPc58-myc, Tip60 and Fe65 plasmids. The authors thank Dr. R. Brandt (University of Osnabrück) for the generously providing the 352tau and 352PHPtau plasmids. The authors acknowledge the University of Georgia Coverdell Core Microscopy Center for access to the Deltavision microscope.

REFERENCES:

1. Eidenmüller, J., Fath, T., Maas, T., Pool, M., Sontag, E., and Brandt, R. (2001) Phosphorylation-mimicking glutamate clusters in the proline-rich region are sufficient to simulate the functional deficiencies of hyperphosphorylated tau protein. *Biochem. J.* **357**, 759-767

2. Fath, T., Eldenmüller, J., and Brandt, R. (2002) Tau-mediated cytotoxicity in a pseudohyperphosphorylation model of Alzheimer's disease. *J. Neurosci.* **22**, 9733-9741

3. Mott, R. T., and Hulette, C. M. (2005) Neuropathology of Alzheimer's disease. *Neuroimaging Clin N Am* **215**, 755-765

4. Gibson, P. H., and Tomlinson, B. E. (1977) Numbers of Hirano bodies in the hippocampus of normal and demented people with Alzheimer's disease. *J Neurol Sci* **33**, 199-206

5. Schochet, S. S., Jr., Lampert, P. W., and Lindenberg, R. (1968) Fine structure of the Pick and Hirano bodies in a case of Pick's disease. *Acta Neuropathol (Berl)* **11**, 330-337

6. Yamamoto, T., and Hirano, A. (1985) Hirano bodies in the perikaryon of the Purkinje cell in a case of Alzheimer's disease. *Acta Neuropathol* **67**, 167-169

7. Hirano, A. (1994) Hirano bodies and related neuronal inclusions. *Neuropathol Appl Neurobiol* **20**, 3-11

8. Mitake, S., Ojika, K., and Hirano, A. (1997) Hirano bodies and Alzheimer's disease. *Kao Hsiung I Hsueh Ko Hsueh Tsa Chih* **13**, 10-18

9. Hartley, D. M., Walsh, D. M., Ye, C. P., Diehl, T., Vasquez, S., Vassilev, P. M., Teplow, D. B., and Selkoe, D. J. (1999) Protofibrillar intermediates of amyloid beta-protein induce acute electrophysiological changes and progressive neurotoxicity in cortical neurons. *J. Neurosci.* **19**, 8876-8884

10. Walsh, D. M., Klyubin, I., Fadeeva, J. V., Cullen, W. K., Anwyl, R., Wolfe, M. S., Rowan, M. J., and Selkoe, D. J. (2002) Naturally secreted oligomers of amyloid beta protein potently inhibit hippocampal long-term potentiation in vivo. *Nature* **416**, 535-539

11. Westerman, M. A., Cooper-Blacketer, D., Mariash, A., Kotilinek, L., Kawarabayashi, T., Younkin, L. H., Carlson, G. A., Younkin, S. G., and Ashe, K. H. (2002) The relationship between Abeta and memory in the Tg2576 mouse model of Alzheimer's disease. *J. Neurosci.* **22**, 1858–1867

12. Cacucci, F., Yi, M., Wills, T. J., Chapman, P., and O'Keefe, J. (2008) Place cell firing correlates with memory deficits and amyloid plaque burden in Tg2576 Alzheimer mouse model. *Proc Natl Acad Sci U S A* **105**, 7863-7868

13. Pimplikar, S. W. (2009) Reassessing the amyloid cascade hypothesis of Alzheimer's disease. *Int. J. Biochem. Cell Biol.* **41**, 1261-1268

14. Zheng, H., and Koo, E. H. (2011) Biology and pathophysiology of the amyloid precursor protein. *Mol Neurodegener* **6**, 27

15. Hardy, J., and Selkoe, D. J. (2002) The amyloid hypothesis of Alzheimer's disease: Progress and problems on the road to therapeutics. *Science* **297**, 353-356

16. Marcello, E., Epis, R., Saraceno, C., and Di Luca, M. (2012) Synaptic dysfunction in Alzheimer's disease. *Adv. Exp. Med. Biol.* **970**, 573-601

17. Koffie, R. M., Hyman, B. T., and Spires-Jones, T. L. (2011) Alzheimer's disease: synapses gone cold. *Mol Neurodeg* **6**, 63-72

18. Benilova, I., Karran, E., and De Strooper, B. (2012) The toxic ab oliogmer and Alzheimer's disease: an emperor in need of clothes. *Nat. Neurosci.* **15**, 349-357

19. Dyrks, T., Weidemann, A., Multhaup, G., Salbaum, J. M., Lemaire, H. G., Kang, J., Muller-Hill, B., Masters, C. L., and Beyreuther, K. (1988) Identification, transmembrane orientation and biogenesis of the amyloid A4 precursor of Alzheimer's disease. *Embo J* **7**, 949-957

20. Glenner, G. G., and Wong, C. W. (1984) Alzheimer's disease: initial report of the purification and characterization of a novel cerebrovascular amyloid protein. *Biochem Biophys Res Commun* **120**, 885-890

21. Kang, J., Lemaire, H. G., Unterbeck, A., Salbaum, J. M., Masters, C. L., Grzeschik, K. H., Multhaup, G., Beyreuther, K., and Muller-Hill, B. (1987) The precursor of Alzheimer's disease amyloid A4 protein resembles a cell-surface receptor. *Nature* **325**, 733-736

22. Hardy, J. (2006) A hundred years of Alzheimer's disease research. *Neuron* **52**, 3-13

23. Muller, T., Meyer, H. E., Egensperger, R., and Marcus, K. (2008) The amyloid precursor protein intracellular domain (AICD) as modulator of gene expression, apoptosis, and cytoskeletal dynamics-relevance for Alzheimer's disease. *Prog Neurobiol* **85**, 393-406

24. Beckett, C., Nalivaeva, N. N., Belyaev, N. D., and Turner, A. J. (2012) Nuclear signalling by membrane protein intracellular domains: The AICD enigma. *Cell Signal* **24**, 402-409

25. Pardossi-Piquard, R., and Checler, F. (2012) The physiology of the b-amyloid precursor protein intracellular domain AICD. *J. Neurochem.* **120 (Suppl. 1)**, 109-124

26. Kosik, K. S., Joachim, C. L., and Selkoe, D. J. (1986) Microtubule-associated protein tau (tau) is a major antigenic component of paired helical filaments in Alzheimer disease. *Proc Natl Acad Sci U S A* **83**, 4044-4048

27. Grundke-Iqbal, I., Iqbal, K., Quinlan, M., Tung, Y. C., Zaidi, M. S., and Wisniewski, H. M. (1986) Microtubule-associated protein tau. A component of Alzheimer paired helical filaments. *J. Biol. Chem.* **261**, 6084-6089

28. Tsuboi, Y. (2009) Clinical, pathological, and genetic characteristics of frontotemporal dementia and parkinsonism linked to chromosome 17 with mutations in the MAPT and PGRN. *Brain Nerve* **61**, 1285-1291

29. Iqbal, K., Liu, F., C.-X., G., and Grundke-Iqbal, I. (2010) Tau in Alzheimer Disease and related tauopathies. *Curr. Alzheimer Res.* **7**, 656-664

30. Roberson, E. D., Scearce-Levie, K., Palop, J. J., Yan, F., Cheng, I. H., Wu, T., Gerstein, H., Yu, G.-Q., and Mucke, L. (2007) Reducing endogenous tau ameliorates amyloid beta-induced deficits in an Alzheimer's disease mouse model. *Science* **316**, 750-754

31. Vossel, K. A., Zhang, K., Brodbeck, J., Daub, A. C., Sharma, P., Finkbeiner, S., Cui, B., and Mucke, L. (2010) Tau reductioin prevents Abeta-induced defects in axonal transport. *Science* **330**, 198-200

32. Sydow, A., Van der Jeugd, A., Zheng, F., Ahmed, T., Balschun, D., Petrova, O., Drexler, D., Zhou, L., Rune, G., Mandelkow, E., D'Hooge, R., Alzheimer, C., and Mandelkow, E. M. (2011) Tau-induced defects in synaptic plasticity, learning, and memory are reversible in transgenic mice after switching off the toxic tau mutant. *J Neurosci* **31**, 2511-2525

33. Ogata, J., Budzilovich, G. N., and Cravioto, H. (1972) A study of rod-like structures (Hirano bodies) in 240 normal and pathological brains. *Acta Neuropathol* **21**, 61-67

34. Fu, Y., Ward, J., and Young, H. F. (1975) Unusual, rod-shaped cytoplasmic inclusions (Hirano bodies) in a cerebellar hemangioblastoma. *Acta Neuropathol* **31**, 129-135

35. Mori, H., Tomonaga, M., Baba, N., and Kanaya, K. (1986) The structure analysis of Hirano bodies by digital processing on electron micrographs. *Acta Neuropathol* **71**, 32-37

36. Hirano, A., Dembitzer, H. M., Kurland, L. T., and Zimmerman, H. M. (1968) The fine structure of some intraganlionic alterations. *J. Neuropathol. Expt. Neurol.* **27**, 167-182

37. Galloway, P. G., Perry, G., Kosik, K. S., and Gambetti, P. (1987) Hirano bodies contain tau protein. *Brain Res* **403**, 337-340

38. Laas, R., and Hagel, C. (1994) Hirano bodies and chronic alcoholism. *Neuropathol Appl Neurobiol* **20**, 12-21

39. Martinez-Saez, E., Gelpi, E., Rey, M., Ferrer, I., Ribalta, T., Botta-Orfila, T., Nos, C., Yague, J., and Sanchez-Valle, R. (2011) Hirano body - rich subtypes of Creutzfeldt-Jakob disease. *Neuropathol Appl Neurobiol*

40. Galloway, P. G., Perry, G., and Gambetti, P. (1987) Hirano body filaments contain actin and actin-associated proteins. *J Neuropathol Exp Neurol* **46**, 185-199

41. Goldman, J. E. (1983) The association of actin with Hirano bodies. *J Neuropathol Exp Neurol* **42**, 146-152

42. Schochet, S. S., Jr., and McCormick, W. F. (1972) Ultrastructure of Hirano bodies. *Acta Neuropathol* **21**, 50-60

43. Izumiyama, N., Ohtsubo, K., Tachikawa, T., and Nakamura, H. (1991) Elucidation of three-dimensional ultrastructure of Hirano bodies by the quick-freeze, deep-etch and replica method. *Acta Neuropathol* **81**, 248-254

44. Maselli, A. G., Davis, R., Furukawa, R., and Fechheimer, M. (2002) Formation of Hirano bodies in Dictyostelium and mammalian cells induced by expression of a modified form of an actin cross-linking protein. *J. Cell Sci.* **115**, 1939-1952

45. Davis, R. C., Furukawa, R., and Fechheimer, M. (2008) A cell culture model for investigation of Hirano bodies. *Acta Neuropathol* **115**, 205-217

46. Ha, S., Furukawa, R., Stramiello, M., Wagner, J. J., and Fechheimer, M. (2011) Transgenic mouse model for the formation of Hirano bodies. *BMC Neurosci* **12**, 97

47. Munoz, D. G., Wang, D., and Greenberg, B. D. (1993) Hirano bodies accumulate C-terminal sequences of beta-amyloid precursor protein (beta-APP) epitopes. *J Neuropathol Exp Neurol* **52**, 14-21

48. Maselli, A. G., Furukawa, R., Thomson, S. A. M., Davis, R. C., and Fechheimer, M. (2003) Formation of Hirano bodies induced by expression of an actin cross-linking protein with a gain of function mutation. *Eucaryot. Cell* **2**, 778-787

49. Ha, S., Furukawa, R., and Fechheimer, M. (2011) Association of AICD and Fe65 with Hirano bodies reduces transcriptional activation and initiation of apoptosis. *Neurobiol Aging* **32**, 2287-2298

50. Lu, D. C., Soriano, S., Bredesen, D. E., and Koo, E. H. (2003) Caspase cleavage of the amyloid precursor protein modulates amyloid beta-protein toxicity. *J. Neurochem.* **87**, 733-741

51. Dickey, C. A., Eriksen, J., Kamal, A., Burrows, F., Kasibhatla, S., Eckman, C. B., Hutton, M., and Petrucelli, L. (2005) Development of a high throughput drug screening assay for the detection of changes in tau levels -- proof of concept with HSP90 inhibitors. *Curr Alzheimer Res* **2**, 231-238

52. Bretteville, A., Ando, K., Ghestem, A., Loyens, A., Begard, S., Beauvillain, J. C., Sergeant, N., Hamdane, M., and Buee, L. (2009) Two-dimensional electrophoresis of tau

mutants reveals specific phosphorylation pattern likely linked to early tau conformational changes. *PLoS One* **4**, e4843

53. Gibson, P. H. (1978) Light and electron microscopic observations on the relationship between Hirano bodies, neuron and glial perikarya in the human hippocampus. *Acta Neuropathol (Berl)* **42**, 165-171

54. Garwood, C. J., Pooler, A. M., Atherton, J., Hanger, D. P., and Noble, W. (2011) Astrocytes are important mediators of Abeta-induced neurotoxicity and tau phosphorylation in primary culture. *Cell Death Dis.* **2**, e167

55. Kinoshita, A., Whelan, C. M., Berezovska, O., and Hyman, B. T. (2002) The gamma secretase-generated carboxyl-terminal domain of the amyloid precursor protein induces apoptosis via Tip60 in H4 cells. *J. Biol. Chem.* **277**, 28530-28536

56. Cao, X., and Südhof, T. C. (2004) Dissection of amyloid-beta precursor protein-dependent transcriptional transactivation. *J. Biol. Chem.* **279**, 24601-14611

57. Alves da Costa, C., Sunyach, C., Pardossi-Piquard, R., Sevalle, J., Vincent, B., Boyer, N., Kawarai, T., Girardot, N., St George-Hyslop, P., and Checler, F. (2006) Presenilin-dependent gamma-secretase-mediated control of p53-associated cell death in Alzheimer's disease. *J. Neurosci.* **26**, 6377-6385

58. Tang, Y., Luo, J., Zhang, W., and Gu, W. (2006) Tip60-dependent acetylation of p53 modulates the decision between cell-cycle arrest and apoptosis. *Mol Cell* **24**, 827-839

59. Sykes, S. M., Mellert, H. S., Holbert, M. A., Li, K., Marmorstein, R., Lane, W. S., and McMahon, S. B. (2006) Acetylation of the p53 DNA-binding domain regulates apoptosis induction. *Mol Cell* **24**, 841-851

60. Sykes, S. M., Stanek, T. J., Frank, A., Murphy, M. E., and McMahon, S. B. (2009) Acetylation of the DNA binding domain regulates transcription-independent apoptosis by p53. *J. Biol. Chem.* **284**, 20197-20205

61. Komarov, P. G., Komarova, E. A., Kondratov, R. V., Christov-Tselkov, K., Coon, J. S., Chernov, M. V., and Gudkov, A. V. (1999) A chemical inhibitor of p53 that protects mice from the side effects of cancer therapy. *Science* **285**, 1733-1737

62. Niedowicz, D. M., Nelson, P. T., and Murphy, M. P. (2011) Alzheimer's disease: Pathological mechanisms and recent insights. *Curr. Neuropharm.* **9**, 674-684

63. Karran, E., Mercken, M., and De Strooper, B. (2011) The amyloid cascade hypothesis for Alzheimer's disease: an appraisal for the development of therapeutics. *Nat. Rev. Drug Discov.* **10**, 698-712

64. Kimberly, W. T., Zheng, J. B., Guenette, S. Y., and Selkoe, D. J. (2001) The intracellular domain of the beta-amyloid precursor protein is stabilized by Fe65 and translocates to the nucleus in a notch-like manner. *J. Biol. Chem.* **276**, 40288-40292

65. Cupers, P., Orlans, I., Craessarts, K., Annaert, W., and De Strooper, B. (2001) The amyloid precursor protein (APP)-cytoplasmic fragment generated by gamma-secretase is rapidly degraded but distributes partially in a nuclear fraction of neurons in culture. *J. Neurochem.* **78**, 1168-1178

66. Weidemann, A., Eggert, S., Reinhard, F. B. M., Vogel, M., Paliga, K., Baier, G., MasterS, C. L., Beyreuther, K., and Evin, G. (2002) A novel ε-cleavage within the transmembrane domain of the Alzheimer amyloid precursor protein demonstrates homology with Notch processing. *Biochemistry* **41**, 2825-2835

67. Ren, Z., Schenk, D., Basi, G. S., and Shapiro, I. P. (2007) Amyloid β-protein precursor jextamembrain domain regulates specificty of γ-secretase-dependent cleavages. *J. Biol. Chem.* **48**, 35350-33560

68. Yamasaki, A., Eimer, S., Okochi, M., Smialowska, A., Kaether, C., Baumeister, R., Haass, C., and Steiner, H. (2006) The GxGD motif of presenilin contributes to catalytic function and substrate identification of γ-secretase. *J. Neurosci.* **26**, 3821-3828

69. Zhang, H., Ma, Q., Zhang, Y.-w., and Xu, H. (2012) Proteolytic processing of the Alzheimer's b-amyloid precursor protein. *J. Neurochen,* **120**, 9-21

70. Perl, D. P. (2010) Neuropathology of Alzheimer's disease. *Mt. Sinai J. Med.* **77**, 32-42

71. Yokoo, H., Oyama, T., Hirato, J., Sasaki, A., and Nakazato, Y. (1994) A case of Pick's disease with unusual neuronal inclusions. *Acta Neuropathol. (Berl)* **88**, 604-

72. Passer, B., Pellegrini, L., Russo, C., Siegel, R. M., Lenardo, M. J., Schettini, G., Bachmann, M., Tabaton, M., and D'Adamio, L. (2000) Generation of an Apoptotic Intracellular Peptide by gamma-Secretase Cleavage of Alzheimer's Amyloid beta Protein Precursor. *J. Alzheimers Dis.* **2**, 289-301

73. Chang, K. A., Kim, H. S., Ha, T. Y., Ha, J. W., Shin, K. Y., Jeong, Y. H., Lee, J. P., Park, C. H., Kim, S., Baik, T. K., and Suh, Y. H. (2006) Phosphorylation of amyloid precursor protein (APP) at Thr668 regulates the nuclear translocation of the APP intracellular domain and induces neurodegeneration. *Mol. Biol. Cell* **26**, 4327-4338

74. Chang, K.-A., and Suh, Y.-H. (2010) Possible roles of amyloid intracellular domain of amyloid precusor protein. *BMB Rep.* **43**, 656-663

75. Borquez, D. A., and Gonzalez-Billault, C. (2012) The amyloid precursor protein intracellular domain-Fe65 multiprotein complexes: As challenge to the amyloid hypothesis for Alzheimer's disease? *Int. J. Alzheimers Dis.* **2012**, 353145-353155

76. Cao, X., and Südhof, T. C. (2001) A transcriptionally active complex of APP with Fe65 and histone acetyltransferase Tip60. *Science* **293**, 115-120

77. Kajiwara, Y., Akram, A., Katsel, P., Haroutunian, V., Schmeidler, J., Beecham, G., Haines, J. L., Pericak-Vance, M. A., and Buxbaum, J. D. (2009) FE65 binds Teashirt, inhibiting expression of the primate-specific caspase-4. *PLoS One* **4**, e5071

78. Ghosal, K., Vogt, D. L., Liang, M., Shen, Y., Lamb, B. T., and Pimplikar, S. W. (2009) Alzheimer's disease-like pathological features in transgenic mice expressing the APP intracellular domain. *Proc Natl Acad Sci U S A* **106**, 18367-18372

79. Nakayama, K., Ohkawara, T., Hiratochi, M., Koh, C.-S., and Nagase, H. (2008) Intracellular domain of amyloid precursor protein induces neuron-specific apoptosis. *Neurosci. Lett.* **444**, 127-131

80. Lu, D. C., Rabizadeh, S., Chandra, S., Shayya, R. F., Ellerby, L. M., Ye, X., Salvesen, G. S., Koo, E. H., and Bredesen, D. E. (2000) A second cytotoxic proteolytic peptide derived from amyloid B-protein precursor. *Nature Medicine* **6**, 397-404

81. Lu, D. C., Shaked, G. M., Masliah, E., Bredesen, D. E., and Koo, E. H. (2003) Amyloid beta protein toxicity mediated by the formation of amyloid-beta protein precursor complexes. *Ann. Neurol.* **54**, 781-789

82. Ghosal, K., Stathopoulos, A., and Pimplikar, S. W. (2010) APP intracellular domain impairs adult neurogenesis in transgenic mice by inducing neuroinflammation. *PLoS One* **5**, e11866

83. Ghosal, K., and Pimplikar, S. W. (2011) Aging and excitotoxic stress exacerbate neural circuit reorganization in amyloid precursor protein intracellular domain transgenic mice. *Neurobiol Aging* **32**, 2320 2321-2329

84. Vogt, D. L., Thomas, D., Galvan, V., Bredesen, D. E., Lamb, B. T., and Pimplikar, S. W. (2011) Abnormal neuronal networks and seizure susceptibility in mice overexpressing the APP intracellular domain. *Neurobiol Aging* **32**, 1725-1729

85. Moehlmann, T., Winkler, E., Xia, X., Edbauer, D., Murrell, J., Capell, A., Kaether, C., Zheng, H., Ghetti, B., Haass, C., and Steiner, H. (2002) Presenilin-1 mutations of leucine 166 equally affect the generation of the Notch and APP intracellular domains independent of their effect on Abeta 42 production. *Proc. Natl. Acad. Sci.. U.S.A.* **99**, 8025-8030

86. McCarthy, J. V., Twomey, C., and Wujek, P. (2009) Presenilin-dependent regulated intramembrane proteolysis and gamma-secretase activity. *Cell Mol. Life Sci.* **66**, 1534-1555

87. Ryan, K. A., and Pimplikar, S. W. (2005) Activation of GSK-3 and phosphorylation of CRMP2 in transgenic mice expressing APP intracellular domain. *J. Cell Biol.* **171**, 327-335

88. Cho, J. H., and Johnson, G. V. (2004) Primed phosphylation of tau at Thr231 by glycogen synthase kinase 3beta (GSK3beta) plays a critical role in regulating tau's ability to bind and stabilize microtubules. *J. Neurochem.* **88**, 349-358

89. Li, W., and Lee, V. M. (2006) Characterization of two VQIXXK motifs for tau fibrillization in vitro. *Biochemistry* **45**, 15692-15701

90. Sengupta, S., Horowitz, P. M., Karsten, S. L., Jackson, G. R., Geschwind, D. H., Fu, Y., Berry, R. W., and Binder, L. I. (2006) Degradation of tau protein by puromycin-sensitive aminopeptidase in vitro. *Biochemistry* **45**, 15111-15119

91. Liu, S. J., Zhang, J. Y., Li, H. L., Fang, Z. Y., Wang, Q., Deng, H. M., Gong, C. X., Grundke-Iqbal, I., Iqbal, K., and Wang, J. Z. (2004) Tau becomes a more favorable substrate for GSK-3 when it is prephosphorylated by PKA in rat brain. *J. Biol. Chem.* **279**, 50078-50088

92. Shahani, N., Subramaniam, S., Wolf, T., Tackenberg, C., and Brandt, R. (2006) Tau aggregation and progressive neuronal degeneration in the absence of changes in spine

density and morphology after targeted expression of Alzheimer's disease-relevant tau constructs in organotypic hippocampal slices. *Neurobiol. Dis.* **26**, 6103-6114

93. Min, S. W., Cho, S. H., Zhou, Y., Schroeder, S., Haroutunian, V., Seeley, W. W., Huang, E. J., Shen, Y., Masliah, E., Mukherjee, C., Meyers, D., Cole, P. A., Ott, M., and Gan, L. (2010) Acetylation of tau inhibits its degradation and contributes to tauopathy. *Neuron* **67**, 953-966

94. Roberson, E. D., Halabisky, B., Yoo, J. W., Yao, J., Chin, J., Yan, F., Wu, T., Hamto, P., Devidze, N., Yu, G. Q., Palop, J. J., Noebels, J. L., and Mucke, L. (2011) Amyloid-b/Fyn-induced synaptic, network, and cognitive impairments depend on tau levels in multiple mouse models of Alzheimer's disease. *J. Neurosci.* **31**, 700-711

95. Cohen, T. J., Guo, J. L., Hurtado, D. E., Kwong, L. K., Mills, I. P., Trojanowski, J. Q., and Lee, V. M. (2011) The acetylation of tau inhibits its function and promotes pathological tau aggregation. *Nat Commun* **2**, 252

96. Fulga, T. A., Elson-Schwab, I., Khurana, V., Steinhib, M. L., Spires, T. L., T., H. B., and Feany, M. B. (2007) Abnormal bundling and accumulation of F-actin mediates tau-induced neuronal degeneration in vivo. *Nat. Cell Biol.* **9**, 139-148

97. Santa-Maria, I., Santpere, G., MacDonald, M. J., de Barreda, E. G., Hernandez, F., Moreno, F. J., Ferrer, I., and Avila, J. (2008) Coenzyme Q induces tau aggregation, tau filaments, and Hirano bodies. *J. Neuropathol. Exp. Neurol.* **67**, 428-434

98. Kim, D. H., Davis, R. C., Furukawa, R., and Fechheimer, M. (2009) Autophagy contributes to degradation of Hirano bodies. *Autophagy* **5**, 44-51

Figure 2.1. Model Hirano bodies protect against APP and C31-induced cell death in N2A cells. N2A cells were transfected with APP/APP-C31 in the presence (CT-GFP, check bars) or absence (GFP, black bars) of model Hirano bodies. Either APP or APP-C31-myc causes low amounts of cell death while the presence of both APP and C31 shows an enhanced increase in cell death. Furthermore, model Hirano bodies are able to protect against the enhanced effect of APP/C31-induced cell death (** $p < 0.01$ between cells with and without Hirano bodies). Error bars represent the standard deviation.

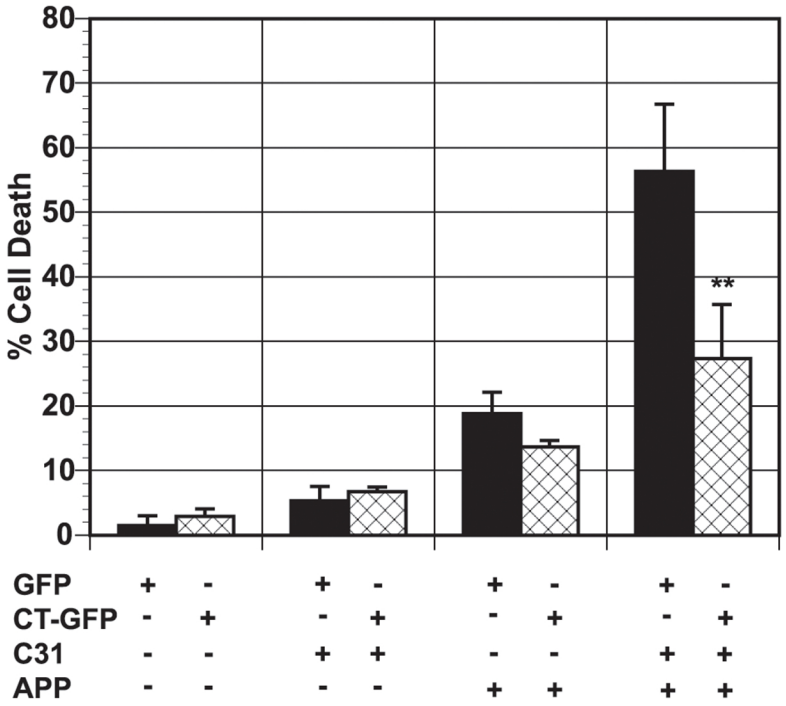
80
70
60
50
40
30
20
10
0
% Cell Death
**
GFP + - + - + - + -
CT-GFP - + - + - + - +
C31 - - + + - - + +
APP - - - - + + + +

Figure 2.2. Model Hirano bodies protect against APP and C31-induced cell death (tau-independent) in H4 cells. Cells were transfected with APP/APP-C31 in the presence (CT-GFP, check bars) or absence (GFP, black bars) of model Hirano bodies. Expression of either APP or APP-C31-myc cause low amounts of cell death while the presence of both APP/C31 caused an enhanced increase in cell death. Furthermore, model Hirano bodies are able to protect against cell death induced by APP (*$p < 0.05$ between cells with and without Hirano bodies) and APP/c31 (** $p < 0.01$ between cells with and without Hirano bodies). Error bars represent the standard deviation.

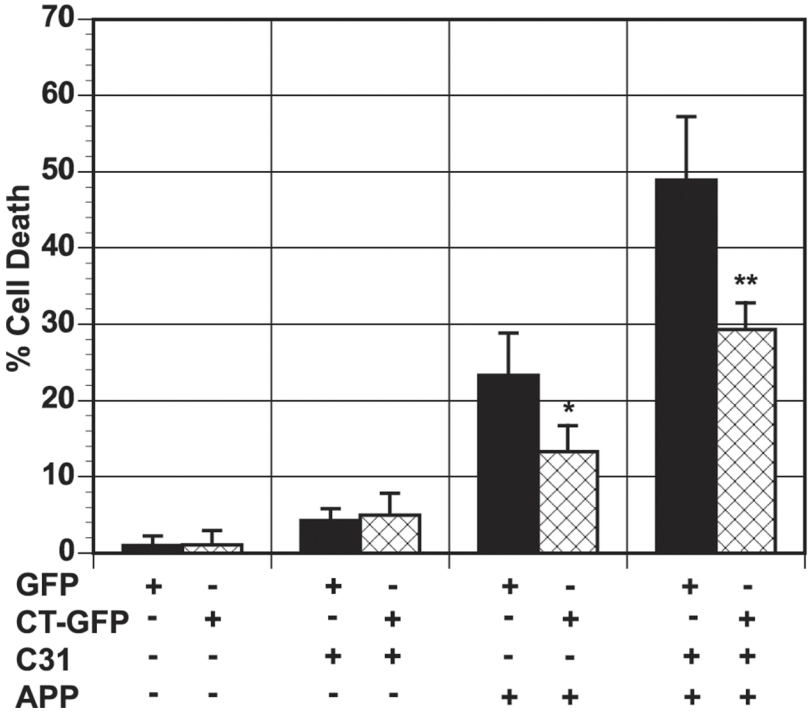
70
60
50
40
30
20
10
0
% Cell Death
*
**
GFP + - + - + - + -
CT-GFP - + - + - + - +
C31 - - + + - - + +
APP - - - - + + + +

Figure 2.3. **Model Hirano bodies protect against AICDc58 and APP/AICDc58-induced cell death.** Cells were transfected with APP and/or AICDc58 in the presence (CT-GFP, check bars) or absence (GFP, black bars) of model Hirano bodies. AICDc58 causes significant cell death in H4 cells in the absence of exogenously expressed APP. Transfection of H4 cells with APP/AICDc58 causes a significant increase in cell death (* $p < 0.05$ in comparison to GFP/AICDc58). The presence of model Hirano bodies significantly protected against AICDc58 and APP-induced cell death (+ $p < .05$ between with and without model Hirano bodies) and APP/AICDc58-induced cell death (++ $p < 0.01$ between with and without model Hirano bodies). Error bars represent the standard deviation.

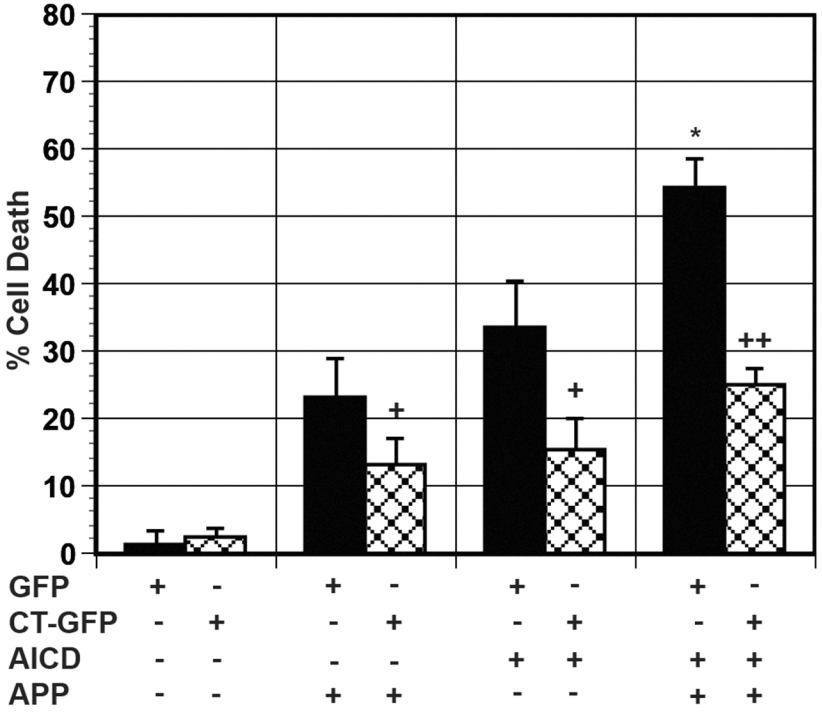
80
70
60
50
40
30
20
10
0
% Cell Death
*
+
+
++
GFP + - + - + - + -
CT-GFP - + - + - + - +
AICD - - - - + + + +
APP - - + + - - + +

Figure 2.4. AICDc58 potentiates 352PHPtau, but not 352WTtau-induced cell death. Cells were transfected with AICDc58/352WTtau or AICDc58/352PHPtau in the presence (CT-GFP, check bars) or absence (GFP, black bars) of model Hirano bodies. Co-transfection of H4 cells with GFP and AICDc58/352WTtau seems to result in cell death that approximates GFP/352WTtau plus GFP/AICDc58 cells. Co-transfection of GFP and AICDc58/352PHPtau significantly enhances cell death compared to GFP/AICDc58 only (***$p < 0.005$) or GFP/AICDc58/352WTtau (**$p < 0.01$). The presence of model Hirano bodies significantly protected against AICDc58-, AICDc58/352WTtau-, and AICDc58/352PHPtau-induced cell death (++$p < 0.01$ compared to cells without model Hirano bodies). Error bars represent the standard deviation.

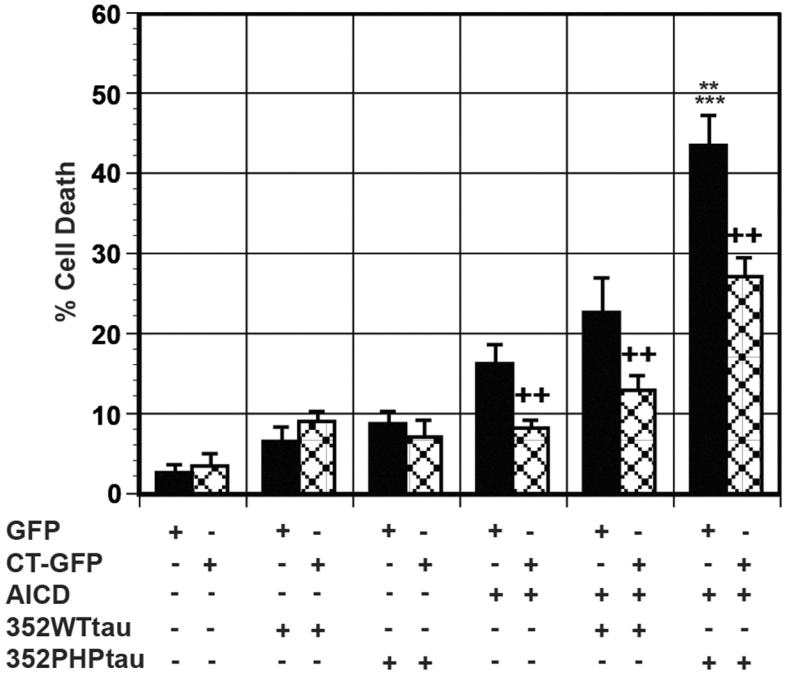
60
50
40
30
20
10
0
% Cell Death
**
***
++
++
++
GFP + - + - + - + - + - + -
CT-GFP - + - + - + - + - + - +
AICD - - - - - - + + + + + +
352WTtau - - + + - - - - + + - -
352PHPtau - - - - + + - - - - + +

Figure 2.5. **Model Hirano bodies protect against tau-dependent cell death.** H4 cells were transfected with APP/C31, and or 353PHPtau in the presence (CT-GFP, check bars) or absence (GFP, black bars) of model Hirano bodies. Transfection of 352PHP tau decreases the amount of exogenous APP (1.5 μg versus 3.0 μg of APP in Figure 2) required to achieve significant enhancement of cell death. Cell death induced by APP/C31/352PHPtau expression is significantly higher than APP/C31 alone (++ $p < 0.01$). Model Hirano bodies protect against tau-dependent cell death (** $p < 0.01$ between with and without model Hirano bodies). Error bars represent the standard deviation.

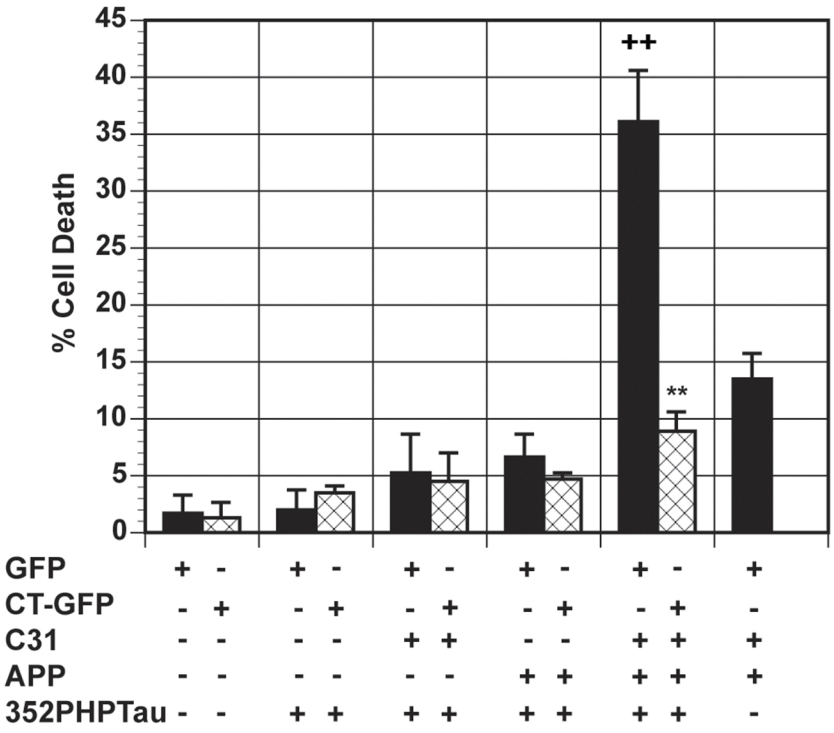
45
40
35
30
25
20
15
10
5
0
% Cell Death
++
**
GFP + - + - + - + - + - +
CT-GFP - + - + - + - + - + -
C31 - - - - + + - - + + +
APP - - - - - - + + + + +
352PHPTau - - + + + + + + + + -

Figure 2.6. **Fe65 contributes to both tau-independent and tau-dependent cell death.** Cells were transfected with either APP/C31 or APP/C31/352PHP/tau in the absence (black bars) or presence of C655F Fe65 (56) (dotted bars). The expression of mutant C655F Fe65 significantly reduced both tau-independent and tau-dependent cell death (*** $p < 0.005$). Error bars represent the standard deviation.

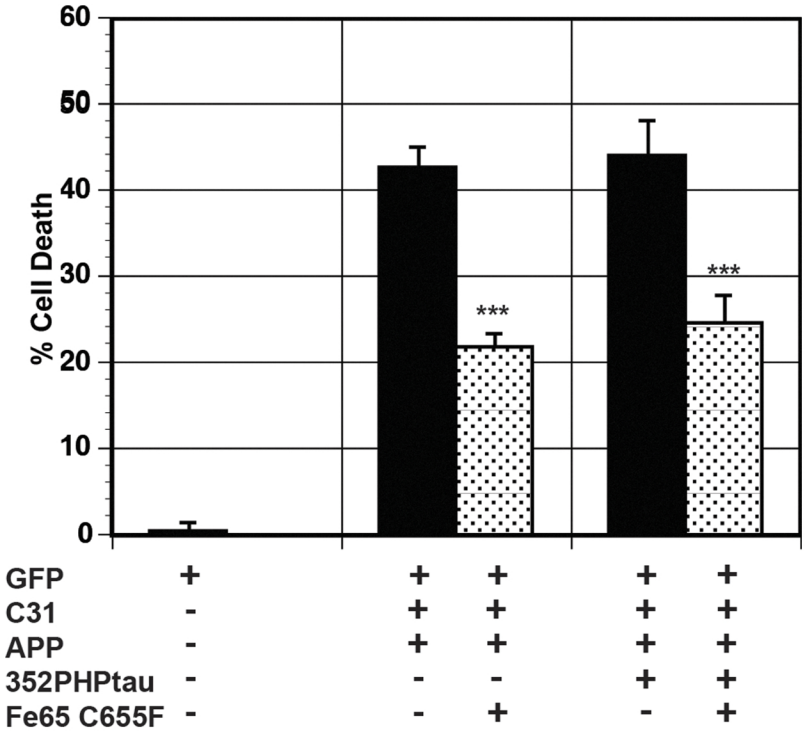
60
50
40
30
20
10
0
% Cell Death
***
***
GFP + + + + +
C31 - + + + +
APP - + + + +
352PHPtau - - - + +
Fe65 C655F - - + - +

Figure 2.7. **Tip60 contributes to both tau-independent and tau-dependent cell death.** Cells were transfected with either APP/C31or APP/C31/352PHPtau in the absence (black bars) or presence (dotted bars) of mutant Q377E G380E Tip60 (mTip60) (55). The expression of mutant Tip60 significantly reduced both tau-independent and tau-dependent cell death (*** $p < 0.005$). Error bars represent the standard deviation.

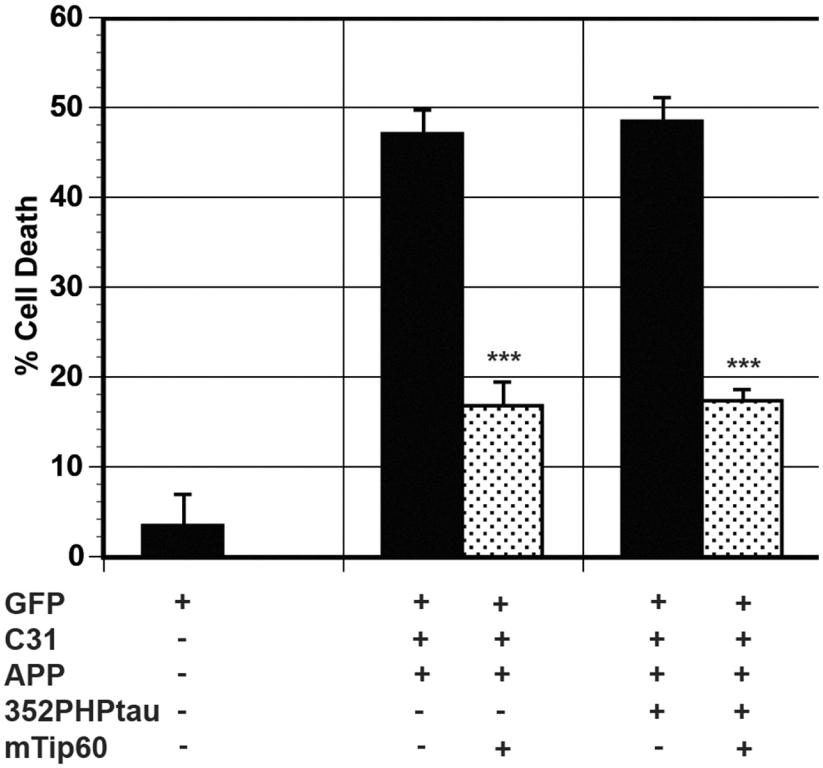
60
50
40
30
20
10
0
% Cell Death
***
***
GFP + + + + +
C31 - + + + +
APP - + + + +
352PHPtau - - - + +
mTip60 - - + - +

Figure 2.8. **p53 contributes to both tau-independent and tau-dependent cell death.** Cells were transfected with either APP/C31 or APP/C31/352PHP/tau in the absence (black bars) or presence (dotted bars) of α-pifithrin. α-pifithrin significantly reduced tau-independent (*** $p < 0.005$) and tau-dependent cell death (** $p < 0.01$). Error bars represent the standard deviation.

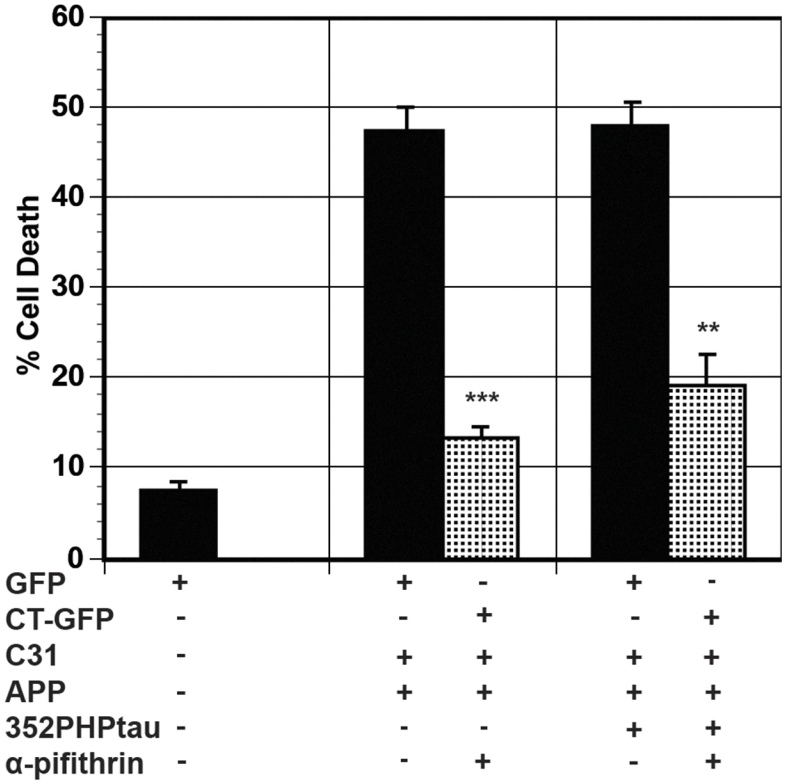
60
50
40
30
20
10
0
% Cell Death
***
**
GFP + + - + -
CT-GFP - - + - +
C31 - + + + +
APP - + + + +
352PHPtau - - - + +
α-pifithrin - - + - +

Figure 2.9. **Caspases contribute to both tau-independent and tau-dependent cell death.** Cells were transfected with either APP/C31 or APP/C31/352PHP/tau in the absence (black bars) or presence of broad caspase inhibitor (Ac-VAD-CHO; striped bar) or caspase 8 inhibitor (Z-IGTD-FMK; white bars) or caspase 3 inhibitor (Z-DEVD-FMK; grey bars). The broad caspase inhibitor and caspase 8 inhibitor significantly reduced tau-independent (APP/C31) cell death (** $p < 0.01$) and tau-dependent cell death (APP/C31/352PHPtau) (* $p < 0.05$). Caspase 3 inhibitor had no significant effect on either kind of cell death. Error bars represent the standard deviation.

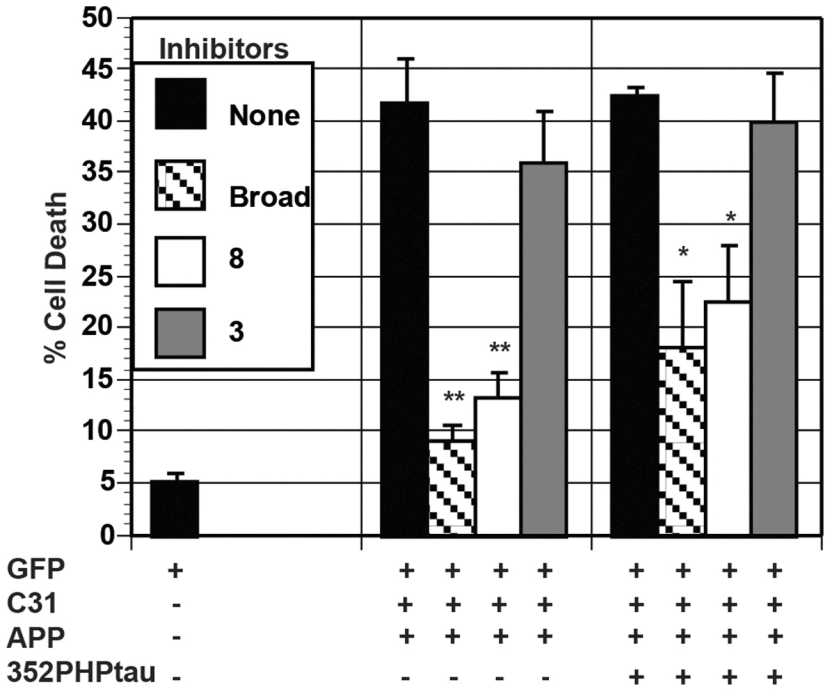
Inhibitors
None
Broad
8
3
% Cell Death
50
45
40
35
30
25
20
15
10
5
0
**
**
*
*
GFP + + + + + + + + +
C31 - + + + + + + + +
APP - + + + + + + + +
352PHPtau - - - - - + + + +

Figure 2.10. **Model Hirano bodies lower tau-dependent and tau-independent apoptosis.** H4 cells were transfected with either APP/C31 or APP/C31/352PHP/tau in the absence (GFP-black bars) or presence of model Hirano bodies (CT-GFP-check bars). H4 cells were stained with the early apoptotic marker annexin V. Sytox orange was used as a control for annexin V false positive cells with compromised membranes. Cells transfected with either GFP/APP/C31 (tau-independent) or GFP/APP/C31/352PHPtau (tau-dependent) showed significant levels of annexin V positive staining. The presence of model Hirano bodies lowered the percent of cells that were annexin V positive in both tau-independent and –dependent cell death (* $p < 0.05$ in comparison to cells without model Hirano bodies). Error bars represent the standard deviation.

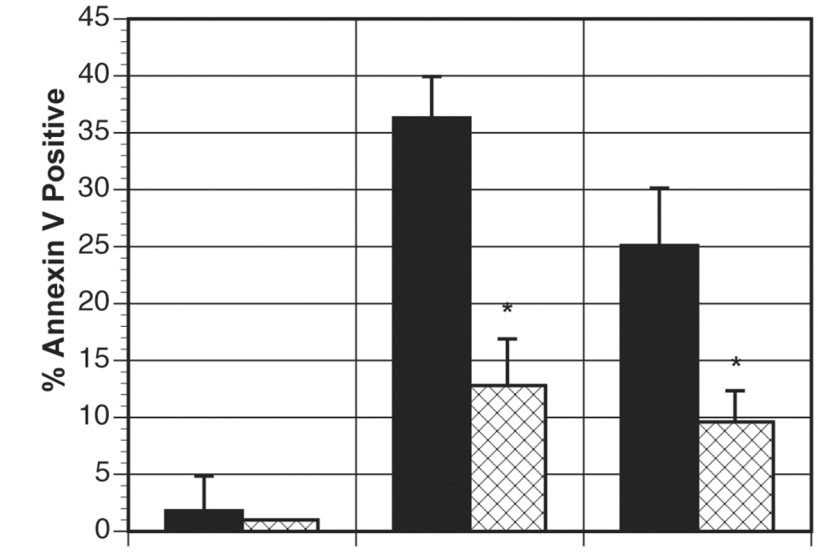

GFP	+	-	+	-	+	-
CT-GFP	-	+	-	+	-	+
C31	-	-	+	+	+	+
APP	-	-	+	+	+	+
352PHPtau	-	-	-	-	+	+

Figure 2.11. **Both 352PHPtau and C31 co-localize with model Hirano bodies**. H4 Cells were transfected with 352PHPtau or C31, and either CT-GFP to induce model Hirano bodies or GFP as a control. In control cells, tau is predominantly found in the cytoplasm while C31 is evenly diffused throughout the cell. In cells expressing CT-GFP, C31 is primarily found co-localizing with model Hirano bodies. Tau also co-localizes with model Hirano bodies, but its overall distribution is not altered. Scale bar 15 μm.

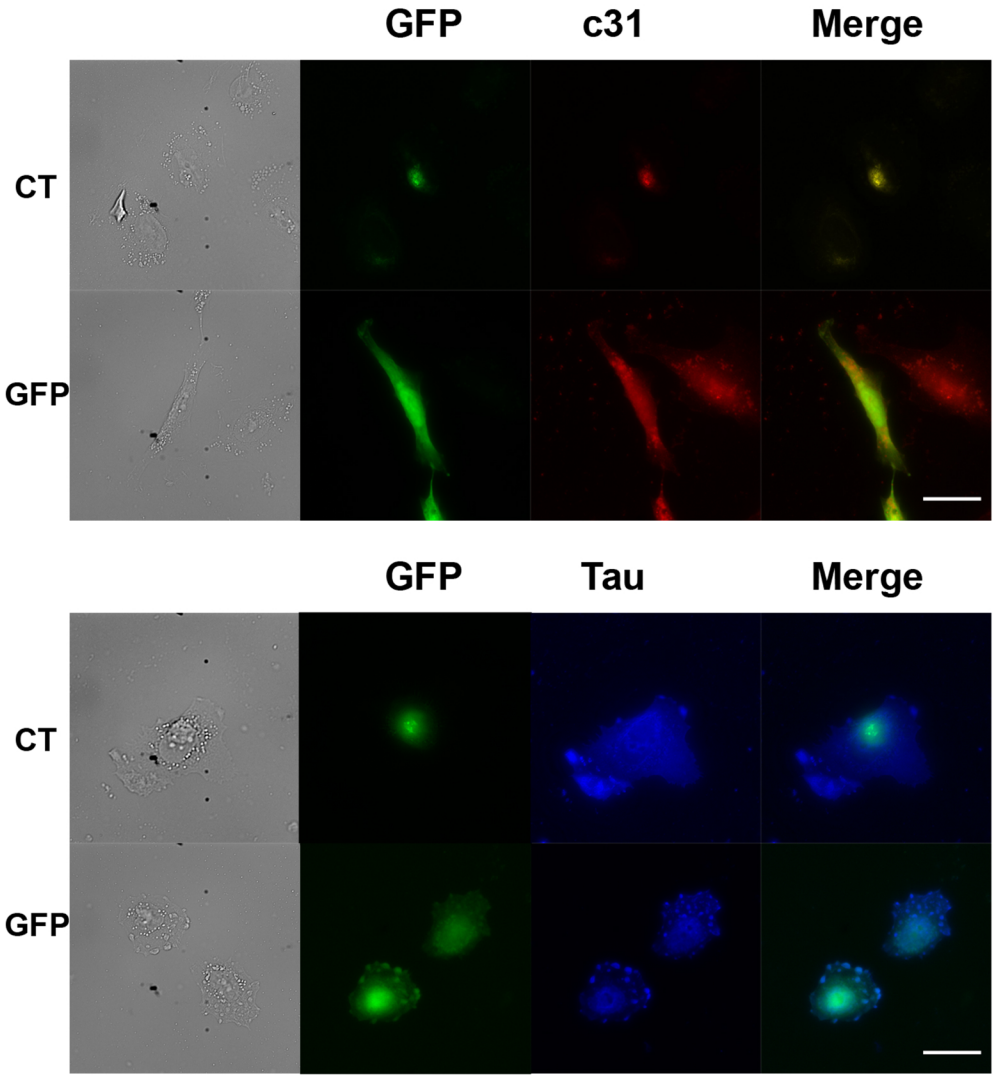
GFP
c31
Merge
CT
GFP
GFP
Tau
Merge
CT
GFP

Figure 2.12. **Model Hirano Bodies do not protect against etoposide-induced cell death.** H4 cells were transfected with CT-GFP to induce Hirano body formation (check bars) or GFP (black bars) as a control. Expression of CT-GFP or GFP alone caused very low levels of cell death in the absence of etoposide. In the presence of 100 μM etoposide, cell death was significantly increased (***$p < 0.005$). The presence of model Hirano bodies had no impact on etoposide-induced cell death. Error bars represent the standard deviation.

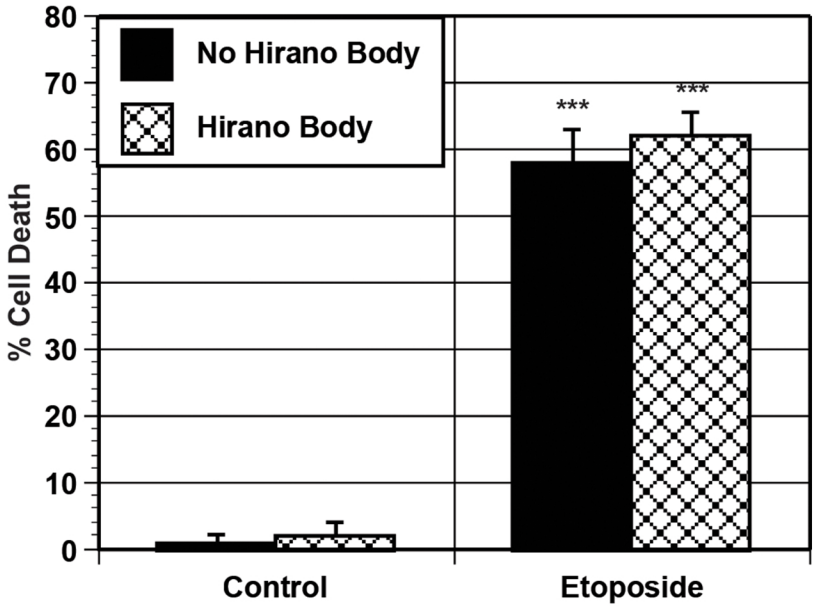
80
70
60
50
40
30
20
10
0
% Cell Death
No Hirano Body
Hirano Body
***
***
Control
Etoposide

Figure 2.13. **Cell death and GFP expression levels are not affected by varying amounts of DNA during co-transfection of multiple plasmids.** H4 cells were transfected with pEGFPN-1 alone or with varying amounts of pcDNA3.1 to replicate co-transfection conditions with 1, 2, or 4 plasmids. Using flow cytometry, it was determined that the median fluorescence intensity of GFP in samples replicating co-transfection of 2 and 4 plasmids were not significantly different from GFP only transfected cells. Additionally, under these conditions cell death levels remained low, indicating that the cell death in our other experiments is not due to an increase in total DNA transfected. Error bar represents the coefficient of variation.

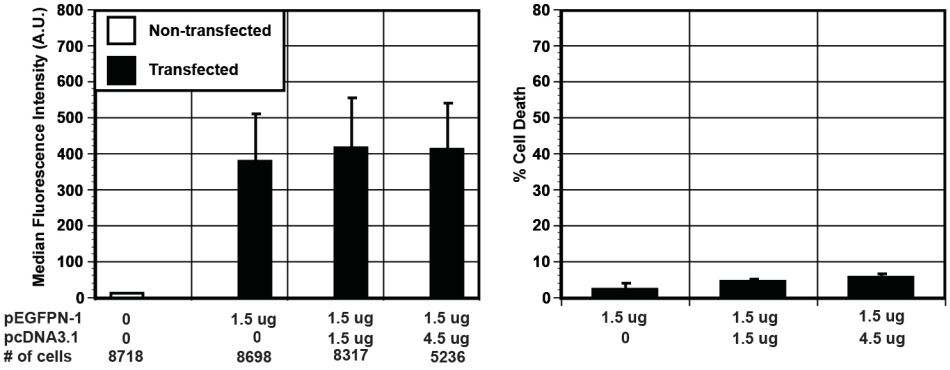
Median Fluorescence Intensity (A.U.)
800
700
600
500
400
300
200
100
0
Non-transfected
Transfected
pEGFPN-1 0 1.5 ug 1.5 ug 1.5 ug
pcDNA3.1 0 0 1.5 ug 4.5 ug
# of cells 8718 8698 8317 5236
% Cell Death
80
70
60
50
40
30
20
10
0
1.5 ug 1.5 ug 1.5 ug
0 1.5 ug 4.5 ug

Figure 2.14. **Representative images of the cell death quantitation**. Live cells transfected with (A) GFP, (B) CT-GFP, GFP/APP/C31 stained with sytox orange (C) or (D) annexin V and Sytox Orange to mark apoptotic cells and rule out compromised membranes, respectively. Green = GFP, Blue = Hoescht 33258 (A and B), annexin V (D). Yellow = GFP and sytox orange. Arrows in C indicate nuclei stained with Sytox Orange. Scale bar = 20 mm

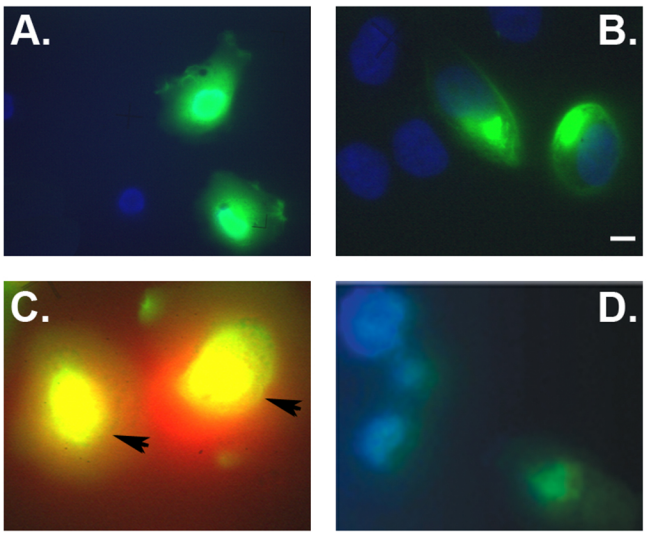
A.
B.
C.
D.

CHAPTER 3

HIRANO BODIES DIFFERENTIALLY MODULATE CELL DEATH INDUCED BY TAU AND THE AMYLOID PRECURSOR PROTEIN INTRACELLULAR DOMAIN[1]

---

[1] Furgerson, M. Spears, W. Sweetnam, J.M. Evans, P. Gearing, M. Fechheimer, M. and R. Furukawa. 2014. *BMC Neuroscience*. 15:74-94 Reprinted here with permission of publisher.

ABSTRACT:

Background: Hirano bodies are actin-rich paracrystalline inclusions found in brains of patients with Alzheimer's disease (AD), frontotemporal dementia (FTD), and in normal aged individuals. Although studies of post-mortem brain tissue provide clues of etiology, the physiological function of Hirano bodies remains unknown. A cell culture model was utilized to study the interactions of mutant tau proteins, model Hirano bodies, and GSK3β in human astrocytoma cells.

Results: Most tau variants showed co-localization with model Hirano bodies. Cosedimentation assays revealed this interaction may be direct, as recombinant purified forms of tau are all capable of binding F-actin. Model Hirano bodies had no effect or enhanced cell death induced by tau in the absence of amyloid precursor protein intracellular domain (AICD). In the presence of AICD and tau, synergistic cell death was observed in most cases, and model Hirano bodies decreased this synergistic cell death, except for forms of tau that caused significant cell death in the presence of Hirano bodies only. A role for the kinase GSK3β is suggested by the finding that a dominant negative form of GSK3β reduces this synergistic cell death. A subset of Hirano bodies in brain tissue of both Alzheimer's disease and normal aged individuals was found to contain tau, with some Hirano bodies in Alzheimer's disease brains containing hyperphosphorylated tau.

Conclusion: The results demonstrate a complex interaction between tau and AICD involving activation of GSK3β in promoting cell death, and the ability of Hirano bodies to modulate this process.

INTRODUCTION:

The cause of sporadic Alzheimer's disease (AD) is unknown, and an intricate interaction between multiple genetic, epigenetic, and environmental risk factors has been proposed (for review, see (1)). However, in approximately 1% of total AD cases, studies show that neurodegeneration results from mutations in the genes encoding the amyloid precursor protein (APP), presenilin 1 (PSEN1), or PSEN2 (2,3). These mutations result in altered processing of APP, increased deposition of amyloid-beta (Aβ), and early onset neurodegeneration. This led to the formation of the amyloid cascade hypothesis, which posits that Aβ initiates a cascade of events leading to tau deposition, synaptic dysfunction and cognitive decline (4). Intramembrane proteolysis of APP by γ-secretase also releases an intracellular fragment known as the amyloid precursor protein intracellular domain (AICD). AICD has been shown to form multi-protein complexes that regulate the induction of apoptosis (for review, see (5,6)). Multiple studies suggest that a downstream effector of AICD is the kinase GSK3β. Studies in neuronal cell cultures and a mouse model report that AICD induces upregulation of total levels of GSK3β as well as increased activation, and thus induces tau hyperphosphorylation (7-9). Abnormal tau phosphorylation is an early marker of AD (10,11) and phosphorylated tau levels correlate with the severity of AD (12). However, the precise mechanisms causing abnormal tau phosphorylation leading to pathological tau formation remain unclear.

Complementary to the amyloid cascade hypothesis was the discovery that mutations in tau cause a familial neurodegenerative disease called frontotemporal dementia with parkinsonism linked to chromosome 17 (FTDP-17) (13). This disease and its sporadic (non-familial) counterparts, forms a family of diseases known as frontotemporal lobar degeneration with tau-positive inclusions (FTLD-tau), are characterized pathologically by the formation of

neurofibrillary tangles (NFTs) and other neuronal and glial inclusions composed of hyperphosphorylated tau (14). Aβ-containing plaques found in AD are not considered a significant invariant pathological feature of these tauopathies. Thus, the amyloid cascade hypothesis posits that Aβ acts upstream of tau to promote neurodegeneration. Nevertheless, significant plaque pathology is often reported in tauopathy patient brain tissue (15-19).

Hirano bodies are inclusion bodies found in significant numbers in the hippocampus in patients with AD compared to age matched controls (20). In addition, Hirano bodies are found in postmortem brain tissue of patients afflicted with a variety of neurodegenerative and other diseases including the tauopathies, and in normal aged individuals (21,22), yet no studies to date explore the cellular basis of this finding. Although the contribution of Hirano bodies to tauopathy is unknown, cell culture and transgenic animal models of FTDP-17 suggest that alterations in the actin cytoskeleton and formation of Hirano bodies are an important event in the pathogenesis of tauopathies (23-25). Tau has been previously shown to bind actin (26-28) and the interaction of tau with the actin cytoskeleton could play a role in disease progression. Hirano bodies are thought to be composed primarily of filamentous actin and actin-associated proteins (29-31), but they have also been shown to contain other components of the neuronal cytoskeleton such the microtubule associated protein tau (32,33). Hirano bodies also accumulate a number of signaling proteins including the transcription factor FAC1 (34), transforming growth factor-β3 (35), and AICD (36,37). Interestingly, Hirano et al., observed a positive correlation between the frequency of NFTs and Hirano bodies in patient samples (38). In that study, Hirano bodies and NFTs were often found in the same cell, although the specific isoforms, mutants, or modifications on tau and physiological consequences of this are unknown.

Early studies of Hirano bodies were reliant on immunohistochemical staining of post-mortem brain tissue due to lack of a model system to study their formation or physiological function. We have developed a cell culture model of Hirano bodies by expressing a truncated form of 34-kDa protein (CT) from *Dictyostelium* (39-42). Truncation of the amino terminus of 34-kDa protein to form CT results in a gain of function in activated actin binding activity and formation of model Hirano bodies in mammalian cells and in transgenic mice (41,43). Model Hirano bodies mitigate the transcriptional activation activity of the APP intracellular domain (AICD), resulting in a decrease in cell death (37). Further, model Hirano bodies decrease cell death potentiated by AICD and a pseudohyperphosphorylated (PHP) tau mimic (44).

We investigated the association of both wild type and mutant forms of tau with Hirano bodies, and their impact on cell death pathways involving tau and AICD. We report that nearly all tau isoforms and mutants tested associate with model Hirano bodies in cells, and bind to actin filaments *in vitro*. Cells expressing both tau and AICD exhibited cell death that was greater than the sum of that observed for tau and AICD alone. This synergistic cell death involved activation of GSK3β, and was eliminated by the presence of model Hirano bodies. These results extend previous reports affirming a specific role for Hirano bodies in aging and disease states and provides further evidence that the presence of Hirano bodies may have an important contribution to the pathogenesis of AD and tauopathies such as FTDP-17.

RESULTS:

The interaction of altered forms of tau with model Hirano bodies and the impact of this interaction on disease pathways leading to cell death was investigated in this study. Mutant tau proteins were chosen on the basis of previous characterization of differential biochemical

properties and their effects on cell death. Expression of mutant tau found in FTDP-17 (R5H, G272V, P301L, R406W) has differential effects on cell death when expressed in cell cultures and in various animal models of tauopathy (24,45,46) and these effects may be attributable to the biochemical properties of tau (47,48). The tau mutant ΔK280 is representative of a group of FTDP-17 mutants previously shown to have increased susceptibility to aggregation compared to WT tau (47-49). However, whether or not tau polymerization is directly neurotoxic continues to be a major question (for review, see (1)) . Previous studies have established a cell culture, *C. elegans*, and mouse model of tau aggregation through expression of a tau fragment comprising only the microtubule binding domain with deletion of lysine 280 (K18ΔK280), which has a high propensity for β-structure and aggregation (50-53). Studies show that expression of K18ΔK280 tau is more lethal than the same fragment without the deletion of lysine 280 (K18), and causes cell death prior to the formation of mature aggregations (50,54,55). The nomenclature of the tau variants and position of the mutation(s) used in this study are shown in Figure 3.1.

FTDP-17 tau mutants and Hirano bodies differentially modulate cell death

The effect of FTDP-17 tau mutants (R5H, G272V, P301L, R406W), 352PHP, and truncated K18 and K18ΔK280 tau on cell death in the presence of model Hirano bodies was investigated. As expected, exogenous expression of wild type tau, 352PHP, and FTDP-17 tau mutants alone, R5H, R406W, G272V, or P301L did not produce significant cell death (Figure 3.2). Consistent with previous reports, expression of K18ΔK280 resulted in significant cell death compared to expression of K18 (figure 3.2D, gray bars ***$p < 0.001$). Coexpression of either 352WT, 441WT, 352PHP, R5H, R406W, K18, or K18ΔK280 tau in the presence of model Hirano bodies resulted only in background levels of cell death (figure 3.2B, check bars). In contrast, expression of either G272V (**$p < 0.01$) or P301L (***$p < 0.001$) in the presence of

model Hirano bodies resulted in significant potentiation of cell death (figure 3.2C, check bars).

Actin Binding

Tau has been previously shown to bind F-actin – albeit not to saturation – and formed F-actin bundles in solution (26-28). We determined the relative F-actin binding for wild type tau and mutant forms of tau to investigate whether the strength of actin binding may correlate with cell death induced by tau and Hirano bodies. Using recombinant protein purified from *E.coli* and cosedimentation with mixtures of F-actin, wild type and mutant forms of tau do not achieve saturation binding to F-actin as shown in Figure 3.3. R406W, G272V, P301L, and 441WT bind F-actin better than 352PHP and R5H, which are greater than 352WT (Figure 3.3). This result is consistent with previous results of wild type recombinant tau (27). Next, we investigated whether tau has an effect on formation of model Hirano bodies since a prior report found that tau promotes the formation of Hirano bodies (56). Transient expression of CT-GFP to induce model Hirano bodies and either 352WT, 441WT, 352PHP, P301L for 48 h did not cause a change in the size of model Hirano bodies (Figure 3.10). Thus, Hirano bodies can form in the absence of tau, and the presence of various forms of tau does not modulate the formation of Hirano bodies.

Hirano bodies, tau, and AICD

Since previous reports have indicated that model Hirano bodies protected against AICD-induced cell death in the presence of 352WT or 352PHP (44), we investigated whether model Hirano bodies would have an effect on cell death induced by FTDP-17 tau (R5H, G272V, P301L, R406W), or truncated tau (K18 or K18ΔK280) in the presence of AICD. Expression of AICD resulted in modest levels of cell death (figure 3.2A, white bars), and the presence of model Hirano bodies significantly lowered this death (white bars, $*p < 0.05$). Coexpression of either

352WT/AICD or 441WT/AICD (black bars) caused an incremental increase in cell death that is similar to what is expected from the additive effects of AICD alone and wild type tau alone (see 3.1). In contrast, a marked potentiation in cell death was observed upon coexpression of 352PHP/AICD (black bars, Table 3.1) consistent with previous data (44). The potentiation of cell death is a synergistic interaction between AICD and 352PHP since the predicted amount of cell death due to AICD alone plus that obtained with 352PHP alone is significantly less than observed when the two are present together (Table 3.1). The presence of model Hirano bodies protected against cell death induced by either 352WT/AICD (stripe bar, ***$p < 0.001$) or 441WT/AICD (stripe bar, **$p < 0.01$), or 352PHP/AICD (stripe bar, ** $p < 0.01$).

The effect of FTDP-17 tau mutants on AICD-induced cell death in the presence or absence of model Hirano bodies was investigated. Similar to 352PHP tau, FTDP-17 tau mutants (R5H, G272V, P301L, R406W) enhance cell death in synergy with AICD (figure 3.2B,C, black bars). The amount of cell death observed is greater than obtained from AICD alone plus that of tau alone (Table 3.1). The presence of model Hirano bodies protected from cell death due to either AICD/R5H or AICD/R406W (Figure 3.2B, stripe bars **$p < 0.01$). However, in cells expressing either G272V/AICD or P301L/AICD, model Hirano bodies had no effect on cell death (figure 3.2C, stripe bars). Expression of K18 and K18ΔK280 with AICD increased cell death synergistically and additively, respectively (black bars, *$p < 0.05$; Table 3.1). The presence of model Hirano bodies lowered cell death (stripe bars *$p < 0.05$) for both K18 and K18ΔK280. These data suggest that model Hirano bodies have a differential effect on cell death induced by tau and/or AICD, depending on the tau variant used.

Collectively, the synergistic versus additive cell death of co-expression of AICD and tau variants suggests a connection by one or more molecular pathways. The effect of Hirano bodies

on cell death may affect AICD, or tau, and/or the synergy that arises from their interaction. Possible routes of this interaction could involve activation of the protein kinase GSK3β, phosphorylation of tau, binding of tau to F-actin, or differential aggregation kinetics of the tau variants.

Hirano bodies differentially influence cell death induced by GSK3β and tau

GSK3β has been implicated in the pathogenesis of AD (for review, see (57)). Specifically, GSK3β is thought to become upregulated and/or activated by Aβ, AICD, and the c-terminal 31 amino acids of APP (C31), triggering a cascade of signaling events leading to tau hyperphosphorylation, apoptosis, and cell death (7,9,58). The contribution of GSK3β and tau to cell death in the presence of model Hirano bodies was investigated using a constitutively active and a dominant negative form of GSK3β. Exogenous expression of a constitutively active mutant of GSK3β (S9A) alone causes cell death similar to that of AICD, and the presence of model Hirano bodies has no effect on this death (figure 3.4A, white bars). In contrast, exogenous expression of GSK3β (S9A) in the presence of 352WT or 352PHP causes significant potentiation of cell death compared to GSK3β (S9A) alone (figure 3.4A, black bars $***p < 0.001$ or $**p < 0.01$, respectively, Table 3.2). Interestingly, although 352WT and 352PHP produce similar amounts of cell death under these conditions, 441WT expression causes only an incremental increase in cell death when expressed with GSK3β (S9A), which is not significantly different from that expected from cell death due to 441WT alone + GSK3β (S9A) alone (Figure 3.4A, black bar; Table 3.2). Exogenous expression of GSK3β (S9A) with either WT tau isoform or 352PHP in the presence of model Hirano bodies causes even further potentiation of cell death (figure 3.4A, check bars, $***p < 0.001$ or $**p < 0.01$).

The effect of FTDP-17 mutant tau expression on cell death induced by GSK3β (S9A) and model Hirano bodies was investigated. Exogenous expression of tau mutants R5H, P301L, and R406W in the presence of GSK3β (S9A) increased cell death synergistically compared to the sum of that observed with expression of GSK3β (S9A) and tau alone (figure 3.4B, black bars; Table 3.2). However, expression of G272V tau in the presence of GSK3β (S9A) resulted in only additive increases in cell death compared to expression of GSK3β (S9A) alone (Figure 3.4A, Table 3.2). We also observed differences in the ability of model Hirano bodies to modulate cell death in the presence of FTDP-17 mutant tau and GSK3β (S9A). Model Hirano bodies enhanced cell death in the presence of GSK3β (S9A)/G272V tau and GSK3β (S9A)/P301L tau (figure 3.4B, check bars ***$p < 0.001$), a result that occurred when either G272V or P301L was expressed with model Hirano bodies. However, model Hirano bodies had no effect on cell death induced by GSK3β (S9A)/R5H tau or GSK3β (S9A)/R406W tau (figure 3.4B, check bars).

GSK3β (S9A) also significantly enhanced cell death in the presence of K18 or K18ΔK280 compared to the sum of the expression of GSK3β (S9A) and tau alone (figure 3.4C, black bars ***$p < 0.001$; Table 3.2). Model Hirano bodies did not have a statistically significant effect on this cell death (figure 3.4C, check bars). We also measured cell death under conditions in which expression of GSK3β (S9A) did not induce significantly greater levels of cell death than GFP controls (figure 3.4D), showing that GSK3β (S9A)-induced cell death is dose dependent. Similar to previous results (figure 3.4A-C), exogenous expression of GSK3β (S9A)/441WT or GSK3β (S9A)/P301L potentiated cell death compared to GSK3β (S9A) alone (figure 3.4D, black bars). In addition, the presence of model Hirano bodies further increased this cell death compared to expression of GSK3β (S9A)/441WT (check bars, *$p < 0.05$) or GSK3β (S9A)/P301L (check bars ***$p < 0.001$). These results show that model Hirano bodies are not

protective against cell death induced by GSK3β and tau, and depending on the mutation, may further increase cell death.

The contribution of dominant negative GSK3β (K85A) (7,59) was used to test the role of GSK3β in cell death induced by tau and model Hirano bodies. GSK3β (K85A) was transiently co-expressed with model Hirano bodies in the presence and absence of G272V (Table 3.3). The unexpectedly higher level of cell death due the presence of G272V and model Hirano bodies was reduced in the presence of GSK3β (K85A) to that expected from the control GFP/G272V + GFP/ GSK3β (K85A) (Table 3.3, $p < 0.02$). This result shows an interaction between F-actin and tau that is more complex than F-actin binding alone and that phosphorylation of tau likely plays a role in cell death.

To determine whether cell death induced by combinations of AICD and tau involve activation of GSK3β and the phosphorylation state of tau, the effect of a dominant negative GSK3β (K85A) was investigated (Figure 3.5). Expression of GSK3β (K85A) with GFP does not significantly increase the cell death due to GFP alone (Figure 3.5, white bars). Further, expression of AICD induces death of approximately 17% of cells, and this number is not significantly changed in the presence of GSK3β (K85A) (Figure 3.5A, white bars). Thus, cell death due to AICD alone does not require activation by GSK3β. Cell death due to wild type, 352PHP, FTDP-17 mutants, and K18 and K18ΔK280 was unaffected by expression of GSK3β (K85A) (Figure 3.5A and D, grey and checked bars). Cell death due to tau + AICD was suppressed by expression of GSK3β (K85A) for 352PHP, G272V, P301L, R5H, and R406W, and K18 (Figure 3.5A-D, black and striped bars). However, expression of GSK3β (K85A) had no effect on cell death induced by AICD/352WT, AICD/441WT, or AICD/K18ΔK280 (Figure 3.5A and D, black and striped bars). Interestingly, cell death of all tau forms + AICD that were

suppressed by expression of GSK3β (K85A) showed synergistic cell death in the presence of GSK3β (S9A) (Table 3.2). These results imply that synergistic cell death due to AICD and tau involve activation of GSK3β, and that phosphorylation of tau is an important factor to cell death. Cell death due to tau forms + AICD that were not suppressed by expression of GSK3β (K85A) had levels of cell death that was not significantly different from the sum of that observed with tau and AICD separately.

Phosphorylation of tau

Results of cell viability in the presence of GSK3β (K85A) suggest that 352PHP, R5H, R406W, G272V, and P301L become phosphorylated by GSK3β in the presence of AICD or CT-GFP. Previously, others have reported that AICD is capable of increasing cellular levels of GSK3β (7-9). Therefore, western blot analysis was performed to determine whether the presence of AICD and/or CT-GFP impact the amount of GSK3β protein in our cell culture system. The presence of exogenous AICD increases total GSK3β levels above that of untransfected cells and also of cells expressing tau only (Figure 3.6A). Furthermore, expression of CT-GFP in the presence of AICD and tau reduces the amount of GSK3β to that of the control (Figure 3.6A). The increase of tau-induced cell death due to the presence of G272V or P301L and CT-GFP was reduced in the presence of GSK3β K85A (Figure 3.5), suggesting CT-GFP may promote phosphorylation of these tau mutants. To test this hypothesis, western blot analysis was performed on different tau mutants to determine if the presence of CT-GFP increases phosphorylation at specific amino acids. 441WT, R406W, and R5H tau showed no increase in phosphorylation at Ser199, Ser202, or Thr231 in the presence of CT-GFP (Figure 3.6B). Interestingly, both P301L and G272V have increased phosphorylation at Ser199 and Ser202 and Thr231 in the presence of CT-GFP (Figure 3.6B). P301L and G272V exhibited synergistic cell

death in the presence of CT-GFP (Figure 3.2C). These results show that the ability of specific mutant tau proteins to induce cell death in the presence of AICD or CT-GFP is due to GSK3β phosphorylation of tau.

Localization of tau and model Hirano bodies

Since preferential accumulation of different forms of tau might indicate physiological function of Hirano bodies, mutant tau and model Hirano body localization was investigated. H4 cells were transiently transfected with CT-GFP to induce model Hirano bodies in the absence or presence of one of the following FLAG-tagged tau constructs: 441WT, 352WT, R5H, G272V, P301L, R406W, 352PHP, K18ΔK280 and K18. All FTDP-17 mutant tau proteins as well as WT tau isoforms were present throughout the model Hirano body or formed a ring-like structure around the periphery of the model Hirano body shown in Figure 3.7. The exception was 352PHP, which was diffusely localized throughout the cell. Further, truncated tau mutants (K18 or K18ΔK280) also showed a strong nuclear localization. These results show that regardless of mutations, tau shows enrichment at sites of F-actin accumulation. However, hyperphosphorylation may decrease this association, as shown for 352PHP tau.

Localization of tau in human brain tissue was performed to confirm that tau is present in Hirano bodies. In AD and control brain sections, 4.1 and 2.7% of Hirano bodies are well stained for tau, respectively (Figure 3.8). Localization of phosphorylated tau (pTau199/202) to Hirano bodies was observed only in AD brain sections and comprised 2.9 % of the total Hirano bodies. These findings are in agreement with prior studies that report tau localized in a fraction of all Hirano bodies in human hippocampus (32,33).

DISCUSSION:

Tau contributes significantly to neurodegeneration in FTDP-17, Alzheimer's disease and other tauopathies by aggregating to form oligomers, paired helical filaments (PHF), and eventually large aggregates including neurofibrillary tangles (NFTs). *In vitro*, formation of oligomers and higher order polymers of tau is thought to occur through the process of nucleation, elongation, and/or autocatalytic growth (60,61). Regulatory pathways may influence the availability of free tau, its phosphorylation state, propensity to aggregate, and inducers of aggregation. Dissecting the formation of oligomeric and higher order polymers of tau *in vivo* and their contribution to cell death require probing these pathways. In this study we have investigated the role of Hirano bodies in modulating tau localization and cell death due to tau.

Proposed cell death pathway involving Hirano bodies, tau, AICD, and GSK3β

The role of tau in cell death induced by the presence or absence of model Hirano bodies and/or AICD is a complex intersection of several variables: 1) affinity of tau for actin; 2) the phosphorylation state and location of the phosphorylated amino acids on tau; and 3) the kinetics and propensity of tau to self-aggregate that could depend on phosphorylation or other modification. As shown in figure 3.9, AICD causes significant cell death when expressed alone. Similarly, expression of K18ΔK280 causes significant cell death unlike expression of all other forms of tau tested (figure 3.9). When coexpressed with AICD, all tau mutants expressed except for 441WT, 352WT, and K18ΔK280 produced synergistic cell death (figure 3.9C). This cell death was ameliorated in the presence of model Hirano bodies, except in the case of P301L or G272V tau (red lines). This could be due to reduction of AICD or tau through indirect or direct binding to F-actin in the model Hirano bodies and/or reduction of GSK3β (Figure 3.6A) and thus affecting the phosphorylation state of tau (Figure 3.6B). Interestingly, the expression of model

Hirano bodies and P301L or G272V tau led to significant cell death in the absence of AICD (Figure 3.2C). This process could be facilitated by a combination of binding to F-actin, increased phosphorylation that reduces F-actin binding, and subsequent tau aggregation. The affinity of tau for F-actin itself is insufficient as R406W and 441WT bound F-actin as well as G272V and P301L.

We also find that expression of a dominant negative form of GSK3β mitigates cell death due to the synergistic effect of AICD and tau in most cases (figure 3.5, 3.9E). This result underscores the importance of GSK3β activation and tau phosphorylation in the synergistic interaction of ACID and tau. In support of this, expression of dominant negative GSK3β (K85A) does not reduce cell death due to expression of AICD alone, or AICD and K18ΔK280, as most GSK3β phosphorylation sites are absent from this mutant. We show that expression of GSK3β (K85A) ameliorates cell death due to G272V in the presence of Hirano bodies, further substantiating the role of GSK3β phosphorylation in our system, even in the absence of exogenously expressed AICD. In summary, these results support the assertion that that a combination of tau phosphorylation and aggregation leads to cell death, which may be either enhanced or mitigated by the presence of model Hirano bodies depending on the form of tau and state of its modification.

These new results resolve an apparent contradiction in previous literature. Expression of mutant forms of tau were shown to induce cell death only after overexpression of actin and subsequent formation of actin-rich structures in a *Drosophila* model (24). However, model Hirano bodies were previously reported to reduce toxicity associated with tau under certain conditions (44). Here we show that Hirano bodies can both promote and protect against cell death initiated by tau depending on the type of tau expressed.

Tau and actin

Multiple studies point to the role of tau as an actin binding protein (25-28,62-66). However, this idea is not without controversy. Studies of tau-actin interactions utilize a range of experimental approaches that yield differential results (67). Tau has been shown to bind and bundle actin *in vitro* (24,27,28,62). Tau bound weakly to actin and did not reach saturation (27). In competitive binding studies with actin, the preferred substrate of tau is tubulin polymerized into microtubules (27,65). Our study is the first to show that all tau mutants tested are able to bind to F-actin with the resultant binding R406W, G272V, P301L, and 441WT > 352PHP and R5H > 352WT (Figure 3.4). R406W, G272V, and P301L have the highest affinity for F-actin yet only G272V and P301L potentiate cell death in the presence of model Hirano bodies and/or AICD (Figure 3.2, Table 3.1). The differences in F-actin binding affinity of the various tau mutants does not explain the differential effect of tau on cell death in the presence of model Hirano bodies. However, since recombinant protein produced in *E.coli* was used, the impact of tau post-translational modifications on F-actin binding was not measured. Other results reported in this study imply that the phosphorylation state of tau is important. In the presence of constitutively active GSK3β (S9A), model Hirano bodies potentiate cell death in the presence of tau (see Table 3.2). In addition, only a small percentage of Hirano bodies in AD brain contain phosphorylated tau (Figure 3.8). Another group was unable to detect pTau-202/205 in Hirano bodies from Alzheimer's patients (68). It is possible that colocalization of tau with Hirano bodies varies from patient to patient and is heavily influenced by post-translational modification, and aggregation state given that Hirano bodies frequently occur in NFT-containing neurons (38). Consistent with this hypothesis, others have shown that phosphorylation of tau at certain sites reduces, but may not abolish its ability to associate with actin filaments (69). Conversely, studies

have suggested that minor phosphorylation of certain residues may enhance actin binding (24,27,70). This suggests a complex, dynamic relationship between tau and actin. This may explain why 352PHP binds F-actin *in vitro* (Figure 3.3), but does not co-localize with model Hirano bodies (Figure 3.7). *In vivo*, tau association with actin has been shown to be critical for tau-induced neurodegeneration (24). We cannot rule out that other modes of actin and tau interaction may be occurring such as intermediate binding proteins or other protein modifications. For example, tau also binds to Fe65 (71), and Fe65 is known to be enriched in Hirano bodies (37).

Phosphorylation of tau

Studies characterizing FTDP-17 tau mutants demonstrated that tau was highly phosphorylated, and depending on the mutation, differentially phosphorylated (72-74). This differential phosphorylation also affects the ability of tau and its mutants to bind to microtubules (75), affects microtubule dynamic instability, and promotes microtubule assembly (for a review, see (76)). It is also well known that tau phosphorylation at multiple sites *in vivo* decreases its association with microtubules (67,77), thus making tau available to aggregate. Hyperphosphorylated tau has a tighter, more folded conformation and in some cases, an increased propensity to aggregate (14,74,78-83).

In all tau constructs tested except for R5H, R406W, K18, or K18ΔK280, expression of exogenous constitutively active GSK3β (S9A) and tau in the presence of model Hirano bodies strongly potentiated cell death compared to expression of GSK3β (S9A) and tau (Figure 3.4). Since GSK3β phosphorylates many substrates, results need to be interpreted with some caution. However, our results suggest that GSK3β or another kinase induces formation of hyperphosphorylated tau species. Model Hirano bodies could potentiate cell death by increasing

the local concentration of tau through F-actin binding, and serving as the nucleation agent in subsequent tau phosphorylation and aggregation. G272V and P301L have a higher propensity to aggregate than 441WT (see below (47)), and may therefore aggregate and induce cell death more easily in the presence of Hirano bodies. G272V and P301L were more phosphorylated in the presence of model Hirano bodies (Figure 3.6), lending credence to this supposition. Further experiments show that expression of dominant negative GSK3β (K85A) in the presence AICD and tau decreases levels of cell death to that expected from an additive effect of cell death induced by AICD + tau alone (Figure 3.2, table 3.1). However, model Hirano bodies did not further enhance cell death in the presence of R406W shown previously to be hypophosphorylated in the presence of GSK3β (7,58) or tau mutants that did not contain the majority of GSK3β phosphorylation sites (K18 and K18ΔK280). Expression of dominant negative GSK3β (K85A) in the presence of G272V and model Hirano bodies lowered cell death to that expected of an additive effect of cell death induced by G272V + model Hirano bodies alone (Figure 3.5). This may suggest a complementary role for phosphorylation and aggregation.

Consistent with this, *in vitro* studies characterizing the 352PHP tau mutant show that these mutations collectively inhibit aggregation compared to WT tau (84). Therefore, transient phosphorylation and dephosphorylation of tau may be critical to formation of a pathologically relevant tau species. This may explain why expression of 352PHP tau and model Hirano bodies does not cause increased cell death in our system. It has been shown that phosphorylation of specific residues on tau is required to prime tau for additional phosphorylation (85-88), and that 352PHP becomes phosphorylated in cell cultures under certain conditions at other serine/threonine residues that are not mutated (89). Therefore, the amino acid charge substitutions used to create the phosphorylation mimics on 352PHP may prime phosphorylation

at other sites. This could explain why expression of either AICD or GSK3β with 352PHP results in a synergistic cell death phenotype. These results support the hypothesis that model Hirano bodies enhance cell death in the presence of highly phosphorylated tau, and reduce cell death in the presence of other tau variants.

Aggregation of FTDP-17 mutant tau

The ability of tau to promote cell death in the presence of model Hirano bodies and/or AICD correlates most strongly with the propensity of tau to self-aggregate. Multiple studies show that FTDP-17 tau mutants vary widely in their ability to form PHFs and NFTs *in vitro*, in cell culture, and *in vivo* as well as the kinetics in which they form (90). Studies with recombinant tau obtained from bacteria showed that ΔK280(441tau) had a greater propensity to form paired helical filaments than P301L>G272V>R406W>441WT with a faster kinetic speed (47). Tau mutants P301L and K18ΔK280 show the greatest tendency to aggregate (47), and potentiated the highest levels of cell death in the presence of model Hirano bodies. All tau mutants except for K18ΔK280 were incapable of inducing cell death alone consistent with previous reports (50,54). The ability of K18ΔK280 to cause cell death was attributed to the ability of this fragment to aggregate since mutation of hexapeptide motifs in tau essential for β-structure and aggregation reduced cell death and rescued neurodegeneration (55,91). Model Hirano bodies have no effect on cell death initiated by expression of exogenous K18ΔK280. Because this mutant is capable of initiating cell death on its own, it likely does not need model Hirano bodies to further aid its aggregation. Although little is known about the R5H tau mutation, R5L has been characterized *in vitro* with increased nucleation rate of aggregation and increased numbers of tau filaments (92), a trait shared with R5H (18). R406W tau does not robustly aggregate *in vitro* or in cell cultures (92-95). In fact, R406W tau has been shown to be hypophosphorylated in resting cells compared

to WT tau (93,95), and hypophosphorylated when exposed to GSK3β *in vitro* (94). Thus, tau phosphorylation may be related to tau aggregation and cell death. The specific tau species responsible for potentiating cell death in our model is unknown, and more studies are needed to determine whether further tau modification and proteolytic processing contributes to cell death. In support of a relationship between aggregation and cell death, some FTDP-17 patients exhibit more aggressive symptoms than AD patients, coincident with robust tau pathology at an earlier age of onset (for review, see (96)).

A possible mechanism for the interaction of model Hirano bodies and tau is that model Hirano bodies increase the local concentration of tau through a direct or indirect interaction. All the full-length tau proteins bound F-actin in our study and all tau proteins with the exception of 352PHP were enriched with model Hirano bodies (Figure 3.3 and 3.7). While tau binds with a lower affinity to actin than microtubules, the concentration of F-actin in a Hirano body could be 360-600 μM based on the actin concentration in F-actin solutions bundled by the *Dictyostelium* 34 kDa actin bundling protein (97). The high local concentration of F-actin in a model Hirano body could compensate for weak tau binding. Phosphorylation, aggregation, or other protein modifications could become more favorable due to the high local concentration. Tau mutants most prone to aggregation then initiate cell death. Previous studies with recombinant tau induced to aggregate by the presence of heparin showed that both P301L and G272V aggregated faster and to a greater extent than R406W or 441WT (47). The truncated K18ΔK280 aggregated exceptionally quickly in contrast to K18. Model Hirano bodies were not able to protect against cell death in the presence of these aggregation-prone tau mutants alone or in addition to AICD. In contrast, WT tau isoforms and tau mutants R406W and R5H did not cause cell death in the presence of model Hirano bodies, and model Hirano bodies were able to protect from cell death

induced by these tau mutants in the presence of AICD. These forms of tau were slower to aggregate and did so to a smaller extent than P301L, G272V, or K18ΔK280 (47).

AICD and tau

Our data is consistent with the idea that tau significantly contributes to cell death in the presence of AICD. This complements previous results showing that expression of exogenous C31/APP/352PHP tau or AICD/352PHP tau results in a potentiation of cell death compared to cells expressing AICD or 352PHP alone (44). In this study, expression of all tau forms tested enhanced cell death in the presence of AICD (albeit at different levels) to a level that was significantly greater than the sum of AICD and tau expressed separately with the exception of 352WT, 441WT, and K18ΔK280 (Table 3.1). It is noteworthy that exogenous expression of dominant negative GSK3β (K85A) with AICD and all forms of tau that previously induced synergistic cell death decreased to an additive sum of AICD alone plus tau alone, while AICD and all forms of tau that do not induce synergistic cell death were unaffected by GSK3β (K85A). In addition, the presence of model Hirano bodies with AICD and tau decreased the amount of GSK3β. These results support a model in which AICD potentiates cell death in the presence of tau and that phosphorylation of tau is important to that process. AICD has been shown to up-regulate or be upstream of GSK3β activation (7). Our results strongly support the conclusion that the interplay between AICD and tau involves activation of GSK3β and phosphorylation of tau, and that there are at least two major effects of AICD. AICD alone activates Fe65, Tip60, and caspases, while the interaction of AICD with tau to cause cell death requires activation of GSK3β.

CONCLUSION:

We provide further evidence that Hirano bodies have a specific effect on the pathogenesis of neurodegenerative disease, with respect to tau and C-terminal fragments of APP. We suggest that Hirano bodies do not serve a general protective function by simply accumulating cytosolic proteins, but rather protect against cell death initiated by AICD and mitigate or enhance cell death dependent on the biochemical properties of tau. This data complements key discoveries made in transgenic animal models and neuronal cell culture reporting abnormal rearrangement of F-actin during cell stress or neurodegeneration, and suggest that Hirano bodies play a complex role in the pathogenesis of disease.

MATERIALS AND METHODS:

Plasmids*:* CT-EGFP was utilized to induce model Hirano bodies as previously described (42,44). Other plasmids utilized encoded GFP (pEGFP-N1, Clontech, Mountain View, CA), AICD (APPc58-myc, c-terminal 58 amino acids of APP-695, a generous gift from Bradley Hyman, Harvard Medical School) (98), and HA-tagged GSK3β (Addgene plasmid 15994) (99). GSK3β (S9A) (constitutively active) (100), and GSK3β (K85A) (dominant negative) (7,59) were constructed from HA-GSK3β using a QuikChange II XL Site-Directed Mutagenesis Kit (Stratagene, La Jolla CA) using mutagenic primers K85A 5'GAACTGGTCGCCATCAAGAAAGTATTGCAGGAC 3' and S9A 5' CCAGAACCACCGCCTTTGCGGAGAGC 3'. The coding sequences of these plasmids were confirmed by sequencing.

A single MAPT gene in the central nervous system generates six tau isoforms by alternative splicing of its pre-mRNA. Isoforms ranging in size from 352-441 residues differ by

exclusion or inclusion of exons 2,3, and 10. Plasmids were constructed to express wild type tau (352WT or 441WT) or mutant forms (352PHP, R5H, G272V, P301L, R406W, K18, or K18ΔK280) in either mammalian or bacterial cells. 352PHP is a tau mutant created in the shortest tau isoform (352WT) in which 10 serine/threonine residues (S198, S199, S202, T231, S235, S396, S404, S409, S413, and S422) were mutated to glutamic acid to mimic a hyperphosphorylated state (generous gifts from Roland Brandt, University of Osnabrück, Osnabrück, Germany) (101) as shown in Figure 3.1. K18 comprises the microtubule-binding domain (amino acids Q244 to E372, numbering from the 441 length tau) (47). To generate N-terminal FLAG-tagged tau constructs with a CMV promoter for expression in mammalian cells (Figure 3.1), the coding sequence of 352PHP was digested from the 352PHP plasmid with ClaI. Using the coding sequence of 441 length human WT tau (441WT) in pET-29b (Addgene plasmid 16316) (102) as a template, ClaI restriction sites were introduced through PCR, and 441WT coding sequence was cloned into the ClaI site of the remainder of the 352PHP plasmid backbone containing the FLAG-tag and CMV promoter. Tau mutants in the 441 length tau in either the mammalian or bacterial expression plasmids were constructed using a QuikChange II XL Site-Directed Mutagenesis Kit (Stratagene, La Jolla CA). Primers for mutagenesis were:

ΔK280 (deletion of K280) 5’ GCAGATAATTAATAAGCTGGATCTTAGC,

R5H 5’ATGGCTGAGCCCCACCAGGAGTTCGAAG,

G272V 5’GCACCAGCCGGGAGTCGGGAAGGTGCAG,

P301L 5’ATCAACACGTCCTGGGAGGCGGCAG, and

R406W 5’GGACACGTCTCCATGGCATCTCAGCAATG. Tau constructs K18 and K18ΔK280 were generated by the introduction of ClaI sites to the 5’ and 3’ end of K18 or K18ΔK280 using either the 441WT or ΔK280 441WT as template, digesting the PCR products, and ligating into

the ClaI site of the remainder of the 352PHP plasmid backbone after deletion of the coding sequence. The coding sequences of all plasmids were verified by sequencing.

Immunofluorescence: Hirano bodies have been proposed to have a glial origin (103), and because glial cells have been shown to be important mediators of cell death induced by Aβ and tau (104), H4 human astroglioma cells were utilized. Furthermore, H4 cells have been shown to contain nearly undetectable levels of endogenous tau (105,106). H4 astroglioma cells (American Type Culture Collection, Manassas, VA) were cultured in Dulbecco's Modified Eagle Medium (DMEM) supplemented with 10% fetal bovine serum (Atlanta Biologicals, Flowery Branch, GA) at 37°C and 5% CO_2. H4 cells were plated onto glass coverslips and allowed to adhere for 24 h. Cells were transiently transfected with equal amounts of plasmid (1 μg each) using Lipofectamine LTX (Invitrogen, Carlsbad, CA) according to manufacturer's instructions. Cells were processed after 24 h for immunofluorescence as previously described (42). Coverslips were visualized with a Zeiss Axioobserver Z1 equipped with an AxioCam MRm controlled by AxioVision4.6 software. Antibodies used were anti-FLAG rabbit antibody to label tau (Sigma-Aldrich, St. Louis, MO), and Alexa Fluor 350 conjugated anti-rabbit secondary antibody (Molecular Probes, Eugene, OR). F-actin was visualized using TRITC-conjugated phalloidin (Sigma-Aldrich, St. Louis, MO), and nuclei were stained with DAPI (Sigma-Aldrich, St. Louis, MO). Characterization of the types of actin-rich structures was performed on H4 cells transfected as described above and processed for immunofluorescence 48 h after transfection. CT-GFP-rich structures were characterized having normal cellular localization, fibrillar structures, Hirano bodies or large Hirano bodies. Hirano body size was determined using NIH ImageJ using the threshold function to eliminate user bias. Large Hirano bodies are those in the fourth quartile.

Significance between samples was determined using the non-parametric Mann-Whitney test. Experiments were performed in a minimum of triplicate.

Immunohistochemistry*:* Samples of human hippocampus were obtained from the Alzheimer's Disease Research Center at Emory University. Samples were screened for presence of Hirano bodies, and were derived from patients with AD, or control subjects that had no known history of neurological disease and no neuropathological changes indicative of neurodegenerative disease at autopsy.

Case number	Age at death	Race/sex
E08-125 (AD)	81	Male
E09-155 (AD)	83	Caucasian male
E10-179 (AD)	66	African American female
E09-170 (control)	88	Caucasian female
E10-142 (control)	94	Caucasian male

All samples were de-identified and coded only by sample number, and supplied as eight-micron, paraformaldehyde-fixed paraffin sections mounted on slides. Mounted sections were dewaxed in xylene and rehydrated in an ethanol gradient prior to antigen retrieval in boiling 10 mM sodium citrate plus 0.05% Tween 20 pH 6.0 for 20 minutes. Endogenous peroxidase activity was inhibited by incubating sections in 3% hydrogen peroxide for 10 minutes prior to washing with phosphate buffered saline (PBS) and blocking with 10 mg/ml bovine serum albumin in PBS overnight. Samples were stained for total tau using mouse tau 5 antibody (1/400 in PBS, 4% BSA) (Santa Cruz Biotechnology, Dallas, TX), or tau phosphorylated at serine 199/202 using

rabbit anti-pTau199/202 (1/300 in PBS, 4% BSA) (Sigma-Aldrich Chemical Co, St. Louis, MO). Anti-mouse and anti-rabbit biotinylated secondary antibodies (1/800 in PBS) (Sigma-Aldrich Chemical Co, St. Louis, MO) followed by a streptavidin-HRP polymer complex (1/1000 in PBS) with diaminobenzidine enhanced substrate system (Vector Laboratory, Burlingame, CA) were utilized as a detection system. Samples were counterstained with hematoxylin/eosin (Sigma-Aldrich Chemical Co, St. Louis, MO) to visualize Hirano bodies. All protocols were approved by the University of Georgia Institutional Biosafety Committee and the Institutional Review Board.

Cell death assays: 24 hours prior to transfection, 8,000 H4 cells/well were plated into 96-well plates (Nalge Nunc, Rochester, NY). Cells were transiently transfected with equal amounts of plasmid (250 ng each) using Lipofectamine LTX (Invitrogen, Carlsbad, CA) according to manufacturer's instructions. In some experiments, the amount of GSK3β (S9A) plasmid was reduced (150 ng) to examine its dose dependent effect while the amounts of the other plasmids were kept constant. 24 hours post-transfection, cell death assays were performed as previously described (44). Briefly, cells were incubated with 9 nM Sytox Orange, a cell impermeable nucleic acid dye (Invitrogen, Carlsbad, CA), and 264 μM Hoechst 33258 (Sigma-Aldrich Chemical Co, St. Louis, MO) for 15 min at 37 °C and 5% CO_2. Due to inefficient transfection, GFP was used as a transfection control. Sytox Orange positive fluorescence was used to indicate dead cells. A minimum of 80 cells was counted per sample and each condition was sampled at least three independent times. Analysis of statistical significance was performed using Student's t-test. The interactions of multiple components and their contributions to cell death were analyzed by using propagation of error, comparing the calculated sum and standard deviations of cell death observed when the two components were separate to that observed when they were

present in the assay together to determine the error of the calculated sum. This strategy and applying Student's t-test allowed determination of whether the cell death observed when the two components were present together was significantly greater than expected, suggesting a biological and/or molecular interaction.

Protein purification: Expression of wild type and mutated forms of tau in pET29-b was induced by the addition of 1 mM IPTG in *E.coli* Bl-21(DE-3) with the exception of 352PHP which required no IPTG. Recombinant tau proteins were purified as previously described (107) with the following modifications. Cells were lysed by the addition of 0.2 mg/ml of lysozyme in the bacterial resuspension buffer and stirred until lysis was complete. The lysate was sonicated prior to the addition of NaCl and subsequent boiling. The lysate was clarified by ultracentrifugation and the supernatant was diluted with cation exchange buffer A without NaCl to a final concentration of 50 mM NaCl, and applied to CM-cellulose column (GE Healthcare Life Sciences, Piscataway, NJ). The column was washed with cation exchange buffer A until the OD reached baseline levels and subsequently eluted with a linear gradient 0.05 – 0.4 M NaCl gradient. Fractions containing tau were identified by SDS-PAGE, collected, diluted with cation exchange buffer A without NaCl to a final concentration of 50 mM NaCl and concentrated on CM-cellulose. The mutant tau was eluted with cation exchange buffer with 0.6 M NaCl. Fractions containing the mutant tau were identified by OD280 nm, sedimented at 13,000xg for 15 min at 4°C, and the supernatant applied directly to sephacryl S-200 (GE Healthcare Life Sciences, Piscataway, NJ) column equilibrated with 10 mM HEPES, pH 7.4, 150 mM NaCl, 1 mM DTT, and 0.02% sodium azide. Fractions containing tau were identified by SDS-PAGE. Individual fractions containing the highest concentrations of tau were frozen at -80C° and used

without further concentrating. Five hours prior to use, the tau was dialyzed versus cosedimentation buffer (see below).

Actin was prepared from rabbit skeletal muscle acetone powder (108,109) and further purified by application to sephadex G-150. The actin was maintained for up to 1 week in cosedimentation buffer (10 mM PIPES, pH 7.0, 100 mM KCl, 1 mM $MgCl_2$, 1 mM ATP, 1 mM DTT, and 0.02% sodium azide) with daily buffer changes. The protein concentrations of actin and tau were determined using bicinchoninic acid method (Pierce Protein Biology, Rockford, IL) (110) with bovine serum albumin as a standard.

Cosedimentation assays were performed as previously described (111). F-actin and/or tau mixtures were incubated 2 h prior to ultracentrifugation. The samples were analyzed by SDS-PAGE and quantified utilizing ChemiDoc™ MP System and Image Lab™ software (Bio-Rad Laboratories, Hercules, CA). The amount of tau in the pellets was corrected for the small amount of tau alone found in the pellet. Experiments were performed in a minimum of triplicate.

Western blot: HEK293T cells (American Type Culture Collection, Manassas, VA) were cultured in Dulbecco's Modified Eagle Medium (DMEM) supplemented with 10% fetal bovine serum (Atlanta Biologicals, Flowery Branch, GA) at 37°C and 5% CO_2. They were plated at a density of 4×10^5 cells per 60 mm diameter dish. Cells were transfected with equal amounts of plasmid (2.5 μg each) using Lipofectamine 2000 (Invitrogen, Carlsbad, CA) according to manufacturer's instructions. At 48 hours after transfection, cells were washed twice with ice-cold PBS and lysed with 20 mM Tris, pH 7.5, 1% triton-X100, 0.1% SDS, 0.5% deoxycholic acid, and 10% glycerol with 10 μL protease inhibitor cocktail (5 mM EGTA, 1 mM DTT, 100 mM leupeptin, 10 mM pepstatin, 0.1 M PMSF, 0.1 M benzamidine, and 0.5 M ε-aminocaproic acid). Cell debris was separated from total homogenate by centrifugation at 13,000g for 15 min

at 4°C. The supernatant was stored at -80°C until used. Protein concentrations of the supernatants were determined by bicinchoninic acid assay using BSA as a standard (110). For western blot analysis, samples were loaded at equal total protein, separated by SDS-PAGE, and transferred to nitrocellulose membranes. Blots were blocked in 5% nonfat dry milk in TBST and probed using with either rabbit anti-pTau199/202 (1/4500) (Sigma-Aldrich Chemical Co, St. Louis, MO), rabbit-anti pTau231 (1/2000) (Acris Antibodies, San Diego, CA), goat-anti pTau396 (1/2000) (Santa Cruz Biotechnology, Dallas, TX), rabbit anti-GFP (1/5000) (Sigma-Aldrich Chemical Co., St. Louis, MO), mouse anti-tau5 (1/5000) (Santa Cruz Biotechnology, Dallas, TX), mouse anti-alpha tubulin (1/8000) (Millipore, Billerica, MA), mouse anti-myc (1/8000) (Cell Signaling Technology, Danvers, MA), or rabbit anti-GSK-3β (1/1000) (Santa Cruz Biotechnology, Dallas, TX). After three washes with TBST, blots were incubated with either goat anti-mouse horseradish peroxidase, goat anti-rabbit horseradish peroxidase (1/10000) (Pierce-lab, Rockford, IL), or donkey anti-goat horseradish peroxidase (1/8000) (Millipore, Billerica, MA) and detected by chemiluminescence using SuperSignal Western Dura Extended Duration Substrate (Thermo Scientific, Rockford IL). Images were captured utilizing ChemiDoc™ MP system and Image Lab™ software (Bio-Rad Laboratories, Hercules, CA). Blots were performed in duplicate.

ACKNOWLEDGEMENTS:

We would like to thank Drs. Stephen Hajduk and Richard Meagher for use of their microscopes. This work was supported by NIH (1R01-NS04645101) (R.F. and M.Fechheimer) and by National Institute of Aging Emory Alzheimer's Disease Research Center P50 AG025688 (M.G.). NIH

REFERENCES:

1. Huang, Y., and Mucke, L. (2012) Alzheimer mechanisms and therapeutic strategies. *Cell* **148**, 1204-1222

2. Sherrington, R., Rogaev, E. I., Liang, Y., Rogaeva, E. A., Levesque, G., Ikeda, M., Chi, H., Lin, C., Li, G., Holman, K., Tsuda, T., Mar, L., Foncin, J. F., Bruni, A. C., Montesi, M. P., Sorbi, S., Rainero, I., Pinessi, L., Nee, L., Chumakov, I., Pollen, D., Brookes, A., Sanseau, P., Polinsky, R. J., Wasco, W., Da Silva, H. A., Haines, J. L., Perkicak-Vance, M. A., Tanzi, R. E., Roses, A. D., Fraser, P. E., Rommens, J. M., and St George-Hyslop, P. H. (1995) Cloning of a gene bearing missense mutations in early-onset familial Alzheimer's disease. *Nature* **375**, 754-760

3. Levy-Lahad, E., Wasco, W., Poorkaj, P., Romano, D. M., Oshima, J., Pettingell, W. H., Yu, C. E., Jondro, P. D., Schmidt, S. D., Wang, K., and et al. (1995) Candidate gene for the chromosome 1 familial Alzheimer's disease locus. *Science* **269**, 973-977

4. Hardy, J., and Selkoe, D. J. (2002) The amyloid hypothesis of Alzheimer's disease: Progress and problems on the road to therapeutics. *Science* **297**, 353-356

5. Beckett, C., Nalivaeva, N. N., and Turner, A. J. (2012) Nuclear signalling by membrane protein intracellular domains: the AICD enigma. *Cell Signal*. **24**, 402-409

6. Pardossi-Piquard, R., and Checler, F. (2012) The physiology of the beta-amyloid precursor protein intracellular domain AICD. *J. Neurochem*. **120 Suppl 1**, 109-124

7. Kim, H.-S., Kim, E.-M., Lee, J.-P., Park, C. H., Kim, S., Seo, J.-H., Chang, K.-A., Yu, E., Jeong, S.-J., Chong, Y. H., and Suh, A. Y.-H. (2003) C-terminal fragments of amyloid precursor protein exert neurotoxicity by inducing glycogen synthase kinase-3b expression. *FASEB J*. **17**, 1951-1954

8. von Rotz, R. C., Kohli, B. M., Bosset, J., Meier, M., Suzuki, T., Nitsch, R. M., and Konietzko, U. (2004) The APP intracellular domain forms nuclear multiprotein complexes and regulates the transcription of its own precursor. *J. Cell Sci.* **117**, 4435-4448

9. Ghosal, K., Vogt, D. L., Liang, M., Shen, Y., Lamb, B. T., and Pimplikar, S. W. (2009) Alzheimer's disease-like pathological features in transgenic mice expressing the APP intracellular domain. *Proc. Natl. Acad. Sci. U.S.A.* **106**, 18367-18372

10. Braak, E., Braak, H., and Mandelkow, E. M. (1994) A sequence of cytoskeleton changes related to the formation of neurofibrillary tangles and neuropil threads. *Acta Neuropathol. (Berl)* **87**, 554-567

11. Braak, H., and Braak, E. (1991) Neuropathological stageing of Alzheimer-related changes. *Acta Neuropathol. (Berl)* **82**, 239-259

12. Holzer, M., Holzapfel, H. P., Zedlick, D., Bruckner, M. K., and Arendt, T. (1994) Abnormally phosphorylated tau protein in Alzheimer's disease: heterogeneity of individual regional distribution and relationship to clinical severity. *Neurosci.* **63**, 499-516

13. Hutton, M., Lendon, C. L., Rizzu, P., Baker, M., Froelich, S., Houlden, H., Pickering-Brown, S., Chakraverty, S., Isaacs, A., Grover, A., Hackett, J., Adamson, J., Lincoln, S., Dickson, D., Davies, P., Petersen, R. C., Stevens, M., de Graaff, E., Wauters, E., van Baren, J., Hillebrand, M., Joosse, M., Kwon, J. M., Nowotny, P., Che, L. K., Norton, J., Morris, J. C., Reed, L. A., Trojanowski, J., Basun, H., Lannfelt, L., Neystat, M., Fahn, S., Dark, F., Tannenberg, T., Dodd, P. R., Hayward, N., Kwok, J. B., Schofield, P. R., Andreadis, A., Snowden, J., Craufurd, D., Neary, D., Owen, F., Oostra, B. A., Hardy, J.,

Goate, A., van Swieten, J., Mann, D., Lynch, T., and Heutink, P. (1998) Association of missense and 5'-splice-site mutations in tau with the inherited dementia FTDP-17. *Nature* **393**, 702-705

14. Lee, V. M., Goedert, M., and Trojanowski, J. Q. (2001) Neurodegenerative tauopathies. *Ann. Rev. Neurosci.* **24**, 1121-1159

15. van Swieten, J. C., Stevens, M., Rosso, S. M., Rizzu, P., Joosse, M., de Koning, I., Kamphorst, W., Ravid, R., Spillantini, M. G., Niermeijer, and Heutink, P. (1999) Phenotypic variation in hereditary frontotemporal dementia with tau mutations. *Ann. Neurol.* **46**, 617-626

16. Mirra, S. S., Murrell, J. R., Gearing, M., Spillantini, M. G., Goedert, M., Crowther, R. A., Levey, A. I., Jones, R., Green, J., Shoffner, J. M., Wainer, B. H., Schmidt, M. L., Trojanowski, J. Q., and Ghetti, B. (1999) Tau pathology in a family with dementia and a P301L mutation in tau. *J. Neuropathol. Exp. Neurol.* **58**, 335-345

17. Miyasaka, T., Morishima-Kawashima, M., Ravid, R., Kamphorst, W., Nagashima, K., and Ihara, Y. (2001) Selective deposition of mutant tau in the FTDP-17 brain affected by the P301L mutation. *J. Neuropathol. Exp. Neurol.* **60**, 872-884

18. Hayashi, S., Toyoshima, Y., Hasegawa, M., Umeda, Y., Wakabayashi, K., Tokiguchi, S., Iwatsubo, T., and Takahashi, H. (2002) Late-onset frontotemporal dementia with a novel exon 1 (Arg5His) tau gene mutation. *Ann. Neurol.* **51**, 525-530

19. Momeni, P., Pittman, A., Lashley, T., Vandrovcova, J., Malzer, E., Luk, C., Hulette, C., Lees, A., Revesz, T., Hardy, J., and de Silva, R. (2009) Clinical and pathological features of an Alzheimer's disease patient with the MAPT Delta K280 mutation. *Neurobiol. Aging* **30**, 388-393

20. Gibson, P. H., and Tomlinson, B. E. (1977) Numbers of Hirano bodies in the hippocampus of normal and demented people with Alzheimer's disease. *J. Neurol. Sci.* **33**, 199-206

21. Hirano, A. (1994) Hirano bodies and related neuronal inclusions. *Neuropathol. Appl. Neurobiol.* **20**, 3-11

22. Martinez-Saez, E., Gelpi, E., Rey, M., Ferrer, I., Ribalta, T., Botta-Orfila, T., Nos, C., Yague, J., and Sanchez-Valle, R. (2011) Hirano body-rich subtypes of Creutzfeldt-Jakob disease. *Neuropathol. Appl. Neurobiol.* **38**, 153-161

23. Minamide, L. S., Striegl, A. M., Boyle, J. A., Meberg, P. J., and Bamburg, J. R. (2000) Neurodegenerative stimuli induce persistent ADF/Cofilin-actin rods that disrupt distal neurite function. *Nat. Cell Biol.* **2**, 628-636

24. Fulga, T. A., Elson-Schwab, I., Khurana, V., Steinhib, M. L., Spires, T. L., T., H. B., and Feany, M. B. (2007) Abnormal bundling and accumulation of F-actin mediates tau-induced neuronal degeneration in vivo. *Nat. Cell Biol.* **9**, 139-148

25. Whiteman, I. T., Minamide, L. S., Goh de, L., Bamburg, J. R., and Goldsbury, C. (2011) Rapid changes in phospho-MAP/tau epitopes during neuronal stress: cofilin-actin rods primarily recruit microtubule binding domain epitopes. *PLoS ONE* **6**, e20878

26. Correas, I., Padilla, R., and Avila, J. (1990) The tubulin-binding sequence of brain microtubule-associated proteins, tau and MAP-2, is also involved in actin binding. *Biochem. J.* **269**, 61-64

27. Roger, B., Al-Bassam, J., Dehmelt, L., Milligan, R. A., and Halpain, S. (2004) MAP2c, but not tau, binds and bundles F-actin via its microtubule binding domain. *Curr. Biol.* **14**, 363-371

28. He, H. J., Wang, X. S., Pan, R., Wang, D. L., Liu, M. N., and He, R. Q. (2009) The proline-rich domain of tau plays a role in interactions with actin. *BMC Cell Biol*. **10**, 81

29. Goldman, J. E. (1983) The association of actin with Hirano bodies. *J. Neuropathol. Exp. Neurol*. **42**, 146-152

30. Galloway, P. G., Perry, G., and Gambetti, P. (1987) Hirano body filaments contain actin and actin-associated proteins. *J. Neuropathol. Exp. Neurol*. **46**, 185-199

31. Maciver, S. K., and Harrington, C. R. (1995) Two actin binding proteins, actin depolymerizing factor and cofilin, are associated with Hirano bodies. *Neuroreport*. **6**, 1985-1988

32. Galloway, P. G., Perry, G., Kosik, K. S., and Gambetti, P. (1987) Hirano bodies contain tau protein. *Brain Res*. **403**, 337-340

33. Peterson, C., Kress, Y., Vallee, R., and Goldman, J. E. (1988) High molecular weight microtubule-associated proteins bind to actin lattices (Hirano bodies). *Acta Neuropathol. (Berl)* **77**, 168-174

34. Jordan-Sciutto, K., Dragich, J., Walcott, D., and Bowser, R. (1998) The presence of FAC1 protein in Hirano bodies. *Neuropathol. Appl. Neurobiol*. **24**, 359-366

35. Peress, N. S., and Perillo, E. (1995) Differential expression of TFG Beta 1, 2, and 3 isotypes in Alzheimer's disease: a comparative immunohistochemical study with cerebral infarction, aged human and mouse control brains. *J. Neuropathol. Exp. Neurol*. **54**, 802-811

36. Munoz, D. G., Wang, D., and Greenberg, B. D. (1993) Hirano bodies accumulate C-terminal sequences of beta-amyloid precursor protein (beta-APP) epitopes. *J. Neuropathol. Exp. Neurol*. **52**, 14-21

37. Ha, S., Furukawa, R., and Fechheimer, M. (2011) Association of AICD and Fe65 with Hirano bodies reduces transcriptional activation and initiation of apoptosis. *Neurobiol. Aging* **32**, 2287-2298

38. Hirano, A., Dembitzer, H. M., Kurland, L. T., and Zimmerman, H. M. (1968) The fine structure of some intraganlionic alterations. *J. Neuropathol. Expt. Neurol.* **27**, 167-182

39. Lim, R. W. L., Furukawa, R., and Fechheimer, M. (1999b) Evidence of intramolecular regulation of the Dictyostelium discoideum 34,000 dalton F-actin bundling protein. *Biochemistry* **38**, 16323-16332

40. Maselli, A. G., Davis, R., Furukawa, R., and Fechheimer, M. (2002) Formation of Hirano bodies in Dictyostelium and mammalian cells induced by expression of a modified form of an actin cross-linking protein. *J. Cell Sci.* **115**, 1939-1952

41. Maselli, A. G., Furukawa, R., Thomson, S. A. M., Davis, R. C., and Fechheimer, M. (2003) Formation of Hirano bodies induced by expression of an actin cross-linking protein with a gain of function mutation. *Eucaryot. Cell* **2**, 778-787

42. Davis, R. C., Furukawa, R., and Fechheimer, M. (2008) A cell culture model for investigation of Hirano bodies. *Acta Neuropathol. (Berl)* **115**, 205-217

43. Ha, S., Furukawa, R., Stramiello, M., Wagner, J. J., and Fechheimer, M. (2011) Transgenic mouse model for the formation of Hirano bodies. *BMC Neurosci.* **12**, 97-113

44. Furgerson, M., Fechheimer, M., and Furukawa, R. (2012) Model Hirano bodies protect against tau-independent and tau-dependent cell death initiated by the amyloid precursor protein intracellular domain. *PLoS ONE* **7**, e44996

45. Ittner, L. M., and Gotz, J. (2011) Amyloid-beta and tau--a toxic pas de deux in Alzheimer's disease. *Nat Rev Neurosci* **12**, 65-72

46. Hoover, B. R., Reed, M. N., Su, J., Penrod, R. D., Kotilinek, L. A., Grant, M. K., Pitstick, R., Carlson, G. A., Lanier, L. M., Yuan, L. L., Ashe, K. H., and Liao, D. (2010) Tau mislocalization to dendritic spines mediates synaptic dysfunction independently of neurodegeneration. *Neuron* **68**, 1067-1081

47. Barghorn, S., Zheng-Fischhofer, Q., Ackmann, M., Biernat, J., von Bergen, M., Mandelkow, E. M., and Mandelkow, E. (2000) Structure, microtubule interactions, and paired helical filament aggregation by tau mutants of frontotemporal dementias. *Biochemistry* **39**, 11714-11721

48. von Bergen, M., Barghorn, S., Li, L., Marx, A., Biernat, J., Mandelkow, E. M., and Mandelkow, E. (2001) Mutations of tau protein in frontotemporal dementia promote aggregation of paired helical filaments by enhancing local beta-structure. *J. Biol. Chem.* **276**, 48165-48174

49. Goedert, M., Jakes, R., and Crowther, R. A. (1999) Effects of frontotemporal dementia FTDP-17 mutations on heparin-induced assembly of tau filaments. *FEBS Lett.* **450**, 306-311

50. Wang, Y. P., Biernat, J., Pickhardt, M., Mandelkow, E., and Mandelkow, E. M. (2007) Stepwise proteolysis liberates tau fragments that nucleate the Alzheimer-like aggregation of full-length tau in a neuronal cell model. *Proc. Natl. Acad. Sci. U.S.A.* **104**, 10252-10257

51. Eckermann, K., Mocanu, M. M., Khlistunova, I., Biernat, J., Nissen, A., Hofmann, A., Schonig, K., Bujard, H., Haemisch, A., Mandelkow, E., Zhou, L., Rune, G., and Mandelkow, E. M. (2007) The beta-propensity of Tau determines aggregation and synaptic loss in inducible mouse models of tauopathy. *J. Biol. Chem.* **282**, 31755-31765

52. Mocanu, M. M., Nissen, A., Eckermann, K., Khlistunova, I., Biernat, J., Drexler, D., Petrova, O., Schonig, K., Bujard, H., Mandelkow, E., Zhou, L., Rune, G., and Mandelkow, E. M. (2008) The potential for beta-structure in the repeat domain of tau protein determines aggregation, synaptic decay, neuronal loss, and coassembly with endogenous Tau in inducible mouse models of tauopathy. *J. Neurosci.* **16**, 737-748

53. Fatouros, c., Pir, G. J., Biernat, J., Koushika, S. P., Mandelkow, E., Mandelkow, E. M., Schmidt, E., and Baumeister, R. (2012) Inhibition of tau aggregation in a novel Caenorhabditis elegans model of tauopathy mitigates proteotoxicity. *Hum. Mol. Genet.* **21**, 3587-3603

54. Khlistunova, I., Biernat, J., Wang, Y., Pickhardt, M., von Bergen, M., Gazova, Z., Mandelkow, E., and Mandelkow, E. M. (2006) Inducible expression of Tau repeat domain in cell models of tauopathy: aggregation is toxic to cells but can be reversed by inhibitor drugs. *J. Biol. Chem.* **281**, 1205-1214

55. Sydow, A., Van der Jeugd, A., Zheng, F., Ahmed, T., Balschun, D., Petrova, O., Drexler, D., Zhou, L., Rune, G., Mandelkow, E., D'Hooge, R., Alzheimer, C., and Mandelkow, E. M. (2011) Tau-induced defects in synaptic plasticity, learning, and memory are reversible in transgenic mice after switching off the toxic Tau mutant. *J. Neurosci.* **31**, 2511-2525

56. Santa-Maria, I., Santpere, G., MacDonald, M. J., de Barreda, E. G., Hernandez, F., Moreno, F. J., Ferrer, I., and Avila, J. (2008) Coenzyme Q Induces Tau Aggregation, Tau Filaments, and Hirano Bodies. *J. Neuropathol. Exp. Neurol.* **67**, 428-434

57. Kremer, A., Louis, J. V., Jaworski, T., and Van Leuven, F. (2011) GSK3 and Alzheimer's Disease: Facts and Fiction. *Front. Mol. Neurosci.* **4**, 17

58. Takashima, A., Noguchi, K., Michel, G., Mercken, M., Hoshi, M., Ishiguro, K., and Imahori, K. (1996) Exposure of rat hippocampal neurons to amyloid beta peptide (25-35) induces the inactivation of phosphatidyl inositol-3 kinase and the activation of tau protein kinase I/glycogen synthase kinase-3 beta. *Neurosci. Lett.* **203**, 33-36

59. Bardai, F. H., and D'Mello, S. R. (2011) Selective toxicity by HDAC3 in neurons: regulation by Akt and GSK3beta. *J. Neurosci.* **31**, 1746-1751

60. Kuret, J., Congdon, E. E., Li, G., Yin, H., Yu, X., and Zhong, Q. (2005) Evaluating triggers and enhancers of tau fibrillization. *Microsc. Res. Tech.* **67**, 141-155

61. Ramachandran, G., and Udgaonkar, J. B. (2013) Mechanistic studies unravel the complexity inherent in tau aggregation leading to Alzheimer's disease and the tauopathies. *Biochemistry* **52**, 4107-4126

62. Kotani, S., Nishida, E., Kumagai, H., and Sakai, H. (1985) Calmodulin inhibits interaction of actin with MAP2 and Tau, two major microtubule-associated proteins. *J. Biol. Chem.* **260**, 10779-10783

63. Kempf, M., Clement, A., Faissner, A., Lee, G., and Brandt, R. (1996) Tau binds to the distal axon early in development of polarity in a microtubule- and microfilament-dependent manner. *J. Neurosci.* **16**, 5583-5592

64. Maas, T., Eidenmuller, J., and Brandt, R. (2000) Interaction of tau with the neural membrane cortex is regulated by phosphorylation at sites that are modified in paired helical filaments. *J. Biol. Chem.* **275**, 15733-15740

65. Farias, G. A., Munoz, J. P., Garrido, J., and Maccioni, R. B. (2002) Tubulin, actin, and tau protein interactions and the study of their macromolecular assemblies. *J. Cell. Biochem.* **85**, 315-324

66. Steinhilb, M. L., Dias-Santagata, D., Fulga, T. A., Felch, D. L., and Feany, M. B. (2007) Tau phosphorylation sites work in concert to promote neurotoxicity in vivo. *Mol. Biol. Cell*

18, 5060-5068

67. Biernat, J., Gustke, N., Drewes, G., Mandelkow, E. M., and Mandelkow, E. (1993) Phosphorylation of Ser262 strongly reduces binding of tau to microtubules: distinction between PHF-like immunoreactivity and microtubule binding. *Neuron* **11**, 153-163

68. Satoh, J., Tabunoki, H., Ishida, T., Saito, Y., and Arima, K. (2013) Ubiquilin-1 immunoreactivity is concentrated on Hirano bodies and dystrophic neurites in Alzheimer's disease brains. *Neuropath. and Appl. Neurobiol.* **39**, 817-830

69. Selden, S. C., and Pollard, T. D. (1983) Phosphorylation of microtubule-associated proteins regulates their interaction with actin filaments. *J. Biol. Chem.* **258**, 7064-7071

70. Griffith, L. M., and Pollard, T. D. (1982) Cross-linking of actin filament networks by self-association and actin-bonding macromolecules. *J. Biol. Chem.* **257**, 9135-9142

71. Barbato, C., Canu, N., Zambrano, N., Serafino, A., Minopoli, G., Ciotti, M. T., Amadoro, G., Russo, T., and Calissano, P. (2005) Interaction of Tau with Fe65 links tau to APP. *Neurobiol. Dis.* **18**, 399-408

72. Vogelsberg-Ragaglia, V., Bruce, J., Richter-Landsberg, C., Zhang, B., Hong, M., Trojanowski, J. Q., and Lee, V. M. (2000) Distinct FTDP-17 missense mutations in tau produce tau aggregates and other pathological phenotypes in transfected CHO cells. *Mol. Biol. Cell* **11**, 4093-4104

73. Krishnamurthy, P., and Johnson, G. V. (2004) Mutant (R406W) human tau is hyperphosphorylated and does not efficiently bind microtubules in a neuronal cortical cell model. *J. Biol. Chem.* **279**, 7893-7900

74. Alonso, A. D., Mederlyova, A., Novak, M., Grundke-Iqbal, I., and Iqbal, K. (2004) Promotion of hyperphosphorylation by frontotemporal dementia tau mutations. *J. Biol. Chem.* **279**, 34873-34881

75. Hong, M., Zhukareva, V., Vogelsberg-Ragaglia, V., Wszolek, Z., Reed, L., Miller, B. I., Geschwind, D. H., Bird, T. D., McKeel, D., Goate, A., Morris, J. C., Wilhelmsen, K. C., Schellenberg, G. D., Trojanowski, J. Q., and Lee, V. M. (1998) Mutation-specific functional impairments in distinct tau isoforms of hereditary FTDP-17. *Science* **282**, 1914-1917

76. Feinstein, S. C., and Wilson, L. (2005) Inability of tau to properly regulate neuronal microtubule dynamics: a loss-of-function mechanism by which tau might mediate neuronal cell death. *Biochim Biophys Acta* **1739**, 268-279

77. Bramblett, G. T., Goedert, M., Jakes, R., Merrick, S. E., Trojanowski, J. Q., and Lee, V. M. (1993) Abnormal tau phosphorylation at Ser396 in Alzheimer's disease recapitulates development and contributes to reduced microtubule binding. *Neuron* **10**, 1089-1099

78. Alonso, A. D., Zaidi, T., Novak, M., Grundke-Iqbal, I., and Iqbal, K. (2001) Hyperphosphorylation induces self-assembly of tau into tangles of paired helical filaments/straight filaments. *Proc. Nat. Acad. Sci. U.S.A.* **98**, 6923-6928

79. Alonso, A. D., Zaidi, T., Novak, M., Barra, H. S., Grundke-Iqbal, I., and Iqbal, K. (2001) Interaction of tau isoforms with Alzheimer's disease abnormally hyperphosphorylated tau and in vitro phosphorylation into disease-like protein. *J. Biol. Chem.* **276**, 37967-37973

80. Perez, M., Hernandez, F., Lim, F., Diaz-Nido, J., and Avila, J. (2003) Chronic lithium treatment decreases mutant tau protein aggregation in a transgenic mouse model. *J. Alz. Dis.* **5**, 301-308

81. Noble, W., Planel, E., Zehr, C., Olm, V., Meyerson, J., Suleman, F., Gaynor, K., Wang, L., LaFrancois, J., Feinstein, B., Burns, M., Krishnamurthy, P., Wen, Y., Bhat, R., Lewis, J., Dickson, D., and Duff, K. (2005) Inhibition of glycogen synthase kinase-3 by lithium correlates with reduced tauopathy and degeneration in vivo. *Proc. Natl. Acad. Sci.U.S.A.* **102**, 6990-6995

82. Alonso, A. D., Adel, C., Li, B., Grundke-Iqbal, I., and Iqbal, K. (2006) Polymerization of hyperphosphorylated tau into filaments eliminates its inhibitory activity. *Proc. Natl. Acad. Sci. U.S.A.* **103**, 8864-8869

83. Jeganathan, S., Hascher, A., Chinnathambi, S., Biernat, J., Mandelkow, E. M., and Mandelkow, E. (2008) Proline-directed pseudo-phosphorylation at AT8 and PHF1 epitopes induces a compaction of the paperclip folding of Tau and generates a pathological (MC-1) conformation. *J. Biol. Chem.* **283**, 32066-32076

84. Eidenmüller, J., Fath, T., Hellwig, A., Reed, J., Sontag, E., and Brandt, R. (2000) Structural and functional implications of tau hyperphosphorylation: information from phosphorylation-mimicking mutated tau proteins. *Biochemistry* **39**, 13166-13175

85. Cho, J. H., and Johnson, G. V. (2004) Primed phosphorylation of tau at Thr231 by glycogen synthase 3beta (GSK3beta) play a critical role in regulating tau's ability to bind and stabilize microtubules. *J. Neurochem.* **88**, 349-358

86. Li, T., and Paudel, H. K. (2006) Glycogen synthase kinase 3beta phosphorylates Alzheimer's disease-specific Ser396 of microtubule-associated protein tau by a sequential mechanism. *Biochemistry* **45**, 3125-3133

87. Sengupta, A., Novak, M., Grundke-Iqbal, I., and Iqbal, K. (2006) Regulation of phosphorylation of tau by cyclin-dependent kinase 5 and glycogen kinase-3 at substrate level. *FEBS Lett* **580**, 5925-5933

88. Liu, S. J., Zhang, J. Y., Li, H. L., Fang, Z. Y., Wang, Q., Deng, H. M., Gong, C. X., Grundke-Iqbal, I., and Iqbal, K. (2004) Tau becomes a more favorable substrate for GSK-3 when it is prephosphorylated by PKA in rat brain. *J. Biol. Chem.* **279**, 50078-50088

89. Shahani, N., Subramaniam, S., Wolf, T., Tackenberg, C., and Brandt, R. (2006) Tau aggregation and progressive neuronal degeneration in the absence of changes in spine density and morphology after targeted expression of Alzheimer's disease-relevant tau constructs in organotypic hippocampal slices. *J. Neurosci.* **26**, 6103-6114

90. Morris, M., Maeda, S., Vossel, K., and Mucke, L. (2011) The many faces of tau. *Neuron* **70**, 410-426

91. von Bergen, M., Friedhoff, P., Biernat, J., Heberle, J., Mandelkow, E. M., and Mandelkow, E. (2000) Assembly of tau protein into Alzheimer paired helical filaments depends on a local sequence motif ((306)VQIVYK(311)) forming beta structure. *Proc. Natl. Acad. Sci. U.S.A.* **97**, 5129-5134

92. Chang, E., Kim, S., Yin, H., Nagaraja, H. N., and Kuret, J. (2008) Pathogenic missense MAPT mutations differentally modulate tau aggregation propensity at nucleation and extension steps. *J. Neurochem.* **107**, 1113-1123

93. Dayanandan, R., Van Slegtenhorst, M., Mack, T. G., Ko, L., Yen, S. H., Leroy, K., Brion, J. P., Anderton, B. H., Hutton, M., and Lovestone, S. (1999) Mutations in tau reduce its microtubule binding properties in intact cells and affect its phosphorylation. *FEBS Lett*. **446**, 228-232

94. Connell, J. W., Gibb, G. M., Betts, J. C., Blackstock, W. P., Gallo, J., Lovestone, S., Hutton, M., and Anderton, B. H. (2001) Effects of FTDP-17 mutations on the in vitro phosphorylation of tau by glycogen synthase kinase 3beta identified by mass spectrometry demonstrate certain mutations exert long-range conformational changes. *FEBS Lett*. **493**, 40-44

95. Gauthier-Kemper, A., Weissmann, C., Golovyashkina, N., Sebo-Lemke, Z., Drewes, G., Gerke, V., Heinisch, J. J., and Brandt, R. (2011) The frontotemporal dementia mutation R406W blocks tau's interaction with the membrane in an annexin A2-dependent manner. *J. Cell Biol*. **192**, 647-661

96. Wszolek, Z. K., Tsuboi, Y., Ghetti, B., Pickering-Brown, S., Baba, Y., and Cheshire, W. P. (2006) Frontotemporal dementia and parkinsonism linked to chromosome 17 (FTDP-17). *Orphanet J. Rare Dis*. **1**, 30

97. Furukawa, R., and Fechheimer, M. (1996) Role of the Dictyostelium 30 kDa protein in actin bundle formation. *Biochemistry* **35**, 7224-7232

98. Kinoshita, A., Whelan, C. M., Berezovska, O., and Hyman, B. T. (2002) The gamma secretase-generated carboxyl-terminal domain of the amyloid precursor protein induces apoptosis via Tip60 in H4 cells. *J. Biol. Chem*. **277**, 28530-28536

99. Summers, S. A., Kao, A. W., Kohn, A. D., Backus, G. S., Roth, R. A., Pessin, J. E., and Birnbaum, M. J. (1999) The role of glycogen synthase kinase 3beta in insulin-stimulated glucose metabolism. *J. Biol. Chem.* **274**, 17934-17940

100. Stambolic, V., and Woodgett, J. R. (1994) Mitogen inactivation of glycogen synthase kinase-3b in intact cells via serine 9 phosphorylation. *Biochem. J.* **303**, 701-704

101. Fath, T., Eldenmüller, J., and Brandt, R. (2002) Tau-mediated cytotoxicity in a pseudohyperphosphorylation model of Alzheimer's disease. *J. Neurosci.* **22**, 9733-9741

102. Hedgepeth, C. M., Conrad, L. J., Zhang, J., Huang, H. C., Lee, V. M., and Klein, P. S. (1997) Activation of the Wnt signaling pathway: a molecular mechanism for lithium action. *Devel. Biol.* **185**, 82-91

103. Gibson, P. H. (1978) Light and electron microscopic observations on the relationship between Hirano bodies, neuron and glial perikarya in the human hippocampus. *Acta Neuropathol. (Berl)* **42**, 165-171

104. Garwood, C. J., Pooler, A. M., Atherton, J., Hanger, D. P., and Noble, W. (2011) Astrocytes are important mediators of Abeta-induced neurotoxicity and tau phosphorylation in primary culture. *Cell Death Dis.* **2**, e167

105. Dickey, C. A., Erickson, J., Kamal, A., Burrows, F., Kasibhatla, S., Eckman, C. B., Hutton, M., and Petrucelli, L. (2005) Development of a high throughput drug sceening assy for detection of changes in tau levels--proof of concept with HSP90 inhibitors. *Curr. Alzheimer Res.* **2**, 231-238

106. Bretteville, A., Ando, K., Ghestem, A., Loyens, A., Begard, S., Beauvillian, J. C., Sergant, N., Hamdane, M., and Buee, L. (2009) Two-dimensional electrophoresis of tau

mutants reveals specific phosphorylation pattern likely linked to early tau conformational changes. *PloS one* **4**, e4843

107. Barghorn, S., Biernat, J., and Mandelkow, E. (2004) Purification of Recombinant Tau Protein and Preparation of Alzheimer-Paired Helical Filaments In Vitro. in *Amyloid Proteins: Methods and Protocols* (Sigurdsson, E. M. ed.), Humana Press, Totowa, NJ. pp 35-51

108. Spudich, J. A., and Watt, S. (1971) The regulation of rabbit skeletal muscle contraction. *J. Biol. Chem.* **246**, 4866-4871

109. MacLean-Fletcher, S. D., and Pollard, T. D. (1980a) Identification of a factor in conventional muscle actin preparations which inhibits actin filament self-association. *Biochem. Biophys. Res. Comm.* **96**, 18-27

110. Smith, P. K., Krohn, R. I., Hermanson, G. T., Mallia, A. K., Gartner, F. H., Provenzano, M. D., Fujimoto, E. K., Goeke, N. M., Olson, B. J., and Klenk, D. C. (1985) Measurement of protein using bicinchoninic acid. *Analytical Biochemistry* **150**, 76-85

111. Fechheimer, M. (1987) The Dictyostelium discoideum 30,000-dalton protein is an actin filament-bundling protein that is selectively present in filopodia. *J. Cell Biol.* **104**, 1539-1551

Figure 3.1: Schematic illustration of tau isoforms, phosphorylation sites and mutations. Point mutations R5H, G272V, P301L, and R406W were created in the 2N4R (441) tau isoform. Arrows represent boundaries of K18 (amino acids 244-372) (54). N1 and N2 represent N-terminal exons 1 and 2. R1, R2, R3, and R4 represent microtubule binding domain repeats 1-4. Yellow circles designate 10 serine/threonine to glutamic acid mutations that occur in 352PHP tau (101). This mutant was created in the 352 tau isoform lacking N1, N2, and R2.

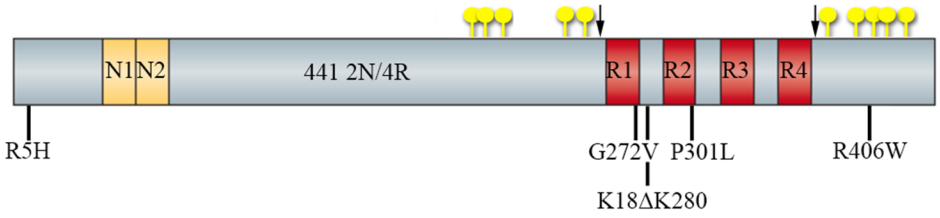
N1
N2
441 2N/4R
R1
R2
R3
R4
R5H
G272V
P301L
R406W
K18ΔK280

Figure 3.2: FTDP-17 tau and model Hirano bodies differentially modulate cell death. H4 cells were transiently transfected with equal amounts of plasmid DNA encoding AICD and/or tau in the presence (check, stripe bars) or absence (gray, black bars) of model Hirano bodies (CT-GFP). Model Hirano bodies protect from cell death induced by AICD and tau, except for tau mutants G272V and P301L. Note that G272V and P301L potentiate cell death in the presence of model Hirano bodies alone. *$p < 0.05$, **$p < 0.01$, ***$p < 0.001$. Error bars represent the standard deviation.

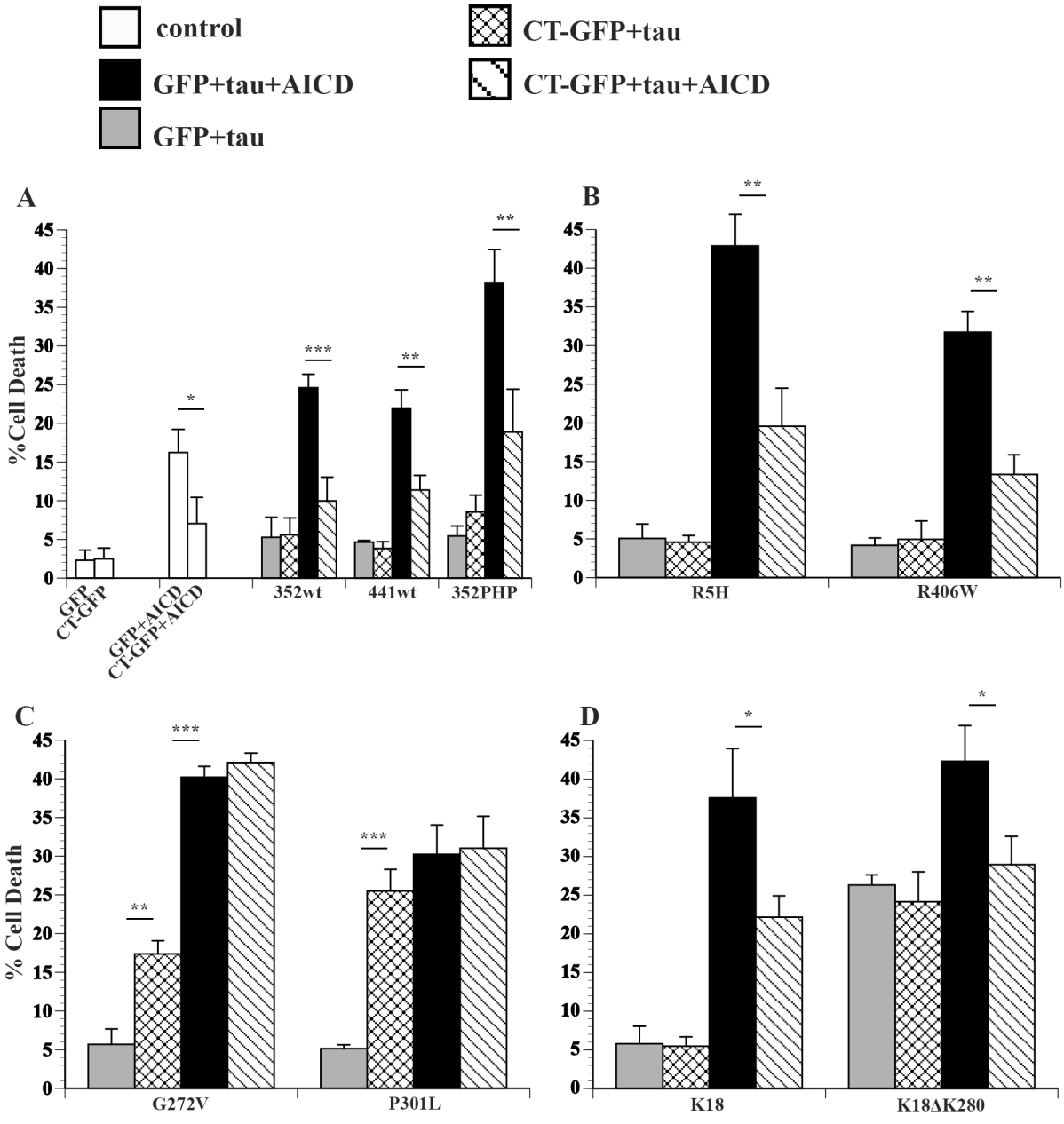
control
GFP+tau+AICD
GFP+tau
CT-GFP+tau
CT-GFP+tau+AICD
A
%Cell Death
GFP
CT-GFP
GFP+AICD
CT-GFP+AICD
352wt
441wt
352PHP
B
R5H
R406W
C
% Cell Death
G272V
P301L
D
K18
K18ΔK280

Figure 3.3: Relative binding of recombinant tau to F-actin. Tau binds differentially to F-actin with binding of R406W (blue square), G272V (red circle), P301L (blue triangle), and 441WT (green triangle) > 352PHP (purple diamond) and R5H (black circle) > 352WT (orange square). The curves are to aid the reader and do not indicate biochemical binding curves. The standard deviations were not shown for clarity.

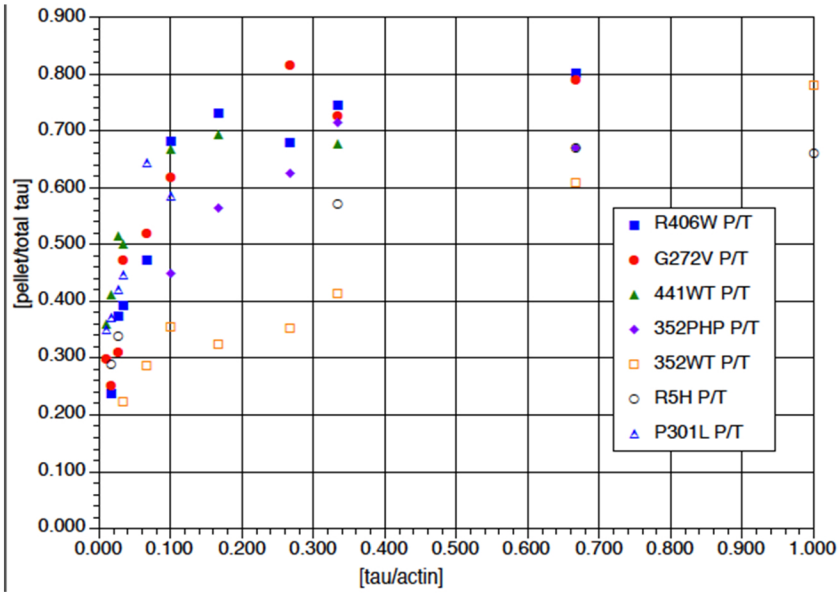
0.900
0.800
0.700
0.600
0.500
0.400
0.300
0.200
0.100
0.000
[pellet/total tau]
0.000
0.100
0.200
0.300
0.400
0.500
0.600
0.700
0.800
0.900
1.000
[tau/actin]
R406W P/T
G272V P/T
441WT P/T
352PHP P/T
352WT P/T
R5H P/T
P301L P/T

Figure 3.4: Model Hirano bodies differentially influence cell death in the presence of GSK3β (S9A) and tau. H4 cells were transiently transfected with equal amounts of plasmid DNA encoding constitutively active GSK3β (S9A) and tau (black bars) or GSK3β (S9A), tau, and model Hirano bodies (check bars). Model Hirano bodies significantly promote cell death induced by GSK3β (S9A) and tau except in tau mutants R5H, R406W, K18, and K18ΔK280, where they have no effect. *$p < 0.05$, **$p < 0.01$, ***$p < 0.001$. Error bars represent the standard deviation.

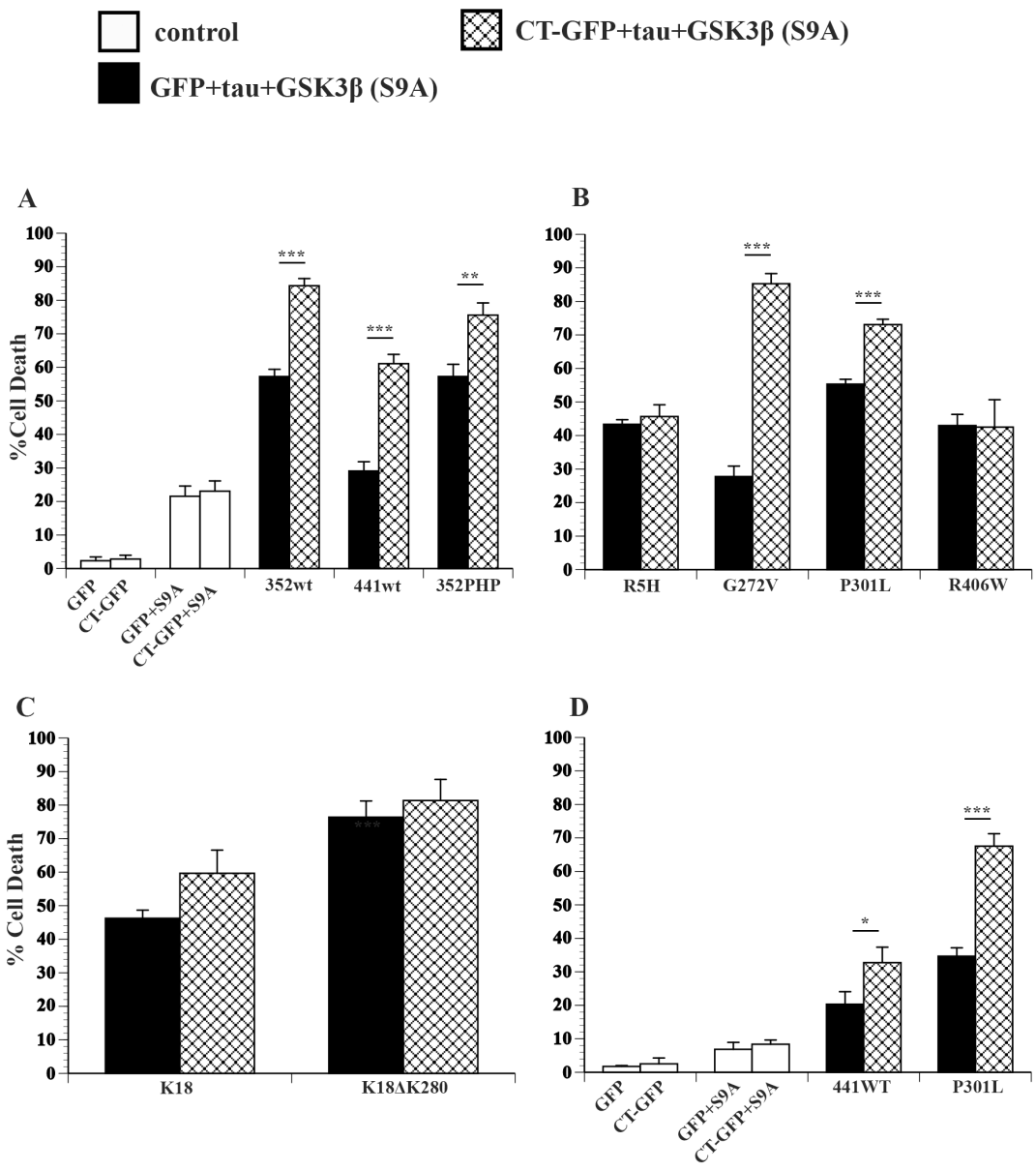
control
GFP+tau+GSK3β (S9A)
CT-GFP+tau+GSK3β (S9A)
A
%Cell Death
GFP
CT-GFP
GFP+S9A
CT-GFP+S9A
352wt
441wt
352PHP
B
R5H
G272V
P301L
R406W
C
% Cell Death
K18
K18ΔK280
D
GFP
CT-GFP
GFP+S9A
CT-GFP+S9A
441WT
P301L

Figure 3.5: GSK3β (K85A) differentially influences cell death in the presence of AICD and tau. H4 cells were transiently transfected with equal amounts of plasmid DNA encoding tau in the absence (grey bars) or presence of AICD (black bars) or dominant negative GSK3β (K85A) and tau in the absence (check bar) or presence of AICD (striped bar). GSK3β (K85A) significantly decreases cell death due to AICD and tau except in tau constructs 352WT, 441WT, K18ΔK280 where there is no effect. *$p < 0.05$, **$p < 0.01$, ***$p < 0.001$. Error bars represent the standard deviation.

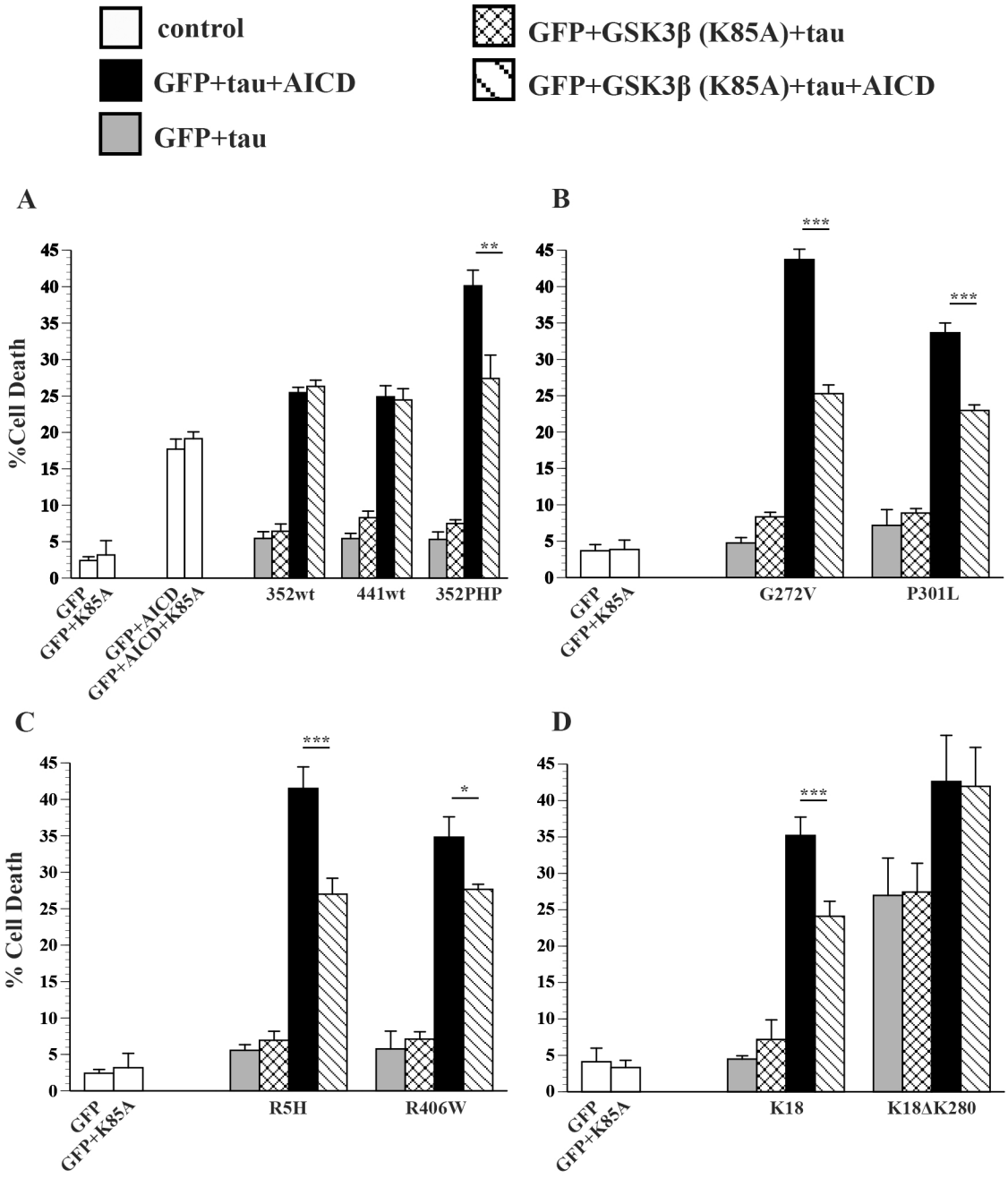
control
GFP+tau+AICD
GFP+tau
GFP+GSK3β (K85A)+tau
GFP+GSK3β (K85A)+tau+AICD
A
B
C
D
%Cell Death
% Cell Death
GFP
GFP+K85A
GFP+AICD
GFP+AICD+K85A
352wt
441wt
352PHP
G272V
P301L
R5H
R406W
K18
K18ΔK280
**
***
*

Figure 3.6: Western blot analysis of GSK3β levels and tau phosphorylation. HEK293 cells were transiently transfected with equal amounts of plasmid. NT = Not Transfected control. A. Expression of exogenous AICD increases total GSK3β protein. Expression of CT-GFP in addition to AICD reduces GSK3β to control levels. Expression of tau has no effect on levels of GSK3β. B. The presence of exogenous CT-GFP increases phosphorylation of G272V at Ser199/Ser202 and Thr231 and of P301L at Ser199/Ser202. Expression of CT-GFP has no effect on 441WT, R406W, or R5H tau phosphorylation at any epitope measured.

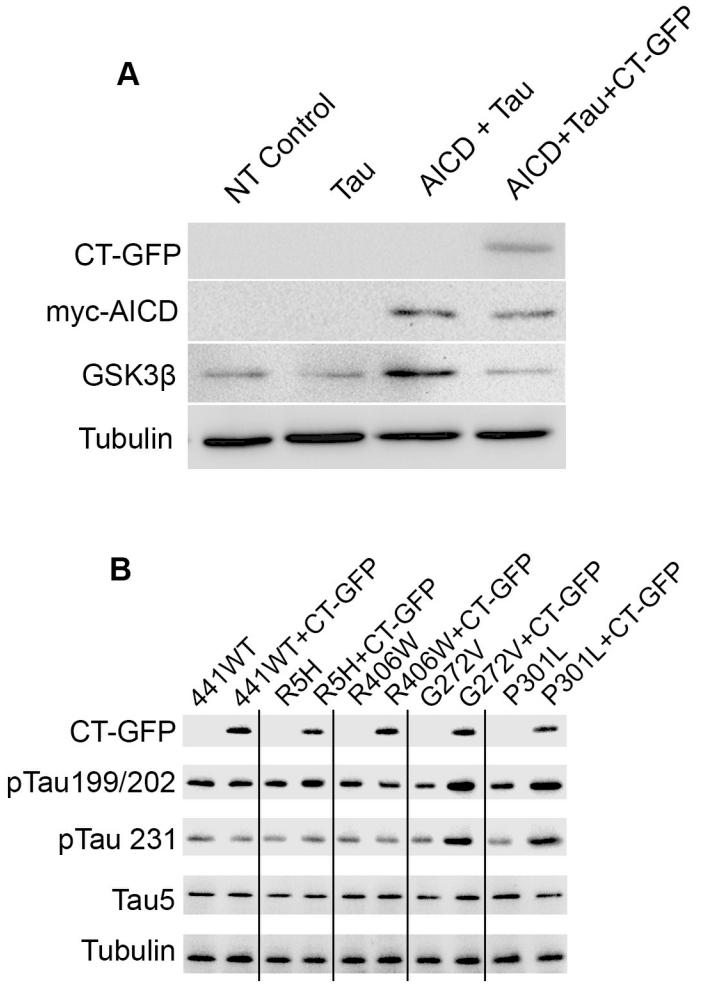
A
NT Control
Tau
AICD + Tau
AICD+Tau+CT-GFP
CT-GFP
myc-AICD
GSK3β
Tubulin
B
441WT
441WT+CT-GFP
R5H
R5H+CT-GFP
R406W
R406W+CT-GFP
G272V
G272V+CT-GFP
P301L
P301L+CT-GFP
CT-GFP
pTau199/202
pTau 231
Tau5
Tubulin

Figure 3.7: Immunofluorescence localization of tau and model Hirano bodies. H4 cells were transiently transfected with FLAG-tagged tau constructs and CT-GFP to induce model Hirano bodies. 24 h post-transfection, cells were fixed and stained for good preservation of F-actin. Tau was stained with anti-FLAG primary antibody and Alexa Fluor350 secondary antibody (blue). F-actin was stained using TRITC-phalloidin (red). All tau isoforms colocalize with model Hirano bodies except 352PHP, which is localized diffusely throughout the cell. A. Control tau 352WT, 441 WT, K18. B. Mutant tau R5H, G272V, P301L, R406W, K18ΔK280, 352PHP. Scale bar = 20 μm.

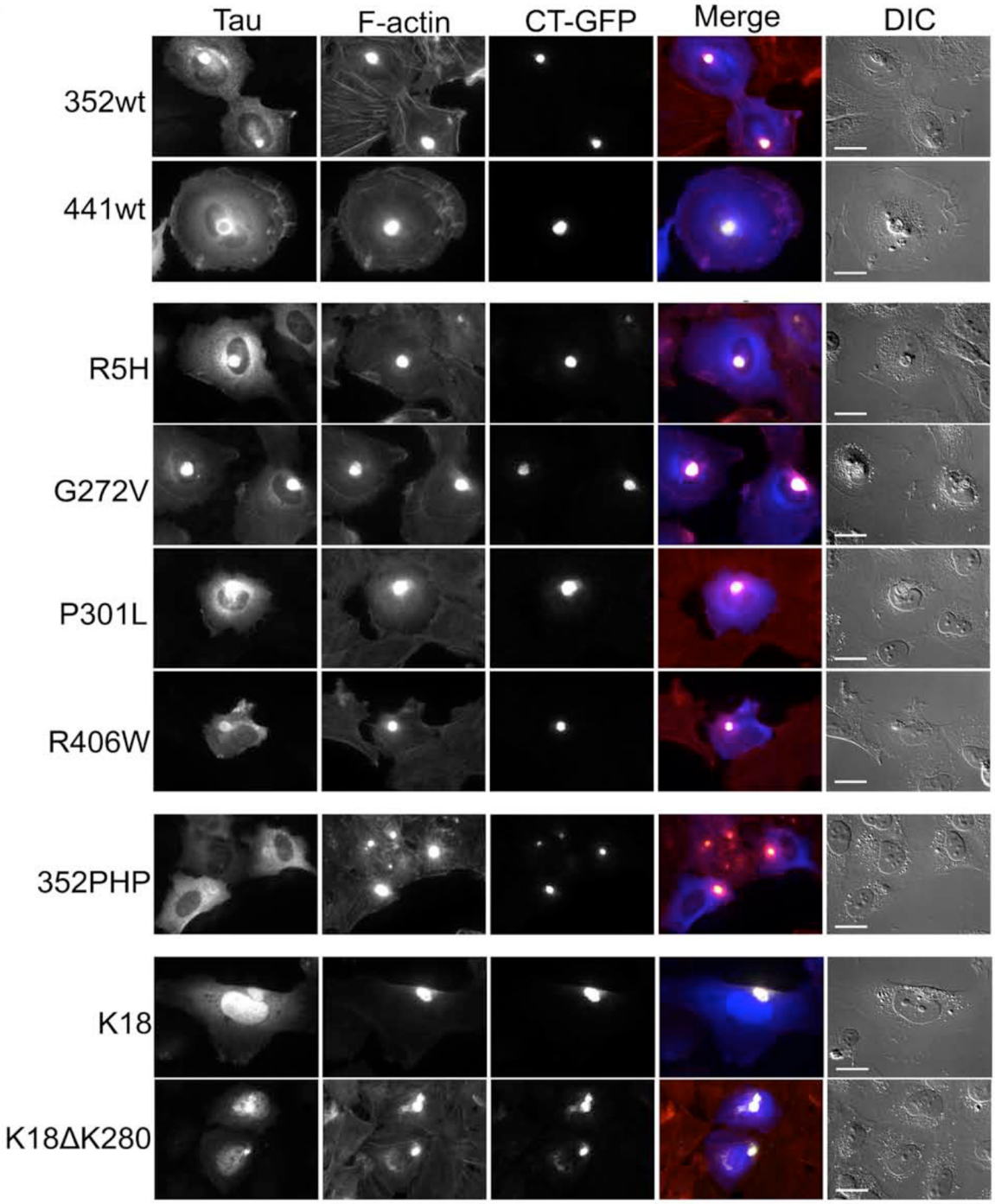
Tau
F-actin
CT-GFP
Merge
DIC
352wt
441wt
R5H
G272V
P301L
R406W
352PHP
K18
K18ΔK280

Figure 3.8: Immunohistochemistry localization of tau and Hirano bodies in human brains. Immunohistochemistry was performed on paraffin embedded human brain sections using Tau5 or pTau-199/202 antibodies following an eosin counterstain to visualize Hirano bodies (arrows). Tau5 antibodies colocalized with Hirano bodies in both Alzheimer diseased and control brains while pTau-199/202 colocalized with Hirano bodies only in Alzheimer diseased brains. Scale bar = 50 μm

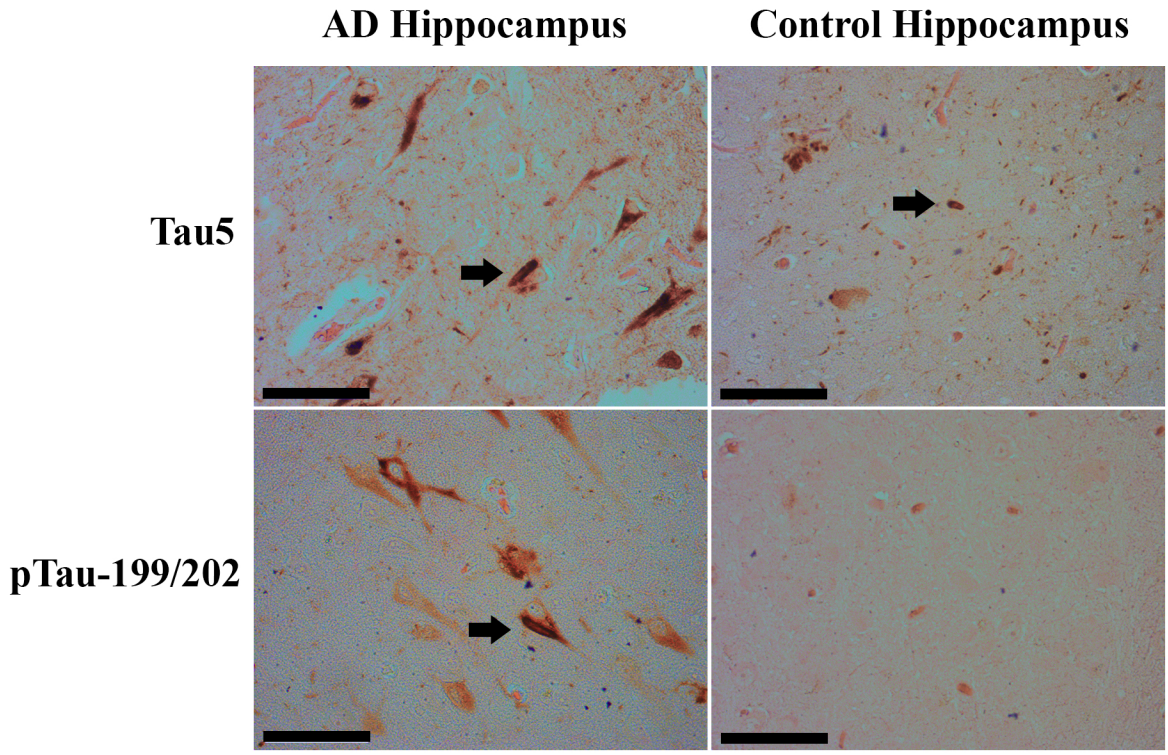
AD Hippocampus
Control Hippocampus
Tau5
pTau-199/202

Figure 3.9: Model of the interplay between AICD, tau, and model Hirano bodies.

A. The black line represents cell death initiated by "AICD only" pathway involving Fe65, Tip60, p53, and caspases (41, 6). B. Blue line represent the modest levels of cell death initiated by "tau only" including K18ΔK280 alone and low levels of cell death from all other tau alone (green boxes). C. The pink arrows represent the synergistic cell death due to AICD and either G272V, P301L, K18, RH5, R406W, or 352PHP tau. 441WT, 352WT, and K18ΔK280 do not synergize with AICD to promote cell death. D. Model Hirano bodies protect against AICD-induced cell death and cell death initiated by AICD and K18, RH5, R406W, or 352PHP tau (red lines). In contrast, model Hirano bodies potentiate AICD-induced cell death in the presence of either P301L or G272V tau (green lines). Model Hirano bodies alone have no impact on K18, R5H, R406W, 352PHP, 441WT, 352WT, or K18ΔK280 tau-induced cell death or have negative consequences. In addition, the synergistic cell death induced by AICD in the presence of G272V or P301L tau is not affected by the presence of model Hirano bodies. E. Expression of the dominant negative GSK3-β (K85A) prevents cell death initiated by synergistic interaction of AICD and tau or model Hirano bodies and G272V or P301L tau (red lines).

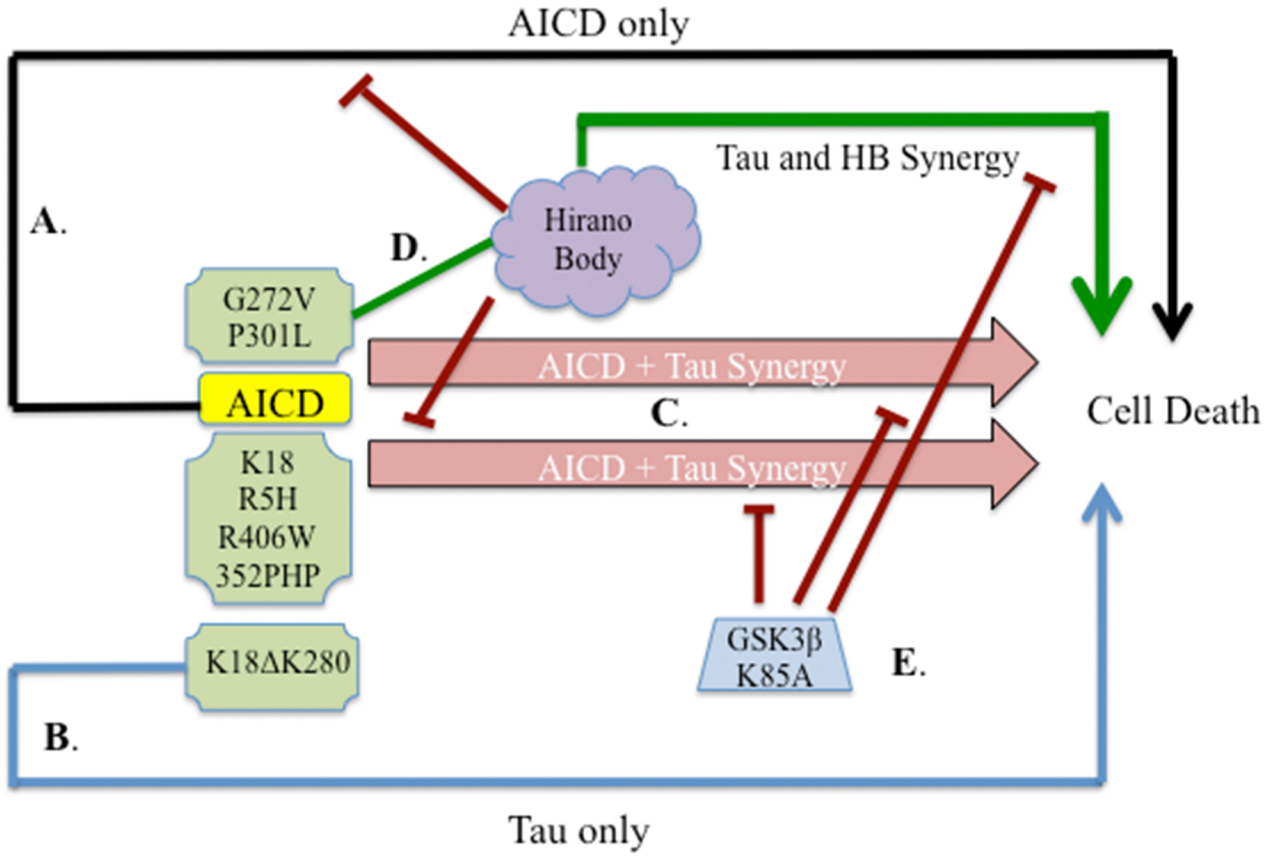
AICD only
A.
Tau and HB Synergy
Hirano Body
D.
G272V
P301L
AICD
AICD + Tau Synergy
C.
Cell Death
K18
R5H
R406W
352PHP
AICD + Tau Synergy
K18ΔK280
GSK3β
K85A
E.
B.
Tau only

Figure 3.10. Mutant tau does not affect model Hirano body formation. H4 cells were transiently transfected with equal amounts of plasmid DNA encoding CT-GFP to induce model Hirano bodies in the absence (white bars) or presence of either 352WT (stripe bar), 441WT (grey bar), 352 PHP (black bar), or P301L crosshatch bar). Cells were fixed after 48 hrs. Model Hirano bodies were characterized as normal, fibrillar, Hirano body, or large Hirano body as determined by GFP fluorescence. There is no difference between the populations of cells. Scale bar = 20 μm.

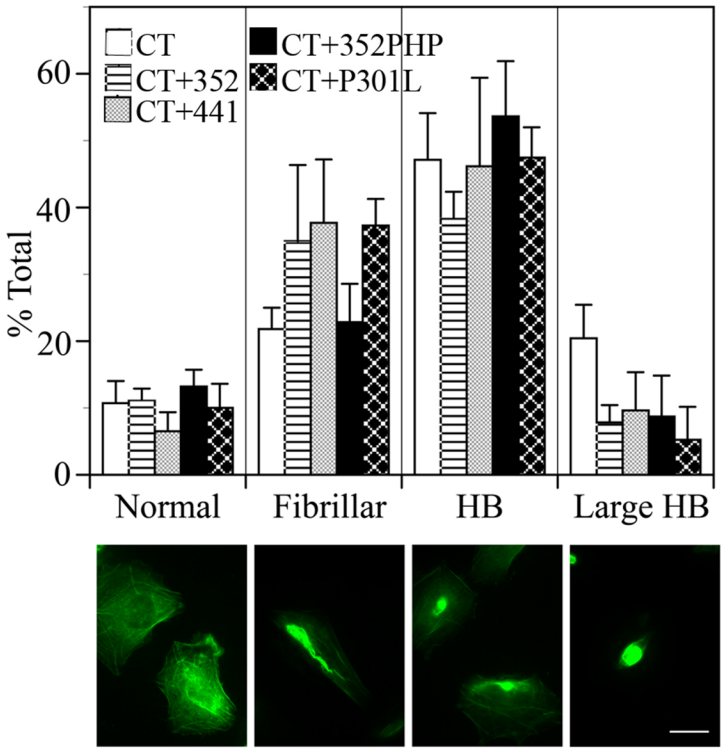
CT
CT+352
CT+441
CT+352PHP
CT+P301L
% Total
60
40
20
0
Normal
Fibrillar
HB
Large HB

Table 3.1. Additive versus synergistic cell death induced by co-expression of AICD and tau. Values of cell death obtained when GFP/AICD or GFP/tau transiently expressed were added together and compared to the actual values of cell death obtained when GFP/AICD/tau were co-expressed. Synergistic cell death (bold entries) was observed when AICD was co-expressed with 352PHP, R5H, K18, P301L, G272V, or R406W. N.S. = not significant

Tau	%Cell Death (Additive)= GFP/AICD+GFP/tau	%Cell Death ±SD (Actual) = GFP/AICD/tau	p value
352tauWT	22.3% ± 1.46	24.6% ± 1.74	N.S.
441tauWT	20.9% ± 2.78	22.0% ± 2.36	N.S.
352tauPHP	**21.7% ± 1.98**	**38.1% ± 4.35**	**p < 0.05**
R5H	**21.3% ± 2.49**	**42.9% ± 4.09**	**p < 0.01**
K18	**22.0% ± 4.24**	**39.0% ± 6.98**	**p < 0.05**
K18ΔK280	42.5% ± 4.28	42.3% ± 4.61	N.S.
P301L	**21.4% ± 2.97**	**30.2% ± 3.79**	**p < 0.05**
G272V	**21.9% ± 2.73**	**40.2% ± 1.40**	**p < 0.01**
R406W	**20.4% ± 3.93**	**31.7% ± 2.70**	**p < 0.05**

Table 3.2. Additive versus synergistic cell death induced by co-expression of tau and GSK3β (S9A). Values of cell death obtained when GFP/GSK3β (S9A) or GFP/tau transiently expressed were added together and compared to the actual values of cell death obtained when GFP/GSK3β (S9A)/tau were co-expressed. Synergistic cell death (bold entries) was observed when GSK3β (S9A) was co-expressed with 352PHP, R5H, K18, K18ΔK280, P301L, or R406W. Interestingly, cell death in the presence of G272V was not affected by the presence of GSK3β (S9A). N.S. = not significant

Tau	%Cell Death (Additive)=GFP/GSK3β(S9A)+ GFP/tau	%Cell Death (Actual) = GFP/GSK3β(S9A)/ tau	p value
352tauWT	**24.1% ± 1.44**	**57.3% ± 1.74**	**p < 0.005**
441tauWT	24.7% ± 0.95	29.1% ± 2.77	N.S.
352tauPHP	**25.5% ± 1.52**	**49.8% ± 3.63**	**p < 0.005**
R5H	**25.1% ± 1.62**	**43.4% ± 1.37**	**p < 0.005**
K18	**25.9% ± 1.40**	**46.3% ± 2.44**	**p < 0.005**
K18ΔK280	**46.4% ± 1.00**	**76.4% ± 4.84**	**p < 0.005**
P301L	**25.2% ± 1.37**	**55.3% ± 1.45**	**p < 0.005**
G272V	25.8% ± 2.88	27.8% ± 3.13	N.S.
R406W	**24.3% ± 1.14**	**43.0% ± 3.33**	**p < 0.005**

Table 3.3. The effect of tau phosphorylation on cell death in the presence of model Hirano bodies. Expression of GSK3β(K85A) reduced the synergistic cell death observed when both G272V and model Hirano bodies are present, to an additive effect, implying that the phosphorylation state is important.

Sample	%Cell Death
Hirano body/GSK3β(K85A)	4.20 ± 0.77
Hirano body/G272V	17.90 ± 2.59
Hirano body/G272V/GSK3β(K85A)	10.20 ± 1.35
GFP/G272V	4.75 ± 0.74
GFP/G272V/ GSK3β(K85A)	5.80 ± 0.56
GFP/G272V + GFP/ GSK3β(K85A)	8.95 ± 2.06

CHAPTER 4

HIRANO BODY EXPRESSION IMPAIRS SPATIAL WORKING MEMORY IN A NOVEL MOUSE MODEL[1]

[1] Furgerson, M. Clark, J.K. Crystal, J.D. Wagner, J.J. Fechheimer, M. and R. Furukawa. Submitted to *Acta Neuropathologica Comm*., 04/15/2014.

ABSTRACT:

Introduction Hirano bodies are actin-rich intracellular inclusions found in the brains of patients with neurodegenerative conditions such as Alzheimer's disease or frontotemporal lobar degeneration-tau. While Hirano body ultrastructure and protein composition have been well studied, little is known about the physiological function of Hirano bodies in an animal model system.

Results Utilizing a Cre/Lox system, we have generated a new mouse model which develops an age-dependent increase in the number of model Hirano bodies present in both the CA1 region of the hippocampus and frontal cortex. These mice develop normally and experience no overt neuron loss. Mice presenting model Hirano bodies have no abnormal anxiety or locomotor activity as measured by the open field test. Mice with model Hirano bodies develop age-dependent spatial working memory impairments. Despite this cognitive impairment, paired pulse stimulation and long-term potentiation measurements in the hippocampus were indistinguishable from control mice. In addition, an inflammatory response can be detected at 8 months of age as assessed by the presence of reactive astrocytes.

Conclusion This study shows that the presence of model Hirano bodies initiates an inflammatory response and impairs spatial working memory in an age-dependent manner. This suggests that Hirano bodies may promote disease progression. This new model mouse provides a tool to investigate how Hirano bodies interact with other pathologies associated with Alzheimer's disease. Hirano bodies likely play a complex and region specific role in the brain during neurodegenerative disease progression.

INTRODUCTION:

Neurodegenerative diseases are characterized by neuronal loss that results in progressive cognitive decline, motor impairments, and changes in behavior (1). The most prevalent neurodegenerative disease is Alzheimer's disease (2,3) which is characterized pathologically by the deposition of protein aggregates (1). The brains of Alzheimer's disease patients develop extracellular amyloid beta plaques and intracellular neurofibrillary tangles (NFTs) (4,5). In addition, patients with Alzheimer's disease and other neurodegenerative diseases may also develop a secondary pathology known as Hirano bodies (6-10).

Hirano bodies are intracellular, eosinophilic rod-shaped inclusions found in both neurons and glia of the central nervous system (6-12). Hirano bodies are paracrystalline structures primarily composed of filamentous actin (F-actin) and actin-associated proteins (7,13). Hirano bodies are differentiated from other types of actin inclusions based on their ultrastructure (14). They have a distinct orientation and spacing of F-actin, the appearance of which changes based on the plane of section. These filaments are approximately 6-10 nm wide with 10-12 nm spacing between parallel filaments (7,15,16). In addition to actin-associated proteins, amyloid precursor protein intracellular domain (AICD) and tau are present in Hirano bodies, implicating these structures in the pathogenesis of Alzheimer's disease (17-19).

Despite decades of research, very little is known about the physiological role of Hirano bodies. Due to a lack of a mammalian model system, research has been limited to studying Hirano body frequency, components, and structure in post-mortem tissue. However, the development of a model system for studying Hirano bodies was made possible through expression of a C-terminal 34 kDa actin-binding protein truncation mutant (CT, amino acids 124-295) in Dictyostelium discoideum (20,21). Expression of CT does not affect total actin

levels, but causes redistribution in the ratio of globular to F-actin (21). These structures slow Dictyostelium growth and development only moderately, and are not detrimental to cell survival (21). Ultrastructural analysis of CT-induced actin-rich deposits revealed highly ordered actin filaments identical to Hirano bodies from human tissue (21). Formation of model Hirano bodies through expression of CT has also been successful in immortal mammalian cell lines as well as primary neurons (22). Cells expressing CT experience no growth or migration phenotypes (22). Model Hirano bodies formed in mammalian cells contain many of the same protein components as Hirano bodies found in humans as well as the same hallmark ultrastructure and filament spacing (22-24).

In addition to structural characterization of model Hirano bodies, limited physiological aspects of these inclusions have also been investigated. Both Hirano bodies found in humans and model Hirano bodies are often seen enclosed in membranes thought to be derived from autophagosomes (12,22). Consistent with this hypothesis, model Hirano bodies are degraded through both the autophagy and proteasome pathways, determined through use of pharmacology and an autophagy mutant Dictyostelium (25). The impact of model Hirano bodies on AICD and tau was investigated in cell culture since these proteins are colocalized with both human and model Hirano bodies (19,22-24). Normally AICD is abundant in the nucleus, where it plays a role in transcription (26,27). The presence of model Hirano bodies drastically reduces AICD nuclear localization (23). The presence of model Hirano bodies was also found to decrease AICD- and tau-induced cell death and AICD-induced transcription (23,24). These results imply both a potentially protective and deleterious role for Hirano bodies.

While cell culture is useful for mechanistic characterization at the cellular level, an in vivo model is needed to provide the appropriate anatomical and physiological context for an

informative assessment of systemic pathology. Therefore, a mouse with brain-specific expression of CT fused to green fluorescent protein under control of the Rosa promoter and induced by Cre/lox technology was generated by crossing a CT-GFP transgenic mouse (R26CT) with a Thy1.2-CRE mouse (28). These mice developed rod-shaped eosinophilic inclusions primarily in the CA3 region of the hippocampus. In addition, these inclusions had an ultrastructure indistinguishable from Hirano bodies found in humans (28). The formation of model Hirano bodies in the mouse hippocampus did not induce neuronal loss or impact long-term plasticity. However, a deficit in presynaptic short-term plasticity in the CA1 region was observed (28). Despite these interesting findings, complex behavioral studies such as motor or learning tasks were not evaluated. Furthermore, Hirano bodies in human disease are found predominately in the CA1 region of the hippocampus, not the CA3 as seen in the previous mouse model (12,16). In order to generate Hirano bodies in the CA1 region of the hippocampus, R26CT mice were crossed with a CamKIIa-CRE mouse, which directs CRE expression predominately to the CA1 region of the hippocampus and forebrain (29,30). In the current study, this new mouse model is characterized utilizing electrophysiological, pathological, and behavioral methods to evaluate the impact of model Hirano bodies on neurophysiology and cognition.

MATERIALS AND METHODS:

Animals: C57Bl/6-Gt(ROSA)26Sor$^{tm1(CT\text{-}GFP)UGA}$ (R26CT) mice (previously described (28)) were crossed with CamKIIa-CRE mice (B6.Cg-Tg(Camk2a-cre)T29-1Stl/J, Jax ID: 005359) (29) to induce expression of CT-GFP (R26CT-CRE). During breeding, CRE was carried maternally,

and all mice were homozygous for the CT-GFP transgene. All R26CT and R26CT-CRE mice used in behavioral and electrophysiological studies were male.

PCR was utilized to genotype the presence of R26CT with primers: P1 5'-TTGGAGGCAGGAAGCACTTG -3' ; P2 5'-CATCAAGGAAACCC TGGACTACTG- 3' ; and P3 5'–CCGACAAAACCGAAAATCTGTG-3' using genomic DNA obtained from the tail as a template. Amplification using P1 and P2 yields a 230 bp product from the R26CT allele, and P1 and P3 yields a 369 bp product from the wild-type Rosa26 allele. To detect the Cre transgene via PCR, the primers were: 5'-CCAGGCCTTTTCTGAGCATACC- 3' and 5'-CAACACCATTTTTTCTGACCCG-3', producing a product of 641 bp.

Mice had ad libitum access to food (except during behavioral studies, see below) and water during this study. All animal protocols and experiments were approved by the University of Georgia Institutional Animal Care and Usage Committee.

Statistics: Test of significance were performed using both paired and unpaired t-test, and mixed ANOVA. Results were considered significant if $p < 0.05$.

Brain sectioning and histology: For cryosections utilized in immunofluorescence, dissected whole brains were fixed in 4% paraformaldehyde in phosphate-buffered saline, pH 7.4 (PBS) overnight, followed by cryoprotection in 30% sucrose, embedding in OCT (Optical Cutting Temperature, Tissue-Tek 4583), and storage in liquid nitrogen. 6-8 μm thick sagittal sections were cut from frozen tissue using a cryostat (Leica CM3050 S, Richmond, IL) and electrostatically attached to Superfrost Plus glass slides (Fisher Scientific, Pittsburgh, PA). For paraffin sections, dissected brains were fixed in 4% paraformaldehyde in PBS, pH 7.4, at 4° C overnight, dehydrated in a graded series of 50, 75, 90, 96 and 100% ethanol, equilibrated with

xylene, embedded in paraffin, sectioned on a sliding microtome (Leica RM2155, Richmond, IL) at a thickness of 5-8 μm, and mounted on slides. H&E staining was performed as follows: after dewaxing with xylene, sections were stained with Gill's No. 2 hematoxylin (Sigma-Aldrich Chemical Co., St. Louis, MO) and eosin solution (Sigma-Aldrich Chemical Co., St. Louis, MO).

Immunohistochemistry: Mounted paraffin sections were dewaxed in xylene and rehydrated in graded ethanol solutions prior to antigen retrieval in boiling 50 mM sodium citrate plus 0.01% Tween20 for 25 minutes. Endogenous peroxidase activity was inhibited through incubation of sections in 3% hydrogen peroxide for 10 minutes prior to washing with PBS and blocking with 10 mg/ml bovine serum albumin (BSA) in PBS overnight. Slices were incubated in mouse anti-GFAP (1/1000) (Sigma-Aldrich Chemical Co., St. Louis, MO) or mouse anti-ED1 (1/400) (Abcam, Cambridge, MA) primary antibodies for 1 hour. Secondary biotinylated goat anti-mouse and goat anti-rabbit antibodies were used at 1/450 dilution for 1 hour. Slices were incubated with streptavidin-HRP polymer complex (1/1000) (Vector Laboratory, Burlingame, CA) for 30 minutes. Slices were washed 3 times for 5 minutes each between antibody and enzyme incubations with TBST (10 mM Tris-HCl, pH 7.4, 150 mM NaCl, 0.1% Tween20). Diaminobenzidine (DAB) enhanced substrate system was used according to the manufacturers instructions (Vector Laboratory, Burlingame, CA). After washing off excess DAB substrate, slides were counterstained with Gill's No. 2 Hematoxylin (Sigma-Aldrich Chemical Co., St. Louis, MO) prior to mounting. Sections were viewed with a Leica DM6000 B microscope (Wetzlar, Germany) with Hamamatsu ORCA-ER digital camera (Hamamatsu, Bridgewater, NJ).

Immunofluorescence: Cryosections were blocked for 1 hour in 2% BSA in TBST and incubated in primary antibody at room temperature overnight. The sections were washed three times in 4% milk in TBST for 5 min each, followed by 1 hour incubation with rabbit anti-GFP (1/500)

(Sigma-Aldrich Chemical Co., St. Louis, MO), FITC labeled goat anti-rabbit secondary (1/1000) (Sigma-Aldrich Chemical Co., St. Louis, MO), TRITC-phalloidin conjugated (1/40) (Sigma-Aldrich Chemical Co., St. Louis, MO), and 264 μM Hoechst 33258 with appropriate washes in between. Slides were visualized with a Zeiss Axioobserver Z1 equipped with an AxioCam MRm controlled by AxioVision4.6 software.

Transmission electron microscopy (TEM): TEM was performed as previously described with slight modification (28). Whole mouse brains were dissected to separate hippocampus from cortex. Hippocampal tissue blocks were fixed by immersion in 4% paraformaldehyde and 2% glutaraldehyde in 0.1 M cacodylate buffer, pH 7.4 overnight, and postfixed in 1% osmium tetroxide for 2 hours. After serial dehydration in ethanol solutions, tissues were embedded in Epon (Embed-812; Electron Microscope Science, Hatfield, PA). Semithin sections were stained with 1% toluidine blue in 1% sodium tetraborate. Ultrathin sections were collected on nickel grids, counterstained with uranyl acetate for 30 minutes, and followed by lead citrate for 5 minutes at room temperature. Samples were observed with a JEOL 100CX with an accelerating voltage of 80 kV.

Western blot: Brain samples were dissected from mice, flash frozen in liquid nitrogen, and stored at -80°C until processed. Tissues were homogenized in a Potter-Elvehjem homogenizer containing 4 brain volumes of Tris buffered saline (25 mM Tris-HCl pH 7.4, 140 mM NaCl, 3 mM KCl, 5 mM EDTA, and 2 mM 1,10-phenanthroline) with 10 μL protease inhibitor cocktail (5 mM EGTA, 1 mM DTT, 100 mM leupeptin, 10 mM pepstatin, 0.1 M PMSF, 0.1 M benzamidine, and 0.5 M ε-aminocaproic acid). Cell debris was separated from total homogenate by centrifugation at 13,000g for 15 min at 4°C. Supernatant was stored at -80°C until used. Protein concentrations of the supernatants were determined by bicinchoninic acid assay using

BSA as a standard (31). For western blot analysis, tissue samples were loaded at equal total protein, separated by SDS-PAGE, and transferred to nitrocellulose membranes. Blots were blocked in 5% nonfat dry milk in TBST and probed using either mouse anti-GFAP (1/2000) (Sigma-Aldrich Chemical Co., St. Louis, MO), rabbit anti-GFP (1/5000) (Sigma-Aldrich Chemical Co., St. Louis, MO), mouse anti-ED1 (1/5000) (Abcam, Cambridge, MA), mouse anti-synaptophysin (1/2000) (AbD Serotec, Raleigh, NC), or mouse anti-alpha tubulin (1/8000) (Millipore, Billerica, MA). After three washes with TBST, blots were incubated with either goat anti-mouse or goat anti-rabbit HRP-conjugated secondary antibodies (1/10000) (Pierce-lab, Rockford, IL) and detected by chemiluminescence using SuperSignal Western Dura Extended Duration Substrate (Thermo Scientific, Rockford IL). Images were captured utilizing ChemiDoc^{TM} MP system and Image Lab^{TM} software (Bio-Rad Laboratories, Hercules, CA).

Assessment of learning and memory in the radial arm maze: Learning and memory assessments were conducted using an 8-arm radial mouse maze (Med Associates, St. Albans, VT) as similarly described for rats (32). This maze consists of eight arms extending from a central chamber with eight guillotine doors positioned at the interface of the central chamber and arms. A 20-mm food dispenser and trough are at the end of each arm. Each arm has two sets of photosensors to track movement of mice in and out of the arms. In addition, the food trough also contains photosensors that detect mouse head entries and dispense food. The sides and top of each arm are composed of clear plastic to allow mice to use visual cues in the room to spatially navigate the maze. A computer in an adjacent room controlled the maze events and data collection. Photosensor, food, and door data were collected using MED-PC software 4.0 (Med Associates, St. Albans, VT) with a resolution of 10 ms. A video camera was mounted above the maze to visualize the mice during the procedure.

Behavioral assessment in the radial arm maze was performed at either 3 or 8 months of age. Thirteen days prior to the start of behavioral testing, mice were individually housed, and a three-day average of individual body weight was determined. Mice were diet restricted to reduce and maintain a body weight of ~87.0% of their ad libitum food body weight for the duration of the behavioral assessment. For four days prior to testing, mice were pre-trained to associate the maze with the experience of obtaining a sucrose-flavored food reward (Bio-Serve F0071, Frenchtown, NJ) by allowing each animal free access to four of the eight arms until one food reward from each arm was retrieved.

The maze was cleaned between subjects with 1/1250-diluted Coverage Plus NPD disinfectant (Steris Life Sciences, Mentor, OH) to prevent a previous mouse's scent from interfering with a subsequent mouse's performance. To further prevent a mouse from using its own scent cues, the entire maze was scent-saturated using cotton bedding from the mouse's home cage.

Radial arm maze training phase (8 arms open, 8 arms baited) to assess spatial short-term memory: Each mouse was placed in the central chamber of the maze for a two minute acclimation period before beginning the procedure. After acclimation, all eight doors opened with the objective of collecting a food reward available at the end of each arm (8 arms open, 8 arms baited). Only one food reward is delivered per arm, and a revisit to a previously visited food trough is considered an error in spatial short-term memory. After either collecting the last food reward or after 15 minutes of elapsed time, the session ends and the doors close. These training phase sessions are performed once a day, at the same time of day per mouse for 10 consecutive days. Results are reported as the mean total errors $\pm$ standard error of the mean (SEM) from the first 3 days or last 3 days of training. Following 10 days of consecutive spatial

memory training, animals proceeded directly to the spatial working memory test with a retention interval.

Radial arm maze test phase (delayed spatial win-shift) to assess spatial working memory: Mice were tested using a delayed spatial win-shift task for 10 consecutive days. This is a 2-phase procedure composed of a study phase and test phase. In the study phase, animals are placed in the central chamber of the maze for a two minute acclimation. Four of the eight doors are opened (randomly chosen by the computer for each mouse every day) and the mouse must collect a food reward that is available at the end of each of the 4 baited arms (4 arms open, 4 arms baited). After collecting the last food reward (or 15 minutes of elapsed time), the doors close. The mouse is subjected to a short retention interval (time delay) by being taken out of the maze and returned to his home cage for 3 minutes, during which the maze was cleaned. The mouse is returned to the maze to begin the test phase. After 1 minute of acclimation, all eight doors of the maze open. Only arms that were previously closed in the study phase are baited in the test phase (8 arms open, 4 arms baited). A revisit to a food trough previously visited in either phase is considered an error in spatial working memory. After either collecting the last food reward or after 15 minutes of elapsed time, the session ends and the doors close. Results are reported as the mean total errors $\pm$ standard error of the mean (SEM) obtained from the first 3 days or last 3 days of the test phase.

Open Field Apparatus: Activity was measured in 43.2 x 43.2 cm square chambers with clear plastic walls and a smooth metal floor (Med Associates, St. Albans, VT, USA). The chambers are individually housed in sound-attenuating cubicles with a 20 lux bulb in each of the two rear corners and a ventilation fan. Two strips containing 16 infrared photobeams perpendicular to each other, with paired photodetectors mounted across from them, create a 16 x 16 photobeam

grid 2 cm from the floor. Activity Monitor software counts photobeam breaks to determine both ambulatory (sequential) and stereotypic (repetitive) movements based on patterning of beam interruptions.

Locomotor activity: Five days after completion of radial arm maze testing, each mouse was placed in the center of the open field apparatus and allowed to roam freely for 60 minutes. Both ambulatory and stereotypic counts were combined into total horizontal counts and binned into 10 minute increments. For center zone analysis, a square zone of 26.3 x 26.3 cm (37.5% of total area) in the center of the chamber was designated to count crossings into this area.

Extracellular field recording: Hippocampal slices were prepared from 3 and 8 month old R26CT and R26CT-CRE mice 10-17 days after completion of radial arm maze testing. Mice were deeply anesthetized with halothane prior to decapitation. The brain was removed and submerged in ice-cold, oxygenated (95% O_2 / 5% CO_2) dissection artificial cerebrospinal fluid (ACSF) containing: 120 mM NaCl, 3 mM KCl, 4 mM $MgCl_2$, 1 mM NaH_2PO_4, 26 mM $NaHCO_3$, and 10 mM glucose. The brain was sectioned into 400 μm thick horizontal slices using a vibratome. The hippocampus was sub-dissected out and a majority of the CA3 portion removed. Slices were placed in a submersion recording chamber and perfused at approximately 1 ml/min with oxygenated (95% O_2 / 5% CO_2) standard ACSF containing: 120 mM NaCl, 3 mM KCl, 1.5 mM $MgCl_2$, 1 mM NaH_2PO_4, 2.5 mM $CaCl_2$, 26 mM $NaHCO_3$, and 10 mM glucose at room temperature. Slices recovered for 45 minutes at room temperature and an additional 45 minutes at 30°C. All recordings were obtained under continuous perfusion of oxygenated ACSF at 30°C. A bipolar stimulating electrode (Kopf Instruments, Tujunga, CA) was placed within the stratum radiatum of CA1, and an extracellular recording microelectrode (1.0 MΩ tungsten recording microelectrode, World Precision Instruments, Sarasota, FL) was positioned in the same

layer. Field excitatory post-synaptic potentials (fEPSPs) were recorded at CA3-CA1 synapses using a stimulus pulse consisting of a single square wave of 270 μs duration. Data were digitized at 10 kHz, low-pass filtered at 1 kHz, and analyzed with pCLAMP 10.2 software (Axon Instruments, Sunnyvale, CA). The initial slope of the population fEPSP was measured by fitting a straight line to a 1 ms window immediately following the fiber volley. Stimulus response curves were obtained at the beginning of each experiment with stimulus pulses delivered at 30, 40, 50, 60, 75, 90, 110, 130, 150, and 170 μA once every 60 s (0.0167 Hz). To begin baseline recording, the stimulation intensity was adjusted to obtain a fEPSP of approximately 35-40% of the linear range between the minimum and maximum response. Paired-pulse responses were performed at intervals of 50, 100, 200, and 500 ms. The slope of paired-pulse responses was measured from an average of five pairs of pulses for each interval. Synaptic responses for long-term potentiation (LTP) experiments were normalized by dividing all fEPSP slope values by the average of the five responses recorded during the 5 minutes immediately prior to high frequency stimulation (HFS). The HFS protocol used to induce LTP in all experiments consisted of three episodes of 100 Hz stimulus trains (100 pulses) for 1 s administered at 20 s inter-train intervals. LTP values for the 1, 2, and 3 hour time points were determined by averaging 5 minutes of normalized slope values immediately prior to the 60, 120, and 180 min time marks post-HFS respectively. Reported n-values (x(y)) indicate the number of slices (x) and the number of mice (y) assessed.

RESULTS:

Mouse characterization

Mice expressing CT-GFP in the hippocampus and frontal cortex were generated by crossing R26CT mice (as described previously (28,29)) to CamKIIa-CRE mice. To verify that CT-GFP was expressed, immunofluorescence was performed on cryosections of 1 month old R26CT and R26CT-CRE mice using anti-GFP antibodies (Figure 4.12). The presence of CT-GFP was also verified by western blot analysis using tissue from cerebral cortex and hippocampus of R26CT and R26CT-CRE mice (Figure 4.12).

To determine if expression of CT-GFP resulted in the production of Hirano bodies, hematoxylin and eosin staining was performed on paraffin sections of brains from 3 and 8 month old R26CT and R26CT-CRE mice. No eosinophilic inclusions were observed in 3 month old R26CT mice in either the cortex or the hippocampus (Figure 4.1). At low frequency, 3 month old R26CT-CRE mice exhibited eosinophilic inclusions in the CA1 region of the hippocampus, but not in the cortex (Figure 4.1). In 8 month old R26CT-CRE mice, eosinophilic inclusions appear predominately in the CA1 of the hippocampus and are found rarely in the pre-frontal cortex (Figure 4.2). To verify that the eosinophilic inclusions found in the brains of R26CT-CRE animals have the same ultrastructure as Hirano bodies found in human brains, hippocampal samples from 8 month old mice were processed and viewed using transmission electron microscopy. R26CT-CRE mice show electron dense inclusions with 10-12 nm spacing similar to human Hirano bodies (Figure 4.12). Structures with the characteristic ultrastructural features of Hirano bodies were not observed in samples from R26CT control mice.

Since inflammation has been widely reported in neurodegenerative diseases (33), we determined whether the presence of model Hirano bodies induces an inflammatory response in

the brains of 3 and 8 month old R26CT and R26CT-CRE mice. Paraffin- embedded brain sections were stained with antibodies against known markers of reactive astrocytes (GFAP) and activated microglia (ED1) using DAB to visualize the product (Figure 4.3, 4.4). During inflammation, the levels of GFAP are significantly higher in reactive astrocytes (34). Therefore, GFAP antibodies were titrated to label only reactive astrocytes using a well established 5xFAD model of Alzheimer's disease known to have inflammation (data not shown) (35). At 3 months of age, neither R26CT nor R26CT-CRE mice show GFAP or ED1 staining in either hippocampus or frontal cortex, indicating that neither reactive astrocytes nor activated microglia are present (Figure 4.3). ED1 staining of 8 month old R26CT and R26CT-CRE brain sections revealed no activated microglia in either hippocampus or cortex (Figure 4.4). Furthermore, 8 month old R26CT mice show no GFAP staining in either hippocampus or cortex. However, 8 month old R26CT-CRE mice have GFAP staining in the hippocampus but not the cortex, indicating that the presence of model Hirano bodies induces inflammation at a later age (Figure 4.4). To verify these results, western blot analysis was performed using brain homogenate from 3 and 8 month old R26CT and R26CT-CRE mice (Figure 4.5). At 3 months of age, neither ED1 nor GFAP levels were significantly different between R26CT and R26CT-CRE mice (Figure 4.5). At 8 months of age, ED1 levels were not different between R26CT and R26CT-CRE mice (Figure 4.5A,B). In contrast, at 8 months of age, GFAP levels were approximately 4-fold higher in R26CT-CRE mice compared to R26CT mice (Figure 4.5C,D). These results are consistent with the immunohistochemistry results indicating that older R26CT-CRE mice have inflammation in the hippocampus as indicated by positive GFAP staining in reactive astrocytes.

Behavioral assessment

Changes in anxiety and cognition are two possible clinical symptoms of patients suffering from neurodegenerative conditions presenting Hirano bodies (36). Behavioral performance of R26CT and R26CT-CRE mice was assessed in an open field test and radial arm maze. In the open field test, locomotor activity and center zone entrances were evaluated in both R26CT (3 month old, n=11; 8 month old, n=11) and R26CT-CRE mice (3 month old, n=12; 8 month old, n=12). There was no difference in locomotor activity between R26CT and R26CT-CRE mice at either age (Figure 4.6A,B). R26CT and R26CT-CRE mice also made a similar number of entrances to the center zone, suggesting no differences in anxiety at either age (Figure 4.6C).

Spatial memory performance of R26CT and R26CT-CRE mice was evaluated at both 3 and 8 months of age utilizing a radial arm maze. The training phase (8 arms open, 8 arms baited) consisted of collecting a food reward at the end of each of the 8 arms without revisiting any previously visited locations as described in Materials and Methods (Figure 4.7A). R26CT (3 month old, n=11; 8 month old, n=11) and R26CT-CRE mice (3 month old, n=12; 8 month old, n=12) performed similarly in this task, as both groups showed significant improvement in performance across sessions from day 1 to day 10 at both 3 and 8 months of age (Figure 4.7B,C). These observations were confirmed by subjecting this training data to an experience (early versus late sessions) X genotype X age analysis of variance (ANOVA). The number of errors declined with experience ($F(1,42)=56.94$, $p<0.001$); none of the other variables or interactions were significant.

At day 11, the same mice from the training phase were evaluated using a delayed spatial win-shift task (Figure 4.7D). In the initial study phase (4 arms open, 4 arms baited), the mice have free access to only 4 arms with 1 food reward per accessible arm. Upon completion of the study phase, mice experience a short retention interval of 3 minutes. In the subsequent test phase

(8 arms open, 4 arms baited), mice have free access to all 8 arms, but only the 4 arms not previously visited (inaccessible during study phase) are now baited and have food rewards. During the study phase, both 3 and 8 month old mice showed no difference between groups or improvement across sessions (data not shown). This was expected, as they had already displayed high performance for this type of task by the end the training phase.

In the test phase, 3 month old R26CT and R26CT-CRE mice show an improvement across sessions (Figure 4.7E) and were not different from each other. At 8 months of age, R26CT mice also showed improvement in performance across sessions (Figure 4.7F). In contrast, the R26CT-CRE mice did not. There was a statistically significant difference between R26CT and R26CT-CRE mice (* $p < 0.05$) at the end of the 10 day testing period (Figure 4.7F, days 18-20). These test phase data were subjected to an experience X genotype X age ANOVA. The number of errors declined with experience ($F(1,42)=28.03$, $p<0.001$). There was also a significant three-way interaction of days x genotype x age ($F(1,42)=8.61$, $p<0.01$); none of the other variables or interactions were significantly different. Next, we conducted experience x genotype ANOVAs separately for ages 3 and 8 months. At both time points, there was a significant effect of experience (3 months: $F(1,21)=17.05$, $p<0.001$; 8 months: ($F1,21)=11.25$, $p<0.01$). However, the interaction of experience and genotype was significant at 8 months ($F(1,21)=14.37$, $p<0.05$) but not at 3 months ($F(1,21)=2.16$, $p=0.16$); none of the other variables were significant. These results indicate R26CT-CRE mice develop impairment in spatial working memory by 8 months of age.

Neurophysiological evaluation

Several neurodegenerative conditions are characterized by synaptic loss or reduction in synaptic density that coincides with cognitive impairment (37-40). Since 8 month old R26CT-CRE mice show cognitive impairments in spatial working memory as measured in the radial arm maze, levels of synaptophysin were measured as a qualitative indicator of synaptic density. In both 3 and 8 month old mice, levels of synaptophysin are approximately equal between R26CT and R26CT-CRE mice suggesting that spatial working memory impairments in R26CT-CRE mice are not due to decreases in synaptic density (Figures 4.5A-D).

In order to determine whether the presence of Hirano bodies impact synaptic function, field excitatory post-synaptic potentials (fEPSPs) were recorded at the Schaffer collateral synapses in the stratum radiatum layer of the CA1 region in slices from the ventral half of the hippocampus. In 3 and 8 month old mice, there was no difference in synaptic response between R26CT (3 month: 10(19) and 8 month: 10(20)) and R26CT-CRE (3 month: 12(18) and 8 month: 12(19)) mice for fEPSPs at any stimulus intensity recorded (Figure 4.8). Short-term synaptic plasticity was evaluated using paired pulse stimulus protocols. There was no difference in the amount of facilitation between R26CT (3 month, n = 10(19); 8 month, n = 10(20)) and R26CT-CRE (3 month, n = 12(18); 8 month, n = 12(21)) mice at any stimulus intensity at either 3 or 8 months of age (Figure 4.9). These results indicate that impairments in spatial working memory in 8 month R26CT-CRE mice are likely not attributed to differences in synaptic density or short-term plasticity.

Long-term synaptic plasticity was evaluated by the induction of long-term potentiation (LTP) using a strong stimulus protocol (3 x 100Hz /1 sec at 20 sec intervals). Following LTP

induction, fEPSP slopes were recorded for 3 hours post-induction to measure early (< 3 hours) and late (> 3 hours) phases of LTP. At both 3 and 8 months of age, fEPSP slope values were not significantly different between R26CT (3 month, n = 10(17); 8 month, n = 9(18)) and R26CT-CRE (3 month, n = 11(16); 8 month, n = 11(18)) mice at both early and late phases of LTP (Figure 4.10). Taken together, these results suggest that expression of CT-GFP and subsequent formation of model Hirano bodies have no impact on synaptic density, baseline synaptic responses, or short and long term synaptic plasticity in the CA1 region of the hippocampus in mice as old as 8 months.

DISCUSSION:

Incidence and ultrastructure of Hirano bodies in transgenic model mice

A new transgenic mouse model was created to study the impact of Hirano bodies in vivo to more closely resemble the presentation of Hirano bodies in Alzheimer's disease. A mouse with model Hirano bodies had been previously studied by crossing R26CT mice with Thy1.2-CRE mice. While Hirano bodies were produced in the hippocampus of homozygous R26CT x Thy1.2-CRE mice, Hirano bodies were predominately reported in the CA3 subregion (28). This is not surprising since the Thy1.2-CRE mouse has been shown to have higher expression of the CRE transgene in the CA3 subregion, rather than the CA1 (28). In the present study, R26CT mice were crossed with a CamKIIa-CRE mouse, which is known to express CRE predominantly in the forebrain and in the CA1 subregion of the hippocampus (29,30,41). This CRE driver was chosen in an attempt to more closely recapitulate human disease conditions in which Hirano bodies are normally found, the pyramidal cell layer of the CA1 region (6,8,12,15,16,42,43). Eosinophilic inclusions were seen predominately in the CA1 region of R26CT-CamKIIa-CRE

mice. In contrast with the previously characterized model Hirano body mice (R26CT x Thy1.2-CRE) in which model Hirano bodies were not detected by light microscopy until 6 months of age, eosinophilic inclusions were found in the hippocampus of R26CT-CamKIIa-CRE mice as early as 3 months of age. It is unclear why eosinophilic inclusions are detected earlier in R26CT mice crossed with CamKIIa-CRE than in R26CT mice crossed with Thy1.2-CRE. Perhaps CA1 pyramidal neurons have a greater propensity to facilitate CT-induced Hirano body formation than do CA3 pyramidal neurons. In human disease, the number of Hirano bodies increases with age and disease severity (15,43,44). Hirano body appearance in humans coincides with aging since pathologists have noted that Hirano bodies are never seen in the brains of humans younger than 11 years old (15). Consistent with these findings, an age-dependent increase in the formation of Hirano bodies was also observed in our mouse model.

There are several characterized actin inclusions found in human disease such as ADF/cofilin rods (AC rods) and hyaline bodies (45-47). Hirano bodies are differentiated from these other actin aggregates by their eosinophilic nature, ability to interact with phalloidin, and distinctive ultrastructure (8,44,46,48). To definitively prove an actin inclusion is a Hirano body, electron microscopy must be performed for ultrastructural analysis. There are a variety of presentations. In humans, they often appear as fingerprint or spheroid/spindle shape (8). Hirano bodies in R26CT-CRE mice also display these alternative patterns (Figure 4.12 A-B). In humans, smaller Hirano bodies observed by electron microscopy (not visible via light microscopy) are more frequent than larger Hirano bodies (16). These smaller Hirano bodies appear less compact and more irregular than those visible through light microscopy (16). R26CT-CRE mice also show similar smaller structures which contain both ordered filaments and amorphous electron dense material (Figure 4.12 D). In Dictyostelium, small nascent model

Hirano body structures observed by TEM fuse together by an unknown process involving microtubules and myosin II to form larger Hirano bodies (21,49,50). Expression of CT in cell culture systems often results in alternative fibrillar structures or small aggregates (22,25). These smaller structures have also been noted in the brains of humans (51) and in the brains of R26CT-CRE mice (Figure 4.12 C). It is likely that a similar formation process of Hirano bodies is occurring in R26CT-CRE mouse brains since several small aggregates can be seen in close proximity in TEM samples (Figure 4.12 C).

Inflammation

Inflammation is a phenomenon occurring in neurodegenerative conditions such as Alzheimer's disease and Parkinson's disease and is characterized by activated microglia and reactive astrocytes (34). Many mouse models of neurodegenerative disease recapitulate reactive microglia or reactive astrocytes as a predominant phenotype (35,52-54). Markers of reactive astrocytes or activated microglia were utilized in order to determine if Hirano bodies accompany an innate immune response in the brain. 3-month- old R26CT-CRE mice had no signs of inflammation (Figure 4.3, 4.5). However, by 8 months of age, R26CT-CRE mice had significantly higher levels of GFAP compared to age-matched R26CT mice (Figure 4.4, 4.5). There are several factors that can initiate astrogliosis including cell damage, ischemia, neuronal hyperactivity, and foreign pathogens including abnormal protein aggregates (55). In Alzheimer's disease, reactive astrocytes are often found in close proximity with deposits of amyloid beta plaques and neurons containing intracellular NFTs (35,56-60). In addition to intracellular NFTs, extracellular NFTs (ghost tangles) have also been reported in brains (61,62). Reactive astrocytes have been reported to surround ghost tangles where they are thought to be clearing these structures from the brain (63,64). Similarly, intracellular Lewy bodies comprised

of alpha synuclein can be exocytosed from neurons in Parkinson's patients and initiate astrogliosis (65-67). Hirano bodies have also been reported to be extruded from neurons, and model Hirano bodies can be cleared from cells through exocytosis (15,25). It is possible that extruded Hirano bodies or intermediate aggregates may initiate an astrocytosis response in the brain. While 3-month-old R26CT-CRE mice have sparse model Hirano bodies, they are more abundant in 8-month-old mice. In 8 month old mice, extracellular model Hirano bodies were observed (Figure 4.12). Release of Hirano bodies may explain why 8 month old R26CT-CRE mice exhibit reactive astrocytes.

Behavioral studies of Hirano body model mice

A central feature of this study is to assess the impact of the behavioral and physiological consequence(s) of Hirano bodies in the brain. To assess the effect of CT-GFP expression and subsequent formation of model Hirano bodies, behavioral studies were performed using both an open field test and an 8-arm radial maze. The open field test has been utilized to measure locomotor activity and anxiety (68). At 3 and 8 months of age, R26CT and R26CT-CRE mice show similar levels of locomotor activity (Figure 4.6A, B). General anxiety was measured by recording the number of center zone entries between R26CT and R26CT-CRE mice (Figure 4.6C). No differences between genotypes at either age were found, implying that the presence of model Hirano bodies does not contribute to anxiety or impair locomotor function.

The training phase (8 arms open, 8 arms baited) of the radial arm maze demonstrated that both R26CT and R26CT-CRE mice have intact spatial learning and navigation since both genotypes learn the reference memory rules associated with completion of the radial arm maze training task. In addition, both R26CT and R26CT-CRE mice appear to have equivalent perception of spatial cues, levels of motivation, and motor control. In the training phase, the task

is continuous and thus the working memory load is low, making the procedure primarily dependent upon immediately accessible information from short-term memory (69,70). The same mice were subsequently tested in a 2-phase delayed spatial win-shift task (with a 3 minute retention interval delay) to more stringently examine spatial working memory. The incorporation of a time delay forces retention of trial-unique spatial information (i.e., the mice must remember which arms were visited in phase 1 in order to successfully complete phase 2, increasing the working memory load). At 3 months of age, spatial working memory appears unimpaired since both R26CT and R26CT-CRE mice perform equally well and improve with training. However, at 8 months of age, the more stringent memory load resulted in discrimination of performance between the R26CT and R26CT-CRE mice. The R26CT mice showed improvement across trials, while the R26CT-CRE mice did not. The test phase results suggest that 8 month R26CT-CRE mice have impaired working memory, (i.e. memory for daily, item-specific locations). This is likely a specific impairment in spatial working memory since the training phase results indicated intact acquisition of reference memory rules, making a general impairment in learning capability unlikely. Furthermore, the memory deficiencies observed at 8 months coincides with the observed increase in frequency of Hirano bodies.

The effect of Hirano bodies on synaptic plasticity

Assessments of spatial memory are known to depend upon intact hippocampal function (69,71,72). In the current studies, electrophysiological recordings in ventral hippocampal slices were utilized to determine if synaptic function is altered in R26CT-CRE mice. Short-term plasticity measurements at 3 and 8 months of age showed that paired-pulse facilitation from R26CT-CRE mice was indistinguishable from R26CT mice (Figure 4.10). This data is in contrast with the previous characterization of the R26CT-CRE mice with a Thy1.2 CRE driver,

which exhibited significant paired-pulse depression at a 50 ms stimulus interval (28). The most obvious explanation for this contrast is due to differences in the expression pattern of CT-GFP. In the current study, CT-GFP expression and Hirano body formation was more predominant in the CA1 subregion of the hippocampus versus the previous mouse model that had predominately CA3 subregion expression and subsequent Hirano body formation (28-30). Our field potential experiments were performed in the stratum radiatum layer of CA1 subregion by activating the Schaffer collateral axons with synapses on the apical dendrites of the pyramidal neurons in the CA3 subregion. In the previous mouse (R26CT x Thy1.2-CRE), Hirano bodies were formed in presynaptic neurons (28). Paired-pulse stimulation is a measurement that reflects the active transport recovery of calcium and trafficking of neurotransmitter-containing vesicles to replenish the ready releasable pool of vesicles (73). The trafficking of these neurotransmitter-containing vesicles is modulated by the actin cytoskeleton. The paired-pulse depression seen in the R26CT x Thy1.2-CRE mice was explained as a change in vesicular trafficking due to sequestration of F-actin in model Hirano bodies (74), decreasing the amount of cellular actin available for cytoskeletal functions. In the current study using R26CT x CamKIIa-CRE mice, Hirano bodies were primarily formed in the postsynaptic CA1 pyramidal neurons. Thus, the difference in the effect of Hirano bodies on paired-pulse responses between the Thy1.2 CRE and CamKIIa-CRE driver models can be readily understood. Furthermore, these results show that the effect of model Hirano bodies on synaptic function depend on the specific location (i.e., presynaptic versus postsynaptic) in which they form.

In addition to evaluating short-term synaptic plasticity, a form of long-term synaptic plasticity, LTP, which has been shown to be involved in spatial learning and memory, was also investigated (75,76). Long-term potentiation has both an early and a late phase. The early phase

relies on redistribution and rearrangement of available synaptic proteins while the latter requires gene expression and protein synthesis to maintain changes in synaptic strength (77). Both the early and late phases of LTP are associated with an increase in actin assembly (78-80). The actin assembly associated with the late stage of LTP involves an increase in the number and size of dendritic spines and expansion of the postsynaptic density (78,79). Model Hirano bodies are known to shift the filamentous to monomeric actin ratio (21), increasing the proportion of cellular F-actin which may consequently impact synaptic plasticity. Therefore, LTP was monitored for 3 hours post induction to determine if the presence of model Hirano bodies could impact either the early (< 3 hours) or late (> 3 hours) phases of LTP. Interestingly, despite the important role of actin in LTP, we found that there was no measurable difference between R26CT and R26CT-CRE mice at either 3 or 8 months of age (Figure 4.10). These results are in contrast with those in the previous study in which R26CT x Thy1.2-CRE mice showed a deficit in the early, but not the late phase LTP (28). Thus, the effect of model Hirano bodies in the CA1 region of the ventral hippocampus of R26CT-CRE mice (current R26CT x CamKIIa-CRE mouse) appears to be negligible as assessed by paired-pulse and LTP measurements.

Despite no significant differences in either short-term or long-term plasticity measurements, 8-month-old R26CT-CRE mice have an impairment in spatial working memory as assessed utilizing a radial arm maze (81-83). This seeming discrepancy could be due to involvement of both the hippocampus and pre-frontal cortex in spatial working memory (69,84). Our electrophysiology measurements were performed on ventral hippocampal slices. The CamKIIa promoter used to drive CRE expression is activated in the hippocampus as well as the prefrontal cortex (29,30). Evidence of this expression is given by the observation that R26CT-CRE mice develop Hirano bodies in the prefrontal cortex at 8 months of age (Figure 4.2). Thus,

it is possible that the electrophysiological measurements in the CA1 of ventral hippocampus performed in this study are either not sensitive enough to detect changes in synaptic physiology or are in an area that is not highly affected by the presence of Hirano bodies. In the future, it will be important to perform electrophysiological experiments in the prefrontal cortex as well as the hippocampus to evaluate the contribution of each brain region to spatial working memory.

CONCLUSION:

The physiological impact of Hirano bodies in the brain has remained elusive. The transgenic mouse generated in this study provides an animal model of Hirano body formation in the mammalian brain. Consistent with data for humans, this transgenic mouse develops Hirano bodies in the CA1 region of the hippocampus as well as in the frontal cortex. Behavioral analyses of mice, which develop model Hirano bodies, indicate that Hirano bodies negatively impact spatial working memory. This study shows that Hirano body formation initiates an inflammatory response in the hippocampus and suggests that Hirano bodies may independently contribute to disease progression or exacerbate the disease state. This model mouse provides a tool to investigate how the presence of Hirano bodies may impact the progression of Alzheimer's disease and other neurodegenerative diseases.

ACKNOWLEDGEMENTS:

Funding for this work was provided by NIH R01 N5046451 (www.ninds.nih.gov/) to R. Furukawa and M. Fechheimer. Disclosure statement: We would like to thank Drs. Richard Meagher and Steve Hajduk for providing access to their microscopes. We would also like to thank the UGA College of Veterinary Medicine, Electron Microscopy Laboratory for their

technical support and expertise with a special thanks to Mary Ard. Finally, we would like to thank Drs. Jim Lauderdale and Nancy Manley for providing access to their cryostat and microtome. All animal protocols and experiments were approved by the University of Georgia Institutional Animal Care Committee.

REFERENCES:

1. Ross, C. A., and Poirier, M. A. (2004) Protein aggregation and neurodegenerative disease. Nat Med 10 Suppl, S10-17
2. Ratnavalli, E., Brayne, C., Dawson, K., and Hodges, J. R. (2002) The prevalence of frontotemporal dementia. Neurology 58, 1615-1621
3. Alzheimer's, A., Thies, W., and Bleiler, L. (2011) 2011 Alzheimer's disease facts and figures. Alzheimers Dement 7, 208-244
4. Terry, R. D. (1963) The Fine Structure of Neurofibrillary Tangles in Alzheimer's Disease. J Neuropathol Exp Neurol 22, 629-642
5. Lynch, T., Sano, M., Marder, K. S., Bell, K. L., Foster, N. L., Defendini, R. F., Sima, A. A., Keohane, C., Nygaard, T. G., Fahn, S., and et al. (1994) Clinical characteristics of a family with chromosome 17-linked disinhibition-dementia-parkinsonism-amyotrophy complex. Neurology 44, 1878-1884
6. Gibson, P. H., and Tomlinson, B. E. (1977) Numbers of Hirano bodies in the hippocampus of normal and demented people with Alzheimer's disease. J Neurol Sci 33, 199-206
7. Hirano, A., Dembitzer, H. M., Kurland, L. T., and Zimmerman, H. M. (1968) The fine structure of some intraganglionic alterations. Neurofibrillary tangles, granulovacuolar bodies and "rod-like" structures as seen in Guam amyotrophic lateral sclerosis and parkinsonism-dementia complex. J Neuropathol Exp Neurol 27, 167-182
8. Schochet, S. S., Jr., Lampert, P. W., and Lindenberg, R. (1968) Fine structure of the Pick and Hirano bodies in a case of Pick's disease. Acta Neuropathol (Berl) 11, 330-337

9. Martinez-Saez, E., Gelpi, E., Rey, M., Ferrer, I., Ribalta, T., Botta-Orfila, T., Nos, C., Yague, J., and Sanchez-Valle, R. (2011) Hirano body - rich subtypes of Creutzfeldt-Jakob disease. Neuropathol Appl Neurobiol

10. Cartier, L., Galvez, S., and Gajdusek, D. C. (1985) Familial clustering of the ataxic form of Creutzfeldt-Jakob disease with Hirano bodies. J Neurol Neurosurg Psychiatry 48, 234-238

11. Okamoto, K., Hirai, S., and Hirano, A. (1982) Hirano bodies in myelinated fibers of hepatic encephalopathy. Acta Neuropathol 58, 307-310

12. Gibson, P. H. (1978) Light and electron microscopic observations on the relationship between Hirano bodies, neuron and glial perikarya in the human hippocampus. Acta Neuropathol (Berl) 42, 165-171

13. Galloway, P. G., Perry, G., and Gambetti, P. (1987) Hirano body filaments contain actin and actin-associated proteins. J Neuropathol Exp Neurol 46, 185-199

14. Hirano, A. (1994) Hirano bodies and related neuronal inclusions. Neuropathol Appl Neurobiol 20, 3-11

15. Ogata, J., Budzilovich, G. N., and Cravioto, H. (1972) A study of rod-like structures (Hirano bodies) in 240 normal and pathological brains. Acta Neuropathol 21, 61-67

16. Schochet, S. S., Jr., and McCormick, W. F. (1972) Ultrastructure of Hirano bodies. Acta Neuropathol 21, 50-60

17. Maciver, S. K., and Harrington, C. R. (1995) Two actin binding proteins, actin depolymerizing factor and cofilin, are associated with Hirano bodies. Neuroreport 6, 1985-1988

18. Galloway, P. G., Perry, G., Kosik, K. S., and Gambetti, P. (1987) Hirano bodies contain tau protein. Brain Res 403, 337-340

19. Munoz, D. G., Wang, D., and Greenberg, B. D. (1993) Hirano bodies accumulate C-terminal sequences of beta-amyloid precursor protein (beta-APP) epitopes. J Neuropathol Exp Neurol 52, 14-21

20. Lim, R. W. L., Furukawa, R., Eagle, S., Cartwright, R. C., and Fechheimer, M. (1999a) Three distinct F-actin binding sites in the Dictyostelium discoideum 34,000 dalton actin bundling protein. Biochemistry 38, 800-812

21. Maselli, A. G., Davis, R., Furukawa, R., and Fechheimer, M. (2002) Formation of Hirano bodies in Dictyostelium and mammalian cells induced by expression of a modified form of an actin cross-linking protein. J. Cell Sci. 115, 1939-1952

22. Davis, R. C., Furukawa, R., and Fechheimer, M. (2008) A cell culture model for investigation of Hirano bodies. Acta Neuropathol 115, 205-217

23. Ha, S., Furukawa, R., and Fechheimer, M. (2011) Association of AICD and Fe65 with Hirano bodies reduces transcriptional activation and initiation of apoptosis. Neurobiol Aging 32, 2287-2298

24. Furgerson, M., Fechheimer, M., and Furukawa, R. (2012) Model Hirano bodies protect against tau-independent and tau-dependent cell death initiated by the amyloid precursor protein intracellular domain. PLOS ONE 7, e44996

25. Kim, D. H., Davis, R. C., Furukawa, R., and Fechheimer, M. (2009) Autophagy contributes to degradation of Hirano bodies. Autophagy 5, 44-51

26. Cao, X., and Südhof, T. C. (2001) A transcriptionally active complex of APP with Fe65 and histone acetyltransferase Tip60. Science 293, 115-120

27. Cao, X., and Südhof, T. C. (2004) Dissection of amyloid-beta precursor protein-dependent transcriptional transactivation. J. Biol. Chem. 279, 24601-14611

28. Ha, S., Furukawa, R., Stramiello, M., Wagner, J. J., and Fechheimer, M. (2011) Transgenic mouse model for the formation of Hirano bodies. BMC neurosci 12, 97

29. Tsien, J. Z., Chen, D. F., Gerber, D., Tom, C., Mercer, E. H., Anderson, D. J., Mayford, M., Kandel, E. R., and Tonegawa, S. (1996) Subregion- and cell type-restricted gene knockout in mouse brain. Cell 87, 1317-1326

30. Shimizu, E., Tang, Y. P., Rampon, C., and Tsien, J. Z. (2000) NMDA receptor-dependent synaptic reinforcement as a crucial process for memory consolidation. Science 290, 1170-1174

31. Smith, P. K., Krohn, R. I., Hermanson, G. T., Mallia, A. K., Gartner, F. H., Provenzano, M. D., Fujimoto, E. K., Goeke, N. M., Olson, B. J., and Klenk, D. C. (1985) Measurement of protein using bicinchoninic acid. Anal. Biochem. 150, 76-85

32. Babb, S. J., and Crystal, J. D. (2006) Episodic-like memory in the rat. Curr Biol 16, 1317-1321

33. Kaushik, D. K., and Basu, A. (2013) A friend in need may not be a friend indeed: role of microglia in neurodegenerative diseases. CNS & neurological disorders drug targets 12, 726-740

34. Glass, C. K., Saijo, K., Winner, B., Marchetto, M. C., and Gage, F. H. (2010) Mechanisms underlying inflammation in neurodegeneration. Cell 140, 918-934

35. Oakley, H., Cole, S. L., Logan, S., Maus, E., Shao, P., Craft, J., Guillozet-Bongaarts, A., Ohno, M., Disterhoft, J., Van Eldik, L., Berry, R., and Vassar, R. (2006) Intraneuronal beta-amyloid aggregates, neurodegeneration, and neuron loss in transgenic mice with five

familial Alzheimer's disease mutations: potential factors in amyloid plaque formation. J Neurosci 26, 10129-10140

36. Rosen, H. J., Hartikainen, K. M., Jagust, W., Kramer, J. H., Reed, B. R., Cummings, J. L., Boone, K., Ellis, W., Miller, C., and Miller, B. L. (2002) Utility of clinical criteria in differentiating frontotemporal lobar degeneration (FTLD) from AD. Neurology 58, 1608-1615

37. Koffie, R. M., Hyman, B. T., and Spires-Jones, T. L. (2011) Alzheimer's disease: synapses gone cold. Mol Neurodegener 6, 63

38. Picconi, B., Piccoli, G., and Calabresi, P. (2012) Synaptic dysfunction in Parkinson's disease. Adv Exp Med Biol 970, 553-572

39. Terry, R. D., Masliah, E., Salmon, D. P., Butters, N., DeTeresa, R., Hill, R., Hansen, L. A., and Katzman, R. (1991) Physical basis of cognitive alterations in Alzheimer's disease: synapse loss is the major correlate of cognitive impairment. Ann Neurol 30, 572-580

40. Scheff, S. W., and Price, D. A. (2006) Alzheimer's disease-related alterations in synaptic density: neocortex and hippocampus. J Alzheimers Dis 9, 101-115

41. Rondi-Reig, L., Libbey, M., Eichenbaum, H., and Tonegawa, S. (2001) CA1-specific N-methyl-D-aspartate receptor knockout mice are deficient in solving a nonspatial transverse patterning task. Proc Natl Acad Sci U S A 98, 3543-3548

42. Schmidt, M. L., Lee, V. M., and Trojanowski, J. Q. (1989) Analysis of epitopes shared by Hirano bodies and neurofilament proteins in normal and Alzheimer's disease hippocampus. Lab Invest 60, 513-522

43. Laas, R., and Hagel, C. (1994) Hirano bodies and chronic alcoholism. Neuropathol Appl Neurobiol 20, 12-21

44. Hirano, A., Dembitzer, H. M., Kurland, L. T., and Zimmerman, H. M. (1968) The fine structure of some intraganlionic alterations. J. Neuropathol. Expt. Neurol. 27, 167-182

45. Ono, S., Abe, H., Nagaoka, R., and Obinata, T. (1993) Colocalization of ADF and cofilin in intranuclear rods of cultured muscle cells. J. Mus. Res. Cell Motil. 14, 195-204

46. Goebel, H. H., and Laing, N. G. (2009) Actinopathies and myosinopathies. Brain Pathol 19, 516-522

47. Bamburg, J. R., and Bloom, G. S. (2009) Cytoskeletal pathologies of Alzheimer's disease. Cell Motil Cytoskeleton 66, 635-649

48. Nishida, E., Iida, K., and Yonezawa, N. (1987) Cofilin is a component of intranuclear and cytoplasmic actin rods induced in cultured cells. Proc. Natl. Acad. U. S. A. 84, 5262-5266

49. Reyes, J. F., Stone, K., Ramos, J., and Maselli, A. (2009) Formation of Hirano bodies after inducible expression of a modified form of an actin-cross-linking protein. Eukaryot Cell 8, 852-857

50. Griffin, P., Furukawa, R., Piggott, C., Maselli, A., and Fechheimer, M. (2014) Requirements for hirano body formation. Eukaryot Cell 13, 625-634

51. Izumiyama, N., Ohtsubo, K., Tachikawa, T., and Nakamura, H. (1991) Elucidation of three-dimensional ultrastructure of Hirano bodies by the quick-freeze, deep-etch and replica method. Acta Neuropathol 81, 248-254

52. Zaheer, S., Thangavel, R., Wu, Y., Khan, M. M., Kempuraj, D., and Zaheer, A. (2013) Enhanced expression of glia maturation factor correlates with glial activation in the brain of triple transgenic Alzheimer's disease mice. Neurochem Res 38, 218-225

53. Duyckaerts, C., Potier, M. C., and Delatour, B. (2008) Alzheimer disease models and human neuropathology: similarities and differences. Acta Neuropathol 115, 5-38

54. Mineur, Y. S., McLoughlin, D., Crusio, W. E., and Sluyter, F. (2005) Genetic mouse models of Alzheimer's disease. Neural Plast 12, 299-310

55. Sofroniew, M. V., and Vinters, H. V. (2010) Astrocytes: biology and pathology. Acta Neuropathol 119, 7-35

56. Akiyama, H., Barger, S., Barnum, S., Bradt, B., Bauer, J., Cole, G. M., Cooper, N. R., Eikelenboom, P., Emmerling, M., Fiebich, B. L., Finch, C. E., Frautschy, S., Griffin, W. S., Hampel, H., Hull, M., Landreth, G., Lue, L., Mrak, R., Mackenzie, I. R., McGeer, P. L., O'Banion, M. K., Pachter, J., Pasinetti, G., Plata-Salaman, C., Rogers, J., Rydel, R., Shen, Y., Streit, W., Strohmeyer, R., Tooyoma, I., Van Muiswinkel, F. L., Veerhuis, R., Walker, D., Webster, S., Wegrzyniak, B., Wenk, G., and Wyss-Coray, T. (2000) Inflammation and Alzheimer's disease. Neurobiol Aging 21, 383-421

57. Wyss-Coray, T., Loike, J. D., Brionne, T. C., Lu, E., Anankov, R., Yan, F., Silverstein, S. C., and Husemann, J. (2003) Adult mouse astrocytes degrade amyloid-beta in vitro and in situ. Nat Med 9, 453-457

58. Sheffield, L. G., Marquis, J. G., and Berman, N. E. (2000) Regional distribution of cortical microglia parallels that of neurofibrillary tangles in Alzheimer's disease. Neurosci Lett 285, 165-168

59. Sheng, J. G., Mrak, R. E., and Griffin, W. S. (1997) Glial-neuronal interactions in Alzheimer disease: progressive association of IL-1alpha+ microglia and S100beta+ astrocytes with neurofibrillary tangle stages. J Neuropathol Exp Neurol 56, 285-290

60. DiPatre, P. L., and Gelman, B. B. (1997) Microglial cell activation in aging and Alzheimer disease: partial linkage with neurofibrillary tangle burden in the hippocampus. J Neuropathol Exp Neurol 56, 143-149

61. Schwab, C., Steele, J. C., and McGeer, P. L. (1998) Pyramidal neuron loss is matched by ghost tangle increase in Guam parkinsonism-dementia hippocampus. Acta Neuropathol 96, 409-416

62. Bancher, C., Brunner, C., Lassmann, H., Budka, H., Jellinger, K., Seitelberger, F., Grundke-Iqbal, I., Iqbal, K., and Wisniewski, H. M. (1989) Tau and ubiquitin immunoreactivity at different stages of formation of Alzheimer neurofibrillary tangles. Prog Clin Biol Res 317, 837-848

63. Cras, P., Kawai, M., Siedlak, S., and Perry, G. (1991) Microglia are associated with the extracellular neurofibrillary tangles of Alzheimer disease. Brain Res 558, 312-314

64. Probst, A., Ulrich, J., and Heitz, P. U. (1982) Senile dementia of Alzheimer type: astroglial reaction to extracellular neurofibrillary tangles in the hippocampus. An immunocytochemical and electron-microscopic study. Acta Neuropathol 57, 75-79

65. Reynolds, A. D., Kadiu, I., Garg, S. K., Glanzer, J. G., Nordgren, T., Ciborowski, P., Banerjee, R., and Gendelman, H. E. (2008) Nitrated alpha-synuclein and microglial neuroregulatory activities. J Neuroimmune Pharmacol 3, 59-74

66. Reynolds, A. D., Glanzer, J. G., Kadiu, I., Ricardo-Dukelow, M., Chaudhuri, A., Ciborowski, P., Cerny, R., Gelman, B., Thomas, M. P., Mosley, R. L., and Gendelman, H. E. (2008) Nitrated alpha-synuclein-activated microglial profiling for Parkinson's disease. J Neurochem 104, 1504-1525

67. Zhang, W., Wang, T., Pei, Z., Miller, D. S., Wu, X., Block, M. L., Wilson, B., Zhang, W., Zhou, Y., Hong, J. S., and Zhang, J. (2005) Aggregated alpha-synuclein activates microglia: a process leading to disease progression in Parkinson's disease. FASEB J 19, 533-542

68. Crawley, J. N. (1985) Exploratory behavior models of anxiety in mice. Neurosci Biobehav Rev 9, 37-44

69. Floresco, S. B., Seamans, J. K., and Phillips, A. G. (1997) Selective roles for hippocampal, prefrontal cortical, and ventral striatal circuits in radial-arm maze tasks with or without a delay. J Neurosci 17, 1880-1890

70. Baddeley, A. (2010) Working memory. Curr Biol 20, R136-140

71. Jarrard, L. E. (1993) On the role of the hippocampus in learning and memory in the rat. Behav Neural Biol 60, 9-26

72. Olton, D. S., and Papas, B. C. (1979) Spatial memory and hippocampal function. Neuropsychologia 17, 669-682

73. Rizzoli, S. O., and Betz, W. J. (2005) Synaptic vesicle pools. Nat Rev Neurosci 6, 57-69

74. Dillon, C., and Goda, Y. (2005) The actin cytoskeleton: integrating form and function at the synapse. Annu Rev Neurosci 28, 25-55

75. Davis, S., Butcher, S. P., and Morris, R. G. (1992) The NMDA receptor antagonist D-2-amino-5-phosphonopentanoate (D-AP5) impairs spatial learning and LTP in vivo at intracerebral concentrations comparable to those that block LTP in vitro. J Neurosci 12, 21-34

76. Borroni, A. M., Fichtenholtz, H., Woodside, B. L., and Teyler, T. J. (2000) Role of voltage-dependent calcium channel long-term potentiation (LTP) and NMDA LTP in spatial memory. J Neurosci 20, 9272-9276

77. Murakoshi, H., and Yasuda, R. (2012) Postsynaptic signaling during plasticity of dendritic spines. Trends Neurosci 35, 135-143

78. Fukazawa, Y., Saitoh, Y., Ozawa, F., Ohta, Y., Mizuno, K., and Inokuchi, K. (2003) Hippocampal LTP is accompanied by enhanced F-actin content within the dendritic spine that is essential for late LTP maintenance in vivo. Neuron 38, 447-460

79. Lin, B., Kramár, E. A., Bi, X., Brucher, F. A., Gall, C. M., and Lynch, G. (2005) Theta stimulation polymerizes actin in dendritic spines of hippocampus. J. Neurosci 25, 2062-2069

80. Ramachandran, B., and Frey, J. U. (2009) Interfering with the actin network and its effect on long-term potentiation and synaptic tagging in hippocampal CA1 neurons in slices in vitro. J. Neurosci 29, 12167-12173

81. Baddeley, A., Logie, R., Bressi, S., Della Sala, S., and Spinnler, H. (1986) Dementia and working memory. Q J Exp Psychol A 38, 603-618

82. Moser, E., Moser, M. B., and Andersen, P. (1993) Spatial learning impairment parallels the magnitude of dorsal hippocampal lesions, but is hardly present following ventral lesions. J Neurosci 13, 3916-3925

83. Bubser, M., and Schmidt, W. J. (1990) 6-Hydroxydopamine lesion of the rat prefrontal cortex increases locomotor activity, impairs acquisition of delayed alternation tasks, but does not affect uninterrupted tasks in the radial maze. Behav Brain Res 37, 157-168

84. Yoon, T., Okada, J., Jung, M. W., and Kim, J. J. (2008) Prefrontal cortex and hippocampus subserve different components of working memory in rats. Learn Mem 15, 97-105

Figure 4.1: Model Hirano bodies detected as eosinophilic inclusions in 3-month-old R26CT-CRE mice. Paraffin-embedded brain sections from 3-month-old R26CT and R26CT-CRE mice were dewaxed and stained with Gill's hematoxylin and counterstained with eosin. 3-month-old R26CT mice show no rod-shaped eosinophilic inclusions in the pyramidal cells of the hippocampus or cerebral cortex. 3-month-old R26CT-CRE mice show no inclusions in the cerebral cortex, but contain rare eosinophilic inclusions in CA1 pyramidal cells of the hippocampus indicated by the arrow. Scale bars represent 20, 50, or 500 μm.

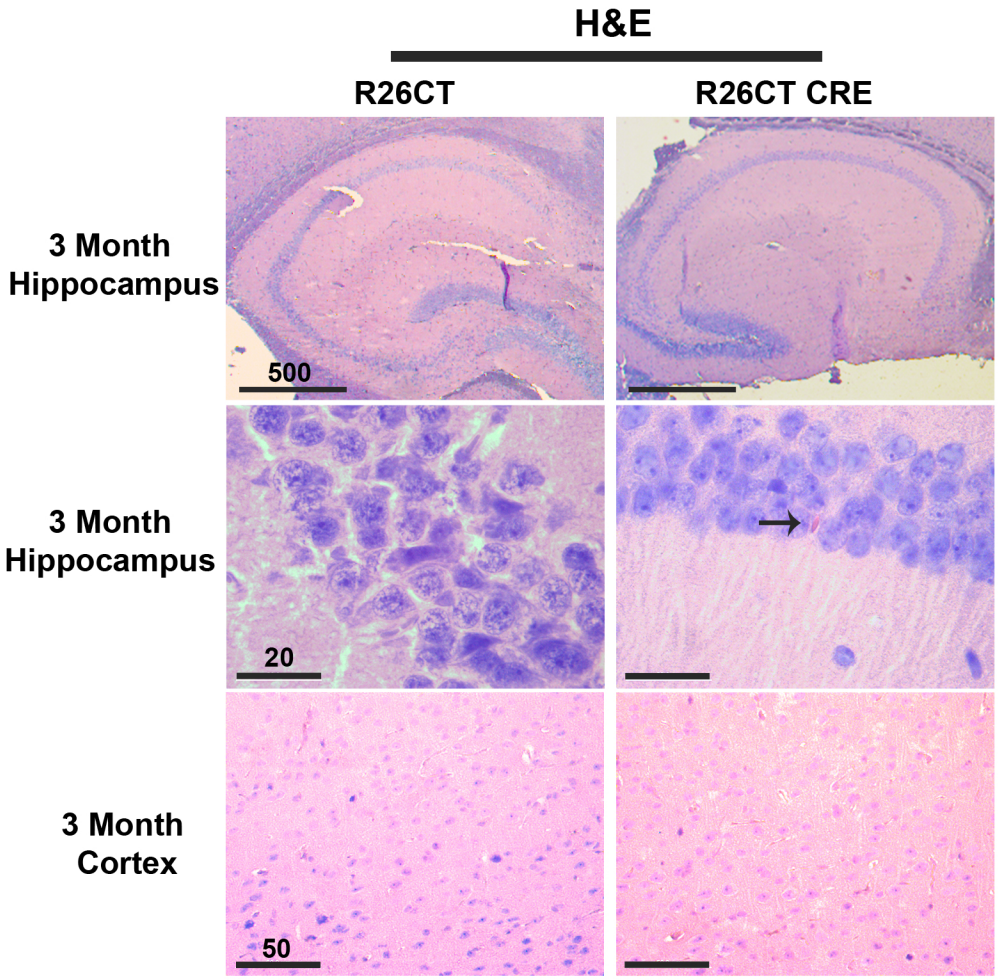
H&E
R26CT
R26CT CRE
3 Month Hippocampus
3 Month Hippocampus
3 Month Cortex
500
20
50

Figure 4.2: Model Hirano bodies detected as eosinophilic inclusions in 8-month-old R26CT-CRE mice. Paraffin-embedded brain sections from 8-month-old R26CT and R26CT-CRE mice were dewaxed and stained with Gill's hematoxylin and counterstained with eosin. 8-month-old R26CT mice show no rod-shaped eosinophilic inclusions in the pyramidal cells of the hippocampus or cerebral cortex. R26CT-CRE mice have eosinophilic inclusions predominately in the CA1 pyramidal cell layer of the hippocampus and rarely in the cerebral cortex. Arrows indicate inclusions. Scale bars represent 20 or 500 μm.

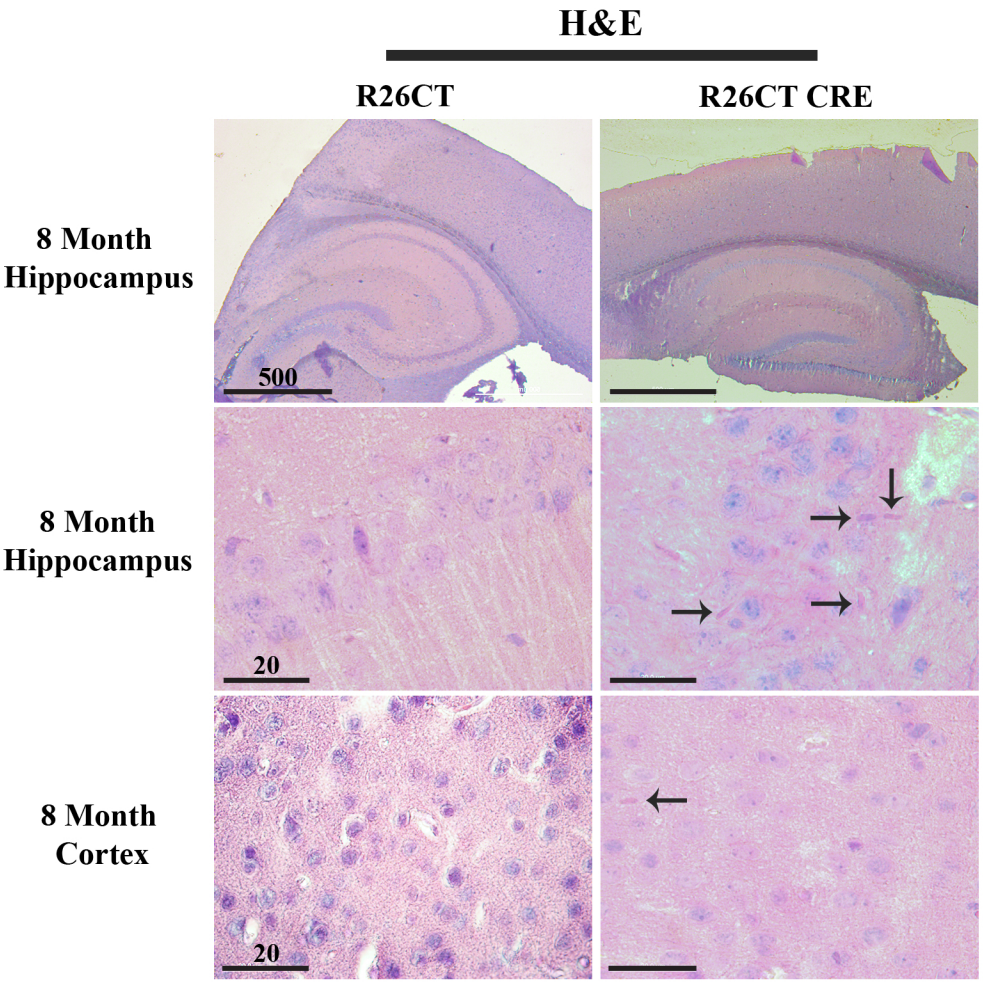
H&E
R26CT
R26CT CRE
8 Month Hippocampus
8 Month Hippocampus
8 Month Cortex
500
20
20

Figure 4.3: Lack of inflammation in microglia and astrocytes of 3-month-old R26CT and R26CT-CRE mice. Paraffin-embedded brain sections from 3 month old R26CT and R26CT-CRE mice were dewaxed and stained with DAB using antibodies against ED1 or GFAP to label activated microglia and reactive astrocytes, respectively. 3-month- old R26CT and R26CT-CRE mice show no GFAP or ED1 staining in either the hippocampus or cortex. Scale bars represent 50 or 500 μm.

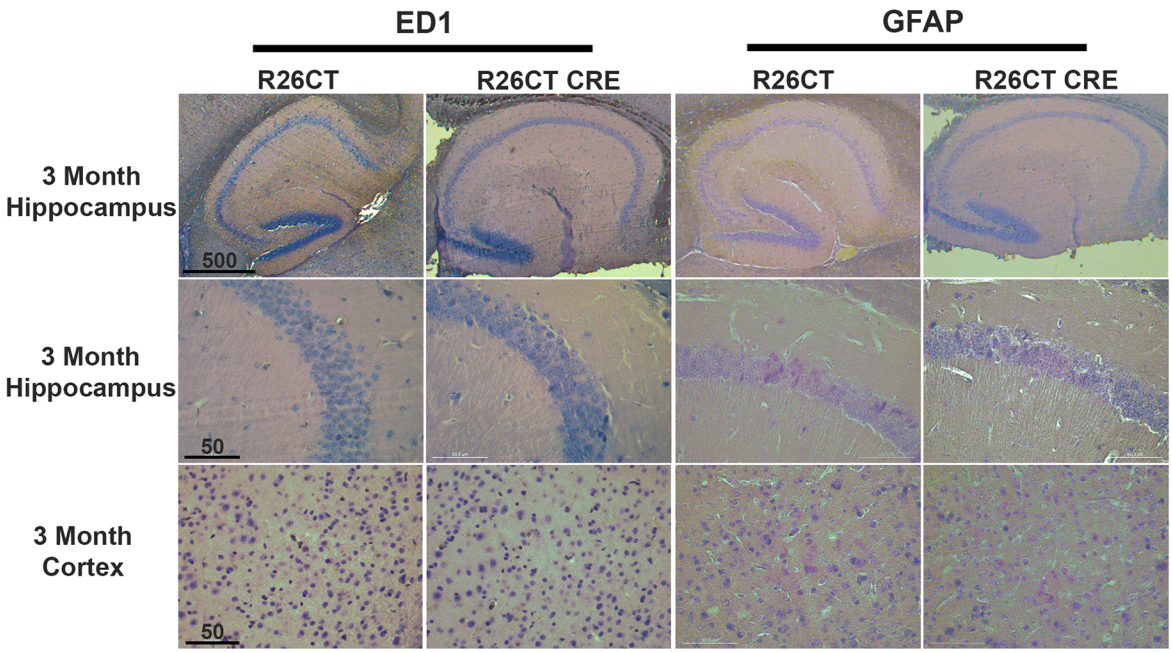
ED1
GFAP
R26CT
R26CT CRE
R26CT
R26CT CRE
3 Month Hippocampus
3 Month Hippocampus
3 Month Cortex
500
50
50

Figure 4.4: Inflammatory response in astrocytes, but not microglia of 8-month-old R26CT-CRE mice. Paraffin-embedded brain sections from 8-month-old R26CT and R26CT-CRE mice were dewaxed and stained with DAB using antibodies against ED1 or GFAP to label activated microglia and reactive astrocytes, respectively. 8-month-old R26CT and R26CT-CRE show no ED1 staining in the hippocampus or cerebral cortex. R26CT mice also show no GFAP staining in either hippocampus or cerebral cortex. R26CT-CRE mice have GFAP staining in the hippocampus but not cerebral cortex. Scale bars represent 50 or 500 μm.

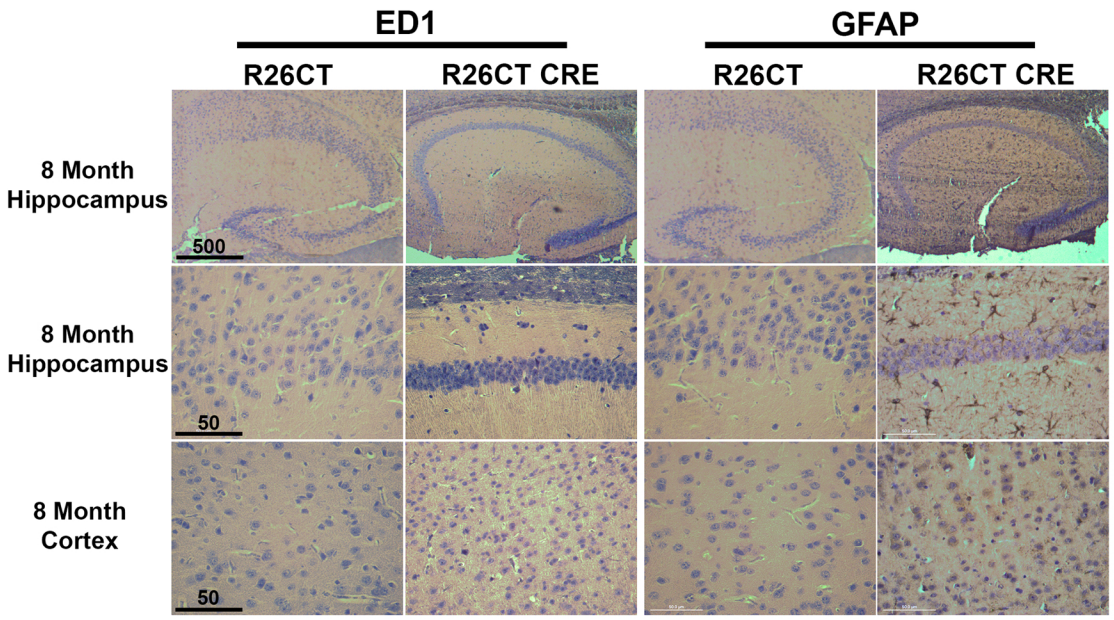
ED1
GFAP
R26CT
R26CT CRE
R26CT
R26CT CRE
8 Month Hippocampus
8 Month Hippocampus
8 Month Cortex
500
50
50

Figure 4.5: Western blot analysis of inflammatory response in 3-and 8-month-old mice. Brain homogenate from 3-and 8-month-old R26CT and R26CT-CRE mice was separated by SDS-PAGE and transferred to nitrocellulose. Blots were probed for tubulin (as a loading control), GFP, ED1, and GFAP. A) At 3 months of age, there is no difference in levels of synaptophysin, GFAP, or ED1 between R26CT and R26CT-CRE mice. B) Quantification of data in A. C) At 8 months of age, there is no difference in levels of ED1 or synaptophysin between R26CT and R26CT-CRE mice. However, R26CT-CRE mice show an increase in GFAP, indicating the presence of an inflammatory response. D) Quantification of data in C. GFAP levels have increased approximately 3.5-fold in R26CT-CRE mice (* $p < 0.05$). Statistics were performed using Student's t-test.

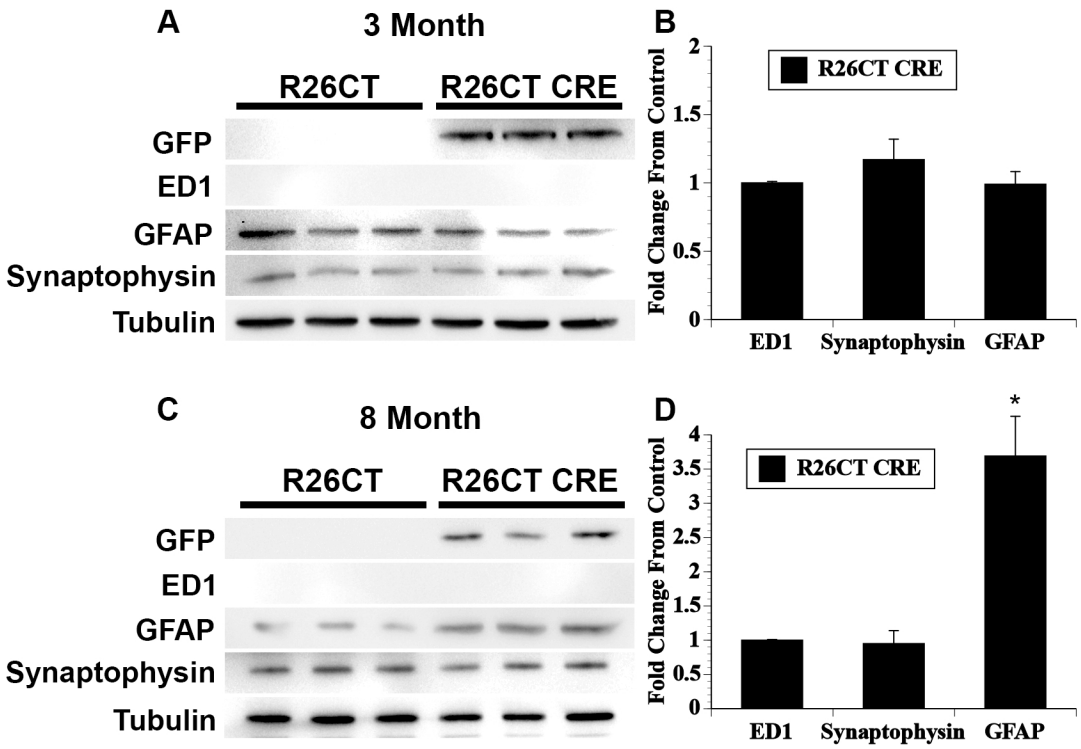
A
3 Month
R26CT
R26CT CRE
GFP
ED1
GFAP
Synaptophysin
Tubulin
B
R26CT CRE
Fold Change From Control
2
1.5
1
0.5
0
ED1
Synaptophysin
GFAP
C
8 Month
R26CT
R26CT CRE
GFP
ED1
GFAP
Synaptophysin
Tubulin
D
R26CT CRE
Fold Change From Control
*
4
3.5
3
2.5
2
1.5
1
0.5
0
ED1
Synaptophysin
GFAP

Figure 4.6: Open field test analysis of 3-and 8-month old R26CT and R26CT-CRE mice. Locomotor activity and center zone entrances of R26CT (3-month-old, n=11; 8-month-old, n=11) and R26CT-CRE (3-month-old, n=12; 8-month-old, n=12) mice were measured utilizing an open field test. A, B) There was no difference in locomotor activity between R26CT (black squares) and R26CT-CRE mice (open circles) at 3 or 8 months of age. C) R26CT (black bars) and R26CT-CRE (white bars) mice made similar entrances to the center zone. At both ages, R26CT and R26CT-CRE mice are not significantly different from each other. Error bars represent SEM.

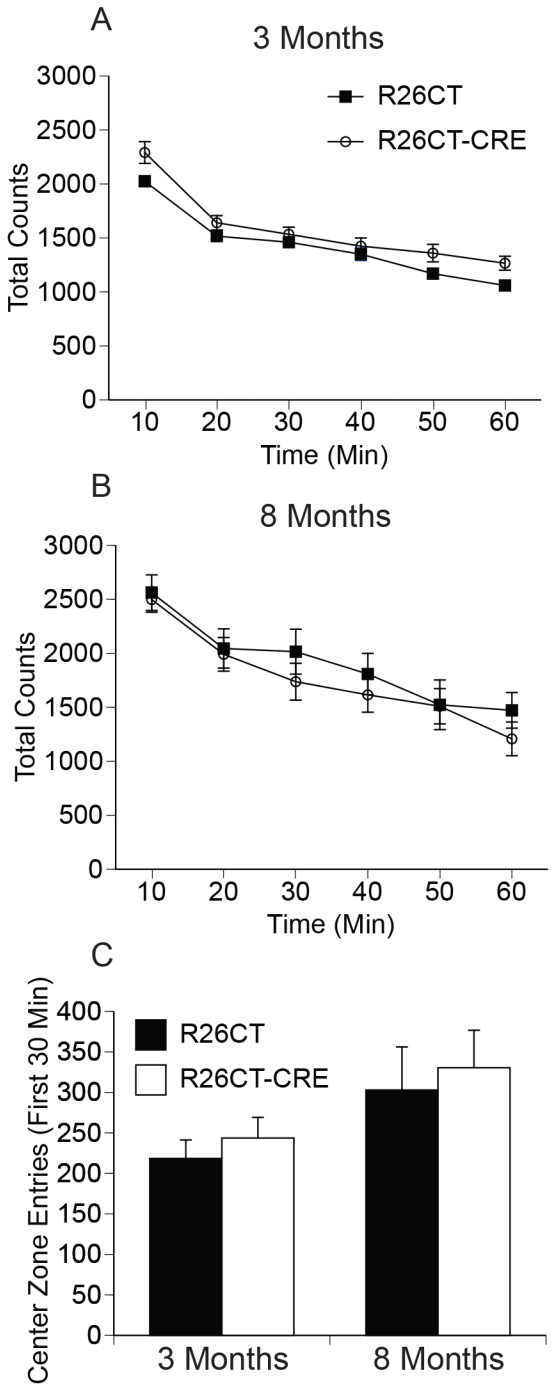
A
3 Months
R26CT
R26CT-CRE
Total Counts
3000
2500
2000
1500
1000
500
0
10
20
30
40
50
60
Time (Min)
B
8 Months
Total Counts
3000
2500
2000
1500
1000
500
0
10
20
30
40
50
60
Time (Min)
C
Center Zone Entries (First 30 Min)
400
350
300
250
200
150
100
50
0
R26CT
R26CT-CRE
3 Months
8 Months

Figure 4.7: Working memory performance in the 8-arm radial maze for R26CT and R26CT-CRE mice. A) Schematic diagram of the training phase procedure (8 arms open, 8 arms baited). B) At 3 months of age: R26CT (black bars, n=11), R26CT-CRE (white bars, n=12). C) At 8 months of age: R26CT (black bars, n=11), R26CT-CRE (white bars, n=12). No significant differences were found between R26CT and R26CT-CRE mice at either 3 or 8 months of age in the training phase (B, C). Performance of both mice improved with experience. D) Schematic diagram of the delayed spatial win-shift assay (RI = retention interval). E) At 3 months of age: R26CT (black bars, n=11), R26CT-CRE (white bars, n=12). Both R26CT and R26CT-CRE mice improved with experience, and there was no significant difference between genotypes at either days 11-13 or 18-20. F) At 8 months of age: R26CT (black bars, n=11), R26CT-CRE (white bars, n=12). R26CT mice improve with experience while R26CT-CRE mice do not. Furthermore, there is a significant difference between R26CT and R26CT-CRE mice during the late time block (days 18-20) indicating that the spatial working memory of R26CT-CRE mice is impaired. Bars represent the mean total error ± SEM of the first 3 days and the last 3 days of either the training or test phase performance. Significance between performance blocks and between genotypes was determined using a mixed ANOVA analysis (*$p < 0.05$, ** $p < 0.01$).

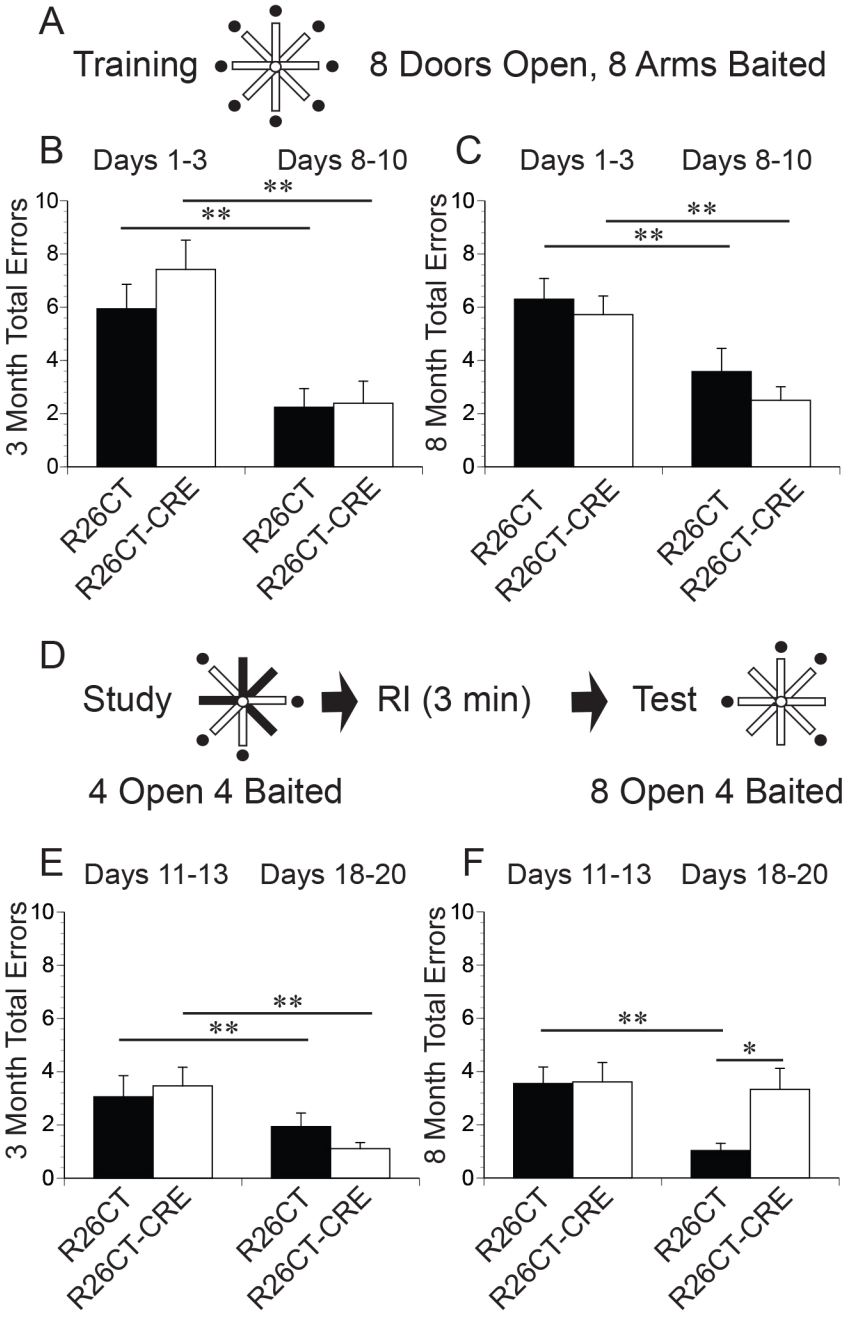
A
Training
8 Doors Open, 8 Arms Baited
B
Days 1-3
Days 8-10
3 Month Total Errors
C
Days 1-3
Days 8-10
8 Month Total Errors
R26CT
R26CT-CRE
D
Study
RI (3 min)
Test
4 Open 4 Baited
8 Open 4 Baited
E
Days 11-13
Days 18-20
3 Month Total Errors
F
Days 11-13
Days 18-20
8 Month Total Errors

Figure 4.8: Field excitatory post-synaptic potentials (fEPSP) recorded from hippocampus in R26CT and R26CT-CRE mice. A, B) Stimulus response curves for R26CT (black squares n=10(19)) and R26CT-CRE (open circles, n=12(18)) mice at 3 months of age. Input intensities are 30, 40, 50, 60, 75, 90, 110, 130, 150, and 170 μA. B) Averaged fEPSP sweeps for each group shown in A. The vertical bar represents 2 mV, and the sweeps are 50 ms in duration. C, D) Same as A and B above except at 8 months of age for R26CT (n=10(20)) and R26CT-CRE (n=12(19)) control mice. The values represent the mean $\pm$ SEM from n slices. There are no significant differences between genotypes at either 3 or 8 months of age. Significance between genotypes was determined using an unpaired t-test.

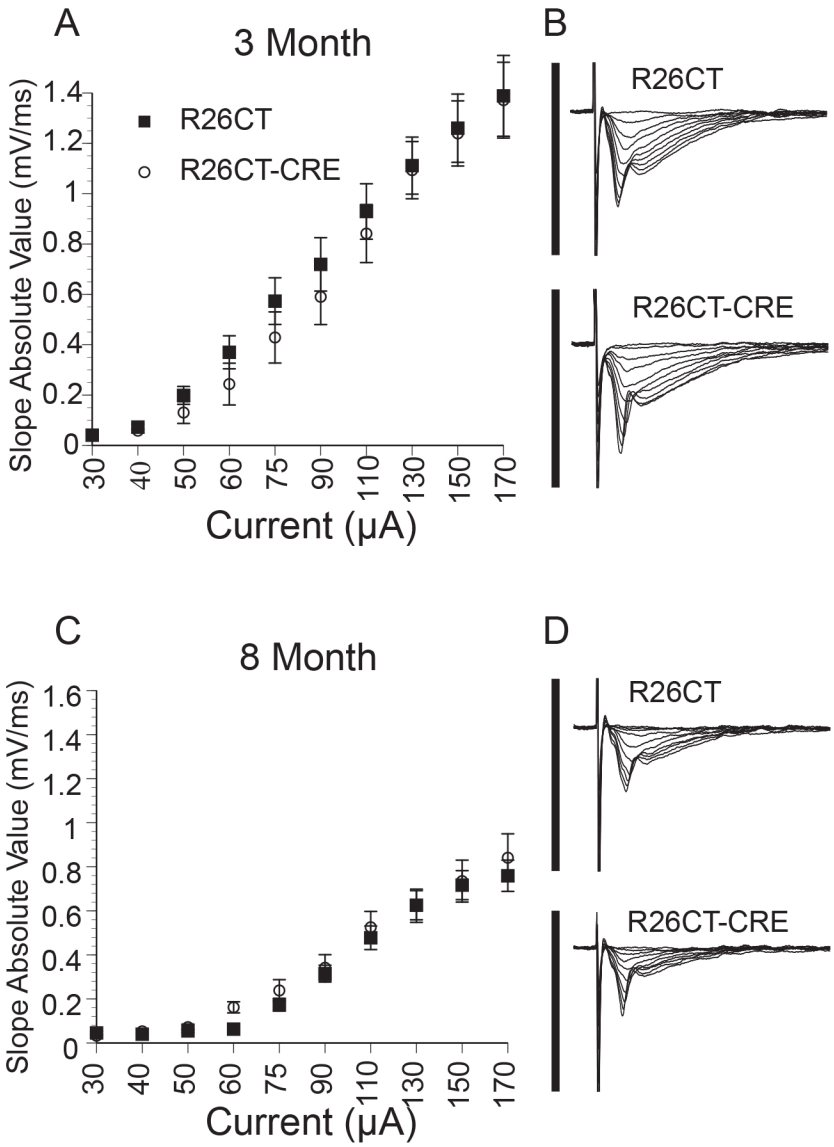
A
3 Month
R26CT
R26CT-CRE
Slope Absolute Value (mV/ms)
Current (µA)
B
R26CT
R26CT-CRE
C
8 Month
Slope Absolute Value (mV/ms)
Current (µA)
D
R26CT
R26CT-CRE

Figure 4.9: Paired-pulse field excitatory post-synaptic potentials (fEPSP) recorded from hippocampus in R26CT and R26CT-CRE mice. A) Paired-pulse ratios at 50, 100, 200, or 500 ms in R26CT (black bars, n=10(19)) and R26CT-CRE (white bars, n=12(18)) mice at 3 months of age. B) Averaged fEPSP sweeps for each group shown in A. The second sweeps for each interval are overlaid. Vertical bars represent 2 mV, and sweeps are 90 ms in duration. C, D) Same as A and B above except at 8 months of age for R26CT (n=10(20)) and R26CT-CRE (n=12(21)) mice. The values represent the mean $\pm$ SEM from n slices. There is no significant difference between genotypes at either age. Significance between genotypes was determined using an unpaired t-test.

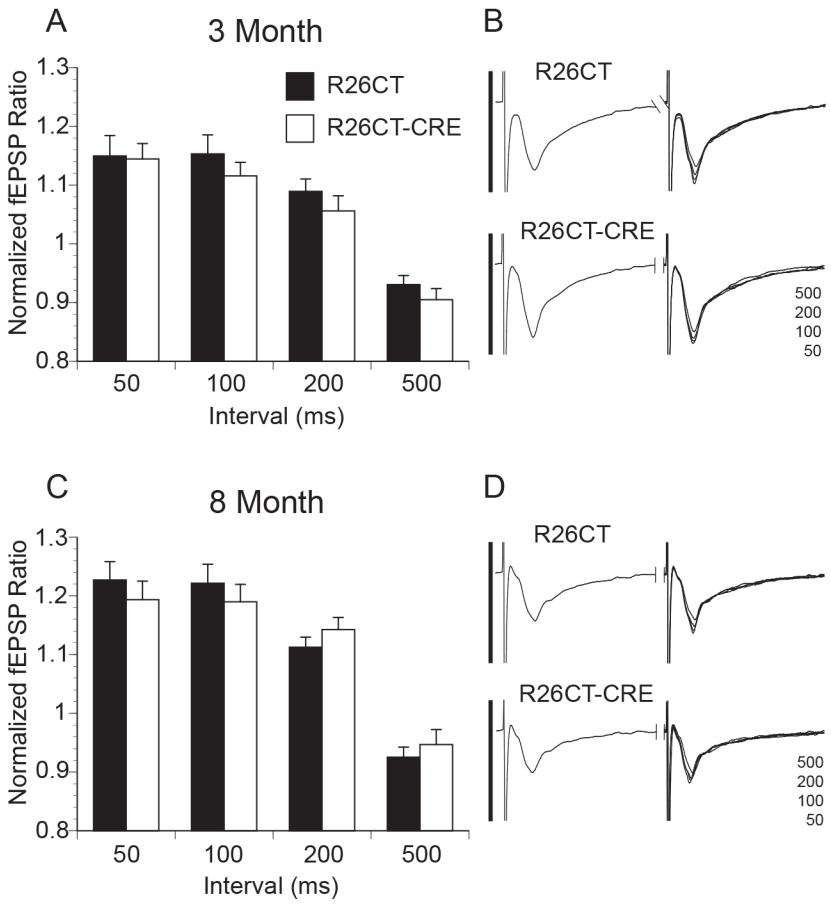
A
3 Month
R26CT
R26CT-CRE
Normalized fEPSP Ratio
1.3
1.2
1.1
1
0.9
0.8
50
100
200
500
Interval (ms)
B
R26CT
R26CT-CRE
500
200
100
50
C
8 Month
Normalized fEPSP Ratio
1.3
1.2
1.1
1
0.9
0.8
50
100
200
500
Interval (ms)
D
R26CT
R26CT-CRE
500
200
100
50

Figure 4.10: Long-term potentiation of field excitatory post-synaptic potentials (fEPSP) recorded from hippocampus in R26CT and R26CT-CRE mice. A) Summary time course of normalized fEPSP slope values in 3-month-old R26CT mice in LTP (black square, (n=10(17)) and R26CT-CRE (open circle, n=11(16)), before and after high frequency stimulation (HFS) (3 x 100 Hz/1 s at 20 s intervals) indicated by the arrow at 30 minutes. Insets represent averaged fEPSP sweeps before and after HFS. B) Summary quantification of LTP for R26CT and R26CT-CRE mice at 1, 2, and 3 hrs post-HFS. C, D) Same as panel A and B above except for 8-month-old R26CT (black square, (n=9(18)) and R26CT-CRE (open circle, (n=11(18)). The values represent the mean $\pm$ SEM from n slices. There is no significant difference between genotypes at either age. Significance was determined using an unpaired t-test between genotypes.

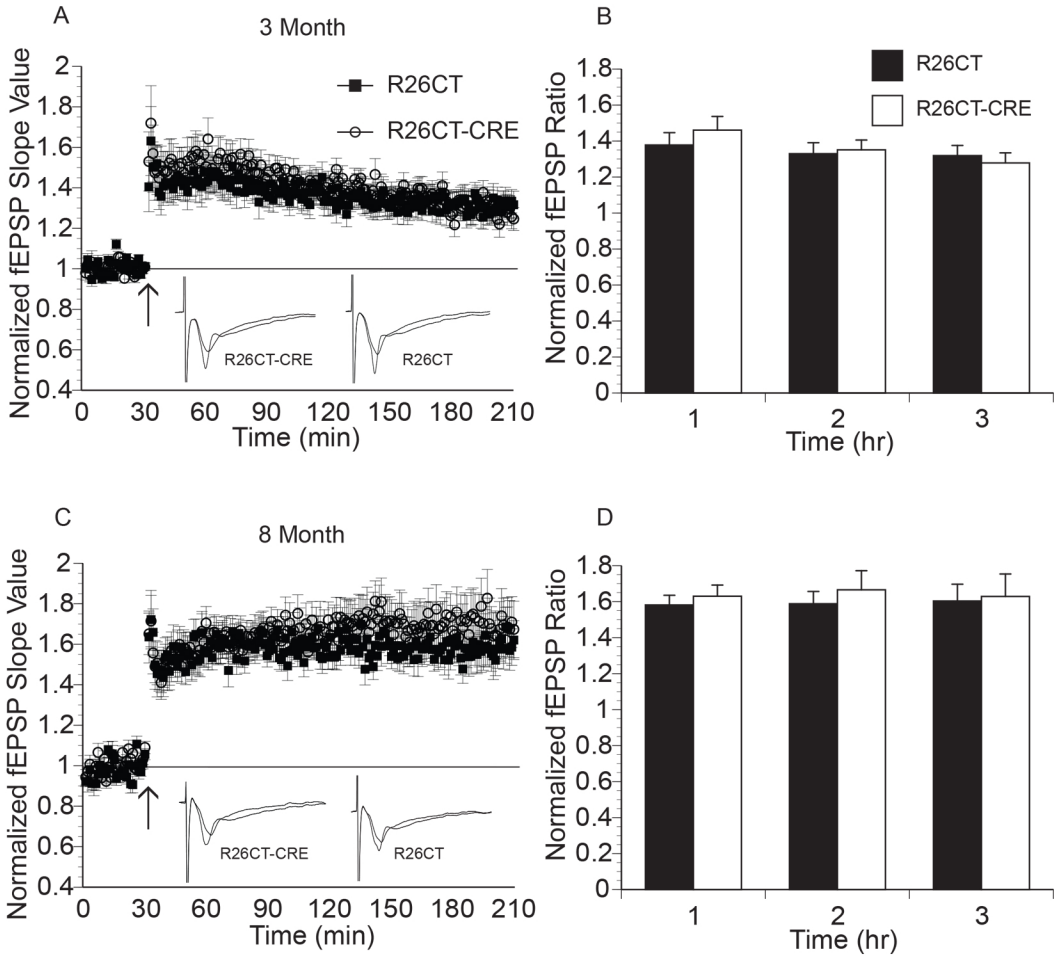
A
3 Month
R26CT
R26CT-CRE
Normalized fEPSP Slope Value
Time (min)
R26CT-CRE
R26CT
B
R26CT
R26CT-CRE
Normalized fEPSP Ratio
Time (hr)
C
8 Month
Normalized fEPSP Slope Value
Time (min)
R26CT-CRE
R26CT
D
Normalized fEPSP Ratio
Time (hr)

Figure 4.11: Immunofluorescence and Western blot of CT-GFP expression in R26CT-CRE mice. A) Immunofluorescence microscopy was performed on cryosections from 1- month-old R26CT and R26CT-CRE mouse brains. Sections were stained with anti-GFP antibodies to visualize expression of CT-GFP and counterstained with DAPI and TRITC-labeled phalloidin to visualize nuclei and F-actin, respectively. R26CT-CRE mice show expression of CT-GFP in the hippocampus while R26CT control mice do not. B) A Western blot was performed using brain homogenate from hippocampus and cortex of 1- month-old R26CT and R26CT-CRE mice using anti-GFP antibodies to detect CT-GFP expression. To ensure that no expression of CT-GFP is detectable in R26CT mice, twice the amount of protein from R26CT samples was loaded compared to R26CT-CRE samples. R26CT-CRE mice show strong expression of CT-GFP in the hippocampus and weak expression in the cortex. R26CT mice have no detectable CT-GFP in either hippocampus or cortex. Scale bar represents 40 or 200 μm.

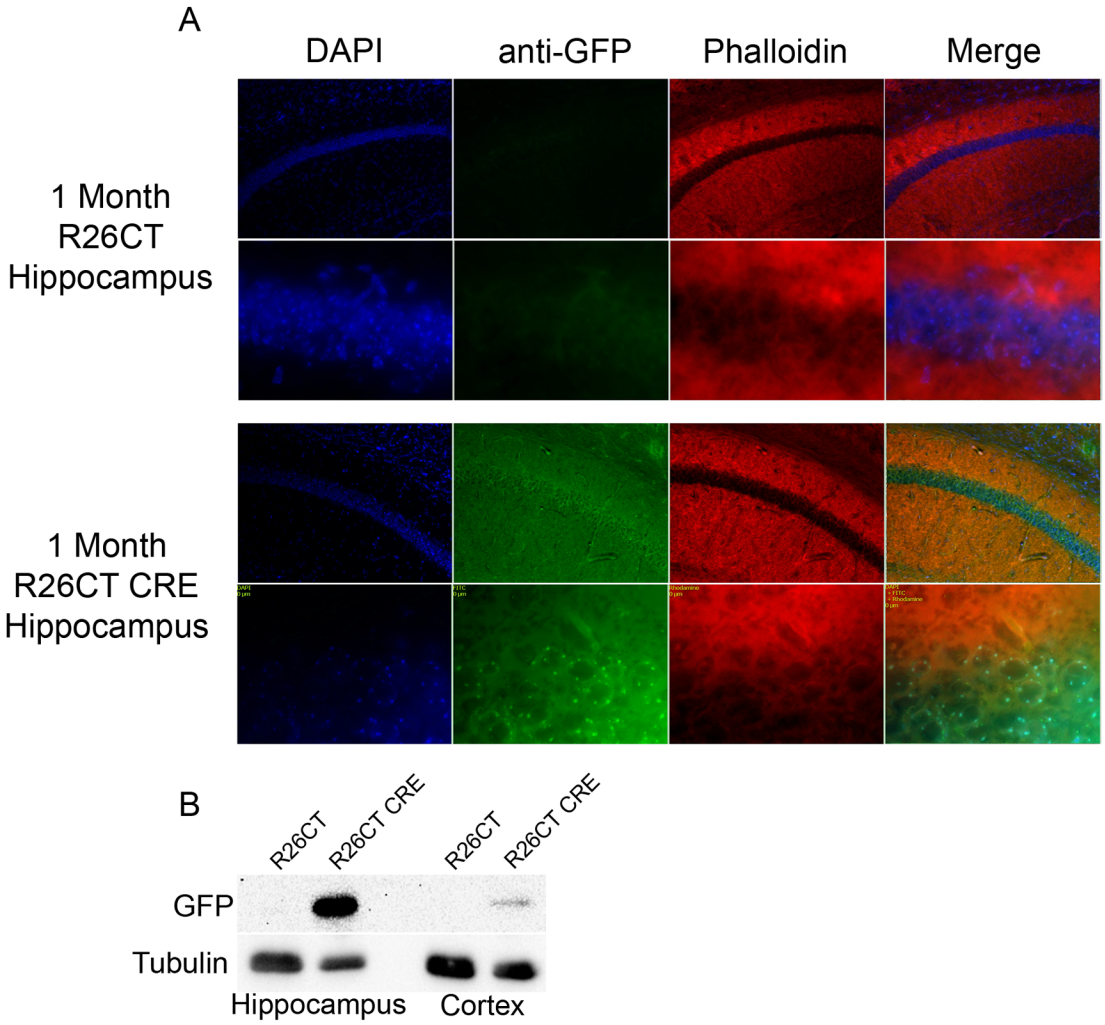
A
DAPI
anti-GFP
Phalloidin
Merge
1 Month
R26CT
Hippocampus
1 Month
R26CT CRE
Hippocampus
B
R26CT
R26CT CRE
R26CT
R26CT CRE
GFP
Tubulin
Hippocampus
Cortex

Figure 4.12: Electron micrographs of inclusions in 8-month-old R26CT-CRE mice. Hippocampal tissue from 8 month old R26CT and R26CT-CRE mice was isolated and prepared for transmission electron microscopy. R26CT-CRE tissue contained electron dense inclusions, which are identical to the ultrastructure of Hirano bodies. These structures were not observed in R26CT mice (data not shown). A, B) The ultrastructure of model Hirano bodies resembling a spheroid or fingerprint pattern similar to those seen in humans (8). C) Intermediate structures were seen in the brains of R26CT-CRE mice similar to those seen in humans and cell culture models (22,25,51). D) R26CT-CRE mice exhibit model Hirano bodies, which contain both ordered filaments and amorphous electron dense material. Arrows indicate Hirano bodies or intermediates magnified in the panels to the right. Scale bars are in nm.

R26CT-CRE Hippocampus

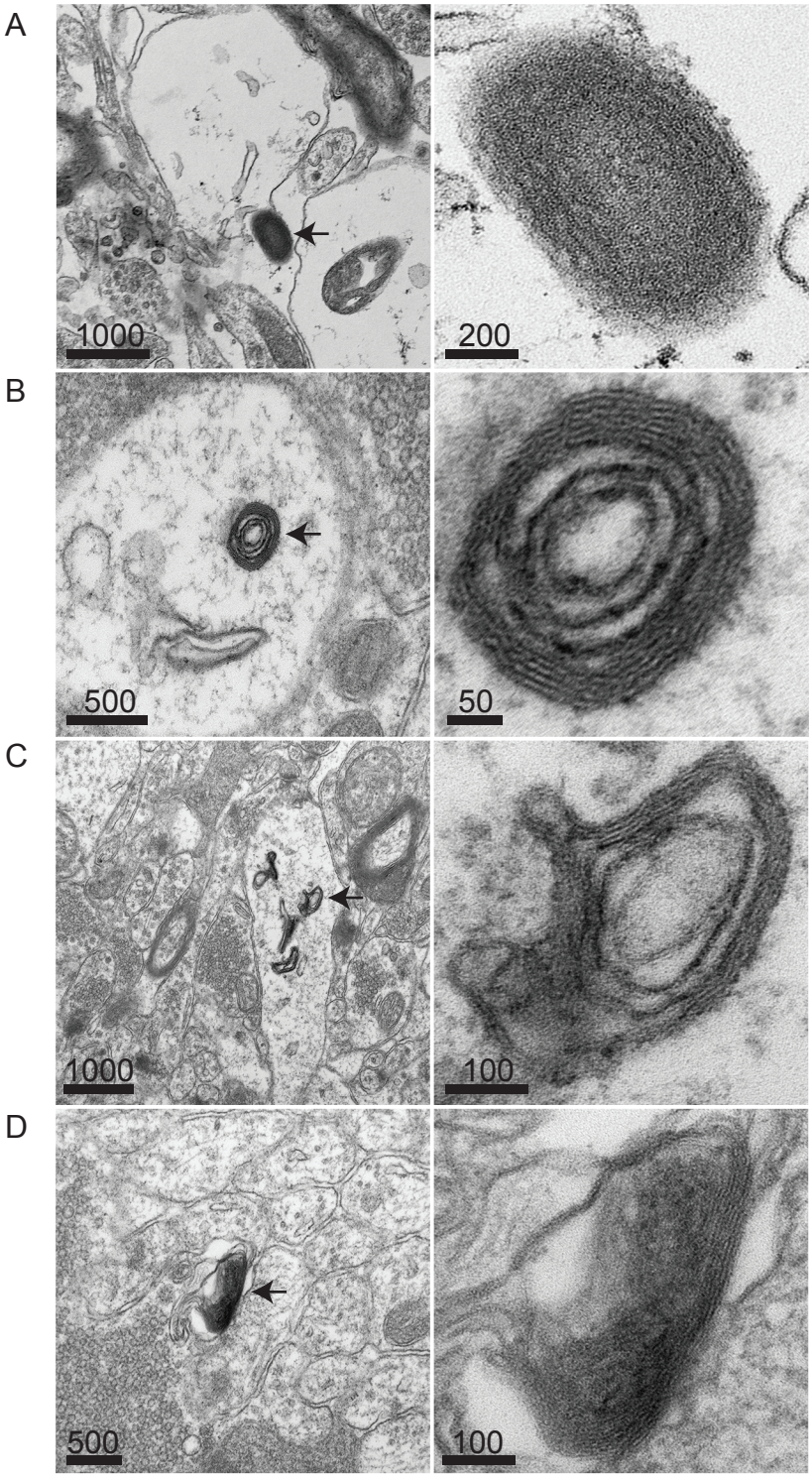

CHAPTER 5

CONCLUSIONS AND FUTURE DIRECTIONS

DISCUSSION:

The overall goal of this dissertation was to investigate the impact of Hirano bodies on normal and disease processes using both cell culture and *in vivo* experimental systems. The initial studies were designed to investigate the interaction of amyloid precursor protein intracellular domains and tau as well as to investigate how Hirano bodies impact these interactions. The work in this dissertation shows that APP and either of its c-terminal fragments C31 or AICD act in synergy to increase cell death and that the presence of tau is not required for this synergistic cell death. However, the addition of a hyperphosphorylated tau mimic 352PHPtau significantly increases cell death in the presence of both APP and C31 or AICD alone. Fe65, Tip60, p53, and caspases play a role in tau-independent and tau-dependent cell death via apoptosis. The presence of model Hirano bodies protected against cell death, indicating Hirano bodies may play a protective role in neurodegeneration. Tau mutants found in FTLD-17 were investigated to determine if they alter this paradigm. Model Hirano bodies had either no effect or enhanced cell death induced by tau in the absence of AICD. In the presence of AICD and tau, synergistic cell death was observed in most cases, and the presence of model Hirano bodies reduced this synergistic cell death in most cases (352PHP, R406W, and R5H tau). The exceptions were those tau mutations that caused significant cell death in the presence of model Hirano bodies in the absence of AICD (G272V and P301L). A role for the kinase GSK3β

is suggested by the finding that a dominant negative form of GSK3β reduces synergistic cell death initiated by AICD and mutant tau. A subset of Hirano bodies in brain tissue of both Alzheimer's disease and normal aged individuals was found to contain tau. Phosphorylated tau was found in some Hirano bodies in Alzheimer's disease tissue. The results demonstrate a complex interaction between tau and AICD involving activation of GSK3β in promoting cell death. Furthermore, these results demonstrate that model Hirano body-dependent modulation of these processes is complex. In addition, these data support previous work indicating that CT-GFP expression to form model Hirano bodies is not detrimental to cells (1-3).

While cell culture systems are useful for mechanistic characterization, an animal model is required for anatomicaly and physiologicaly assessment of systemic pathology. Therefore, a mouse with brain-specific expression of CT-GFP (R26CT-CRE) was generated by crossing a CT-GFP transgenic mouse (R26CT) with a CamKIIa-CRE mouse. These mice develop rod-shaped eosinophilic inclusions in the CA1 region of the hippocampus and cortex, and these inclusions have an identical ultrastructure to authentic Hirano bodies (4-6). Although the formation of model Hirano bodies did not lead to cell death, they were found to induce an inflammatory response as measured by the presence of reactive astrocytes. Open field test results suggest that there are no overt deficits in general anxiety or locomotor activity. Older R26CT-CRE mice showed an impairment in spatial working memory as measured in the radial arm maze. These impairments are likely not attributable to a loss of synaptic density since levels of the synaptic protein synaptophysin were unchanged in R26CT-CRE mice compared to R26CT mice. Furthermore, there were no detectable electrophysiological differences in R26CT-CRE mice compared to R26CT mice that might mechanistically explain the working memory impairments. The radial arm maze task is known to heavily rely on both hippocampus and

prefrontal cortex. Perhaps electrophysiology measurements in the prefrontal cortex could help explain our behavioral results.

Work performed using a mouse model and cell culture system has given valuable insight into the physiological role of Hirano bodies. Experiments performed in cell culture indicate that CT-GFP expression has no severe phenotypes. Model Hirano body formation after CT expression did not significantly impact *Dictyostelium* growth and development and were not detrimental to cell survival (1,7). Later experiments using mammalian cell culture systems corroborated these results (2). Consistent with the cell culture work, CT-GFP expressing mice appear to be developmentally normal. Furthermore, expression of CT-GFP did not induce neuron loss in these mice. While CT-GFP expression in cell culture systems appears to have no negative consequences, CT-GFP expressing mice have an inflammatory response and working memory impairments. However, there is no correlate of these two phenotypes in cell culture models. These findings stress the importance of using animal model systems. While the presence of model Hirano bodies alone do not have a negative impact on cells and minor impact on mice, model Hirano bodies in combination of disease-relevant molecules such as APP and tau have a complex differential effect in cell culture.

Future Directions: The association of AICD/C31 and Hirano bodies in a cell culture system.

Model Hirano bodies are found to mitigate cell death induced by APP and C-terminal fragments of the amyloid precursor protein. Since both AICD and C31 colocalize with human and model Hirano bodies, it is likely that Hirano bodies act as a sink and sequester specific proteins. Therefore, sequestration of AICD/C31 likely prevents downstream apoptotic signaling events attributed to AICD and C31 (8,9). Hirano bodies are classically described as being

comprised primarily of F-actin and actin- associating proteins (10-12). However, other proteins, which are unable to interact with actin, are associated with Hirano bodies (13-23). It is unclear whether the interaction between AICD/C31 and Hirano bodies is direct or indirect. AICD/C31 is known to interact with the scaffolding protein Fe65 (via PTB2 domain), and this interaction is required for AICD/C31-induced apoptosis (8,9,24). Fe65 is also found colocalized with model Hirano bodies, which suggests that AICD may indirectly associate with Hirano bodies through Fe65 (3). While Fe65 is unable to interact with actin directly, it can associate with the actin-binding protein Mena via its WW domain (25). In addition, Mena has also been shown to colocalize with model Hirano bodies (unpublished data Fechheimer lab). Several experiments can be performed to determine whether the AICD/C31 association with model Hirano bodies involves Fe65 and Mena. First, *in vitro* studies of AICD/C31 interaction with F-actin can be performed through F-actin cosedimentation assays. F-actin can be incubated with a combination of AICD/C31, Fe65, or Mena alone as well as in combination. Combinations that promote AICD/C31 binding to F-actin will pellet with F-actin after centrifugation. Association of these proteins can then be quantified via SDS-PAGE and Western blots. Transient expression of AICD/C31 and CT-GFP in Fe65 or Mena knockout cell lines can also be utilized to investigate the association of AICD/c31 with model Hirano bodies. For instance, immunofluorescence assays can be used to determine if AICD/C31 still colocalizes with model Hirano bodies in Mena and/or Fe65 knockout cell lines. The immunofluorescence results can be followed up with rescue experiments through reintroduction of Fe65 or Mena to knockout cell lines. Model Hirano bodies have been shown to protect against AICD-induced apoptosis. If Fe65 and Mena are shown to be important for AICD/C31 association with model Hirano bodies, it would be interesting to perform cell death experiments. Expression of AICD with and without CT-GFP

can be performed in Mena-knockout cells. The inability of model Hirano bodies to protect against AICD-induced cell death in the absence of Mena would argue that AICD association with model Hirano bodies is important for protection by model Hirano bodies. Furthermore, it would indicate that Mena is required for this interaction. As a control experiment it would be important to perform electron microscopy on model Hirano bodies formed in Mena knockout cell lines to verify that the absence of Mena does not impact model Hirano body structure and formation.

Future Directions: The association of AICD/C31 and Hirano bodies in a mouse model.

The association of AICD and Hirano bodies can also be investigated using a mouse model system. An Alzheimer's disease mouse model (FeCγ25) has been generated through brain specific expression of AICD and Fe65 driven by CamKIIa promoters (26). FeCγ25 mice exhibit many features observed in Alzheimer's disease including GSK3β activation, tau hyperphosphorylation, tau aggregation, neuronal loss, and memory impairments (26-29). To determine if model Hirano bodies can protect against AICD initiated insults *in vivo*, CT-GFP expressing mice could be crossed with the FeCγ25 mice. Since model Hirano bodies sequester, and prevent AICD-induced cell death in cell culture, they may protect against neuronal loss in FeCγ25 mice. I hypothesize that the sequestration of AICD by model Hirano bodies may prevent AICD-induced increases in GSK3β and consequently tau phosphorylation and aggregation. It would be interesting to see how CT-GFP expression impacts working memory deficits in FeCγ25 mice. Memory impairments in FeCγ25 correlate with tau aggregation (26,27). If sequestration of AICD reduces tau phosphorylation and aggregation, it may reduce working memory impairments in FeCγ25 mice. However, our R26CT-CRE model Hirano body model

mice show working memory deficits in an 8-arm radial maze. Therefore, any protective effect of model Hirano bodies on AICD-induced memory deficits may be masked by CT-GFP working memory impairments. It would be interesting to investigate this paradigm.

AICD is known to play a role in transcriptional regulation (30,31). However, studies have been performed in cell culture systems using microarrays and have yielded inconsistent results (32-34). Our laboratory has reported that model Hirano bodies reduce AICD transcriptional transactivation (3). It would be worthwhile to investigate transcriptional targets of AICD in a mouse model to determine how model Hirano bodies impact these targets. This can be accomplished by dissecting different brain regions from control, FeCγ25, and FeCγ25 x CT-GFP transgenic mice and then performing RNA deep sequencing analysis to generate transcriptome libraries.

Future Directions: The impact of AICD and model Hirano bodies on tau in cell culture.

Expression of AICD and mutant tau leads to synergistic cell death indicating a putative link between AICD and tau. Multiple studies suggest that a downstream effector of AICD/C31 is the kinase GSK3β. Studies in cell culture and mice report that AICD either induces transcriptional upregulation of GSK3β or increases GSK3β activation (via phosphorylation) resulting in downstream tau hyperphosphorylation (34-36). Our use of the dominant-negative GSK3β (K85A) implicates GSK3β in the signaling between AICD and tau variants. Through Western blot analysis we found that AICD increases total levels of GSK3β. Furthermore, we found that CT-GFP expression mitigates these AICD -induced changes in GSK3β protein levels. It would be important to determine if AICD- induced increases in GSK3β coincide with an increase in tau phosphorylation. Western blots could be performed using phospho-tau specific

antibodies to determine if there is an increase in tau phosphorylation in the presence of AICD and whether CT-GFP expression reduces these phosphorylation states. If AICD increases tau phosphorylation, it would be worthwhile to investigate whether dominant negative GSK3β (K85A) reduces AICD-mediated phosphorylation of tau using Western blot analysis.

While AICD and tau have an interesting and dynamic interaction, the association between CT-GFP and tau is also intriguing. Particularly, G272V and P301L tau variants were unique in their ability to significantly increase cell death in the presence of CT-GFP. Furthermore, this increase in cell death was drastically reduced in the presence of a dominant-negative GSK3β (K85A) mutant. Based on these results, Western blots were performed to determine if CT-GFP increased phosphorylation of G272V and P301L tau, but not other tau variants. We found that G272V and P301L tau variants had an increase in phosphorylation at several serine and threonine amino acids in the presence in CT-GFP while other tau variants did not. There are multiple potential interpretations of these results. Since tau colocalizes with model Hirano bodies, CT-GFP expression may increase local concentrations of tau making it a better substrate for interaction with endogenous GSK3β. Additionally, CT-GFP expression may directly or indirectly increase either activated (phosphorylated) GSK3β levels or levels of total GSK3β protein. Since we showed that CT-GFP reduces AICD-induced increases in GSK3β levels, it seems unlikely that CT-GFP increases protein levels of GSK3β in the absence of AICD. However, one attempt to test these possibilities would be through Western blot analysis using antibodies against pan-GSK3β to detect total protein and either anti-Tyr216 GSK3β or anti-Tyr279 GSK3β antibodies to detect activated forms of GSK3β.

Model Hirano bodies appear to have a differential impact on mutant tau-induced cell death. While model Hirano bodies protect against cell death initiated by AICD and most tau

variants, model Hirano bodies potentiated G272V and P301L-induced cell death as mentioned above. These data appears to correlate with the propensity of tau to aggregate as G272V and P301L have a greater propensity to self-aggregate as compared to the other mutants tested (37-39). In addition to manipulating tau phosphorylation, model Hirano bodies may act as a sink to increase local concentrations of tau and induce a nucleation event for mutants, which aggregate readily. In order to test this hypothesis, tau aggregation could be measured in cells expressing mutant tau with and without CT-GFP expression. Tau aggregates are rich in beta sheet structure and are sarkosyl insoluble (40-42). Tau aggregation could be visualized in cells by labeling with Thioflavin-S or Congo red, fluorescent compounds that interact with beta sheet-rich aggregates (43). Western blot analysis could also be performed on sarkosyl soluble and insoluble fractions using tau antibodies. If model Hirano bodies modify tau aggregation, levels of sarkosyl-insoluble tau will change.

Future Directions: The impact of AICD and Hirano bodies on tau in mouse models.

Our work in a cell culture system implies that AICD is able to signal downstream to tau through GSK3β. While cell culture experiments allow a fast and easy manipulation of variables, they may not recapitulate mechanisms in a more complex system such as the brain. Therefore, *in vivo* studies are required to verify our cell culture results. Others have also implicated the importance of APP to tau signaling events *in vivo*. Alzheimer's disease model mice expressing familial mutant amyloid precursor protein or presenilin exhibit many of the characteristics of disease progression. Knockout of endogenous tau in some of these models lessens disease severity (44,45). GSK3β activation, tau hyperphosphorylation, and tau aggregation all occur in the AICD transgenic Alzheimer's disease model mouse (FeCγ25). Furthermore, tau pathology

correlates with memory impairments in these animals. (26-29). It would be interesting to see if reduction of tau in FeCγ25 mice would also improve behavioral and pathological phenotypes reported in these animals.

Genetic crosses between CT-GFP transgenic mice and mutant tau mice would help us understand how different forms of tau promote toxicity. Both P301L and R406W transgenic mice have all been created and extensively characterized. P301L tau- expressing mice are the most well characterized FTLD-tau mouse model (46-48). These animals exhibit robust tau hyperphosphorylation, NFT formation, astrocytosis, apoptotic neuronal loss, and spatial memory deficits (46-48). Our work in cell culture shows that model Hirano bodies promote P301L tau-induced cell death in a cell culture system. Therefore, it is possible that model Hirano bodies will also increase P301L-induced aggregation and neuronal loss in a mouse. Furthermore, both P301L tau and CT-GFP transgenic mice independently develop astrogliosis and spatial memory impairments. Therefore, it is likely that CT-GFP expression would also exacerbate reactive astrocytes and increase memory deficits in P301L tau mice.

R406W-tau expressing mice exhibit late-age tau hyperphosphorylation, tau aggregation, and were found to have associative memory deficits, which correlate with tau pathology (42). In our cell culture system, model Hirano bodies had no impact on cell death initiated by R406W tau. When AICD signaling was bypassed through expression of a constitutively active GSK3β (S9A) mutant, model Hirano bodies lost their protective ability. This implies that model Hirano bodies protect against AICD or factors upstream of GSK3β. Based on these results, model Hirano bodies would likely not impact pathological phenotypes associated with R406W animals. While we evaluated spatial working memory in CT-GFP transgenic mice, associative memory was never measured. Therefore, it is uncertain how model Hirano bodies would impact this type

of memory in R406W tau transgenic mice. Nevertheless, repeating our P301L and R406W tau experiments *in vivo* is of value. The experiments we have performed have given us valuable insight, and we are now beginning to appreciate the complex nature of Hirano bodies under various conditions. Therefore, the future direction experiments proposed in this chapter would give an important understanding of the physiological role of Hirano bodies in various disease states.

REFERENCES:

1. Maselli, A. G., Davis, R., Furukawa, R., and Fechheimer, M. (2002) Formation of Hirano bodies in Dictyostelium and mammalian cells induced by expression of a modified form of an actin cross-linking protein. *J. Cell Sci.* **115**, 1939-1952
2. Davis, R. C., Furukawa, R., and Fechheimer, M. (2008) A cell culture model for investigation of Hirano bodies. *Acta Neuropathol* **115**, 205-217
3. Ha, S., Furukawa, R., and Fechheimer, M. (2011) Association of AICD and Fe65 with Hirano bodies reduces transcriptional activation and initiation of apoptosis. *Neurobiol Aging* **32**, 2287-2298
4. Schochet, S. S., Jr., Lampert, P. W., and Lindenberg, R. (1968) Fine structure of the Pick and Hirano bodies in a case of Pick's disease. *Acta Neuropathol (Berl)* **11**, 330-337
5. Hirano, A., Dembitzer, H. M., Kurland, L. T., and Zimmerman, H. M. (1968) The fine structure of some intraganglionic alterations. Neurofibrillary tangles, granulovacuolar bodies and "rod-like" structures as seen in Guam amyotrophic lateral sclerosis and parkinsonism-dementia complex. *J Neuropathol Exp Neurol* **27**, 167-182
6. Schochet, S. S., Jr., and McCormick, W. F. (1972) Ultrastructure of Hirano bodies. *Acta Neuropathol* **21**, 50-60
7. Maselli, A. G., Furukawa, R., Thomson, S. A. M., Davis, R. C., and Fechheimer, M. (2003) Formation of Hirano bodies induced by expression of an actin cross-linking protein with a gain of function mutation. *Eucaryot. Cell* **2**, 778-787

8. Kinoshita, A., Whelan, C. M., Berezovska, O., and Hyman, B. T. (2002) The gamma secretase-generated carboxyl-terminal domain of the amyloid precursor protein induces apoptosis via Tip60 in H4 cells. *J. Biol. Chem.* **277**, 28530-28536

9. Park, S. A., Shaked, G. M., Bredesen, D. E., and Koo, E. H. (2009) Mechanism of cytotoxicity mediated by the C31 fragment of the amyloid precursor protein. *Biochemical and biophysical research communications* **388**, 450-455

10. Goldman, J. E. (1983) The association of actin with Hirano bodies. *J Neuropathol Exp Neurol* **42**, 146-152

11. Galloway, P. G., Perry, G., and Gambetti, P. (1987) Hirano body filaments contain actin and actin-associated proteins. *J Neuropathol Exp Neurol* **46**, 185-199

12. Maciver, S. K., and Harrington, C. R. (1995) Two actin binding proteins, actin depolymerizing factor and cofilin, are associated with Hirano bodies. *Neuroreport* **6**, 1985-1988

13. Fernandez, L. A. (1968) Hirano J, Masson GM: Effects of dietary sodium on hypertensive disease caused by renin. *Lab Invest* **18**, 8-14

14. Galloway, P. G., Perry, G., Kosik, K. S., and Gambetti, P. (1987) Hirano bodies contain tau protein. *Brain Res* **403**, 337-340

15. Munoz, D. G., Wang, D., and Greenberg, B. D. (1993) Hirano bodies accumulate C-terminal sequences of beta-amyloid precursor protein (beta-APP) epitopes. *J Neuropathol Exp Neurol* **52**, 14-21

16. Renkawek, K., Bosman, G. J., and de Jong, W. W. (1994) Expression of small heat-shock protein hsp 27 in reactive gliosis in Alzheimer disease and other types of dementia. *Acta Neuropathol* **87**, 511-519

17. Jordan-Sciutto, K., Dragich, J., Walcott, D., and Bowser, R. (1998) The presence of FAC1 protein in Hirano bodies. *Neuropathol Appl Neurobiol* **24**, 359-366

18. Munch, G., Cunningham, A. M., Riederer, P., and Braak, E. (1998) Advanced glycation endproducts are associated with Hirano bodies in Alzheimer's disease. *Brain Res* **796**, 307-310

19. Lee, S. C., Zhao, M. L., Hirano, A., and Dickson, D. W. (1999) Inducible nitric oxide synthase immunoreactivity in the Alzheimer disease hippocampus: association with Hirano bodies, neurofibrillary tangles, and senile plaques. *J Neuropathol Exp Neurol* **58**, 1163-1169

20. Rossiter, J. P., Anderson, L. L., Yang, F., and Cole, G. M. (2000) Caspase-cleaved actin (fractin) immunolabelling of Hirano bodies. *Neuropathol. Appl. Neurobiol.* **26**, 342-346

21. Zhu, X., Raina, A. K., Rottkamp, C. A., Aliev, G., Perry, G., Boux, H., and Smith, M. A. (2001) Activation and redistribution of c-jun N-terminal kinase/stress activated protein kinase in degenerating neurons in Alzheimer's disease. *J Neurochem* **76**, 435-441

22. Lee, H. G., Ueda, M., Miyamoto, Y., Yoneda, Y., Perry, G., Smith, M. A., and Zhu, X. (2006) Aberrant localization of importin alpha1 in hippocampal neurons in Alzheimer disease. *Brain Res* **1124**, 1-4

23. Rohn, T. T. (2008) Caspase-cleaved TAR DNA-binding protein-43 is a major pathological finding in Alzheimer's disease. *Brain Res* **1228**, 189-198

24. Borg, J. P., Ooi, J., Levy, E., and Margolis, B. (1996) The phosphotyrosine interaction domains of X11 and FE65 bind to distinct sites on the YENPTY motif of amyloid precursor protein. *Molecular and cellular biology* **16**, 6229-6241

25. Ermekova, K. S., Zambrano, N., Linn, H., Minopoli, G., Gertler, F., Russo, T., and Sudol, M. (1997) The WW domain of neural protein FE65 interacts with proline-rich motifs in mena, the mammalian homolog of Drosophila enabled. *J. Biol. Chem.* **272**, 32869-32877

26. Ryan, K. A., and Pimplikar, S. W. (2005) Activation of GSK-3 and phosphorylation of CRMP2 in transgenic mice expressing APP intracellular domain. *The Journal of cell biology* **171**, 327-335

27. Ghosal, K., Vogt, D. L., Liang, M., Shen, Y., Lamb, B. T., and Pimplikar, S. W. (2009) Alzheimer's disease-like pathological features in transgenic mice expressing the APP intracellular domain. *Proc Natl Acad Sci U S A* **106**, 18367-18372

28. Ghosal, K., Stathopoulos, A., and Pimplikar, S. W. (2010) APP intracellular domain impairs adult neurogenesis in transgenic mice by inducing neuroinflammation. *PLOS ONE* **5**, e11866

29. Ghosal, K., and Pimplikar, S. W. (2011) Aging and excitotoxic stress exacerbate neural circuit reorganization in amyloid precursor protein intracellular domain transgenic mice. *Neurobiol Aging* **32**, 2320 2321-2329

30. Cao, X., and Südhof, T. C. (2001) A transcriptionally active complex of APP with Fe65 and histone acetyltransferase Tip60. *Science* **293**, 115-120

31. Cao, X., and Südhof, T. C. (2004) Dissection of amyloid-beta precursor protein-dependent transcriptional transactivation. *J. Biol. Chem.* **279**, 24601-14611

32. Aydin, D., Filippov, M. A., Tschape, J. A., Gretz, N., Prinz, M., Eils, R., Brors, B., and Muller, U. C. (2011) Comparative transcriptome profiling of amyloid precursor protein family members in the adult cortex. *BMC genomics* **12**, 160

33. Müller, T., Concannon, C. G., Ward, M. W., Walsh, C. M., Tirniceriu, A. L., Tribl, F., Kogel, D., Prehn, J. H. M., and Egensperger, R. (2007) Modulation of gene expression and cytoskeletal dynamics of the amyloid precursor protein intracellular domain (AICD). *Mol. Biol. Cell* **18**, 201-210

34. von Rotz, R. C., Kohli, B. M., Bosset, J., Meier, M., Suzuki, T., Nitsch, R. M., and Konietzko, U. (2004) The APP intracellular domain forms nuclear multiprotein complexes and regulates the transcription of its own precursor. *J. Cell Sci.* **117**, 4435-4448

35. Kim, H.-S., Kim, E.-M., Lee, J.-P., Park, C. H., Kim, S., Seo, J.-H., Chang, K.-A., Yu, E., Jeong, S.-J., Chong, Y. H., and Suh, A. Y.-H. (2003) C-terminal fragments of amyloid precursor protein exert neurotoxicity by inducing glycogen synthase kinase-3b expression. *FASEB J.* **17**, 1951-1954

36. Ghosal, K., Vogt, D. L., Liang, M., Shen, Y., Lamb, B. T., and Pimplikar, S. W. (2009) Alzheimer's disease-like pathological features in transgenic mice expressing the APP intracellular domain. *Proc. Natl. Acad .Sci. U.S.A.* **106**, 18367-18372

37. von Bergen, M., Barghorn, S., Li, L., Marx, A., Biernat, J., Mandelkow, E. M., and Mandelkow, E. (2001) Mutations of tau protein in frontotemporal dementia promote aggregation of paired helical filaments by enhancing local beta-structure. *J Biol Chem* **276**, 48165-48174

38. Barghorn, S., Zheng-Fischhofer, Q., Ackmann, M., Biernat, J., von Bergen, M., Mandelkow, E. M., and Mandelkow, E. (2000) Structure, microtubule interactions, and paired helical filament aggregation by tau mutants of frontotemporal dementias. *Biochemistry* **39**, 11714-11721

39. Goedert, M. (1999) Filamentous nerve cell inclusions in neurodegenerative diseases: tauopathies and alpha-synucleinopathies. *Phil. Trans. Roy. Soc. Lond. B-Biol. Sci.* **354**, 1101-1118

40. von Bergen, M., Friedhoff, P., Biernat, J., Heberle, J., Mandelkow, E. M., and Mandelkow, E. (2000) Assembly of tau protein into Alzheimer paired helical filaments depends on a local sequence motif ((306)VQIVYK(311)) forming beta structure. *Proc Natl Acad Sci U S A* **97**, 5129-5134

41. Hundelt, M., Fath, T., Selle, K., Oesterwind, K., Jordan, J., Schultz, C., Gotz, J., von Engelhardt, J., Monyer, H., Lewejohann, L., Sachser, N., Bakota, L., and Brandt, R. (2009) Altered phosphorylation but no neurodegeneration in a mouse model of tau hyperphosphorylation. *Neurobiol Aging*

42. Tatebayashi, Y., Miyasaka, T., Chui, D. H., Akagi, T., Mishima, K., Iwasaki, K., Fujiwara, M., Tanemura, K., Murayama, M., Ishiguro, K., Planel, E., Sato, S., Hashikawa, T., and Takashima, A. (2002) Tau filament formation and associative memory deficit in aged mice expressing mutant (R406W) human tau. *Proc Natl Acad Sci U S A* **99**, 13896-13901

43. Friedhoff, P., Schneider, A., Mandelkow, E. M., and Mandelkow, E. (1998) Rapid assembly of Alzheimer-like paired helical filaments from microtubule-associated protein tau monitored by fluorescence in solution. *Biochemistry* **37**, 10223-10230

44. Roberson, E. D., Scearce-Levie, K., Palop, J. J., Yan, F., Cheng, I. H., Wu, T., Gerstein, H., Yu, G.-Q., and Mucke, L. (2007) Reducing endogenous tau ameliorates amyloid beta-induced deficits in an Alzheimer's disease mouse model. *Science* **316**, 750-754

45. Ittner, L. M., Ke, Y. D., Delerue, F., Bi, M., Gladbach, A., van Eersel, J., Wolfing, H., Chieng, B. C., Christie, M. J., Napier, I. A., Eckert, A., Staufenbiel, M., Hardeman, E., and Gotz, J. (2010) Dendritic function of tau mediates amyloid-beta toxicity in Alzheimer's disease mouse models. *Cell* **142**, 387-397

46. Lewis, J., McGowan, E., Rockwood, J., Melrose, H., Nacharaju, P., Van Slegtenhorst, M., Gwinn-Hardy, K., Paul Murphy, M., Baker, M., Yu, X., Duff, K., Hardy, J., Corral, A., Lin, W. L., Yen, S. H., Dickson, D. W., Davies, P., and Hutton, M. (2000) Neurofibrillary tangles, amyotrophy and progressive motor disturbance in mice expressing mutant (P301L) tau protein. *Nature genetics* **25**, 402-405

47. Gotz, J., Tolnay, M., Barmettler, R., Chen, F., Probst, A., and Nitsch, R. M. (2001) Oligodendroglial tau filament formation in transgenic mice expressing G272V tau. *The European journal of neuroscience* **13**, 2131-2140

48. Gotz, J., Chen, F., Barmettler, R., and Nitsch, R. M. (2001a) Formation of neurofibrillary tangles in P301L tau transgenic mice induced by Abeta 42 fibrils. *Science* **293**, 1491-1495

APPENDICES

DOCUMENENT A

LOSS OF NMDAR-DEPENDENT LTP COINCIDES WITH DEFICITS IN SPATIAL WORKING MEMORY IN 3XTG-AD MICE[1]

---

[1] Furgerson, M. Clark, J.K. Crystal, J.D. Fechheimer, M. Furukawa, R. and J.J. Wagner. Submitted to *Neurobiology of Aging*, 04/18/14

ABSTRACT:

Alzheimer's disease is a neurodegenerative condition believed to be initiated by production of amyloid beta peptide, which leads to synaptic dysfunction and progressive memory loss. In a mouse model of Alzheimer's disease (3xTg-AD), an 8-arm radial maze and field potential recordings from the CA1 region of ventral hippocampal slices were utilized to determine the contribution of both NMDA and non-NMDA receptor-dependent mechanisms of long-term potentiation in spatial working memory. Our study shows that 3xTg-AD mice have a reduction in NMDA receptor-dependent LTP and an increase in non-NMDA receptor-dependent LTP, leading to a total LTP that is similar between 3xTg-AD and control mice at 3 months of age. Both young (3 month) and older (8 month) 3xTg-AD mice exhibit reductions in paired-pulse facilitation and NMDA receptor-dependent LTP that coincides with an impairment in spatial working memory. This impairment correlates with increased amounts in amyloid beta 42, demonstrating that the onset of behavioral and neurophysiological alterations in 3xTg-AD mice occurs before the detectable presence of plaques and tangles.

INTRODUCTION:

Alzheimer's disease is a disease of aging characterized by progressive memory loss and dementia. It is differentiated from other forms of dementia based on two pathological hallmarks, amyloid plaques and neurofibrillary tangles (1). Amyloid plaques are derived from the aggregation of the amyloid beta (Aβ) peptide, which is generated through sequential cleavage of the amyloid precursor protein by beta and gamma-secretase (1-4). During disease progression, the microtubule associated protein tau is subject to extensive post-translational modification including hyper-phosphorylation and acetylation. These modifications are prerequisites to tau

aggregation and formation of neurofibrillary tangles (5-9). The exact mechanism linking these pathologies to memory impairment is unknown. However, a growing body of evidence suggests the inability of neurons to maintain calcium homeostasis as an underlying factor during the early events of Alzheimer's disease (10,11).

One aspect of calcium signaling related to cellular mechanisms of learning and memory involves the mechanisms underlying long-term potentiation (LTP) of synaptic strength. LTP represents the most current model for information storage within the brain, and therefore is suspected to play an important role in cognitive processes such as learning and memory (12,13). Large, transient increases in intracellular calcium and a subsequent series of calcium-mediated responses lead to the induction of LTP (14). At least two different mechanisms of LTP are known to coexist at hippocampal CA3-CA1 synapses, N-methyl-D-aspartate receptor-dependent LTP (NMDAR LTP; (13) and non-NMDA receptor-dependent LTP (non-NMDAR LTP) mediated via activation of L-type calcium channels ((15). Pharmacological evidence indicates that both forms of LTP can contribute to spatial memory, as both NMDAR antagonists (16) and calcium channel antagonists (17) impair spatial learning.

NMDA receptors play an important role in assessments of spatial working memory using the radial arm maze (18-20). More recent experiments in which the NMDAR subunits NR2B and NR2A are specifically blocked by bilateral infusion of antagonists directly into the CA1 region of hippocampus show a significant reduction in working memory using a T-maze delayed alternation task (21). $NR2A^{-/-}$ mice show impairments in working memory but not reference memory in the 6-arm radial maze (22), demonstrating the contribution of specific NMDARs to memory functions. Finally, studies in humans have also shown that blockage of NMDARs with ketamine leads to decreased accuracy on spatial working memory tests (23).

In this study, neurophysiology, spatial working memory, and Aβ levels were characterized and correlated on an individual basis in a mouse model of Alzheimer's disease (3xTg-AD) (24) at 3 months and 8 months of age. The results of this study reveal that young 3xTg mice show impairments in spatial working memory but not a difference in total LTP compared to control mice. The contribution of non-NMDAR LTP to total LTP was significantly higher in 3xTg mice than control mice. As the 3xTg-AD mice aged, non-NMDAR LTP declined, and impairments in both learning and memory become more progressive. These changes correlated with the amount of Aβ on an individual mouse comparison.

MATERIAL AND METHODS:

Animals and euthanasia

All animals used in this study were male mice and consisted of either non-transgenic control mice (B6129SF2/J) (NonTg), were obtained from Jackson Laboratories (101045 JAX, Bar Harbour, ME), or Alzheimer's model mice homozygous for three mutant alleles APPSwe, Psen I, and tauP301L (B6/129-*Psen1*^{tm1Mpm} Tg(APPSwe, tauP301L)1Lfa/Mmjax) (3xTg-AD) obtained from MMRRC ID 034830-JAX. Mice were housed individually with the same color enrichment housing inserts in an AAALAC accredited facility on a 12-hour light/dark timed schedule and had ad libitum access to food (except during behavioral studies, see below) and water during this study. Mice began testing in the radial arm maze at 2.5 and 7.5 months old. After completion of the radial arm maze testing, approximately 10 days elapsed before electrophysiological studies commenced to reduce any potential temporary enrichment from the maze environment. Euthanasia of mice occurred under deep anesthesia with halothane followed

by decapitation. The University of Georgia Institutional Animal Care and Usage Committee approved all animal protocols and experiments.

Chemicals and reagents

Except where noted, specialty chemicals and antibodies were obtained from Sigma Aldrich (St. Louis, MO).

Radial arm maze apparatus and mouse preparation

Learning and memory assessments were conducted using an 8-arm radial mouse maze (Med Associates, St. Albans, VT) as similarly described previously for rats (25). This maze consists of eight arms extending from a central chamber with eight guillotine doors positioned at the interface of the central chamber and arms. A 20 mg food dispenser and trough are at the end of each arm. Each arm has two sets of photosensors to track movement of the mice in and out of the arms. At the end of each arm is a food trough containing a photosensor that detects mouse head entries and dispenses 20 mm food upon interruption of the photobeam. The sides and top of each arm are composed of clear plastic to allow mice to use visual cues within the room to spatially navigate the maze. A computer in an adjacent room controls the maze events and data collection. Photosensor, food, and door data were collected using MED-PC software 4.0 (Med Associates, St. Albans, VT) with a resolution of 10 ms. A video camera was mounted above the maze to visualize the mice during the procedure.

Behavioral assessment in the radial arm maze was measured at either 3 or 8 months of age. Thirteen days prior to the start of behavioral testing, mice were individually housed, and a three-day average of individual mouse body weight was determined. Mice were diet-restricted to reduce and maintain a body weight of ~87.0% of their ad libitum food body weight for the duration of the behavioral assessment. For four days prior to testing, mice were pretrained to

associate the maze with the experience of obtaining a sucrose-flavored food reward (Bio-Serve F0071, Frenchtown, NJ) by allowing each animal free access to four of the eight arms until one food reward from each arm was retrieved.

The maze was cleaned between subjects with 1/1250-diluted Coverage Plus NPD disinfectant (Steris Life Sciences, Mentor, OH) to prevent a previous mouse's scent from interfering with a subsequent mouse's performance. To further prevent a mouse from using scent cues, the entire maze was scent-saturated using cotton bedding from the mouse's home cage after cleaning the maze.

Radial arm maze training phase (8 arms baited, 8 arms open)

This procedure was utilized to assess spatial short-term memory. Each mouse was placed in the central chamber of the maze for a two minute acclimation period. After acclimation, all eight doors opened with the objective of collecting a food reward available at the end of each baited arm (8 arms open, 8 arms baited) using visual cues within the room to navigate the maze. Only one food reward is delivered per arm, and a revisit to a previously visited food trough is considered an error in spatial short-term working memory. After either collecting the last food reward or after 15 minutes of elapsed time, the session ends and the doors close. In the training phase, the dependent measure is the number of errors in the first eight choices. The experiments are performed once a day, at the same time of day per mouse for 10 consecutive days. Mice achieving the criterion of no more than 2 errors within the first 10 choices by the 10th day of training continued in the study. Results from either the first two or last two days are reported as the mean $\pm$ standard error of the mean (SEM). Following 10 consecutive days of spatial memory training, animals proceeded directly to the spatial memory test with a retention interval.

Radial arm maze test phase (delayed win-shift) to assess spatial working memory

On the following day after completion of the training phase, spatial working memory was tested using a delayed spatial win-shift procedure for 10 consecutive days. This is a two-phase procedure consisting of a study phase followed by a test phase. In the study phase, the mouse is placed in the central chamber of the maze for a two minute acclimation period. Afterwards, four of the eight doors are opened (randomly chosen for each mouse on each day). Each mouse must navigate the maze using visual cues within the room to obtain a food reward that is available upon triggering a photobeam located within the food trough at the end of the arm (4 arms open, 4 arms baited). Only one food reward is delivered per baited arm, and a revisit to a previously visited food trough is considered an error in spatial short-term memory. After collecting the last food reward or after 15 minutes of elapsed time, the doors close. The mouse is subjected to a short retention interval by being taken out of the maze and returned to his home cage for 3 minutes while the maze was cleaned. The mouse was returned to the maze to begin the test phase. After 1 minute of acclimation, all eight doors of the maze open. Only arms that were previously closed in the study phase are now baited in the test phase (8 arms open, 4 arms baited). The mouse must navigate the maze to collect a food reward at each newly baited arm. A revisit to a food trough previously visited in either the study or test phase is considered an error in spatial working memory. The session ends after collecting the last food reward, or after 15 minutes of elapsed time. In the test phase, the dependent variable is the number of errors in the first 4 choices. Results from either the first two or last two days are reported as the mean $\pm$ standard error of the mean (SEM).

Immunohistochemistry

Tissue from naive animals not used in behavioral or electrophysiological testing was fixed overnight with 4% paraformaldehyde at 4°C, embedded with paraffin, and cut into 6-10 μm

sections using a Leica RM2155 microtome. Mounted sections were dewaxed in xylene and rehydrated in an ethanol gradient prior to antigen retrieval in boiling 50 mM sodium citrate plus 0.01% Tween 20 for 25 minutes. Endogenous peroxidase activity was inhibited by incubating sections in 3% hydrogen peroxide for 10 minutes prior to washing with phosphate-buffered saline (PBS) and blocking with 10 mg/ml bovine serum albumin in PBS overnight. Primary antibodies BAM-10, pTau-199/202, pTau231 (Acris Antibodies, San Diego, CA), and pTau396 were used at a concentration of 1/250, 1/200, 1/450, and 1/300, respectively. Secondary biotinylated goat anti-mouse and goat anti-rabbit antibodies were used at 1/450 dilution. Slices were incubated with 1/1000 streptavidin-HRP polymer complex (Vector Laboratory, Burlingame, CA). Slices were washed 3 times for 5 minutes each between antibody and enzyme incubations with 0.02% Tween-20 in PBS. Diaminobenzidine-enhanced substrate system was used according to the manufacturer's instructions. After washing off excess diaminobenzidine substrate, slides were counterstained with Gill's No. 2 hematoxylin prior to mounting coverslips. Sections were viewed with a Leica DM6000 B microscope (Wetzlar, Germany) with Hamamatsu ORCA-ER digital camera (Hamamatsu, Bridgewater, NJ).

Amyloid-beta extraction

Aβ extraction was performed as previously described (26). Briefly, ventral hippocampal tissue from behaviorally tested animals taken at the time of sacrifice for electrophysiological testing was obtained and stored at -80C°. The tissue was transferred to a Potter-Elvehjem homogenizer containing 4 brain volumes of Tris-buffered saline (25 mM Tris-HCl pH 7.4, 140 mM NaCl, 3 mM KCl, 5 mM EDTA, and 2 mM 1,10-phenathroline) with 10 μL protease inhibitor cocktail (5 mM EGTA, 1 mM DTT, 10 mg/mL leupeptin, 1 μL/mL pepstatin, 0.1 M PMSF, 0.1 M benzamidine, and 0.5 M e-aminocaproic acid). After homogenization, 6.25 M

guanidine HCl in 50 mM Tris, pH 8.0 was added to samples after transfer to a 1.5 mL microcentrifuge tube. Samples were rocked on a platform for 2 hours at room temperature before centrifugation at 12,000 rpm for 30 minutes.

Enzyme linked immune-sorbent assay (ELISA)

ELISAs were performed as previously described (26-28). Briefly, 96-well Costar plates were coated with 4.0 mg/mL BAM-10 for capture of all Ab isoforms. $A\beta_{1-42}$ (Aβ42) levels were detected using a 1/250 dilution of rabbit Ab42 antibody. Wells were subsequently incubated with 100 mL of 1/500 biotinylated anti-rabbit antibody followed by incubation with (1/1000) avidin-horseradish peroxidase (Vector Laboratory, Burlingame, CA). Wells were washed 3 times for 1 minute each with Tris-buffered saline plus 0.05% Tween 20 after each incubation step. QuantaBlu substrate kit was used according to the manufacturers protocol (Pierce Biotechnology, Rockford, IL) and fluorescence of the HRP-substrate reaction was measured on a Biotek Synergy 2 plate reader (EX 340, EM 400) (Winooski, VT).

Extracellular field recording

Hippocampal slices were prepared from behaviorally tested 3 and 8 month old 3xTg-AD and NonTg mice as previously described 10-17 days after completion of the radial arm maze testing as previously described (29). Mice were deeply anesthetized with halothane prior to decapitation. The brain was removed and submerged in ice-cold, oxygenated (95% O_2/ 5% CO_2) dissection artificial cerebrospinal fluid (ACSF) containing 120 mM NaCl, 3 mM KCl, 4 mM $MgCl_2$, 1 mM NaH_2PO_4, 26 mM $NaHCO_3$, and 10 mM glucose. The brain was sectioned into 400 mm thick horizontal slices using a vibratome. The hippocampus was sub-dissected out and the CA3 portion removed. Slices were placed in a submersion recording chamber and perfused at approximately 1 mL/min with oxygenated (95% O_2 / 5% CO_2) standard ACSF containing: 120

mM NaCl, 3 mM KCl, 1.5 mM $MgCl_2$, 1 mM NaH_2PO_4, 2.5 mM $CaCl_2$, 26 mM $NaHCO_3$, and 10 mM glucose at room temperature. Slices were allowed to recover for 45 minutes at room temperature and an additional 45 minutes at 30°C. All recordings were obtained under continuous oxygenated perfusion of ACSF at 30°C. A bipolar stimulating electrode (Kopf Instruments, Tujunga, CA) was placed within the stratum radiatum of CA3, and an extracellular recording microelectrode (1.0 MΩ tungsten recording microelectrode, World Precision Instruments, Sarasota, FL) was positioned in the same layer of CA1. Field excitatory post-synaptic potentials (fEPSPs) were recorded at CA3-CA1 synapses using a stimulus pulse consisting of a single square wave of 270 μs duration. Data were digitized at 10 kHz, low-pass filtered at 1 kHz, and analyzed with pCLAMP 10.2 software (Axon Instruments, Sunnyvale, CA). The initial slope of the population fEPSP was measured by fitting a straight line to a 1 ms window immediately following the fiber volley. Stimulus-response curves were obtained at the beginning of each experiment with stimulus pulses delivered at 40, 50, 60, 75, 90, 110, 130, and 150 μA once every 60 s (0.0167 Hz). To begin baseline recording, the stimulation intensity was adjusted to obtain a fEPSP of approximately 35-40% of the linear range between the minimum and maximum response. Paired-pulse responses were performed at intervals of 50, 100, 200, and 500 ms. The slope of paired-pulse responses was measured from an average of five pairs of pulses for each interval. Synaptic responses for long-term potentiation (LTP) experiments were normalized by dividing all fEPSP slope values by the average of the five responses recorded during the 5 minutes immediately prior to high frequency stimulation (HFS). The HFS protocol used to induce LTP in all experiments consisted of four episodes of 200 Hz/0.5 s stimulus trains (100 pulses) administered at 5 s inter-train intervals. For separation of the NMDAR from the non-NMDAR component of LTP, the NMDAR antagonist DL-AP5 (50 μM) (Tocris Bioscience,

Minneapolis, MN) was bath applied for 30 minutes prior to HFS, continued for 5 minutes post-HFS, and subsequently removed for the remainder of recording. LTP values for the 1 hour time point were determined by averaging 5 minutes of normalized slope values at 55-60 minutes post-HFS. Reported n-values (x(y)) indicate the number of slices (x) and the number of mice (y) assessed.

Statistics

Tests of significance for planned comparisons were performed using either the paired or unpaired t-test, as appropriate.

RESULTS:

Spatial working memory was evaluated in individual NonTg or 3xTg-AD mice at 3 or 8 months. Electrophysiological recordings of synaptic transmission and synaptic plasticity in the ventral hippocampal CA1 region of these same mice were obtained as well as quantification of total Aβ42 levels. Together, these studies permit direct correlations between memory, electrophysiology, and pathology on an individual mouse basis.

Spatial memory testing

Spatial memory was tested in an 8-arm radial maze utilizing two different procedures. The first, a training phase (8 arms open, 8 arms baited), consisted of collecting a food reward at the end of each of the 8 arms without revisiting locations where the reward was collected (Figure 1A,B). Only 1 food reward was available per arm. NonTg (3 month, n=11; 8 month, n=11) and 3xTg-AD mice (3 month n=12; 8 month, n=11) performed similarly with both genotypes showing significant improvement in performance from day 1 to day 10.

At day 11, the same mice from the training phase were evaluated using a delayed spatial win-shift procedure as shown in the schematic diagram (Figure 2A). In the study phase (4 arms open, 4 arms baited), the mice have free access to only 4 arms with 1 food reward per accessible arm. Upon completion of the study phase, a 4 minute short retention interval occurs before the subsequent test phase (8 arms open, 4 arms baited) where the mice have free access to all 8 arms. Only the 4 arms not previously visited (inaccessible during study phase) were baited and have food rewards. During the study phase, mice at both 3 and 8 months of age showed no difference between genotypes or improvement across sessions (data not shown).

In contrast to training phase results, test phase results showed significant differences between NonTg and 3xTg-AD mice at both 3 and 8 months (Figure 2B,C). NonTg mice showed a significant increase in performance across sessions at both 3 and 8 months ($p < 0.01$, paired t-test, days 11-12 compared to days 19-20). In contrast, 3xTg-AD mice did not (Figure 2B,C). In addition, the inability of 3xTg-AD mice to improve with increasing sessions was not age-dependent. Although at three months, NonTg mice make fewer spatial working memory errors at days 19-20 than did the 3xTg-AD, this trend is not statistically significant. However, at eight months, the NonTg mice make significantly fewer spatial working memory errors at days 19-20 than do 3xTg-AD mice ($p < 0.05$, unpaired t-test, Figure 2C). These results demonstrate that the onset of impairment of spatial working memory performance can be observed as early as 3 months of age in 3xTg-AD mice but only after increasing memory load requirements such as that seen using the delayed spatial win-shift procedure.

Characterization of 3xTg-AD pathology and progression

To verify the pathological state of our 3xTg-AD mice, immunohistochemical analysis at 3 and 8 months was performed (Supplemental Figure 1). Using a non-isoform specific Aβ

antibody (BAM-10), intraneuronal Aβ localization was detected in CA1 pyramidal neurons at both 3 and 8 months in 3xTg-AD mice, but not in NonTg mice. Bam-10 localization also revealed small disperse plaque deposits in the hippocampus of 8-month-old 3xTg-AD mice, but not in NonTg or 3-month-old 3xTg-AD mice. To determine relative levels of tau hyper-phosphorylation, three antibodies that recognize site-specific phosphorylation of tau at Ser199/202, Thr231, and Ser396 were utilized. No detectable phospho-tau within CA1 pyramidal neurons of NonTg or 3-month 3xTg-AD mice was found. However, in 8-month 3xTg-AD mice, phospho-tau was readily detectable in CA1 pyramidal neurons of the hippocampus with all antibodies.

To test whether Aβ correlated with behavioral measurements of spatial working memory, Aβ from ventral hippocampal brain tissue was extracted from the same mice that were tested in the radial arm maze. Since soluble Aβ (40 or 42), as well as total Aβ40, has been shown to remain relatively stable with age in 3xTg-AD mice (24,30), ELISA assays were used to measure total Aβ42 since it is the most abundant species in 3xTg-AD mice, and because of its more aggressive nature during disease progression (1,24,31). Consistent with the immunohistochemistry, 3xTg-AD mice show an age-dependent increase in total Aβ42 levels while Aβ42 in NonTg mice is virtually undetectable (Figure 3A). At both 3 and 8 months, 3xTg-AD mice show a significant correlation between total Aβ42 and spatial working memory as measured by the number of errors that occurred in the test phase before visiting the last baited arm (Figure 3B) (3 months: $r^2 = 0.354$; Pearson correlation coefficient 0.6, $p < 0.05$; 8 months: $r^2 = 0.404$, Pearson correlation coefficient 0.8, $p < 0.01$). The results suggest that within a given age cohort, increased levels of total Aβ42 correspond with decreased cognitive performance.

Electrophysiology

To determine if neurophysiological differences exist between 3xTg-AD and NonTg mice, fEPSPs at CA3-CA1 synapses from the stratum radiatum in hippocampal slice preparations were recorded as a measure of synaptic function. At 3 months of age, baseline fEPSPs for both groups were similar. The 3xTg-AD mice (n=54(12)) exhibited significantly lower fEPSP slopes than NonTg mice (n=47(11)) at the highest stimulus intensities (Figure 4A, 130 and 150 μA, $p < 0.05$). At 8 months of age, fEPSP slopes at intensities greater than 50 μA, were significantly reduced in 3xTg-AD mice (n=39(11)) compared to NonTg (n=47(11)) (Figure 4B, $p < 0.01$).

A paired-pulse stimulus protocol was utilized to evaluate short-term synaptic plasticity. At 3 months, both 3xTg-AD and NonTg mice showed paired pulse facilitation at all intervals except 500 ms (Figure 5A). The 3xTg-AD mice showed significantly less facilitation than NonTg mice ($p < 0.01$), ((n=58(11)) NonTg; n=54(12)) in 3xTg-AD). Paired-pulse facilitation on 8-month-old mice showed similar results (Figure 5B). The 3xTg-AD mice showed significantly less facilitation than NonTg mice at all stimulus intervals including 500 ms ($p < 0.01$, $p< 0.05$ at 500 ms, (n=42(11)) NonTg; n= n=36(11)) in 3xTg-AD).

Long term synaptic plasticity was induced using a multiple train stimulus induction protocol previously shown to elicit a compound potentiation consisting of both NMDAR and non-NMDAR components of LTP (15). At 3 months, there was no significant difference in total LTP between 3xTg-AD (47 ± 3.8%; n=23(12)) and NonTg mice (45 ± 2.5%; n=25(10)) (Figure 6A-C). The non-NMDAR component of LTP was measured using the selective NMDAR antagonist, DL-AP5. At 1 hour post-tetanus in the presence of 50 μM DL-AP5, the fEPSP slope value was potentiated 28 ± 2.7% in NonTg mice (n=25(10)), in contrast to 42 ± 3.9% in 3xTg-AD mice (n=25(12)) (Figure 6A-C). This non-NMDAR component of LTP was significantly

greater in 3xTg-AD mice than in the NonTg mice ($p < 0.01$), constituting 89% of the total LTP observed in the 3xTg-AD mice and 62% in the NonTg mice.

At 8 months, the total LTP was significantly reduced ($p < 0.05$) in 3xTg-AD mice (32 ± 3.8%, n=15(11)) compared to NonTg mice (46 ± 4.2%, n=19(9)) (Figure 6D-F). The non-NMDAR component of LTP did not differ significantly between the NonTg (24 ± 2.4%, n=23(11)) and the 3xTg-AD mice (27 ± 4.6%, n=18(11)) (Figure 6D-F). This result is in contrast to the significant difference observed between these groups at 3 months of age (Figure 6C). Thus, the significant decrease in total LTP at 8 months of age in the 3xTg-AD mice is due to the decrease in the non-NMDAR component of LTP.

Within each genotype, the total LTP remained constant for the NonTg mice at 3 and 8 months of age (cf. Figure 6C and F). In contrast, the total LTP of the 3xTg-AD mice decreased significantly during this time period. These results agree with a previous report describing the delayed onset of impairment in total LTP magnitude in the 3xTg-AD mice (24). The relative contribution of the non-NMDAR LTP to the total LTP is the same for both genotypes at 8 months as compared with 3 months. These results demonstrate that 3xTg-AD mice exhibit a significantly reduced NMDAR-dependent component of LTP at both 3 and 8 months, and this deficit occurs concomitantly with significant impairments in spatial working memory.

DISCUSSION:

Using the radial arm maze, both 3-and 8-month-old 3xTg-AD mice failed to demonstrate improvements in working memory performance in a delayed spatial win-shift test phase with increasing session days as compared with NonTg (Figure 2). This is in contrast to the results obtained from the training phase assessment of short-term memory (8 arms open, 8 arms baited) where improvement across session days occurred in 3xTg-AD mice (Figure 1). The total

magnitude of LTP in the CA1 region of the hippocampus was equivalent for the NonTg and 3xTg-AD mice at 3 months; however, the contribution of non-NMDAR LTP was significantly greater in 3xTg-AD than NonTg (Figure 6). Together, these results suggest that the impairment in spatial working memory in the test phase of the delayed win-shift protocol was concurrent with the loss of the NMDAR-dependent component of LTP in both 3-and 8-month 3xTg-AD mice. In addition, impairments in spatial working memory of individual 3xTg-AD mice were correlated with total Aβ42 levels in both of these age groups (Figure 3).

The training phase results (8 arms open, 8 arms baited) demonstrate that both 3xTg-AD and NonTg control mice have intact spatial learning and navigation (i.e., they show equivalent levels of learning the reference memory rules used in the radial maze task, equivalent perception of spatial cues, equivalent levels of motivation and motor control). In the training phase, the task is continuous and thus the working memory load is low, making the procedure primarily dependent upon immediately accessible information from short-term memory (32,33). In order to specifically examine working memory, the mice were tested in a 2-phase delayed spatial win-shift assay, which included a brief retention interval delay. The incorporation of a time delay forces retention of trial-unique spatial information (i.e., the mice must remember which arms were visited in phase 1 in order to successfully complete phase 2), which increases working memory load. This allowed discrimination in performance between NonTg and 3xTg-AD mice as the NonTg mice showed improvement but the 3xTg-AD mice did not. The test phase results suggest that 3xTg-AD mice have impaired spatial working memory (i.e. memory for daily item-specific locations). This is likely profound working memory impairment since the training phase results indicated intact acquisition of reference memory rules, making impairment in learning capability unlikely. At 3 months, our test phase results are in contrast to Morris water maze

studies with 3xTg-AD mice in which no impairments are shown at early time points (30). This apparent discrepancy is likely due to the Morris water maze performance being evaluated primarily as a test of spatial reference memory, rather than spatial working memory (34,35). The retention interval delay in our radial maze test phase served to increase memory load, which revealed an impairment of spatial working memory in the 3 month 3xTg-AD mice.

Assessments of spatial learning and memory depend upon intact hippocampal function (32,36-38). More recently, a primary role for the ventral sector of the hippocampus in spatial working memory has been reported (39), consistent with the direct anatomical connection between the ventral hippocampus and the medial prefrontal cortex (40). It is clear that the dorsal and ventral sectors of the hippocampus are distinct entities, both anatomically and functionally (41). Therefore, in the current studies we have obtained electrophysiological recordings in hippocampal slices taken from the ventral third of the hippocampus to determine if synaptic function is altered in the 3xTg-AD mice when behavioral effects were evident in a spatial working memory task dependent upon intact function in this brain region. With respect to Alzheimer's disease, evidence indicating that early loss of hippocampal tissue is more prominent in the anterior (ventral) sector (42,43) supports our findings of early behavioral impairment in spatial working memory in the 3xTg-AD mice.

Previous investigations of short-term synaptic plasticity have shown that measurements of paired pulse facilitation in the CA1 region of both 1 and 6 month old 3xTg-AD mice are not different from NonTg mice (24). In contrast, our results demonstrate that the paired-pulse facilitation ratio is significantly decreased in 3xTg-AD mice at both 3 and 8 months (Figure 5). Other previous work has shown dysregulation of calcium homeostasis in 3xTg-AD mice resulting in higher resting calcium levels as early as 6 weeks of age (44). This increase in resting

presynaptic calcium levels would be expected to result in a greater initial release of neurotransmitter and a subsequent decrease in paired-pulse facilitation ratio (45). Thus, our observation here of a reduction in paired-pulse ratio in ventral hippocampal slices from 3xTg-AD mice may be an early neurophysiological indicator of a functional synaptic abnormality that is consistent with the dysregulation of calcium homeostasis and excitatory neurotransmission (46).

In addition to evaluating short-term synaptic plasticity, we also investigated a form of long-term synaptic plasticity, long-term potentiation. At least two forms of LTP are known to occur at CA3-CA1 synapses in the hippocampus, NMDAR-dependent (13) and non-NMDAR-dependent (15). As both of these forms of LTP have been shown to be involved in spatial learning and memory performance (47,48), we investigated the potential involvement of these two forms of LTP in behaviorally tested 3xTg-AD mice. Our results show that NMDAR LTP is significantly reduced in 3xTg-AD mice at both 3 and 8 months, coinciding with the failure to show improvement in the test phase assessment of spatial working memory. This is in contrast to the training phase results, which show no impairment in a spatial short-term memory task. Together these results suggest a specific role for NMDAR LTP in spatial working memory, as has been previously demonstrated (49). Interestingly, at 3 months the relative contribution of each component of LTP is different between the 3xTg-AD and NonTg mice. Non-NMDAR LTP is increased in 3xTg-AD mice and as a result the combination of NMDAR LTP with non-NMDAR LTP yields a total LTP that is not significantly different between groups. This could explain previous findings in which LTP assessed at earlier ages was not found to be altered in the 3xTg-AD mice (24). Our results demonstrate a specific relationship between loss of NMDAR

LTP in the ventral hippocampus and impaired performance in the test phase of our spatial working memory task.

By 8 months, our 3xTg-AD mice show a significant reduction in total LTP. Elevated levels of soluble Aβ42 disrupts synaptic function and is responsible for decreases in LTP (50), enhanced activation of long-term depression (51), and synaptic loss (52). Aβ42 levels in the brains of 3xTg-AD animals are significantly elevated by 4 months (30), and in our current study a significant increase of total Aβ42 in the ventral hippocampus of 3xTg-AD mice is observed by 3 months. This increase in Aβ42 levels in our mice coincides with the behavioral and electrophysiological alterations observed at this age as discussed previously. At 8 months, total Aβ42 levels continue to increase, but with similar influence on maze performance as compared to 3 months. Given that soluble Aβ42 levels remain constant over a period of 2-6 months (30), the continued increase in total Aβ42 measured at 8 months is likely due to its accumulation within amyloid plaques (Figure S1). Interestingly, a comparison of Aβ42 levels with the total number of errors accrued in the test phase from individual mice show there is a relationship between total Aβ42 levels and spatial working memory performance (Figure 3). This observation adds further support to the suggestion that soluble Aβ may be important for early synaptic deficits associated with the disease state (52). For the 3xTg-AD model, our findings of behavioral impairment in spatial working memory at the 3 month time point is the earliest noted to date and is at least 3 months before the observation of plaque formation in these animals (30). A correlation between individual Aβ42 burden and behavioral performance in the Morris water maze has been identified at a time when amyloid plaque is present (53). Notably, here we have demonstrated that a behavioral impairment in spatial working memory can be observed prior to evidence of amyloid plaque accumulation in the ventral hippocampus.

In the current series of studies, we have characterized early behavioral and electrophysiological alterations in 3xTg-AD model mice. The earliest reported observation of plaque formation in these animals occurs at 6 months, and the large majority of assessments of cognitive function in these younger mice describe them as being presymptomatic with respect to their behavioral performance in spatial memory tasks. Our findings of altered synaptic function that coincide with significant impairments in radial arm maze performance provide an example linking the loss of particular components of synaptic plasticity, such as decreased paired-pulse facilitation and NMDAR LTP in the ventral hippocampus, with a specific form of spatial working memory. These observations demonstrate that 3-month 3xTg-AD mice show functional and behavioral signs that are present at an age previously referred to by many investigators as presymptomatic. The significant correlation between total Aβ42 levels and spatial working memory performance in the 3-month age group indicates that individuals producing more Aβ42 suffer greater memory impairment prior to the presence of amyloid plaque deposition in the hippocampus. Our additional finding that 3xTg-AD mice also show an increase in non-NMDAR LTP at a young age is intriguing, and warrants further investigation into this potentially compensatory mechanism in the early stages of Alzheimer's disease.

ACKNOWLEDGEMENTS:

Funding for this work was provided by NIH R01 N5046451 (www.ninds.nih.gov) to R. Furukawa and M. Fechheimer. Disclosure statement: There are no conflicts of interest. All animal protocols and experiments were approved by the University of Georgia Institutional Animal Care Committee.

REFERENCES:

1. Hardy, J. (2006) A hundred years of Alzheimer's disease research. *Neuron* **52**, 3-13
2. Glenner, G. G., and Wong, C. W. (1984) Alzheimer's disease: initial report of the purification and characterization of a novel cerebrovascular amyloid protein. *Biochem Biophys Res Commun* **120**, 885-890
3. Dyrks, T., Weidemann, A., Multhaup, G., Salbaum, J. M., Lemaire, H. G., Kang, J., Muller-Hill, B., Masters, C. L., and Beyreuther, K. (1988) Identification, transmembrane orientation and biogenesis of the amyloid A4 precursor of Alzheimer's disease. *EMBO J.* **7**, 949-957
4. Kang, J., Lemaire, H. G., Unterbeck, A., Salbaum, J. M., Masters, C. L., Grzeschik, K.-H., Multhaup, G., Beyreuther, K., and Muller-Hill, B. (1987) The precursor of Alzheimer's disease amyloid A4 protein resembles a cell-surface receptor. *Nature* **325**, 733-736
5. Kosik, K. S., Joachim, C. L., and Selkoe, D. J. (1986) Microtubule-associated protein tau (tau) is a major antigenic component of paired helical filaments in Alzheimer disease. *Proc. Natl. Acad. Sci. U.S.A.* **83**, 4044-4048
6. Bancher, C., Grundke-Iqbal, I., Iqbal, K., Fried, V. A., Smith, H. T., and Wisniewski, H. M. (1991) Abnormal phosphorylation of tau precedes ubiquitination in neurofibrillary pathology of Alzheimer disease. *Brain Res.* **539**, 11-18
7. Grundke-Iqbal, I., Iqbal, K., Quinlan, M., Tung, Y. C., Zaidi, M. S., and Wisniewski, H. M. (1986) Microtubule-associated protein tau. A component of Alzheimer paired helical filaments. *J. Biol. Chem.* **261**, 6084-6089
8. Noble, W., Olm, V., Takata, K., Casey, E., Mary, O., Meyerson, J., Gaynor, K., LaFrancois, J., Wang, L., Kondo, T., Davies, P., Burns, M., Veeranna, Nixon, R., Dickson, D.,

Matsuoka, Y., Ahlijanian, M., Lau, L. F., and Duff, K. (2003) Cdk5 is a key factor in tau aggregation and tangle formation in vivo. *Neuron* **38**, 555-565

9. Cohen, T. J., Guo, J. L., Hurtado, D. E., Kwong, L. K., Mills, I. P., Trojanowski, J. Q., and Lee, V. M. (2011) The acetylation of tau inhibits its function and promotes pathological tau aggregation. *Nat Commun* **2**, 252
10. Yu, J. T., Chang, R. C., and Tan, L. (2009) Calcium dysregulation in Alzheimer's disease: from mechanisms to therapeutic opportunities. *Prog. Neurobiol.* **89**, 240-255
11. Berridge, M. J. (2011) Calcium signalling and Alzheimer's disease. *Neurochem. Res.* **36**, 1149-1156
12. Peng, S., Zhang, Y., Zhang, J., Wang, H., and Ren, B. (2011) Glutamate receptors and signal transduction in learning and memory. *Mol. Biol. Rep.* **38**, 453-460
13. Bliss, T. V., and Collingridge, G. L. (1993) A synaptic model of memory: long-term potentiation in the hippocampus. *Nature* **361**, 31-39
14. Citri, A., and Malenka, R. C. (2008) Synaptic plasticity: multiple forms, functions, and mechanisms. *Neuropyschopharmacology* **33**, 18-41
15. Grover, L. M., and Teyler, T. J. (1990) Two components of long-term potentiation induced by different patterns of afferent activation. *Nature* **347**, 477-479
16. Morris, R. G., Anderson, E., Lynch, G. S., and Baudry, M. (1986) Selective impairment of learning and blockade of long-term potentiation by an N-methyl-D-aspartate receptor antagonist, AP5. *Nature* **319**, 774-776

17. Maurice, T., Bayle, J., and Privat, A. (1995) Learning impairment following acute adminstration of the calcium channel antagonist nimodipine in mice. *Behav. Pharmacol.* **6**, 167-175

18. Butelman, E. R. (1989) A novel NMDA antagonist, MK-801, impairs performance in a hippocampal-dpendent spatial learning task. *Pharmacol. Biochem. Behav.* **34**, 13-16

19. Bolhuis, J. J., and Reid, I. C. (1992) Effects of intraventricular infusion of the N-methyl-D-aspartate (NMDA) receptor antagonist AP-5 on spatial memory of rats in a radial arm maze. *Behav. Brain Res.* **47**, 151-157

20. Ward, L., Mason, S. E., and Abraham, W. C. (1990) Effects of the NMDA antagonists CPP and MK-801 on radial arm maze performance in rats. *Pharmacol. Biochem. Behav.* **35**, 785-790

21. Zhang, X. H., Liu, S. S., Yi, F., Zhuo, M., and Li, B. M. (2013) Delay-dependent impairment of spatial working memory with inhibition of NR2B-containing NMDA receptors in hippocampal CA1 region of rats. *Mol. Brain* **6**, 13-33

22. Niewoehner, B., Single, F. N., Hvalby, O., Jensen, B., Meyer zun Altern Borloh, S., Seeburg, P. H., Rawlins, J. N., Sprengel, R., and Bannerman, D. M. (2007) Impaired spatial working memory but spared spatial reference memory following functional loss of NMDA receptors in the dentate gyrus. *Eur. J. Neurosci.* **25**, 837-846

23. Driesen, N. R., McCarthy, G., Bhagwagar, Z., Bloch, M. H., Calhoun, V. D., D'Souza, D. C., Gueorguieva, R., He, G., Leung, H. C., Ramani, R., Anticevic, A., Suckow, R. F., Morgan, P. T., and Krystal, J. H. (2013) The impact of NMDA receptor blockade on human working memory-related prefrontal function and connectivity. *Neuropsychopharmacology* **38**, 2613-26622

24. Oddo, S., Caccamo, A., Shepherd, J. D., Murphy, M. P., Golde, T. E., Kayed, R., Metherate, R., Mattson, M. P., Akbari, Y., and LaFerla, F. M. (2003b) Triple-transgenic model of Alzheimer's disease with plaques and tangles: intracellular Abeta and synaptic dysfunction. *Neuron* **39**, 409-421

25. Babb, S. J., and Crystal, J. D. (2006) Episodic-like memory in the rat. *Curr. Biol.* **16**, 1317-1321

26. Hemming, M. L., Selkoe, D. J., and Farris, W. (2007) Effects of prolonged angiotensin-converting enzyme inhibitor treatment on amyloid beta-protein metabolism in mouse models of Alzheimer disease. *Neurobiol. Dis.* **26**, 273-281

27. Hemming, M. L., and Selkoe, D. J. (2005) Amyloid beta-protein is degraded by cellular angiotensin-converting enzyme (ACE) and elevated by an ACE inhitor. *J. Biol. Chem.* **280**, 37644-37650

28. Johnson-Wood, K., Lee, M., Motter, R., Gordon, G., Barbour, R., Khan, K., Gordon, M., Tan, H., Games, D., Lieberburg, I., Schecnk, D., Seubert, P., and McConlogue, L. (1997) Amyloid precursor protein processing and Ab42-deposition in a transgenic mouse model of Alzheimer disease. *Proc. Natl .Acad. Sci. U. S. A.* **94**, 1550-1555

29. Ha, S., Furukawa, R., Stramiello, M., Wagner, J. J., and Fechheimer, M. (2011) Transgenic mouse model for the formation of Hirano bodies. *BMC Neurosci.* **12**, 97-113

30. Billings, L. M., Oddo, S., Green, K. N., McGaugh, J. L., and LaFerla, F. M. (2005) Intraneuronal Ab causes the onset of early Alzheimer's disease-related cognitive deficits in transgenic mice. *Neuron* **45**, 675-688

31. Oddo, S., Caccamo, A., Kitazawa, M., Tseng, B. P., and LaFerla, F. M. (2003a) Amyloid deposition precedes tangle formation in a triple transgenic model of Alzheimer's disease. *Neurobiol Aging* **24**, 1063-1070

32. Floresco, S. B., Seamans, J. K., and Phillips, A. G. (1997) Selective roles for hippocampal, prefronal cortical, and ventral striatal circuits in radial-arm maze tasks with or without a delay. *J. Neurosci.* **17**, 1880-1890

33. Baddeley, A. (2010) Working memory. *Curr. Biol.* **20**, R136-140

34. Morris, R. G. (1984) Developments of a water-maze procedure for studying spatial learning in the rat. *J. Neurosci. Methods* **11**, 47-60

35. Wenk, G. L. (2004) Assessment of spatial memory using the radial arm maze and Morris water maze. in *Curr. Protoc. Neurosci.* (Crawley, J. N. ed.), J. Wiley, New York, NY. pp

36. Jarrard, L. E. (1993) On the role of the hippocampus in learning and memory in the rat. *Behav. Neural. Biol.* **60**, 9-26

37. Olton, D. S., and Papas, B. C. (1979) Spatial memory and hippocampal function. *Neuropsychopharmacology* **17**, 669-682

38. Becker, J. T., Walker, J. A., and Olton, D. S. (1980) Neuroanatomical bases of spatial memory. *Brain Res.* **200**, 307-320

39. O'Neill, P. K., Gordon, J. A., and Sigurdsson, T. (2013) Theta oscillations in the medial prefrontal cortex are modulated by spatial working memory and synchronize with hippocampus through its ventral subregion. *J. Neurosci.* **33**, 14211-14224

40. Degenetais, E., Thierry, A. M., Glowinski, J., and Gioanni, Y. (2003) Synaptic influence of hippocampus on pyramidal cells of the rat prefrontal cortex: an in vivo intracellular recording study. *Cereb. Cortex* **13**, 782-792

41. Fanselow, M. S., and Dong, H. W. (2010) Are the dorsal and ventral hippocampus functionally distinct structures? *Neuron* **65**, 7-19

42. Qiu, A., Fennema-Nostine, C., Dale, A. M., Miller, M. I., and Alzheimer's Disease Neuroimaging, I. (2009) Regional shape abnormalities in mild cognitive impairment and Alzheimer's disease. *Neuroimage* **45**, 656-661

43. Frisoni, G. B., Ganzola, R., Canu, E., Rub, U., Pizzini, F. B., Alessandrini, F., Zoccatelli, G., Beltramello, A., Caltagirone, C., and Thompson, P. M. (2008) Mapping local hippocampal changes in Alzheimer's disease and normal ageing with MRI at 3 tesla. *Brain* **131**, 3266-3276

44. Stutzmann, G. E., Smith, I. F., Caccamo, A., Oddo, S., LaFerla, F. M., and Parker, I. (2006) Enhanced ryanodine receptor recruitment contributes to Ca+2 disruptioins in young, adult, and aged Alzheimer's disease mice. *J. Neurosci.* **26**, 5180-5189

45. Zucker, R. S., and Regehr, W. G. (2002) Short-term synaptic plasticity. *Annu. Rev. Physiol.* **64**, 355-405

46. Paula-Lima, A. C., Britto-Moreira, J., and Ferreira, S. T. (2013) Deregulation of excitatory neurotransmission underlying synapse failure in Alzheimer's disease. *J. Neurochem.* **126**, 191-202

47. Davis, S., Butcher, S. P., and Morris, R. G. (1992) The NMDA receptor antagonist D-2-amino-5-phosphonopentanoate (D-AP5) impairs spatial learning and LTP in vivo at

intracerebral concentrations comparable to those that block LTP in vitro. *J. Neurosci.* **12**, 21-34

48. Borroni, A. M., Fichtenholtz, H., Woodside, B. L., and Teyler, T. J. (2000) Role of voltage-dependent calcium channel long-term potentiation (LTP) and NMDA LTP in spatial memory. *J. Neurosci.* **20**, 9272-9276

49. Bannerman, D. M., Niewoehner, B., Lyon, L., Romberg, C., Schmitt, W. B., Taylor, A. C., Sanderson, D. J., Cottam, J., Sprengel, R., Seeburg, P. H., Kohr, G., and Rawlins, J. N. (2008) NMDA receptor subunit NR2A is required for rapidaly acquired spatial working meory but not incremental spatial reference memory. *J. Neurosci.* **28**, 3623-3630

50. Walsh, D. M., Klyubin, I., Fadeeva, J. V., Cullen, W. K., Anwyl, R., Wolfe, M. S., Rowan, M. J., and Selkoe, D. J. (2002) Naturally secreted oligomers of amyloid beta protein potently inhibit hippocampal long-term potentiation in vivo. *Nature* **416**, 535-539

51. Kim, J. H., Anwyl, R., Suh, Y. H., Djamgoz, M. B., and Rowan, M. J. (2001) Use-dependent effects of amyloidogenic fragments of (beta)-amyloid precursor protein on synaptic plasticity in rat hippocampus in vivo. *J. Neurosci.* **21**, 1327-1333

52. Mucke, L., Masliah, E., Yu, G.-Q., Mallory, M., Rockenstein, E. M., Tatsuno, G., Hu, K., Kholodenko, D., Johnson-Wood, K., and McConlogue, L. (2000) High-level neuronal expression of Abeta $_{1-42}$ in wild type human amyloid protein precursor transgenic mice: synaptotoxicity without plaque formation. *J. Neurosci* **20**, 4050-4058

53. Puolivali, J., Wang, J., Heikkinen, T., Heikkila, M., Tapiola, T., van Groen, T., and Tanila, H. (2002) Hippocampal Abeta 42 levels correlate with spatial memory deficit in APP and PS1 double transgenic mice. *Neurobiol Dis* **9**, 339-347

Figure 1. Training phase results for 3xTg-AD and NonTg mice in the 8-arm radial maze at 3 and 8 months. Mice collect food rewards in each open, baited arm (8 arms open, 8 arms baited as illustrated in the schematic). Revisits to arms where the food rewards were previously obtained are errors. A) NonTg (black bars, n=11) and 3xTg-AD (white bars, n=12) mice at 3 months old. B) NonTg (black bars, n=11) and 3xTg-AD (white bars, n=11) at 8 months old. Both the NonTg and 3xTg-AD mice significantly improved their performance as the number of training sessions increased, as evidenced by a decrease in errors (* $p < 0.05$, ** $p < 0.01$). There were no differences between the genotypes or ages of the mice. The values represent mean $\pm$ SEM of the first 2 days or the last 2 days of the training phase.

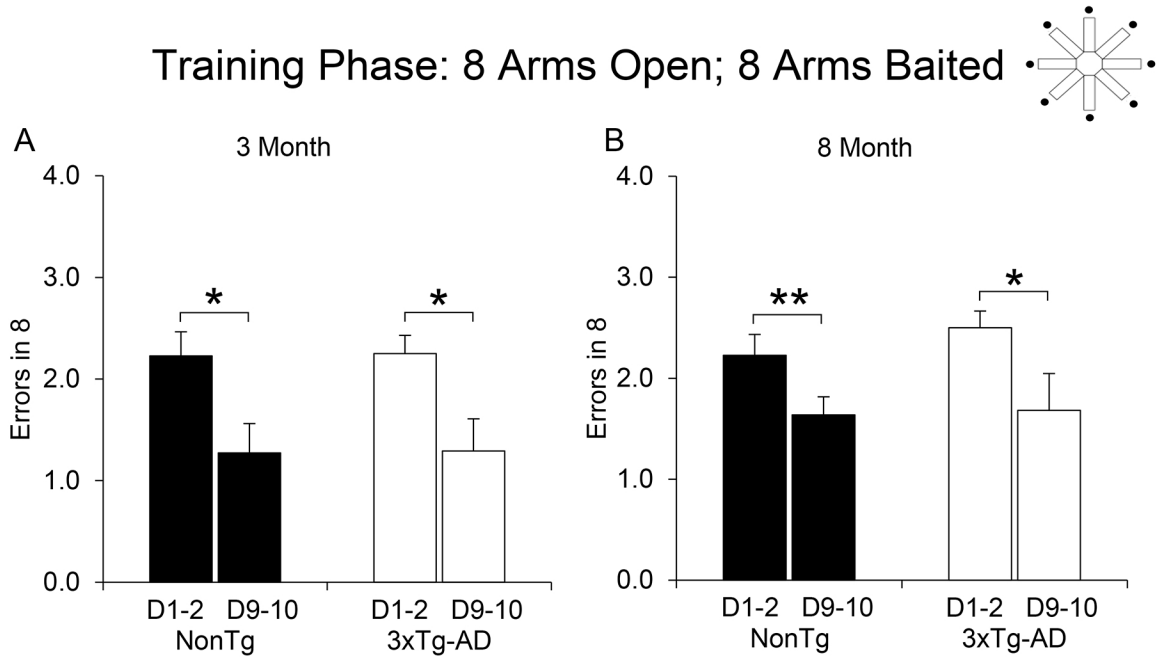
Training Phase: 8 Arms Open; 8 Arms Baited
A
3 Month
Errors in 8
4.0
3.0
2.0
1.0
0.0
*
*
D1-2
D9-10
D1-2
D9-10
NonTg
3xTg-AD
B
8 Month
Errors in 8
4.0
3.0
2.0
1.0
0.0
**
*
D1-2
D9-10
D1-2
D9-10
NonTg
3xTg-AD

Figure 2. Test phase results for 3xTg-AD and NonTg mice in the 8-arm radial maze using a delayed spatial win-shift procedure at 3 and 8 months. A) Schematic illustration of 2-phase delayed spatial win-shift procedure. Mice collect food rewards in each open, baited arm (4 arms open (white), 4 arms baited (•)) in the study phase. The black arms represent inaccessible arms. A short retention interval of 4 minutes occurs between the study and test phase. During the test phase, 8 arms are open with the 4 previously inaccessible arms now baited. Revisits to food troughs where the food rewards were previously obtained are errors. B) NonTg (black bars, n=11) and 3xTg-AD (white bars, n=12) mice at 3 months old. C) NonTg (black bars, n=11) and 3xTg-AD (white bars, n=12) at 8 months old. The NonTg mice significantly improved their performance as the number of training sessions increased as evidenced by a decrease in errors at both 3 and 8 months (* $p < 0.05$). In contrast, the 3xTg-AD mice do not improve at either 3 or 8 months. In addition, there is a significant difference between the performance of the NonTg and the 3xTg-AD mice at days 19-20 at 8 months. The values represent mean $\pm$ SEM of the first 2 days or the last 2 days of the test phase. Significance was determined using either a paired t-test (within genotype, ** $p < 0.01$) or unpaired t-test (between genotypes, *$p < 0.05$).

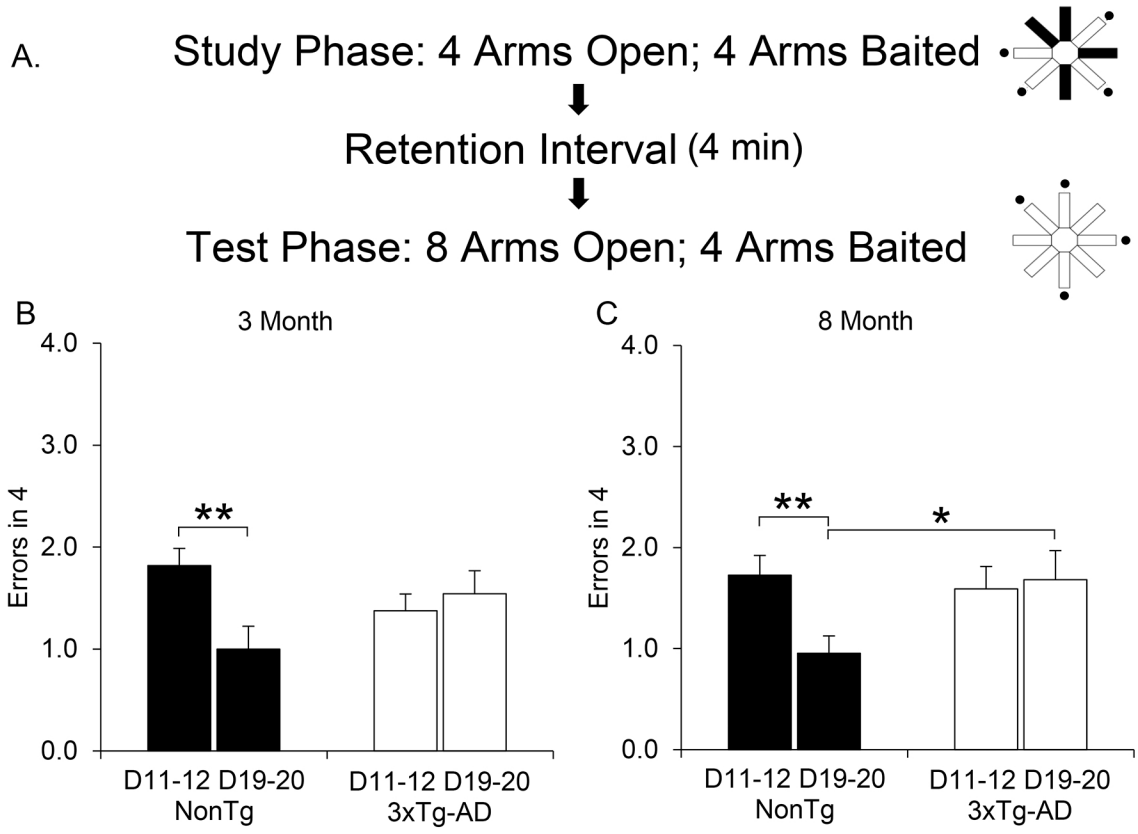
A.
Study Phase: 4 Arms Open; 4 Arms Baited
Retention Interval (4 min)
Test Phase: 8 Arms Open; 4 Arms Baited
B
3 Month
Errors in 4
4.0
3.0
2.0
1.0
0.0
**
D11-12 D19-20
NonTg
D11-12 D19-20
3xTg-AD
C
8 Month
Errors in 4
4.0
3.0
2.0
1.0
0.0
**
*
D11-12 D19-20
NonTg
D11-12 D19-20
3xTg-AD

Figure 3. Aβ42 quantification and relation to maze performance in 3xTg-AD and NonTg mice. A) Comparison of total Aβ42 levels in ventral hippocampal tissue at 3 and 8 months for 3xTg-AD (white bars, 3 months, n=12; 8 months, n=11) and NonTg mice (black bars, 3 months, n=8; 8 months, n=10). Values represent the mean ± SEM; significance was determined using an unpaired t-test between genotypes (**$p < 0.01$). B) Total Aβ42 versus total errors in the delayed win-shift test phase at 3 and 8 months in 3xTg-AD (open and light grey circles, respectively) and NonTg (black and dark grey circles, respectively) mice. At both 3 and 8 months, 3xTg-AD mice show a significant correlation between total Aβ42 and total errors ($p < 0.05$, $p < 0.01$, respectively). Significance was determined using Pearson's correlation coefficient.

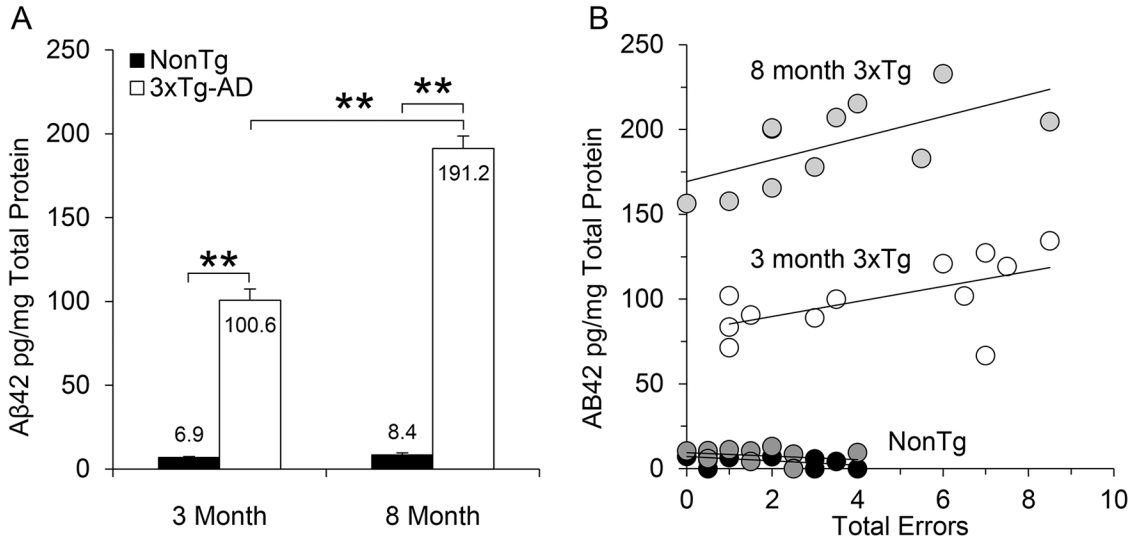
A
NonTg
3xTg-AD
Aβ42 pg/mg Total Protein
250
200
150
100
50
0
**
**
**
6.9
100.6
8.4
191.2
3 Month
8 Month
B
AB42 pg/mg Total Protein
8 month 3xTg
3 month 3xTg
NonTg
0
2
4
6
8
10
Total Errors

Figure 4. Field Excitatory Post-Synaptic Potentials (fEPSP) recorded from the CA1 region of ventral hippocampus in 3xTg-AD and NonTg control mice. A) Stimulus-response curves for 3xTg-AD (white circles, n=54(12)) and NonTg (black circles, n=56(11)) mice at 3 months. Input intensities are 40, 50, 60, 75, 90, 110, 130, and 150 μA. The insets above are averaged fEPSP sweeps for stimulus-response curves in panel A. The vertical bar represents 2 mV and the sweeps are 50 ms in duration. Line values represent the mean ± SEM from n slices. The 3xTg-AD mice exhibited significantly lower fEPSP than NonTg mice at the highest stimulus intensities, 130 and 150 μA. B. Same as panel A except at 8 months for 3xTg-AD (n=39(11)) and for NonTg (n=47(11)) mice. The 3xTg-AD mice exhibited significantly lower fEPSP than NonTg mice at stimulus intensities greater than 60 μA. Significance between genotypes was determined using an unpaired t-test (*$p < 0.05$; **$p < 0.01$)

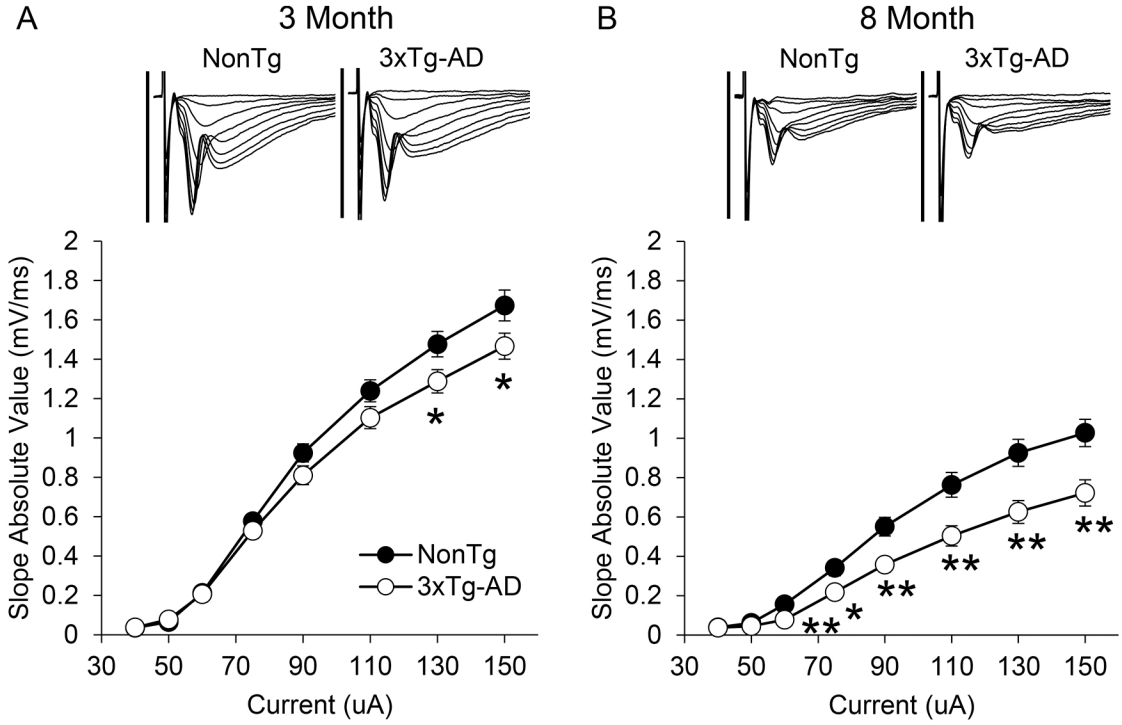
A
3 Month
NonTg
3xTg-AD
Slope Absolute Value (mV/ms)
Current (uA)
NonTg
3xTg-AD
B
8 Month
NonTg
3xTg-AD
Slope Absolute Value (mV/ms)
Current (uA)

Figure 5. Paired-pulse Field Excitatory Post-Synaptic Potentials (fEPSP) recorded from the CA1 region of ventral hippocampus in 3xTg-AD and NonTg control mice. A) Paired-pulse ratios at 50, 100, 200, and 500 ms in 3xTg-AD (open bars, n=54(12)) and NonTg (black bars, n=58(11)) control mice at 3 months. Inset above represents averaged fEPSP sweeps for paired-pulse ratios in panel A. The vertical bar represents 2 mV, and the sweeps are 90 ms in duration. B) Same as panel A except at 8 months for 3xTg-AD (n=36(11)) and NonTg (n=42(11)) control mice. Bar graph values represent the mean ± SEM from n slices. Significance between genotypes was determined using an unpaired t-test (* = $p < 0.05$).

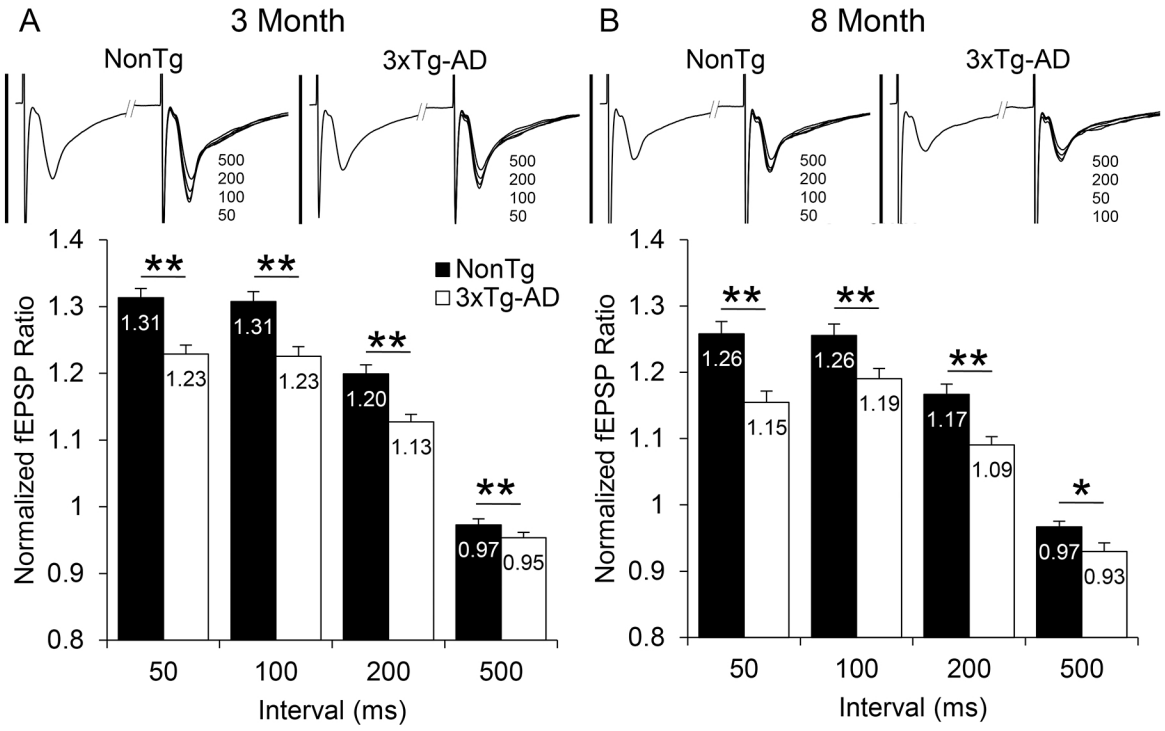
A
3 Month
NonTg
3xTg-AD
500
200
100
50
B
8 Month
NonTg
3xTg-AD
500
200
50
100
Normalized fEPSP Ratio
1.4
1.3
1.2
1.1
1
0.9
0.8
**
*
NonTg
3xTg-AD
1.31
1.23
1.31
1.23
1.20
1.13
0.97
0.95
1.26
1.15
1.26
1.19
1.17
1.09
0.97
0.93
50
100
200
500
Interval (ms)

Figure 6. Long-Term Potentiation (LTP) of Field Excitatory Post-Synaptic Potentials (fEPSP) recorded from the CA1 region of ventral hippocampus in 3xTg-AD and NonTg mice. A) Summary plot of normalized fEPSP slope values in 3-month-old NonTg mice for total LTP (black circle, (n=25(10)) and bath-applied DL-AP5 (50 μM) representing non-NMDAR LTP (dark grey circle, n=25(10)), before and after high frequency stimulation (HFS) (4 x 200Hz/0.5 sec at 5 sec intervals) indicated by the arrow at 30 minutes. Insets above represent averaged fEPSP sweeps before and after HFS for total LTP and non-NMDAR LTP. B) Same as panel A except in 3-month-old 3xTg-AD mice for total LTP (white circle, (n=23(12)) and non-NMDAR LTP (light grey circle, n=25(12)). C) Summary quantification of total LTP and non-NMDAR LTP for NonTg and 3xTg-AD mice at 1 hr post-HFS. There is no significant difference in total LTP between the 3xTg-AD and NonTg mice. In the presence of DL-AP5, the non-NMDAR component of LTP is significantly greater in 3xTg-AD than NonTg mice. D, E, & F) Same as A, B, & C above except at 8 months of age. There was a significant decrease in the total LTP of 3xTg-AD mice. In addition, the non-NMDAR component constitutes a larger proportion of the total LTP than NonTg mice, similar to that found at 3 months. For NonTg mice (total LTP, n=17(9); Non-NMDAR LTP, n=23(11)), and 3xTg-AD mice (total LTP, n=15(11); Non-NMDAR LTP, n=18(11)). Values represent the mean ± SEM from n slices. Significance was determined using an unpaired t-test, both between genotypes and within genotype for component LTP comparison (*$p < 0.05$, **$p < 0.01$).

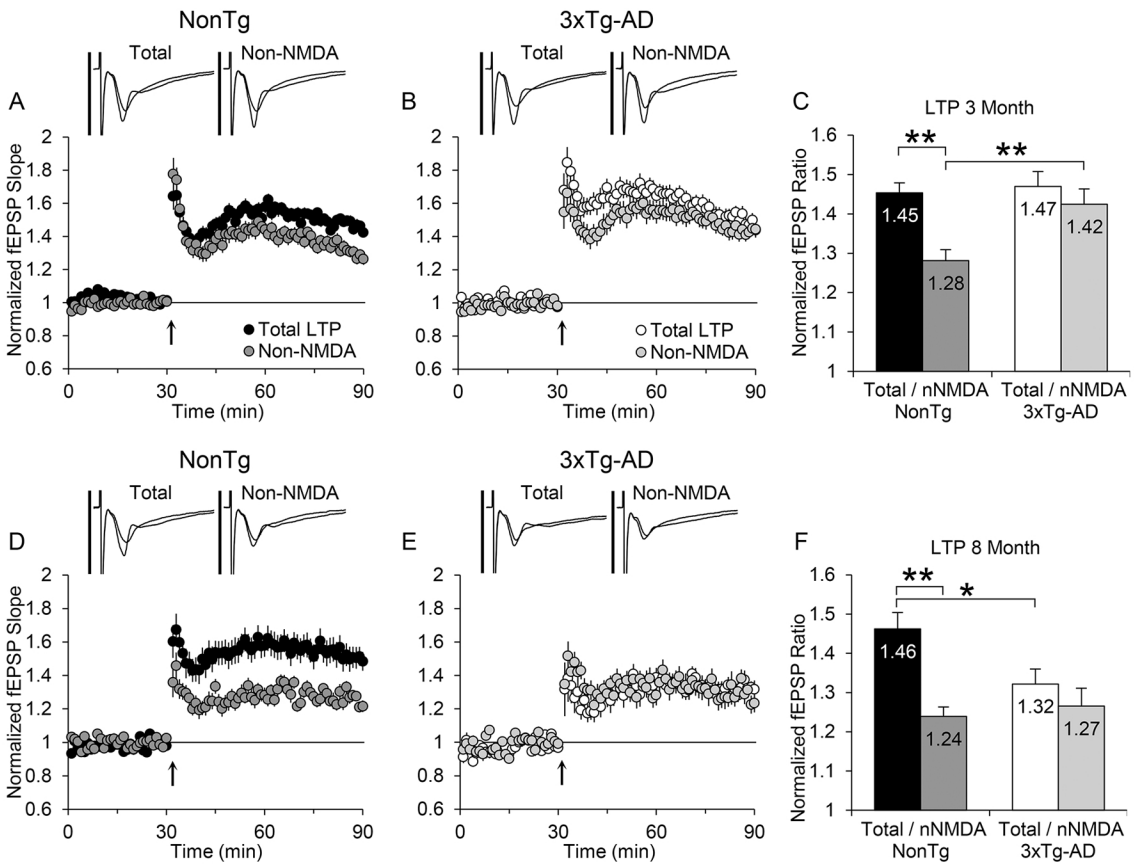
NonTg
3xTg-AD
Total
Non-NMDA
A
B
C
D
E
F
Normalized fEPSP Slope
Time (min)
Total LTP
Non-NMDA
LTP 3 Month
LTP 8 Month
Normalized fEPSP Ratio
1.45
1.28
1.47
1.42
1.46
1.24
1.32
1.27
Total / nNMDA
NonTg
Total / nNMDA
3xTg-AD

Figure S1. Supplementary Figure 1. Characterization of 3xTg-AD pathology in the CA1 region of ventral hippocampus. Sections of 3xTg-AD and NonTg mice at 3 and 8 months were stained with BAM-10 (specific for total Aβ), pTau199/202 (site-specific phosphorylation of tau at Ser 199 and 202), pTau231 (site-specific phosphorylation of tau at Thr 231), and Tau396 (site-specific phosphorylation of tau at Ser 396). 3xTg-AD mice exhibit intra-neuronal Aβ at both 3 and 8 months. Small plaque deposits can be seen at 8 months, but not 3 months in 3xTg-AD mice. Phosphorylated tau is present at 8 months but not 3 months in 3xTg-AD mice. Scale bar = 50 μm.

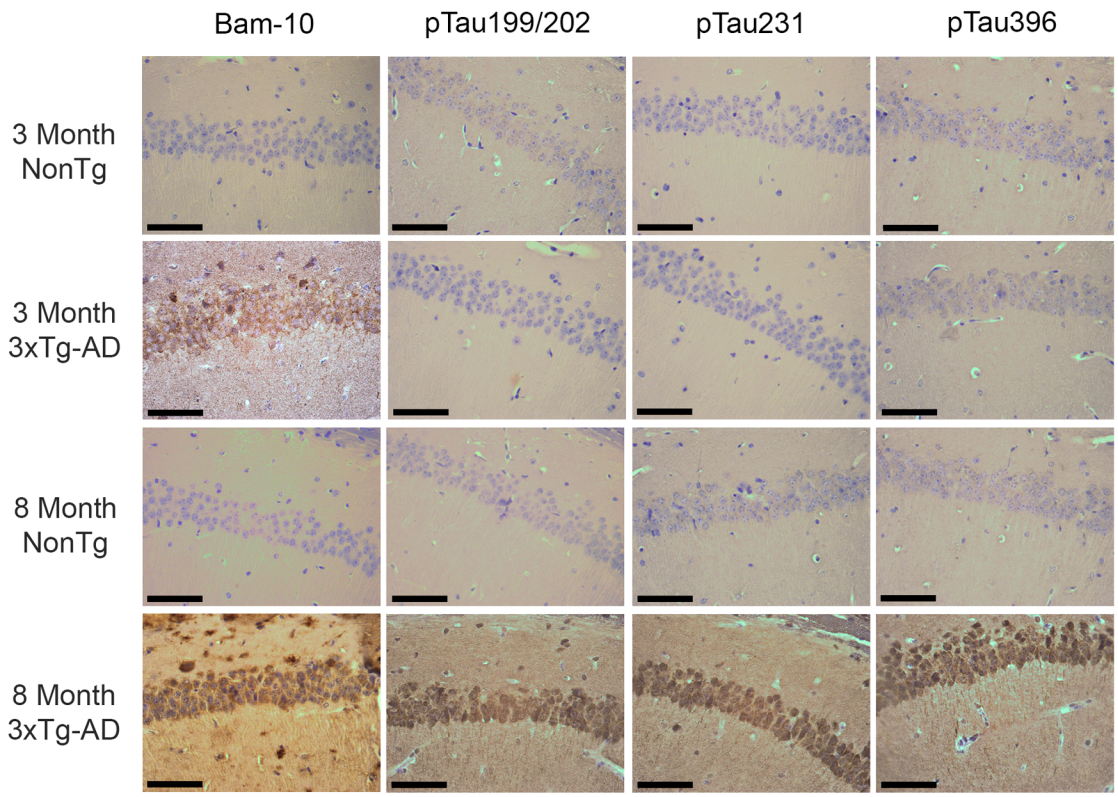
Bam-10
pTau199/202
pTau231
pTau396
3 Month NonTg
3 Month 3xTg-AD
8 Month NonTg
8 Month 3xTg-AD